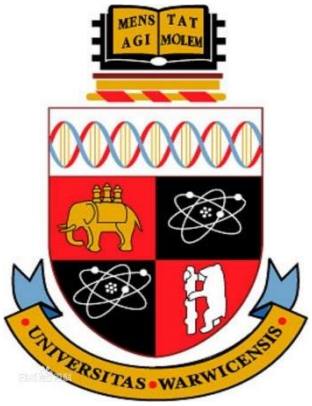

Seismic Design and Assessment of Resilient Steel Frames with Visco-Plastic Dampers

A thesis submitted to the

University of Warwick

for the degree of

Doctor of Philosophy

by

Jaehoon BAE

School of Engineering

Supervised by

Prof Theodore Karavasilis and Dr Georgia Kremmyda

January 2019

Table of Contents

List of Illustrations and Tables

Chapter 1

Chapter 2

Chapter 3

Chapter 4

Chapter 5

Appendix

List of Abbreviations

Abbreviation	Explanation
ACMR	Adjusted Collapse Margin Ratio
ADRS	Acceleration-Displacement Response Spectrum
ATC	Applied Technology Council
BPOE	Basic Performance Of Existing Buildings
BRB	Buckling-Restrained Brace
CMR	Collapse safety Margin Ratio
CSM	Capacity Spectrum Method
DBE	Design Based Earthquake
EC	Euro Code
FEMA	Federal Emergency Management Agency
IDA	Incremental Dynamic Analysis
LATBSDC	Los Angeles Tall Buildings Structural Design Council
MCE	Maximum Considered Earthquake
MDOF	Multi-Degree-Of-Freedom
NRH	Non-linear Response History
PBSD	Performance-Based Seismic Design
PGA	Peak Ground Acceleration

PGV	Peak Ground Velocity
PSA	Pseudo-Spectral Acceleration
SDOF	Single-Degree-Of-Freedom
SEAOC	Structural Engineers Association Of California
SEANC	South’s Leading State Employees’ Association
SF	Scale Factor
SMRFs	Steel Moment-Resisting Frames
SVD	Super-elastic Viscous Dampers
TBI	Tall Buildings Initiative
VPD	Visco-Plastic Damper
WHPs	Web Hourglass shape Pins

Acknowledgements

"Research and industry are always complementary and link together."
After concluding my previous consulting engineer role, I decided to embark on a PhD. Throughout the duration of my PhD I have received valuable help from many people in the School of Engineering at the University of Warwick.

Above all, I greatly appreciate the help of my supervisor, Professor Theodore Karavasilis, for his invaluable supervision and influential attitude as a researcher. I have learned a lot and gained confidence in my research through conversation with him. I would also like to thank my other supervisors, Dr. Georgia Kremmyda, Professor Toby Mottram, and Professor Irwanda Laory, for their encouragement and thoughtful suggestions.

I would also like to express my gratitude to the professors who became my referees, Professor Sang-dae Kim, Professor Sang-eul Han and Professor Young-kyu Ju. Also, I appreciate my superiors and previous employers, Dr. Tae-sang An, Dr. Young-ju. Their advice broadened my thinking, strengthened my self-belief that I have been achieved and helped me to develop an in-depth understanding of practical structural engineering aspects. Thanks to my wife, Sunju Kim, and my son, Hyunjun Bae. Their endless support has given me the strength and confidence to succeed in my PhD. I also want to thank my father, mother and my family for their unlimited support.

Finally, thanks to the many people who have supported me that I have not mentioned and, above all, thanks to the Lord for giving me the opportunity to proceed on this journey.

Declaration

This thesis is submitted to the University of Warwick in support of my application for the degree of Doctor of Philosophy. It has been composed by myself and has not been submitted in any previous application for any degree.

Parts of this thesis have been published in the following international journals:

Jaehoon, B., Theodore L, Karavasilis. (2018) Seismic Design and Assessment of Steel Frames with Visco-plastic Dampers, *International Journal of Earthquake and Impact Engineering* .

Jaehoon, B., Theodore, K., Youngju, K., Taesang A. (2018) Seismic Design and Assessment of Resilient Steel Frames with Visco-Plastic Dampers. *16th European Conference on Earthquake Engineering*, June 18-21, Thessaloniki, Greece.

January 2019

Jaehoon (Nicolas) BAE

Abstract

In recent years, many new buildings have been designed for low-damage seismic performance in order to achieve earthquake resilience, contrary to seismic design codes, which primarily focus on life safety (ASCE/SEI 7-10, 2010). Many researchers have investigated a variety of approaches to increase the resilience of buildings against wind or earthquake loads. Supplemental passive damper systems such as viscous and visco-elastic dampers are considered effective and affordable means of improving seismic resilience. However, these rate-dependent dampers may unintentionally overstress the columns of the building since their force output depends on inter-storey velocity. One way of reducing the aforementioned detrimental effect is to control the peak damper force using a hybrid damper system. This paper evaluates the seismic performance of steel frames equipped with visco-plastic dampers. The visco-plastic damper is realised by the in-series combination of a viscoelastic damper and a friction device. The main goal of exploiting the visco-plastic damper in resilience-based seismic design is the reduction of storey drifts without increasing the base shear force, i.e., a design objective that is difficult to achieve with conventional viscous or viscoelastic dampers.

A prototype steel building is designed as a high ductility steel moment-resisting frame (MRF). This MRF is then equipped with viscoelastic or visco-plastic dampers to achieve high seismic performance. Parametric designs are carried out by designing visco-plastic dampers with different activation forces for their friction devices. Non-linear dynamic analyses for a set of 20 earthquake ground motions scaled to the design and maximum considered earthquake intensities are carried out in OpenSees. The response results highlight the advantages of the visco-plastic damper. Moreover, they provide the basis to identify the appropriate range of activation force values for the visco-plastic damper's friction device so that drift reduction and control of the peak base shear force can be simultaneously achieved. Also, peak residual drifts that are directly related to the earthquake resilience of the building are

compared between the frames with viscoelastic and visco-plastic dampers under DBE and MCE levels. Furthermore, IDA (Incremental Dynamic Analysis) are carried out on the MRFs with viscoelastic and visco-plastic dampers using a set of 20 far-field seismic records to evaluate vulnerability to collapse.

The results highlight the effectiveness of the visco-plastic damper in controlling drifts, residual drifts, and the base shear force, while also providing adequate seismic collapse resistance.

Chapter 1

Introduction

1.1 Backgrounds

Conventional seismic-resistant yielding structures, such as steel moment-resisting frames (MRFs), are designed to ensure life safety under strong earthquakes (Eurocode 8, 2013); yet they have certain limitations in terms of providing earthquake resilience. Much research has already been carried out to explore economical means of improving buildings' resilience against earthquakes. To this end, passive damper systems are widely used in many fields (buildings, bridges, etc.) because of their superior efficiency, easy installation and cost effectiveness, as compared to conventional reinforcement methods. For instance, research by Christopoulos et al. (2013) highlights that this supplementary damper system is widely used to not only control earthquakes, but also wind forces. This is reinforced by Zheng Lu et al. (2017), who discuss the possible application of particle dampers and define such an energy dissipating system as the core technology of the future. In the same vein, the popularity of this method has grown since its effectiveness has been validated by several researches (Chen et al., 2003; Apostolakis et al., 2010; Kallavasilis et al., 2012). With regards to tall buildings fitted with passive damper systems, according to Lin et al. (2009), the impact of wind energy can be reduced with the use of viscous dampers. Symans et al. (2008) also holds the view that this implementation can reduce the side-sway effect of top displacement. According to Longarini et al. (2017), seismic resistance of tall buildings is significantly enhanced by using viscous dampers that reduce base shear and peak acceleration. A number of other authors have also examined the effects of the damper system in terms of reducing the side-sway and acceleration caused by wind loads on tall buildings (Wakahara et al., 1992; Qin et al., 2008; Zemp et al., 2011; Christopoulos et al., 2013).

Considering the evidence mentioned above, it is clear that the damper system is an effective influence on tall structures, not only in relation to wind, but

also earthquake loads. Rate-dependent passive dampers, such as viscous, viscoelastic, and elastomeric, are now a mature and readily available technology for resilience-based seismic design (Christopoulos and Filiatrault, 2006). Such dampers are available at a relatively low cost and can be easily installed. Therefore, with a slight increase in initial cost, the socio-economic losses caused by earthquakes during the life-cycle of a building can be significantly reduced, if not minimized. Prior numerical and experimental research has shown that rate-dependent dampers are highly effective in reducing plastic deformations, drifts, residual drifts, and the probability of collapse of steel MRFs (Karavasilis et al., 2011; Karavasilis et al., 2012; Seo et al., 2014).

However, rate-dependent dampers produce forces that increase with inter-storey velocities, and therefore may induce high axial forces in the columns. Constantinou and Symans (1993) identified the harmful effect of additional axial force caused by adding a viscoelastic damper to a structure. This detrimental effect becomes more pronounced when the steel MRF experiences plastic deformation. In such case, damper forces may not be out of phase with the peak bending moments and shear forces in the columns. For example, Karavasilis (2016) assessed the response of tall steel MRFs with viscous dampers under strong earthquakes, and indeed, identified plastic mechanisms involving plastic hinges in the columns. To address this issue, Kariniotakis and Karavasilis (2017) have recently proposed a modified capacity design rule for columns of steel MRFs with viscous dampers that guarantees a plastic mechanism similar to that of conventional steel MRFs. Another way to address the detrimental effect of large peak damper forces is to develop hybrid devices capable of imposing a limit on the peak force that they exert to structural members attached to them. For example, a hybrid device consisting of an elastomeric damper in-series connected to a buckling restrained steel brace has been proposed by Ibrahim et al. (2007). In the latter work, yielding of the buckling-restrained brace imposes a limit on the peak force of the hybrid device during earthquake loading. Furthermore, oil dampers or viscous fluid dampers with a relief valve that limits their peak force are available on the market (SANWA TEKKI, 2017). It should be

pointed out that activation of the peak force control mechanism in the previously mentioned hybrid devices results in loss of velocity-dependent supplemental viscous damping, and therefore compromises the capability of the devices to reduce drifts.

Because of the value of hybrid dampers, recent research has studied the counterbalance between the benefits and drawbacks of each component passive damper. Silwal et al. (2016) introduced super-elastic viscous dampers (SVD) combining a viscoelastic device and shape memory alloy cables in parallel, and verified the effectiveness of hybrid dampers in reducing residual drift and increasing resilience against collapse due to seismic intensity. Similarly, Marshall et al. (2010), and Rawlinson et al. (2014) introduced a new hybrid damper which combines high-damping rubber dampers in series with a buckling-restrained brace (BRB). In this research, the performance of the hybrid damper is verified through experimentation and FEM analysis. The results show a high ability to dissipate seismic energy under all levels of seismic ground intensity. Rawlinson et al. (2014) emphasised the role of different types of passive control combinations in increasing resilient capability throughout the non-linear dynamic analysis of a single-degree-of-freedom (SDOF) system. Lee et al. (2017) introduced a hybrid energy dissipation device which combines a steel-slit damper and rotational friction dampers in parallel. Based on the paper, the hybrid damper can be effectively applied in seismic retrofits to reduce the probability of collapse. Several other studies have assessed the benefits of hybrid dampers in reducing seismic hazard and probability of collapse (Chang-Hwan et al., 2016; Jinkoo et al., 2017).

1.2 The problem dampers increasing column loads

According to the capacity design rules, plastic hinges should be placed at the beam end zone (ductile components), not on the columns (Brittle components) while experiencing inelastic deformation under strong earthquake cyclic loading (Fig. 1.1(a)). The significant problem faced when the velocity damper system is used with MRF is that plastic hinges may be placed on the column of the structure, which may lead to the structural collapse (weak story failure), as can be seen in Fig. 1.1(b).

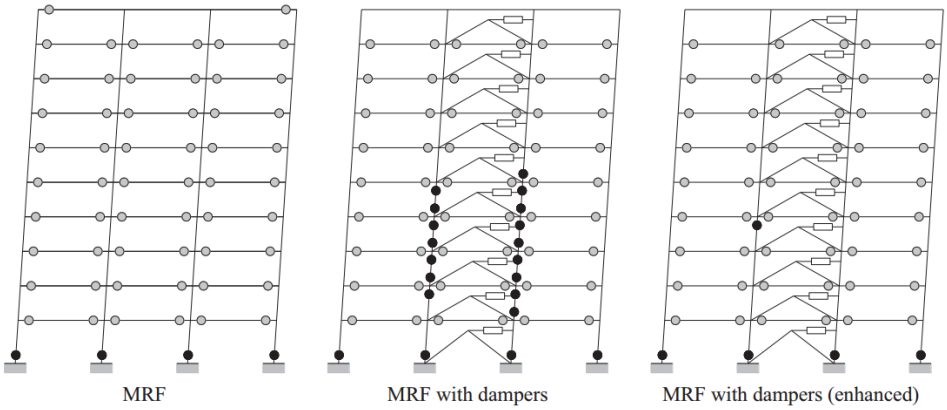

(a) MRF with velocity damper plastic mechanism (adapted from Karavasilis, 2016)

(b) Story failure at the Kobe City Hall (adapted from Wada et al., 2010)

Fig. 1.1 MRF with velocity damper plastic mechanism and story failure at the Kobe City Hall

1.3 Limitations of current seismic design guidelines and structural systems

Ghobarah (2001) pointed out that the fundamental philosophy of current building codes is established on precautions to ensure life safety in the event of frequently occurring small and medium earthquakes, and collapse prevention under rare large-scale earthquakes (Table 1.1). In other words, current seismic design codes overlook building resilience performance, since the design philosophy focusses on saving human life rather than protecting the building. This leads to limitations in terms of providing diversified performance levels, and therefore requires the development of separate performance stages to deal with not only danger to life, but also building resilience against different seismic hazard levels (Ghobarah, 2001). From this perspective, Ghobarah stressed the importance of quantifying seismic performance in the future. Table 1.1 shows the proposed earthquake hazard.

Table 1.1 Proposed earthquake hazard level (Ghobarah, 2001)

Earthquake frequency	Return period in years	Probability of exceedance
Frequent	43	50% in 30 years
Occasional	72	50% in 50 years
Rare	475	10% in 50 year
Very rare	970	5% in 50 years
Extremely rare	2475	or 10% in 100 years 2% in 50 years

In addition, compatibility with reality and ambiguity for current standards must also be resolved. In terms of compatibility with reality, the respond spectrum analysis, which is widely used in practice, is based on the theory of elastic analysis used in the SDOF (single-degree of freedom) system and considers only the maximum response corresponding to a specific period calculated by the structural dynamics equation. In reality, however, many of the current buildings are composed of MDOF (multi-degree of freedom) systems, and the increase in the effective period due to ongoing plastic

deformation during an earthquake causes a compatibility problem with the existing respond acceleration spectrum analysis method, as it is based on a specific period. In addition, there has been controversy surrounding the reliability of a response modification factor known as 'R' in US standards, 'q' factor in Eurocode, and displacement amplification factor 'Cd' (Uang, 1991). Uang (1991) holds the view that force reduction (R-factor) and displacement amplification factors (Cd factor) play a significant role in the development of seismic design procedures, however they are ambiguous and unreliable. In Uang's major study, the significant problem facing seismic design provision is that the elastic design procedure makes it difficult for designers to estimate the actual strength of the structure beyond the elastic range caused by rare earthquakes. This view is supported by Ghobarah (2001), who states that current code-based design cannot accurately predict the performance of the structure over the elastic range, or the actual displacement assumed by multiplying amplification factor 'Cd' to the elastic displacement result from the respond spectrum analysis. Another problem is that it is difficult to achieve the anticipated seismic performance under severe seismic ground motion if the structural strength reserved is less than that of the results from the seismic provisions. Uang (1991) also points out that the maximum inelastic deformation cannot be calculated using the elastic analysis that is a fundamental of the code. He noted that there are limitations in defining the structure ductility factor for multi-storey buildings; R and Cd factors do not offer a guaranteed safety margin against structural collapse.

1.4 Performance-based seismic design

In order to solve many restrictions caused by code based design and to provide a more reliable alternative, performance-based design has been introduced in the field of earthquake engineering with the development of experience and engineering technology. To date, various studies have assessed the efficacy of the performance-based design methodology in earthquake engineering (Ghobarah, 2001; Vamvatsikos et al., 2015; Deierlein et al., 2003; Allahvirdizadeh et al., 2017). According to the existing design method, a structure satisfying the required performance (code, standards) is generated

by following the design philosophy, a process-oriented procedure, provided as a manual. However, even if the required performance is achieved, there are an infinite number of combinations that satisfy this requirement. In other words, a performance-based design tool is more suitable when simultaneously applying several new technologies, since it is a result-oriented procedure. Similarly, the main purpose of performance-based design is to remove uncertainty and to reduce the possibility of loss under seismic hazards (Liu et al., 2013). This view is supported by Basim & Estekanchi (2015), who stated that performance-based design is an effective means of ensuring losses caused by earthquake remain within an acceptable range. They also cited that performance-based design has developed over two stages. In the first generations, the performance level varied according to the degree of damage. Target performance levels are governed by structural characteristics, as shown in Fig. 1.2 (Ghobarah, 2001). Performance targets are diversified from serviceability, life safety and collapse prevention stages where displacement and drift quantity can be used as an indicator of performance achievement. Table 1.2 shows the seismic performance objective suggested by SEAOC Vision 2000.

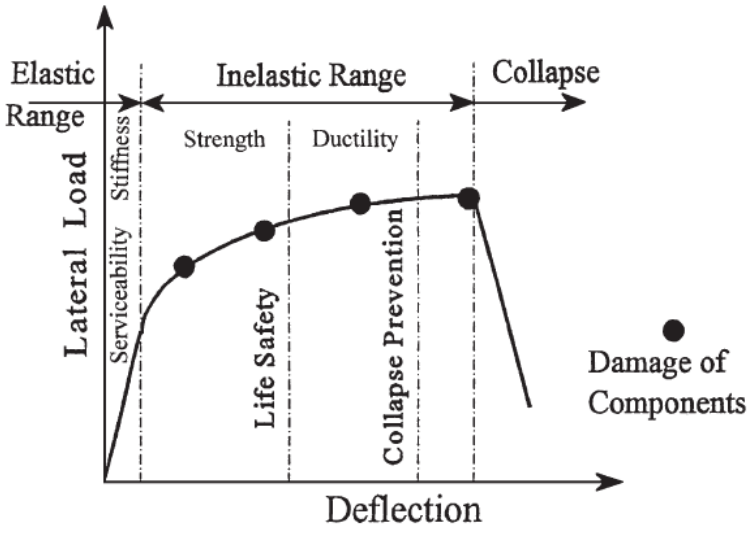

Fig. 1.2 Typical performance curve (adapted from Ghobarah, 2001)

Table 1.2 Seismic performance objective (SEAOC Vision 2000)

		Earthquake Performance Level			
		Fully Operational	Operational	Life safe	Near collapse
Earthquake Damage Level	Frequent (43 years)	Basic objective	×	×	×
	Occasional (72 years)	Essential/ hazardous	Basic objective	×	×
	Rare (475 years)	Safety critical	Essential/ hazardous	Basic objective	×
	Very rare (975 years)	Not feasible	Safety critical	Essential/ hazardous	Basic objective

Fig.1.3 shows the first generation of performance-based design in the FEMA 273 Report, NEHRP Guidelines for the Seismic Rehabilitation of Buildings (ATC, 1997), and Performance-Based Seismic Engineering of Buildings (SEAOC, 1995). FEMA356 and ASCE 41-06 provide practical performance level guidelines. The capacity spectrum method (CSM) was developed through ATC-40, where CSM was first introduced, and FEMA356, where the modification factor was adjusted (Share et al., 2009).

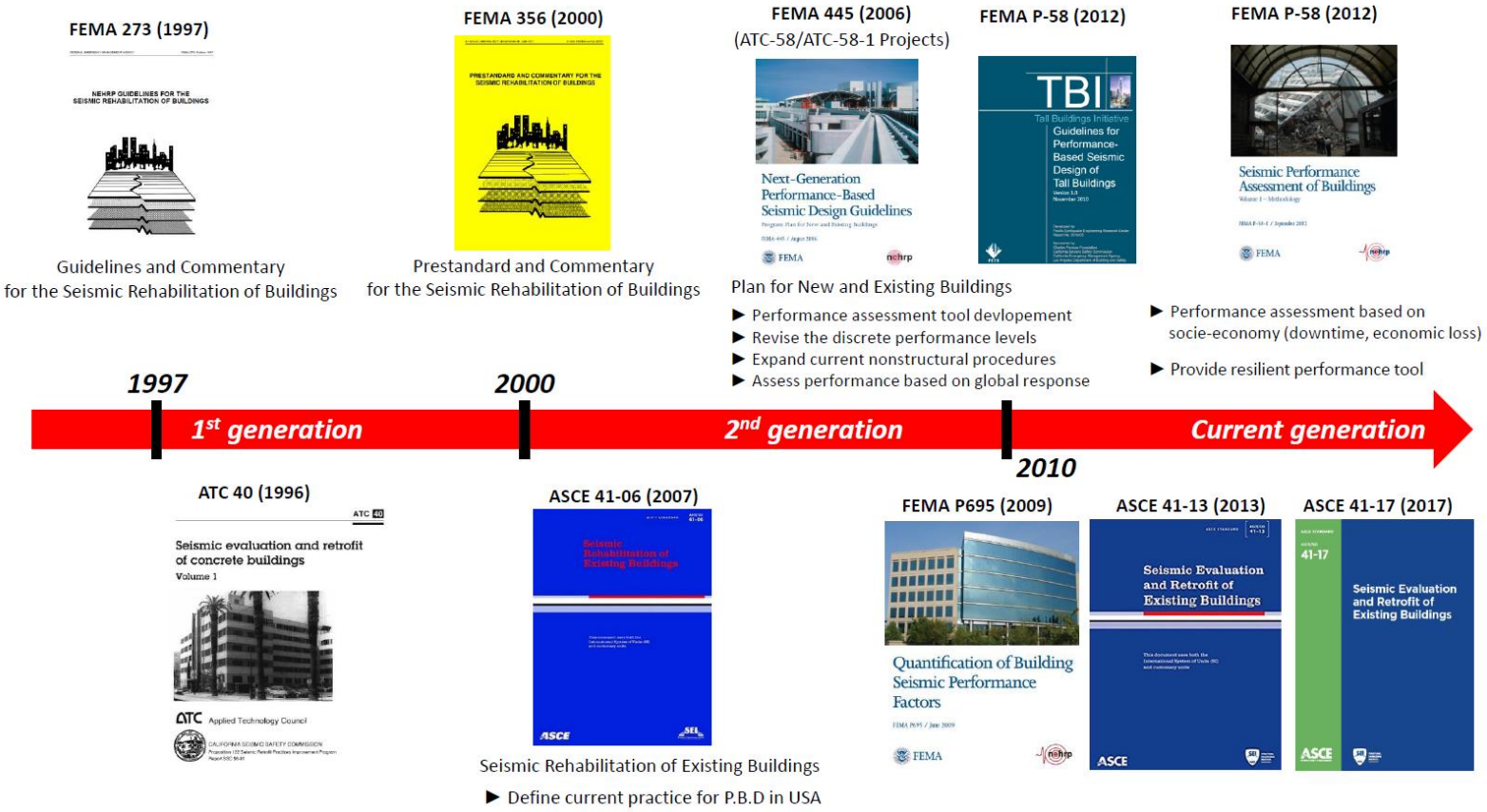

Fig. 1.3 The development of performance-based seismic design

Share (2009) introduced the procedure for estimating the performance point with the ATC-40 capacity spectrum method as follows (Fig. 1.4): 1) Select seismic spectrum with 5% damping. 2) Consider the modification factor that represents the relationship between soil and structure. 3) Transfer spectrum to ADRS (Acceleration-Displacement Response Spectrum) format followed by the ATC-40 procedure. 4) Conduct a pushover analysis to estimate the capacity spectrum of the structure and transfer it to ADRS format for comparison with the performance points. 5) Reduce the spectrum to consider the effective damping and ductility of the structure. 6) Determine the performance point at the intersection of reduced demand spectrum and capacity spectrum and verify it against the target performance.

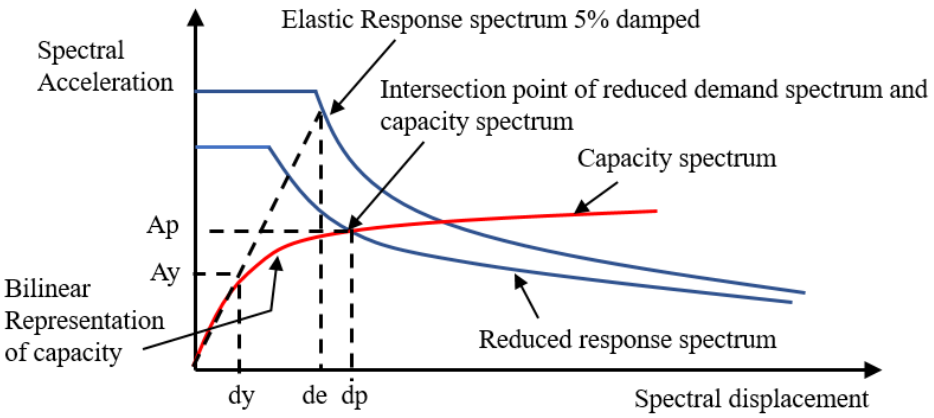

Fig. 1.4 Performance point with capacity spectrum method ATC-40, adapted from Share et al. (2009)

The next generation performance-based design has advanced in terms of reducing the impact of limitations such as uncertainty (e.g. ground motions and the objective of performance levels.) Performance-based design provides a reliable tool that helps stakeholders communicate more easily.

FEMA 445, which was regarded as a next generation performance-based design, shows the advancement in the development of assessment tools on the global scale, diversifying performance levels and expanding non-structural procedures. In terms of FEMA P695, this provision allowed the selection of the seismic reduction factor (R, Cd factor) based on non-linear dynamic analysis. The performance assessment procedure can be summarised as follows (Fig. 1.5);

(1) Determine overstrength factor (Ω) and ductility factor (μ) of the structure by conducting push-over (non-linear static) analysis.
(2) Conduct non-linear dynamic analysis, IDA (incremental dynamic analysis) and estimate the collapse safety margin (CMR) that is the ratio of medium collapse intensity acceleration over MCE acceleration value.
(3) Estimate adjusted collapse margin ratio (ACMR) considering the safety factor, which is dependent on the fundamental periods and ductility of the structure.
(4) Conduct the performance evaluation if calculated ACMR is within the allowable $ACMR_{10\%}$ and $ACMR_{20\%}$, considering the modified uncertainty of the collapse by looking at record-to-record uncertainty, design requirement uncertainty, test data uncertainty, and modelling uncertainty.

Tall building guideline: According to Moehle (2004), performance-based design is used widely in the construction of tall buildings in the USA. This has been formalised by institutions such as SEANC (2007), LATBSDC (2008), and TBI (2010). Performance quantity is measured by structural demand parameters such as storey drifts, accelerations, and residual drifts, however, repair damage costs from probabilistic earthquake hazards are more important for tall building project stakeholders (Moehle, 2004).

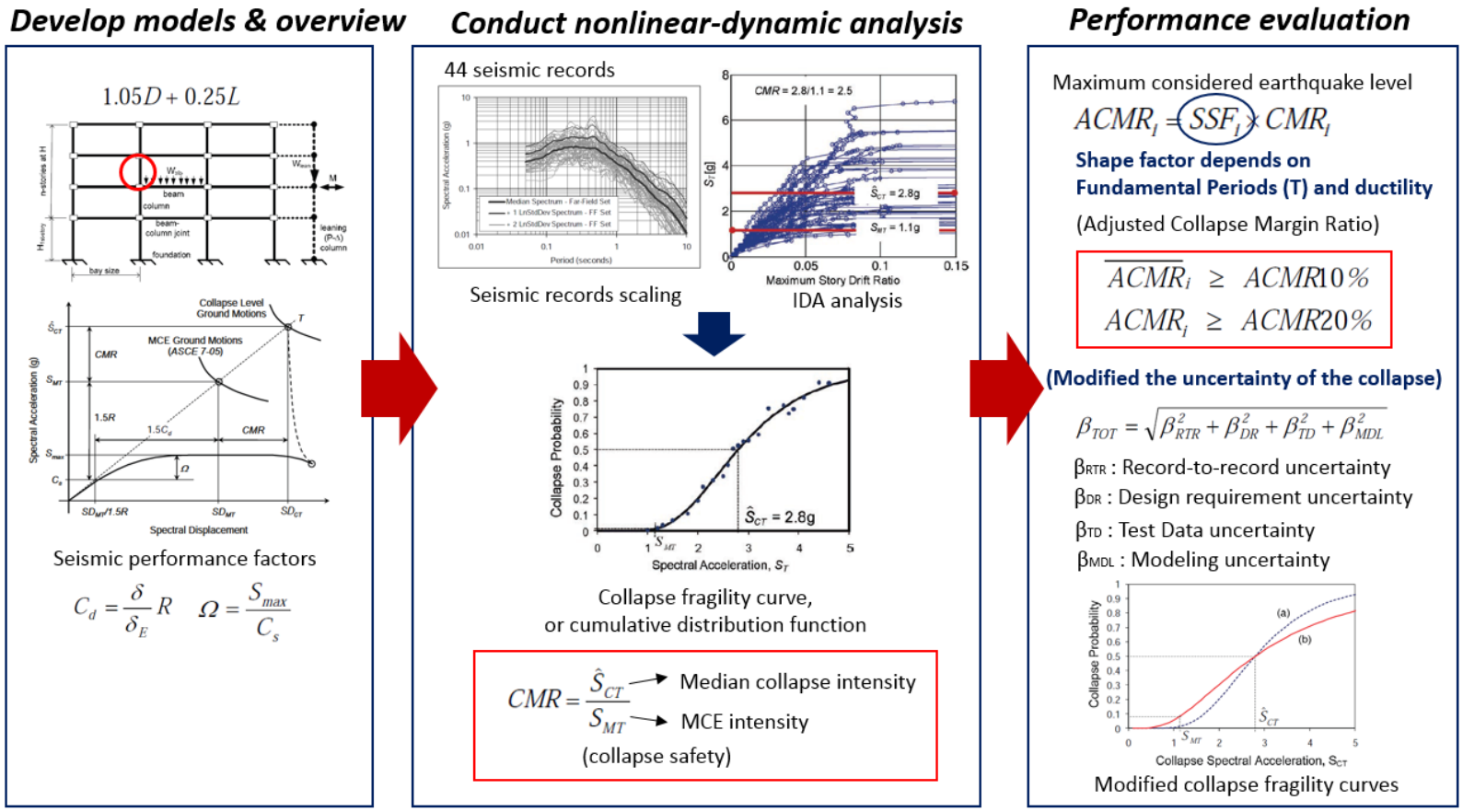

Fig. 1.5 FEMA P695 performance evaluation process

Since 2010, performance-based design has pursued more reliable analysis results, more diverse performance levels, and has increased consideration of the socio-economic effects of different seismic hazards.

Fig. 1.6 shows the code considered to be the current generation of performance-based design tools. FEMA P-58 introduced evaluation of building performance in terms of direct economic loss and collapse (2012). FEMA P-58 also provides new design tools with which socio-economic impact, downtime, economic loss, and performance loss can be determined.

Fig. 1.6 Current generation of performance-based design guidelines (ASCE 41-17 & FEMA P-58)

The development of FEMA P-58, FEMA P695, and the Tall Building Guidelines are regarded as crucial in the development of more reliable performance-based design. Regarding the FEMA P-58 provisions, FEMA P-58 provides tools to estimate casualties, direct and indirect losses from earthquake damage, and repair time and downtime. Assessment can be divided into three approaches (Fig. 1.7):

(1) Intensity-based assessment: Specified acceleration respond spectrum used to calculate the performance.

(2) Scenario-based assessment: Building site and earthquake fault rupture spectral intensity and intensity dispersion is considered.

(3) Time-base assessment: All effects including site and probability of occurrence at a specific time are considered.

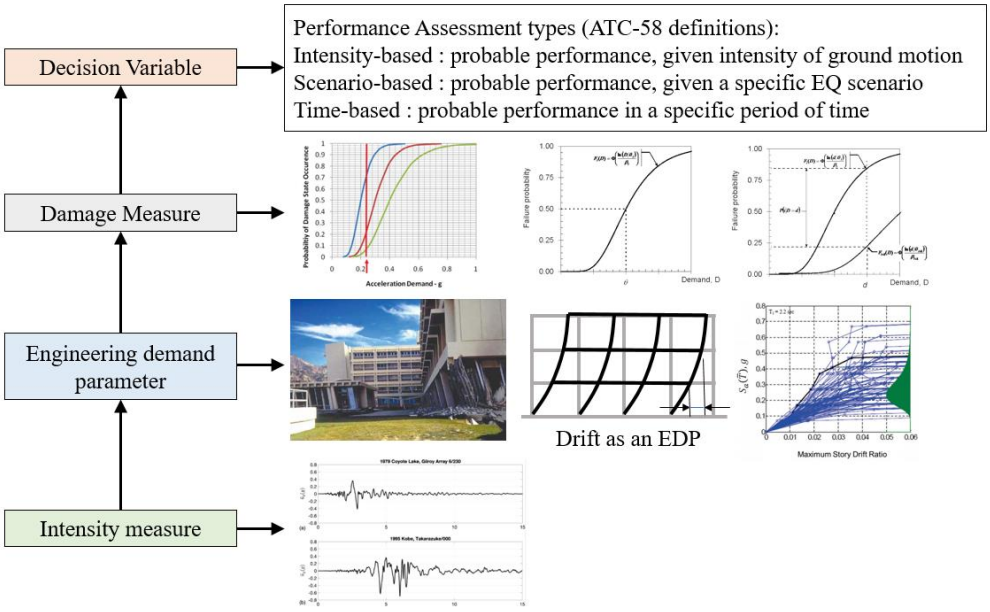

Fig. 1.7 Performance-based framework adapted from Krawinkler & Deierlein (2014)

ASCE 41-17 are focused on resilience performance, economic impact, and building downtime, and attempt to understand these together. According to a report by 2017 SEAOC COVENTION PROCEEDINGS (2017), ASCE 41-13 has been used to evaluate the seismic performance of existing buildings and retrofits. The report reveals that the major critical hazard level for Basic Performance of Existing Buildings (BPOE) corresponds to 2/3rds of maximum considered earthquake level, which is 20% exceedance probability in 50 years (Table 1.3).

Table 1.3 ASCE 41 Seismic hazard level (SEAU 5th Education Conference)

	New Building		Existing Building	
Category	BSE-2N	BSE-1N	BSE-2E	BSE-1E
Hazard level	ASCE7-10 MCE level	2/3rds of ASCE 7-10 MCE level	-	-
Exceedance probability	2% in 50 years	10% in 50 years	5% in 50 years	20% in 50 years
Return periods	2400-year	475-year	975-year	225-year

According to the ASCE 41-17 provisions, there has been a change in ground motion parameters, site factor, and non-linear response history analysis.

The ASCE 41-17 provisions provide performance guidelines under various seismic intensities for both new and existing buildings.

Specifically, ASCE 41-17 provisions deal not only with structural component performance, but also non-structural component performance. Fig. 1.8 suggests that structural performance levels can be divided into six ranges, and non-structural performance levels into five.

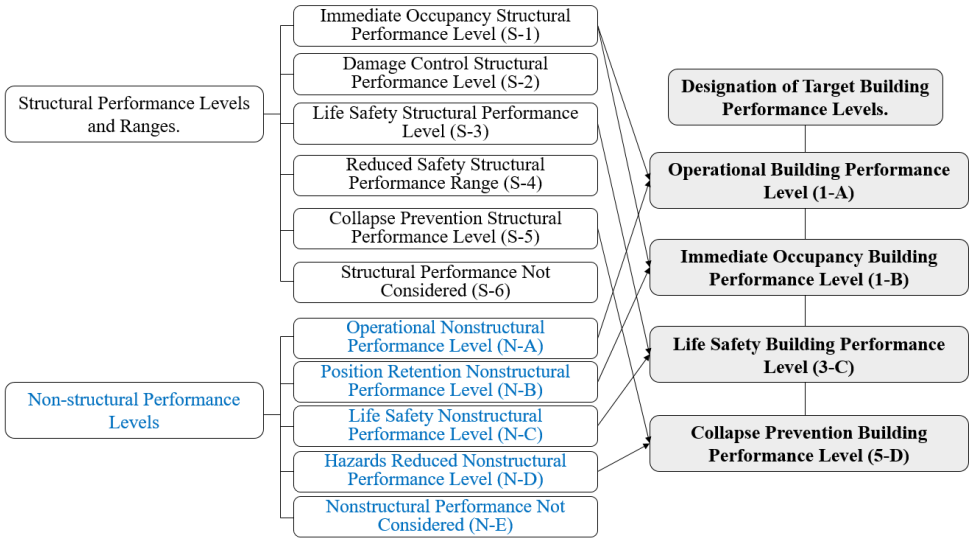

Fig. 1.8 ASCE 41-17 Performance level (ASCE 41-17)

Fig. 1.9 briefly illustrates the damage levels for structural and non-structural components.

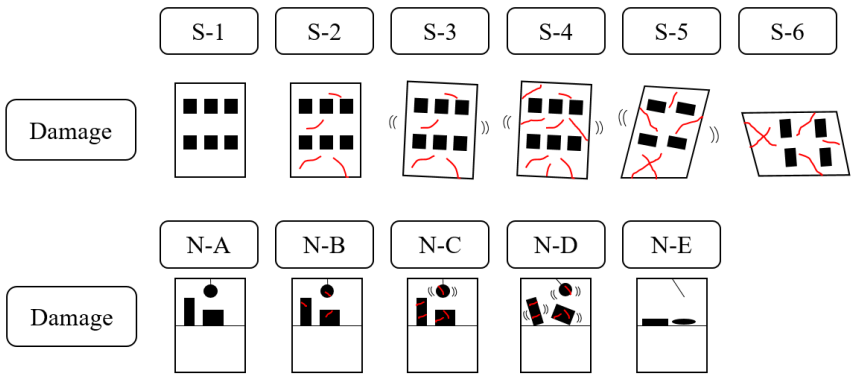

Fig. 1.9 ASCE 41-17 new damage level for structural & non-structural components

Risk categories are divided into I, II, III, IV stages according to damage status, where BSE-1E is the basic standard for existing buildings, and 1E corresponds with similar intensity to the DBE level ASCE7-10 suggests.

ASCE 41-17 classifies earthquake hazards according to Category I, II, III, and IV, as shown in Fig. 1.10, and classifies the performance targets according to the degree of damage to the structural members and non-structural components. As shown in the figure, the criteria for distinguishing between BSE-1E and BSE0-1N in ASCE 41-17 sets distinct target performance for existing facilities and new buildings. The difference is that the performance targets for Category I, II, and IV differ from those for non-structural components, with the goal of setting performance targets for new buildings one step higher.

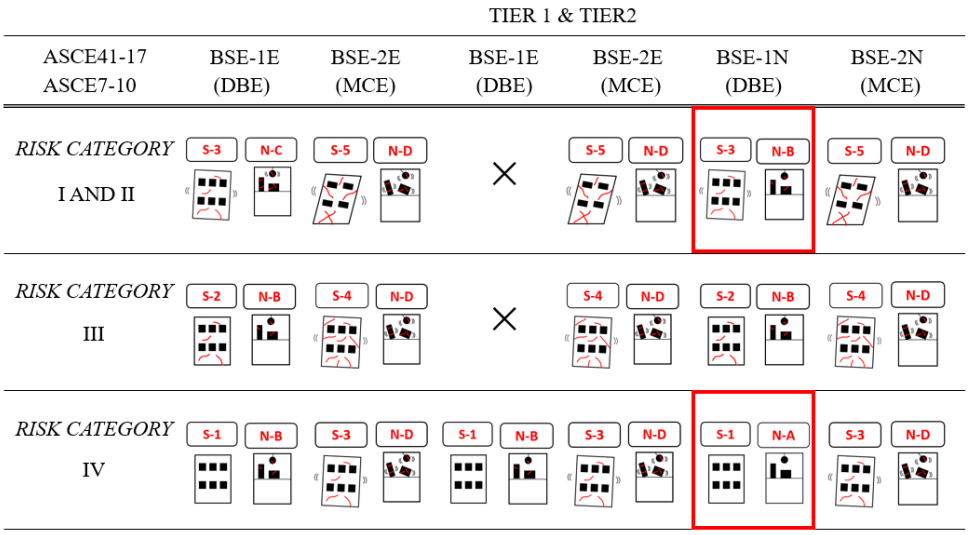

Fig. 1.10 Risk category & damage level

In Europe, performance-based design has developed on its own. Eurocode 8 introduced seismic design which adapted a limit-state design approach. However, there is a limitation in providing information regarding verification of ductility. Instead, ductility was realised by the strict rule in the code (Pinto & Franchin, 2004). EC8-3 standards introduce different performance levels that are similar to the international code (Fig. 1.11).

Hazard level	Performance level
T_R = 2,475 years (2 % in 50 years)	Near collapse (NC): heavily damaged, very low residual strength and stiffness, large permanent drifts but still standing
T_R = 475 years (10 % in 50 years)	Significant damage (SD): significantly damaged, some residual strength and stiffness, non-structural components damaged, uneconomic to repair
T_R = 225 years (20 % in 50 years)	Limited damage (LD): only lightly damaged, damage to non-structural components economically repairable

Fig. 1.11 Performance objective in Eurocode 8 from Pinto & Franchin (2004)

In Japan, after the Kobe earthquake, performance-based design was adopted. The recent trend in performance-based design is to diversify performance goals and develop a more practical performance-based design. Akiyama (1985) introduced a methodology focused on energy-based performance. He insisted that determining detailed damage distribution is crucial to earthquake engineering. According to Akiyama, energy equilibrium and energy-based seismic design can effectively and reliably enhance performance measurements. Fischinger (2014) agreed that the energy-based design method allows performance objectives to be achieved more efficiently.

Shi et al. (2016) introduced distinct seismic performance objectives in different countries according to seismic hazard standards set by the Eurocode, United States, Japan and China. These are compared in Fig. 1.12.

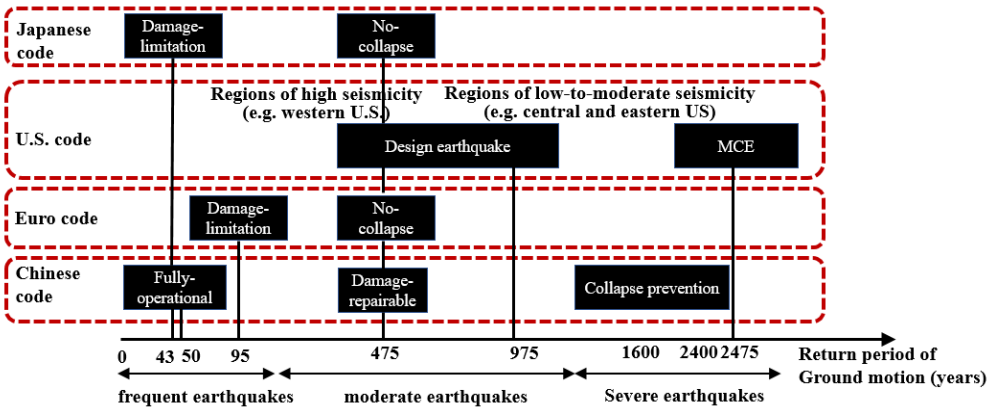

Fig. 1.12 Seismic hazard levels and performance requirements for different nations (adapted from Shi et al., 2016)

As can be seen in Fig. 1.12 above, Chinese code suggests three stages of performance requirements, whereas Japanese and Eurocode performance requirements are stricter - suggesting “no collapse” even for moderate earthquakes.

Performance-based design has developed and is now widely used all over the world, yet more research on the following limitations is necessary to solve the:

(1) unreliability of probabilistic seismic risk analysis,
(2) uncertainty of non-linear modelling and analysis results,
(3) the absence of a widely acceptable quantification of diversified performance.

1.5 Need for earthquake resilience

Aside from the earlier mentioned limitations, earthquake engineering must also concentrate on the economic effects to society. Many researches have focused on developing a robust structure against rare earthquakes to reduce damage to the structure and increase target performance. Resilience vulnerability of specific buildings against earthquakes can cause severe socio-economic damage. Of note is the movement of performance-based design interests from focusing on reducing casualties to mitigating building damage by suggesting additional damage-free structures such as self-centering, supplementary dampers and isolation systems (Cimellaro, 2016). Cimellaro (2016) suggested pre-prevention through state-of-the art technology such as self-centering against earthquake events can mitigate seismic losses and reduce the residual drift, which allows rapid recovery from earthquake damage. These systems are considered as a structural system at the preliminary stage of a project to reduce the risk of uncertain earthquake hazards (Krawinkler & Deierlein, 2014). Krawinkler and Deierlein also insisted that resilience-based design, the next generation of performance-based design, has developed in an area of new methodology to assess probabilistic seismic hazard analysis, advanced modelling, non-linear response analysis and measurement of damage to component members. Similarly, quantification of the performance level allows the development of performance-based earthquake design. Fig.1.13 represents the resilience concept - how the system recovers to its original status after being damaged in an earthquake. Krawinkler & Deierlein (2014) clarify that the main purpose of resilience-based design is the capacity to recover from the detrimental effects of an earthquake at the preliminary stage. Cimellaro (2016) acknowledges the concept of "resilience" as a management process that deals with hazardous events, since human beings cannot prevent natural incidents

such as typhoons and earthquakes, and it is also impossible to predict them. Therefore, the most significant aspect of resilience-based design is reducing the time taken to recover from unexpected consequences to the social and economic community. Many researches suggest that effective resilience performance will see a building recover to the equilibrium state as soon as possible after a natural disaster (Fig. 1.13).

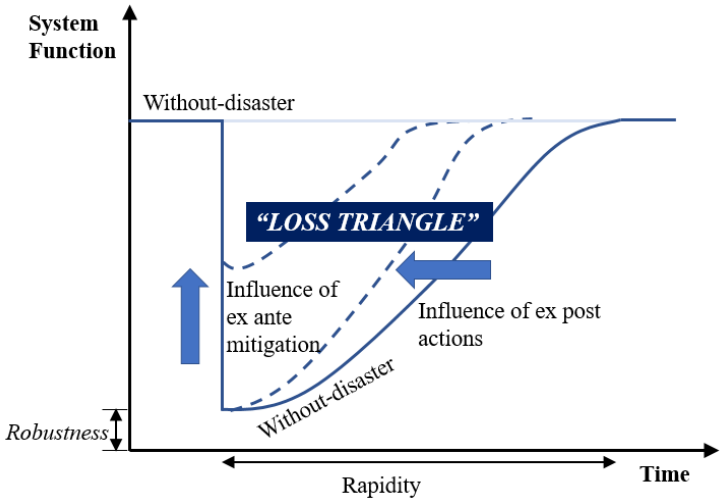

Fig. 1.13 Idealised concept of resilience (Krawinkler & Deierlein, 2014 adapted from NRC 2011)

In other words, resilience performance is a process that uses several different techniques (e.g. self-centering, isolation, damper systems) to reduce the damage from hazardous events and recover to the original status so as to achieve the intended performance objective (Fig. 1.14).

Disturbance		
(1)	Hazard	Any
	Hazard Level	Expected
	Affected Area	Community
	Disruption Level	Moderate

Restoration times		
(2)	30%	Restored
	60%	Restored
	90%	Restored
(3)	X	Current

Functional Category: Cluster	(4) Support Needed	(5) Target Goal	Overall Recovery Time for Hazard and Level Listed								
			Phase 1 -- Response			Phase 2 -- Workforce			Phase 3 -- Community		
			Days 0	Days 1	Days 1-3	Wks 1-4	Wks 4-8	Wks 8-12	Mos 4	Mos 4-36	Mos 36+
Critical Facilities		A									
Emergency Operation Centers			90%								
First Responder Facilities			90%								
Acute Care Hospitals			90%								
Emergency Housing		B									
Temporary Emergency Shelters				90%							
Single and Multi-family Housing				90%							
Housing/Neighborhoods		B									
Critical Retail				30%	60%	90%					
Churches and Spiritual Centers				30%	60%	90%					
Schools					30%	60%	90%				
Community Recovery		C									
Businesses						30%		60%		90%	

Fig. 1.14 Resilient evaluation matrix (adapted from NIST, 2015)

1.6 Research objectives and thesis outline

This thesis aims to contribute to the state-of-the-art in design of steel MRFs with visco-plastic dampers to reduce the detrimental effect caused by the use of velocity-dependent supplementary damper systems such as viscous and visco-elastic dampers. In the long run, this hybrid damper system will increase resilience performance against seismic hazards. The visco-plastic damper is realised by the in-series combination of a viscoelastic damper and a friction device. A prototype steel building is designed as a high ductility steel MRF. This MRF is then equipped with viscoelastic or visco-plastic dampers to achieve high seismic performance. Parametric designs are carried out by designing visco-plastic dampers with different activation forces for their friction devices. Non-linear dynamic analyses for a set of 20 earthquake ground motions scaled to the design and maximum considered earthquake intensities are carried out in OpenSees. The response results provide the basis to identify the appropriate range of values for the activation force of the friction device of the visco-plastic damper so that drift reduction and control of the peak base shear force can be simultaneously achieved. Also, peak residual drift that is directly related to the resilience performance of the building is compared between the frame with viscoelastic dampers and the frame with visco-plastic dampers under DBE and MCE level. To estimate the seismic vulnerability to collapse, IDA (Incremental Dynamic Analysis) was conducted for both MRF with viscoelastic and with visco-plastic dampers using a set of 20 seismic records and the collapse probability was evaluated using the fragility curve.

This dissertation is divided into six chapters, including this introduction and appendices.

Chapter 1 covers the limitations of current seismic design guidelines and structural systems, explains the fundamentals of performance-based seismic design, and highlights the need for earthquake resilience.

Chapter 2 looks at seismic advanced resilient systems, supplementary passive dampers and their use in seismic design and/or retrofit. The effectiveness of passive dampers is then investigated. Seismic design methods for buildings with viscous or viscoelastic dampers are also discussed.

Chapter 3 describes the visco-plastic damper (VPD), looks at the mechanical characteristics of the visco-plastic damper, its practical structural details, a simplified design procedure, and suggests an adequate level of friction resistance (defined through the λ factor explained in the same chapter).

Chapter 4 compares the seismic performance of 5, 10, and 20 storey buildings with viscoelastic and visco-plastic dampers. First, the results of pushover analysis are presented. Then, a scaling procedure for non-linear time history analysis utilising 20 far field seismic records is described. A comparison of the results of the MRFs, MRFs with viscous dampers, and MRFs with viscoelastic dampers in terms of peak drifts, residual drifts, as well as peak base shear is then provided. Finally, optimum λ factors based on seismic performance under the design and maximum considered earthquake intensities are suggested.

Chapter 5 evaluates the collapse resistance of a building with visco-plastic dampers on the basis of IDA and a FEMA P-58 fragility curve. Then, the effect of λ factor on collapse fragility is quantified.

Chapter 6 summarises the previous chapters, presents conclusions.

Chapter 2

Literature Review

2.1 Introduction

In this chapter, seismic advanced resilient systems and passive damper usage for seismic retrofits will be investigated and the passive damper types and their seismic effectiveness will be introduced. Then, a simplified seismic design procedure for passive damper systems will be briefly explored.

2.2 Seismic advanced resilient performance systems

Resilient performance can be advanced through systems such as self-centering, pre-tensioned wire. Many studies related with increasing seismic resilient performance have been conducted in recent years. The Doc-bone concept , an effective methodology to control easily replaceable plastic mechanisms to increase resilient performance of the structures, was first introduced by Balut and Gioncu (2003). Under strong earthquakes, beam plastic hinge occurred at the end of the beam. If this local plastic hinge can be replaceable, it shows more easily replaceable that means progressive resilient performance. Baiguera (2016) developed dual seismic resistant steel frame with high post-yielding energy-dissipative braces using the concept of Doc-bone. Recently, advanced resilient system can be widely used not only with steel frames but it also with timber structure. Hashemi et al.(2017) introduced rocking coupled walls with innovative Resilient Slip Friction (RSF) joints that is of steel-timber wall system showing effectiveness in reducing showing self-centering behavior. Feng et al. (2018) proposed a hinged wall with buckling-restrained braces (BRBs) Fig. 2.1 shows different examples of innovative resilient performance systems (Balut and Gioncu, 2003; Baiguera et al., 2016; Kamperidis et al., 2018)

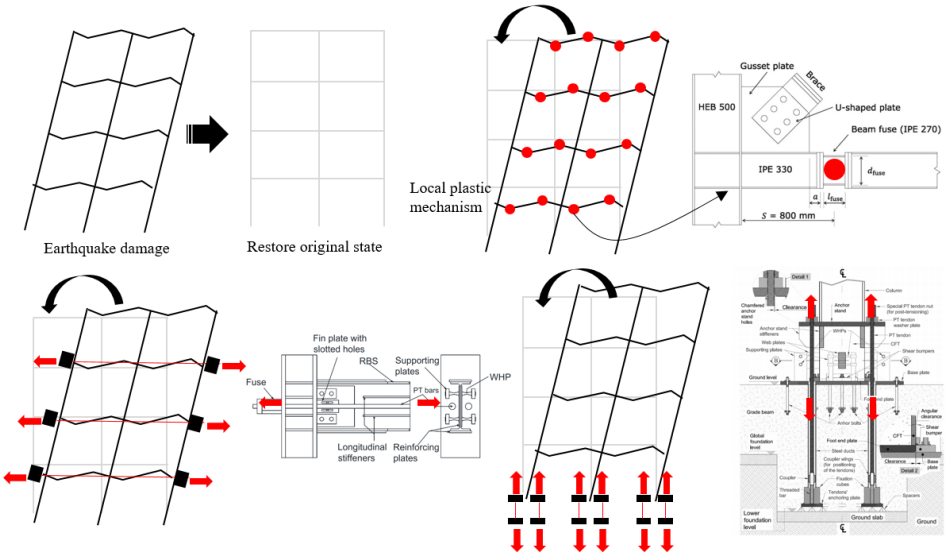

Fig. 2. 1 Resilient advanced system adopted from Balut and Gioncu (2003); Baiguera et al. (2016); Kamperidis et al. (2018)

2.3 Seismic retrofit and passive damper systems

2.3.1 Seismic retrofit strategy

Before the introduction of the seismic design, many buildings were built without considering earthquake vulnerability, hence it is now necessary for them to be re-evaluated and undergo a reinforced seismic retrofit. Some buildings do not abide by current standards and fail to achieve the intended performance level because they have lost their original seismic capability. According to Wasti et al. (2006), there are many strategic approaches to implementing seismic retrofit. Fig. 2.2 introduces three techniques to increase seismic resilience that are commonly used in practice. The first is to strengthen the structural elements so that they can withstand an earthquake, as can be seen Fig.2.3. This involves increasing the stiffness to have shear resistant force itself, which is the traditional method of retrofit. The second is to use a seismic control device passive damper to increase the seismic capacity. Finally, seismic isolation is used to prolong the building's fundamental periods. This makes it possible to reduce the influence of the

overall seismic load as a result of avoiding the effect of the strong earthquake load of the short period of the seismic wave (Fig.2.3).

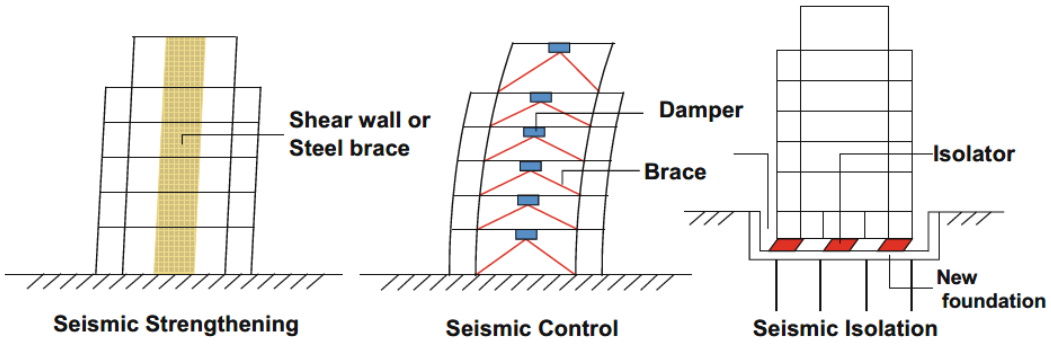

Fig. 2.2 Seismic rehabilitation types, adapted from Wasti et al. (2006)

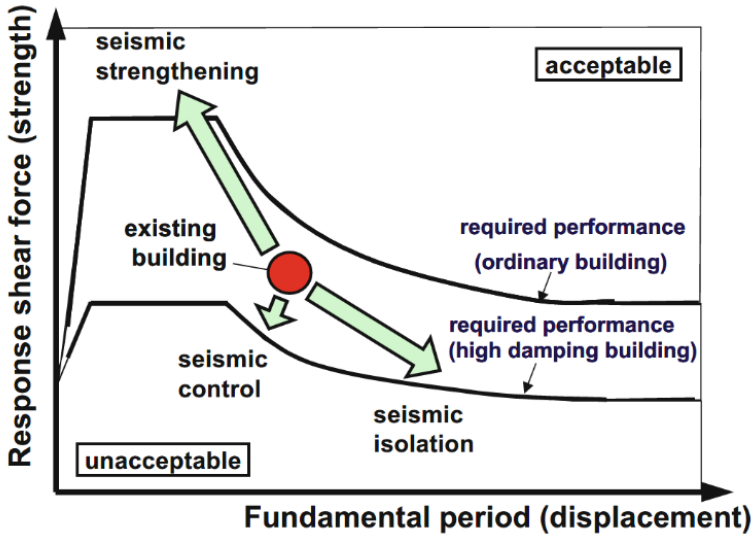

Fig. 2.3 Seismic rehabilitation method, adapted from Wasti et al. (2006)

2.3.2 The effectiveness of passive dampers

One of the most effective uses of the passive damper is that it mimics reducing spectral acceleration by adding supplementary damping to the structure. There are other positive influences of using damper systems, such as reducing displacement and drift and reducing velocity and acceleration, which is crucial for non-structural components (Seo et al., 2014). For instance,

Christopoulos and Montgomery (2013) studied viscous dampers to determine whether they can increase the seismic performance of tall buildings against wind and seismic loads. The results of the study have shown that modular viscoelastic coupling dampers (VCDs) can play a major role in sustaining a large shear deformation and even reducing torsional velocity, as well as lateral accelerations. The most obvious finding to emerge from their study is that viscous dampers help increase the stability of buildings, retrofits, and efficiency without changing original dynamic periods. The metallic damper is also commonly used because of its cost-effectiveness and ease of replacement (Lee et al., 2014). According to Chen (2001), the metallic damper is also used to reduce acceleration. Chen (2001) has shown that a low level of energy can also be dissipated by the metallic damper. The second major finding of the study is that the action of the metallic damper is similar to that of an isolation device, which ensures that damage is localised within the damper so that the main structure remains undamaged. The effectiveness of the passive damper is verified by many researches (Tse et al., 2012; Marshall et al., 2010; Lee et al., 2016; Silwal et al., 2016; Kim et al., 2017). Regarding the increased cost of application of the passive damper, Tse (2012) stated that an approximate additional 2% to total building construction costs would be expected in the use of a passive damper system. He also insisted that the maintenance cost is below 0.2% of the total budget, and that these costs depend on the conditions in which the passive damper is applied, the damper types, and the different target performances. However, the additional costs of passive damper application can be offset by the reduced weight of structural components as a result of the damper system, as stated by Symans et al. (2008).

2.3.3 Types of passive damper

The categories of passive damper are varied and can be divided into several criteria, as already explained in many studies. Tanaka et al. (2004) have identified two main types of viscous damper: the shearing resistance type, and the fluid resistance type. The shearing resistance type is related to temperature variation and, therefore, a sustained standard temperature is required for accurate evaluation. Kasai et al. (1998) also identify the damper system by the type of installment and the process of function (Fig. 2.6). According to experts, including Kibayashi et al. (2004), such a damper system can be divided into four types: brace, wall, shear link, and stud. On the other hand, Connor et al. (2014), and Heysami (2015) distinguish the different passive control systems by their functions: viscous damper, oil damper, visco-elastic damper, friction damper, and steel damper, based on criteria supported by several authors (Cherry and Filiatrault, 1993; Siahpolo, 2013). According to Hussain et al. (1998), the viscous damper is similar to the automobile shock-absorber, as the silicon acts as a damping fluid (Fig. 2.6). Its damping effect comes from the behaviour of the piston and depends on the velocity force induced. Hussain also (1998) notes that the relationship between the damping force and relative velocity is expressed as F=CV. Recently, hybrid damper systems have been introduced to compensate for the weaknesses of each damper type. One example is the SAFE damper that consists of a combination of a friction damper and a metallic damper (Chang-Hwan et al., 2015). Similarly, Christopoulos (2013) announced the viscoelastic coupling damper as a hybrid system (Fig. 2.4).

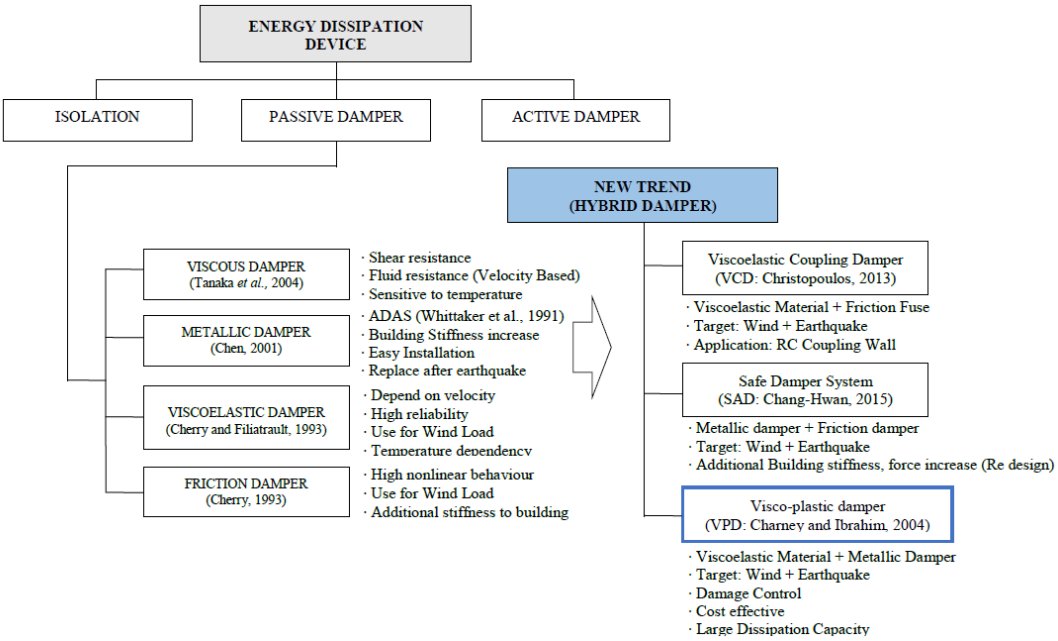

Fig. 2.4 Summary of energy dissipation device & new trend

Passive dampers can also be classified according to application type, as stated in Fig. 2.5 (Guo et al., 2015).

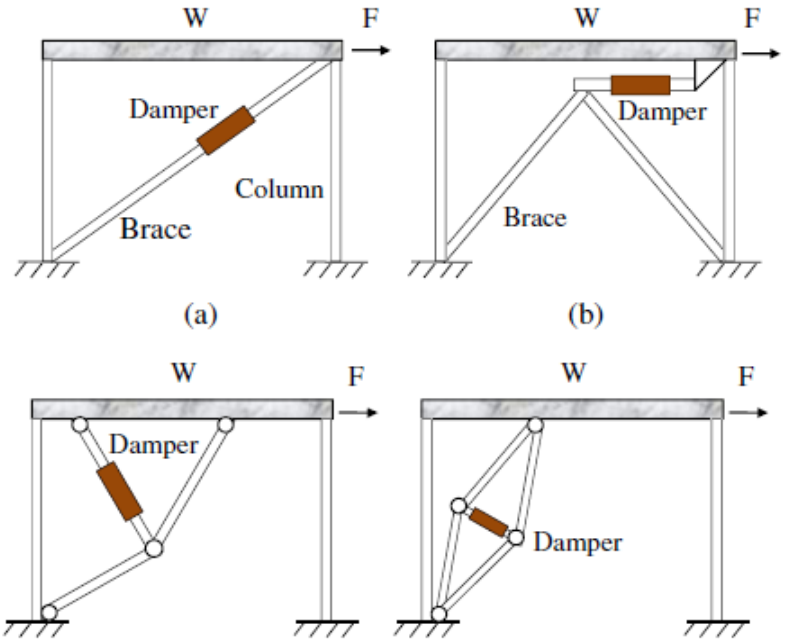

Fig. 2.5 Damper application type, adapted from Guo et al. (2015) (a) Diagonal (b) Chevron (c) Toggle (d) Scissor

Damper Type	Hysteresis	Figure	Brace type	Wall type	Shear Link type	Stud type
Viscous damper ([1]Velocity based)	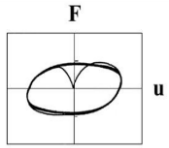	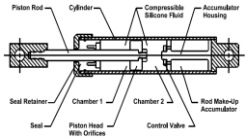				
Viscoelastic damper ([2]Deformation based)	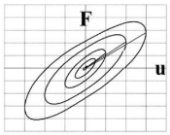	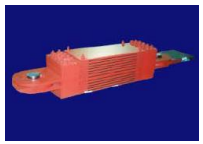				
Steel damper (Deformation-based)	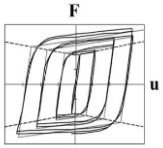					

Fig. 2. 6 Different damper types adapted from Kibayashi et al. (2004); Charney (2004); Hussain (1998)

1 Energy dissipated by the density of velocity, temperature sensitive
2 Device designed to use relative displacement of both dissipate dampers (elastic-plastic behaviour)

2.4 Viscous damper

Various dampers have been widely used on the site, and the efficacy of the viscous damper has been assessed for its superior capability in dissipating energy when used in new builds and retrofits (Karavasilis, 2016; Seo et al., 2014; Miyamoto and Gilani, 2013). According to Symans et al. (2008), viscous damper force is dependent on the velocity stated in Eq. (1). Fig. 2.7 shows the fluid viscous damper that is commonly used on the site. Its configuration is shown in Fig. 2.8.

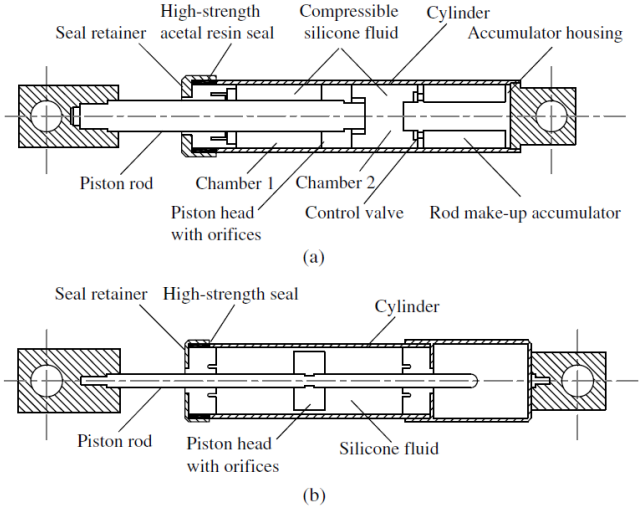

Fig. 2.7 Configuration of fluid viscous damper, adapted from Guo et al. (2014)

$$f = c\left|\dot{u}\right|^{\alpha}\operatorname{sgn}(\dot{u}) \qquad (2\text{-}1)$$

Where, c=damping coefficient; α =constant exponent; $\dot{u}$=relative velocity; sgn= symbolic function adapted from Guo et al. (2014)

Fig. 2.8 Seismic fluid viscous damper adapted from Taylor devices inc. homepage

In 2015, Guo et al. (2014) introduced a design procedure for the seismic upgrade of existing buildings using a fluid viscous damper. In his research, the fluid viscous damper is cost-effective and rapidly implementable. Guo pointed out several limitations in the course of application, dependent on the site situation, damper layout as a result of building design, construction budget, and target performance. Similarly, Hamidia et al. (2014) provided an updated design equation regarding prediction of a more accurate viscous damping ratio. This equation is more conservative when used for non-linear viscous dampers than the existing FEMA273 formula.

Several studies have used a numerical method to examine the seismic efficiency of the viscous damper. Researchers (Karavasilis, 2016; Kariniotakis & Karavasilis, 2018) have verified the seismic resistance by comparing the IDA (Incremental Dynamic Analysis) results of steel MRF and steel MRF fitted with viscous dampers following Eurocode 8. The results reveal that steel MRFs with viscous dampers show more plastic hinges for the columns than steel MRFs without. This can be solved by following the capacity design rule. Seo et al. (2014) also provided a simplified design procedure for the MRF with viscous dampers. Although there are several advantages to using a supplementary damper in terms of reducing absolute acceleration, velocity and storey drift, Seo pointed out that base shear can be significantly increased according to the additional damping ratio because of the large force induced by using a viscous damper. According to Dimopoulos et al. (2016), different seismic resistance systems such as SC-MRFs and viscous damper frames were evaluated to compare the effectiveness of the systems in terms of economical loss under DBE (Design Based Earthquake) and MCE (Maximum Considered Earthquake) level, and verify the seismic performance of the viscous damper at all seismic intensities. He also highlighted the mitigation of residual drifts when using a viscous damper.

2.5 Viscoelastic damper

The viscoelastic damper was first applied to tall building structures (Fig. 2.9) because of its superior performance in reducing displacement and acceleration. In Tsai et al. (1993), the seismic and wind resistance of a frame with viscoelastic dampers was verified through a simulation model and a FEM analytical model to consider the effect of temperature. Similarly, Shen et al. (1995) found that the energy dissipation capability of a viscoelastic damper is superior in mitigating the vibration caused by wind loading. Several authors have focused on questions concerning viscoelastic dampers and wind load (Mahmoodi & Keel, 1989). Mahmoodi & Keel highlight the crucial role of the viscoelastic damper in reducing excessive acceleration regarding serviceability aspects.

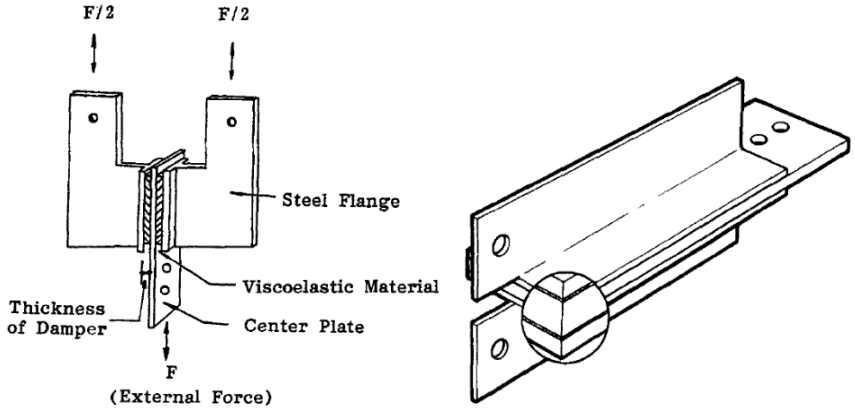

Fig. 2.9 Typical viscoelastic damper figure, adapted from Tsai et al. (1993), and a typical damper used in the World Trade Center from Samali et al. (1995)

Fu and Kasai (1998) clarified the differences between viscous and viscoelastic dampers through a parameter study. In their research, the significant difference between the two systems was that the viscous damper mainly provides damping under low frequencies, whereas the viscoelastic damper provides damping as well as damper stiffness, and added stiffness is dependent upon both damper stiffness and interaction force with other structural members (Fig. 2.10).

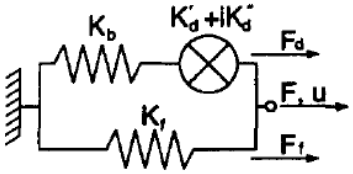

(a) Viscoelastic damper basic model

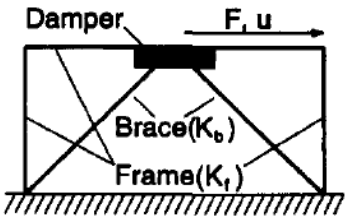

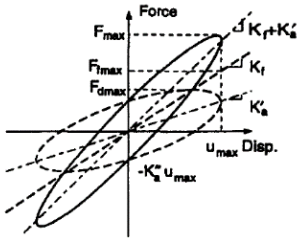

(b) Frame (c) Hysteresis loop of a viscoelastic damper

Fig. 2.10 Frame and hysteresis loop of viscous and viscoelastic damper, adapted from Fu and Kasai (1998)

Therefore, the viscoelastic damper is superior to the viscous damper under the condition of impulse excitation, since stiffness plays a key role in reducing peak displacement. Regarding energy dissipation, it was found that a viscous damper performs slightly better than a viscoelastic damper. The most significant finding of this research is the recommendation to use a stiffness ratio of brace stiffness to frame stiffness equal to 10 in both viscous and viscoelastic dampers. Aside from this, numerous researches verify the performance of viscoelastic dampers against seismic and wind loads, experimentally and through analytical methodology (Aiken, 1990; Lin et al., 1991; Zhang and Soong 1992; Lobo et al., 1993; Chang et al., 1993; Samali & Kwok, 1995). According to Samali & Kwok (1995), the properties of viscoelastic dampers were designed in consideration of the effect on seismic performance. Mahmoodi and Keel (1990) highlighted the disadvantage of increased acceleration and its negative consequences on building residents due to the high amplitudes of wind loading in a tall building. Therefore, increasing the stiffness or damping effect using a viscoelastic damper to prevent excess acceleration was suggested. To better understand the mechanisms of shear stress and shear strain behaviour, Karavasilis et al. (2011) analysed the viscoelastic damper using a GM model (Fig. 2.11).

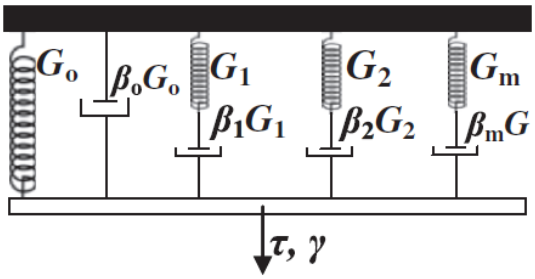

Fig. 2.11 GM visco-elastic damper model adapted from Karavasilis et al. (2011)

In the paper, the viscoelastic damper is selected by the equation Ad = (k_d × t_d) / G(w_1, temp), where A_d is the area of the visco-elastic damper and t_d is its thickness, and G(w_1, temp) represents the storage shear modulus.

As can be seen in Fig. 2.12, the properties of shear storage modulus G´, shear loss modulus G´´, loss factor are crucial for the viscoelastic damper, where G´ reflects the property of elastic behaviour, and G´´ represents the characteristic of the viscous damping effect.

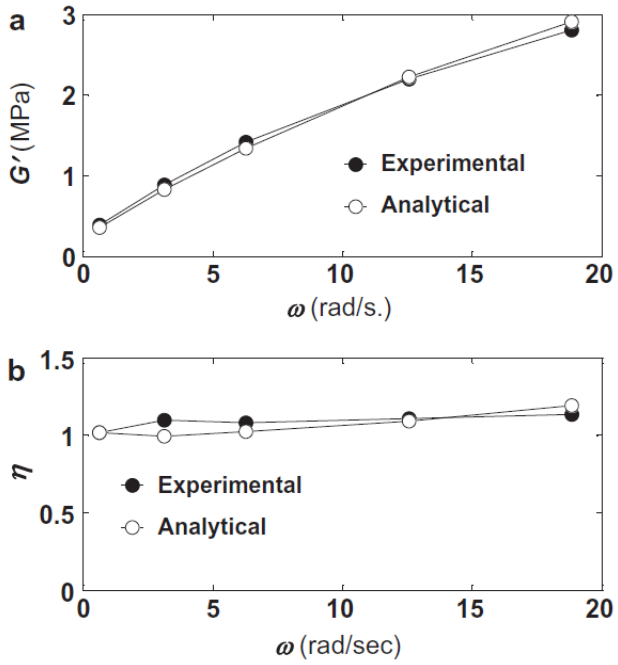

Fig. 2.12 Comparison of experimental and analytical values of the mechanical properties of the viscoelastic material at 24°C G´ and η, adapted from Karavasilis et al. (2011)

In the same way, Karavasilis et al. (2012) introduced an elastomer structural damper that is realised by pre-compressing a high-damping elastomeric material into steel tubes. In the paper, hysteretic behaviour and its performance have been assessed. The basic elastomeric damper model uses a modified Bouc-Wen model and a non-linear dashpot in parallel and is tested against sinusoidal loadings at various frequencies and vibrations. A simplified design method was also introduced. According to the results, the damper is not only superior in terms of reducing the weight of the steel required, but also in diminishing storey drifts as well as plastic hinge rotations. The visco-elastic damper is widely applied to skyscrapers in the USA and Japan due to its effectiveness in reducing induced earthquake and wind loading. Fig. 2.13 shows viscoelastic damper efficiency in reducing acceleration.

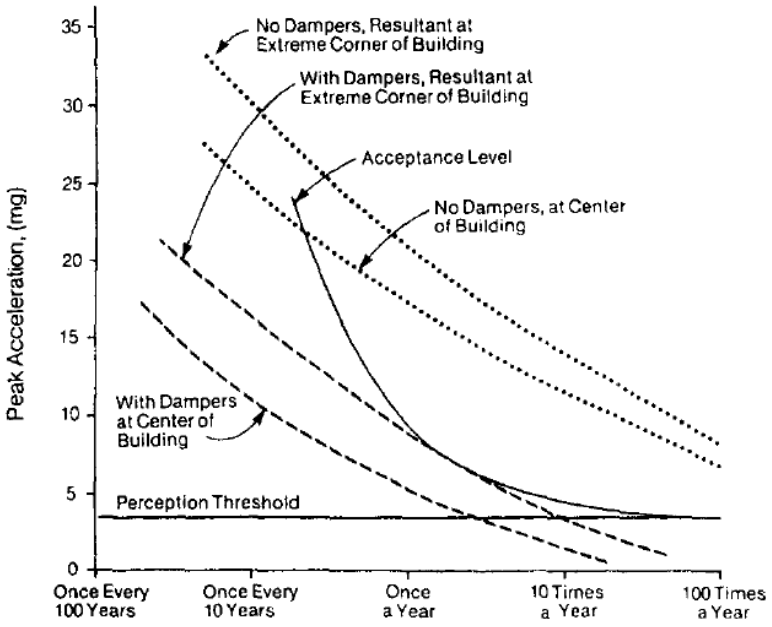

Fig. 2.13 Efficiency of the viscoelastic damper in reducing acceleration, adapted from Samali et al. (1995)

2.6 Steel damper

Regarding the steel damper, several types can be utilised on the site (Fig. 2.14), even in regions of low-to-moderate size seismic hazards, since steel dampers easily yield and dissipate seismic energy at low earthquake intensities (Kim et al., 2016).

	Slit damper	Honeycomb damper	ADAS	TADAS	Proposed damper in this study	BRB
Configuration	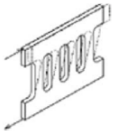	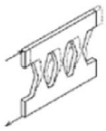	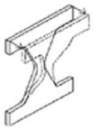			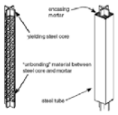
Boundary condition	Fixed-fixed	Fixed-fixed	Fixed-fixed	Fixed-free (Cantilever type)	Fixed-free (Cantilever type)	-
Deformation mechanism of steel plate	In-plane deformation	In-plane deformation	Out-of-plane deformation	Out-of-plane deformation	In-plane deformation	Axial deformation
Characteristics	• High elastic stiffness	• High elastic stiffness • Decrease of stress concentration	• Decrease of stress concentration • Large deformation capacity	• Decrease of stress concentration • Large deformation capacity	• High elastic stiffness • Decrease of stress concentration • Minimization of loss of steel material	• High elastic stiffness • Large deformation capacity • Prevention of local buckling of core member

Fig. 2.14 Different types of steel damper, adapted from Kim et al. (2016)

Khazaei (2013) conducted a non-linear dynamic analysis to verify the effectiveness of the ADAS damper. It was found that shear force can be reduced when a frame incorporates an ADAS damper. Regarding the design of the ADAS damper, Landi & Merenda (2014) suggest a simplified design procedure for structures using this system. The researchers performed a non-linear time history analysis on different masonry buildings.

Several different types of steel damper have been proposed. Oh et al. (2009) introduced a new system where a slip damper is used in the beam to column connection, and has the characteristics of being easily replaceable and showing advanced seismic performance under rare strong earthquakes. Kim et al. (2016) proposed a cantilever type steel damper that is superior in terms of energy dissipation capability and has been verified to restore stability throughout an experimental method. Lee & Kim (2017) introduced a box type slit steel damper using four steel slit plates for the seismic retrofit. Through non-linear time history analysis, this showed that energy can be dissipated in the damper with the other structural members maintaining their elastic status.

2.7 Friction damper

Filiatrault & Cherry (1990) introduced a simplified design process related to the MRF with friction damper system and suggested an optimised methodology in the slip-load distribution relation. Fu & Cherry (2000) stated that a friction damper's seismic capacity can vary depending on the slip-force of the friction damper, frame yielding and damper stiffness, and suggested adequate parameter ranges to be a brace stiffness ratio of 4 to 10, a slip-force factor of 4 to 8, and a frame ductility of 1 to 1.5. They also introduced a quasi-static design procedure for the frame with friction damper that can be applied to other displacement dependent damper systems. Ng & Xu (2006) also conducted shaking table tests to verify the seismic performance of the friction damper. The results showed advanced seismic resistance when the frame is fitted with a passive friction damper by displaying its effectiveness in reducing maximum acceleration. New types of friction damper are also being introduced. Filiatrault (2000) invented a friction-based ring spring damper showing a self-centering friction mechanism. This showed identical damper behaviour regardless of the frequency considered in this study and verified via shaking table test the advanced capability of the damper in terms of reducing acceleration and lateral displacement.

Khoo et al. (2015) proposed a new type of connection friction damper (Fig. 2.15), and pointed out that moment-shear-axial force can cause the reduction of shear resistance for friction connections. Therefore, as a way of solving this problem, Asymmetric Friction Connection (AFC) was introduced. This is a slotted/bolted connection type, and its performance was verified through experiment.

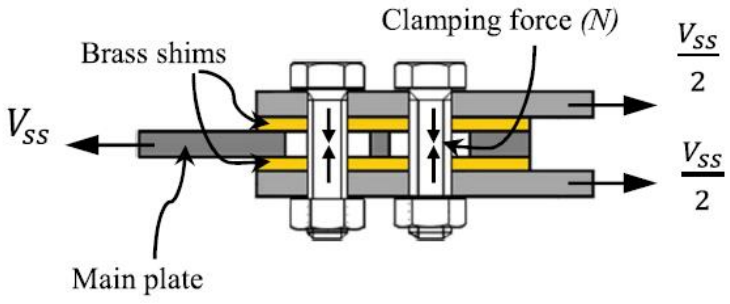

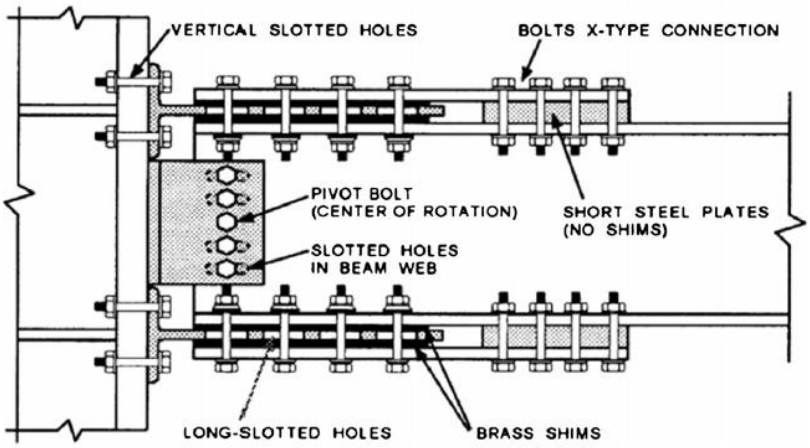

Fig. 2.15 Friction connection, adapted from Khoo et al. (2015)

Friction dampers can also be used in the retrofit of an existing building. For instance, Moon et al. (2017) proposed a friction damper design procedure for the retrofit of low and medium height regular RC buildings. In the research of Nikoukalam et al. (2015), Shear Slotted Bolted Connection (SSBC) was introduced for improving the frame with minimal change to the existing structure, which can be easy applicable in practice. This used a shear fuse and aimed to reduce shear plastic deformation. Cavallaro et al. (2018) shows in experimental results that friction torque procedures accurately match target preload. An interesting finding of his research was that time dependent tighten loss is mainly determined by the first tightening.

2.8 Hybrid damper

Several new types of hybrid damper have been introduced to make full use of the capabilities of each component damper whilst offsetting their disadvantages. For example, such a damper will mitigate the unintentional force created by a velocity dependent damper because velocity dampers produce forces that increase with inter-storey velocity, which may induce high axial force in structural columns. Hybrid damper systems are capable of imposing a limit on the peak force that they exert onto the structural members they are attached to. This kind of hybrid device consisting of an elastomeric

damper in-series connected to a buckling restrained steel brace has been proposed by Ibrahim et al. (2007). In the latter work, yielding of the buckling-restrained brace imposes a limit on the peak force of the hybrid device during earthquake loading. Furthermore, oil dampers or viscous fluid dampers with a relief valve that limits their peak force are available (SANWA TEKKI, 2017). It should be pointed out that activation of the peak force control mechanism in the previously mentioned hybrid devices results in loss of velocity-dependent supplemental viscous damping and, therefore, compromises the capability of the devices to reduce drifts. Because of the value of hybrid dampers, recent research has studied the counterbalance between the benefits and drawbacks of each component passive damper. Silwal et al. (2016) introduced super-elastic viscous dampers (SVD) combining a viscoelastic device and shape memory alloy cables in parallel and verified the effectiveness of hybrid dampers in reducing residual drift and increasing resilience against collapse due to seismic intensity. Similarly, Marshall et al. (2010), and Rawlinson et al. (2014) introduced a new hybrid damper which combines high-damping rubber dampers in series with a buckling-restrained brace (BRB). In this research, the performance of the hybrid damper is verified through experimentation and FEM analysis. The results show a high ability to dissipate seismic energy under all levels of seismic ground intensity. Rawlinson et al. (2014) emphasised the role of different types of passive control combinations in increasing resilience capability throughout the non-linear dynamic analysis of a single-degree-of-freedom (SDOF) system. Lee et al. (2017) introduced a hybrid energy dissipation device which combines a steel-slit damper and rotational friction dampers in parallel. Based on the findings of the paper, the hybrid damper can be effectively applied in seismic retrofits to reduce the probability of collapse. Several other studies have assessed the benefits of hybrid dampers in reducing seismic hazard and probability of collapse (Lee et al., 2016; Kim et al., 2017).

2.9 Visco-plastic damper

2.9.1 Introduction of the visco-plastic damper

Charney and Ibrahim (2004) were the first to introduce the concept of the visco-plastic damper composed of steel and viscoelastic substances. The device is shaped by two steel plates fixed to both sides with viscoelastic materials inserted between them (Fig. 2.16, top). As noted by Charney and Ibrahim (2004), the behaviour procedures of this device can be summarised in three steps. First, at the normal stage, this device acts against the wind, diminishes the vibration from small and moderate earthquakes, and shows the viscoelastic hysteretic loop. If a strong earthquake is induced in a building and, in case the steel damper is yielding, the damper system will show the steel damper action where the earthquake energy can be dissipated with hysteretic plastic deformation (The expected hysteresis curve of the visco-plastic damper is illustrated in Fig. 2.16, bottom).

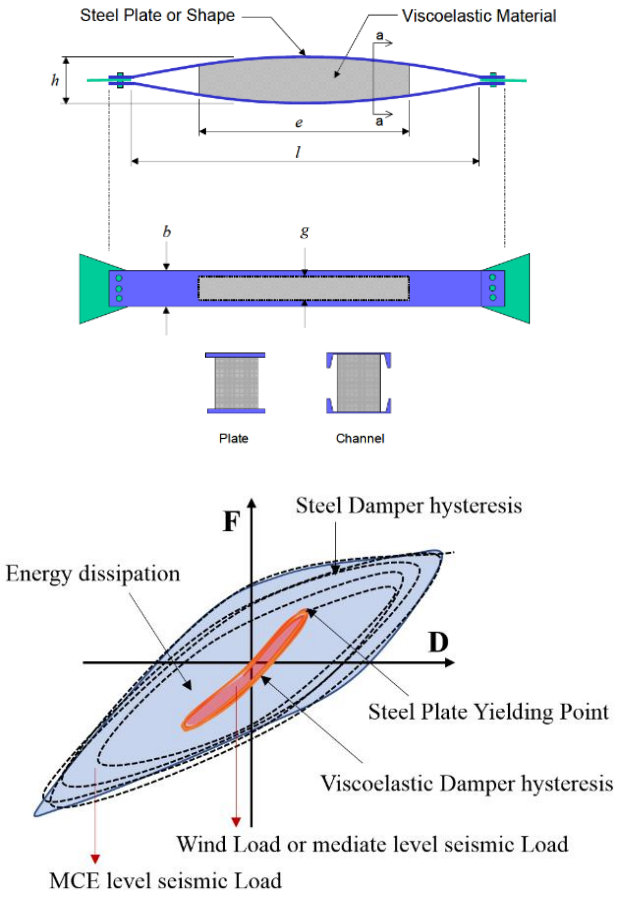

Fig. 2.16 Visco-plastic device detail by Ibrahim (2007) and hysteresis curve

2.9.2 Characteristics of visco-plastic dampers

A study by Sheikholeslami and Behnamfar (2012) examines the advantages of visco-plastic devices by performing a cyclic loading test. They found that a visco-plastic damper has a quick restore capability. According to Charney and Ibrahim (2004), the capacity of a visco-plastic damper can be easily controlled because the damper has many parameters (Ibrahim et al., 2007). This study highlights the importance of the design detail, such as the connection between steel and viscoelastic material, the bending adequacy, and a further bending effectiveness test. Also, Bardar et al. (2015) state that there is an almost thirty percent reduction in displacement when a visco-plastic damper is used in a nine-storey steel frame. Similarly, Siahpolo et al. (2013) state that the visco-plastic damper significantly reduces the roof displacements both near to and far from the epicentre. Considering the evidence mentioned above, the characteristics of a visco-plastic device can be summarised as follows:

1) Damage Control: easy optimisation using design parameters.
2) Easy installation: easy installation in any type of structure (buildings, bridges, etc.).
3) Large Dissipation Capacity: visco-elastic material behaviour produces large strain deformation for small deformation, thus leading to an increase in energy dissipation capacity.
4) Wind or Earthquake: regardless of the degree of vibration, it increases the resilience of buildings via the hybrid interaction of steel and visco-elastic device.
5) Cost Effective: the fabrication process is straightforward because of the simplicity of the device.

2.10 Seismic design methods for building with passive dampers

2.10.1 MRF with viscous dampers

This procedure is followed by the methods proposed by Seo et al. (2014). In this thesis, (Step 1-1) damping target ratio is established as total damping and inherent damping is assumed. Therefore, equivalent damping is calculated by subtracting inherent damping from total damping ($\zeta_{total} = \zeta_{equivalent} + \zeta_{inherent}$) (Step 1-2). Reverse triangular force is applied to the un-damped frame to estimate each storey's lateral stiffness. The storey stiffness is then calculated by the equation: $K = \frac{\sum v}{\Delta u}$ (2-1) α value (the ratio of brace stiffness to the total storey MRF lateral stiffness) is used equal to 10 following the two criteria of Lin and Chopra (2003). The α value equal to 10 was recommended by Kasai et al. (1998). (Step 1-3) According to the equation below (2-2), the combination of damping coefficient value is varied to satisfy the same equivalent damping. However, it is recommended that it should be proportional to the stiffness of the total frame, as Ci=εKo (Christopoulos and Filiatrault, 2006). If the equivalent damping is used proportionally to the stiffness of the frame, it can prove more economical, thereby leading to savings in practical terms by matching the damping to the force requirement.

$$\zeta_{eq} = \frac{T_1}{4\pi} \times \frac{\sum_i C_i(\phi_i - \phi_{i-1})^2}{\sum_i m_i \times \phi_i^2} \quad (2\text{-}2)$$

Where mi and φi are the mass and mode shape displacement at Floor i. This supplemental damping is added to the inherent damping ratio of the steel MRF (i.e. 3%) to calculate the total damping ratio ζtot. This damping ratio is used to calculate the damping reduction factor (Whittaker et al., 2003), which can be then used to reduce the elastic design spectrum of Eurocode 8 (Fig. 2.17, left).

2.10.2 MRF with viscoelastic dampers

The design is performed following the procedure presented by Seo et al. (2014), which involves the following steps:

(Step 2-1): Define the performance objectives. i.e. significantly lower than the drifts of the high ductility steel MRF.

(Step 2-2): Define the β factor, which is equal to Ki/Ko,i, where Ki is the viscoelastic damper stiffness and Ko,i is the horizontal stiffness of Storey i. The Ko,i of each storey of the steel MRF is calculated as the ratio of the inter-storey displacement over the total shear force of the storey on the basis of a simple static analysis for an inverted triangular height-wise distribution of lateral forces.

(Step 2-3): The fundamental period of vibration of the steel MRF with dampers is obtained on the basis of modal analysis. In this analysis, the dampers are represented by springs with a stiffness equal to K_i. The dampers are assumed to be supported by stiff braces.

(Step 2-4): The required area of viscoelastic material is calculated as $A_i=(k_i \times t_i)/G'$, where ti is the thickness of the viscoelastic material and G′ is the storage shear modulus, dependent on frequency and temperature. If the calculated areas Ai are too large for practical application, the designer should revert to Step 2-2 and select a smaller β factor value.

(Step 2-5): In this step, the loss shear modulus of the viscoelastic material is calculated as $G'' = G' \times \eta$ (2-3), where η is the loss factor. Then the damping coefficient of the viscoelastic damper can be calculated as $Ci = G'' \times A_i/(\omega_1 \times t_i)$ (2-4), where $\omega_1=2\pi/T_1$. (2-5)

(Step 2-6): The supplemental equivalent damping ratio provided by the viscoelastic dampers is calculated by the paper (Whittaker et al., 2003). This procedure follows the same course of calculating the equivalent damping of the viscous damper (Fig. 2.17, right).

2.11 Summary

In this chapter, supplementary passive dampers and their use in seismic design and/or retrofit are reviewed together with a recent seismic rehabilitation technique. Then, the effectiveness of passive dampers is discussed in terms of structural, non-structural and cost aspects. Different types of damper systems are introduced, such as viscous, viscoelastic, steel, friction, and the new hybrid damper system that is popular in passive supplementary dampers.

In the final section, seismic design methods for buildings with passive dampers are discussed, focusing on a simplified methodology for MRFs with viscous or viscoelastic dampers..

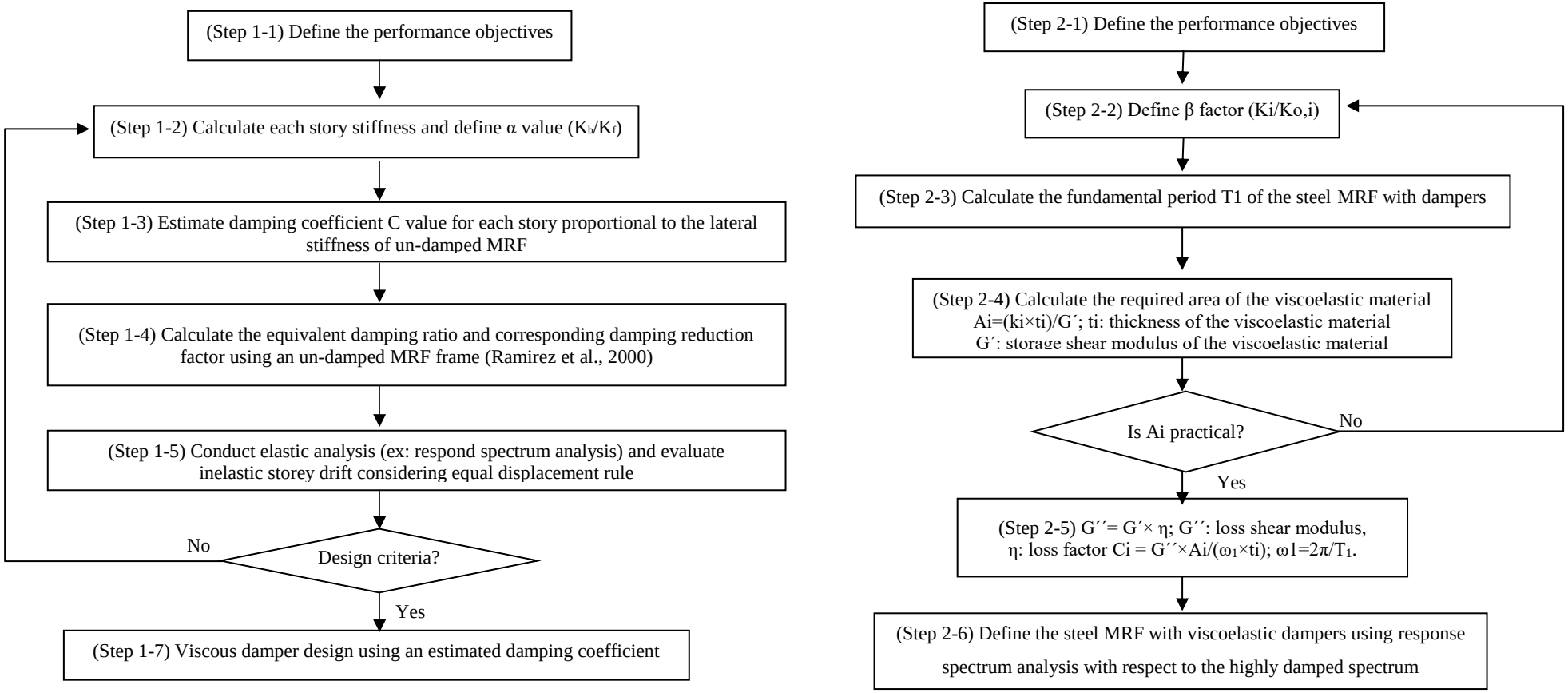

Fig. 2. 17 Simplified design process MRF with viscous (Seo et al., 2014) and viscoelastic dampers (Lee et al., 2005)

Chapter 3.

Visco-Plastic Damper (VPD)

3.1 Introduction

This chapter introduces a hybrid damper with visco-plastic behaviour. The characteristics of the visco-plastic damper and structural details for its practical implementation in steel frames will be discussed. Then, a simplified design method developed for visco-plastic dampers will be introduced and the need for research to identify optimum values of parameters involved in the design process will be highlighted.

3.2 Characteristics of a VPD

Fig. 3.1(a) shows a basic model of the visco-plastic damper which uses the Kelvin model of a dashpot (K_d) and spring (K_b) connected in parallel. The visco-plastic damper utilizes viscoelastic and steel or friction devices connected in series. Fig. 3.1(b) shows the hysteresis graph of the VPD. More specifically, it presents the elastic behaviour showing an inclined elliptical trace under small amplitude. As the amplitude is increased, the friction component begins to activate under large amplitude.

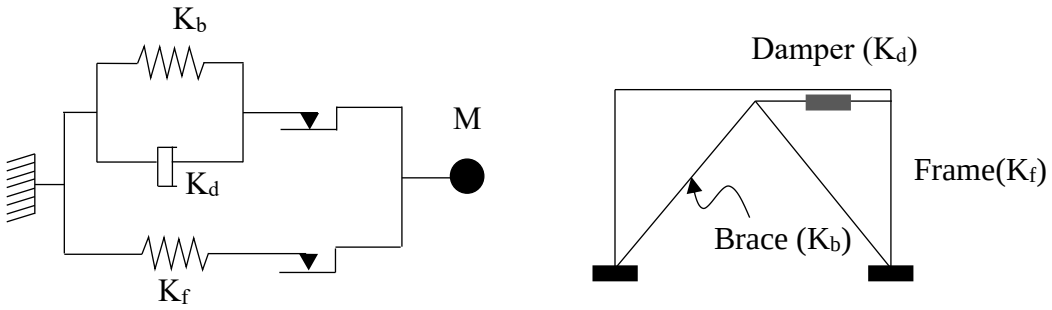

(a) Ideal model of the visco-plastic damper

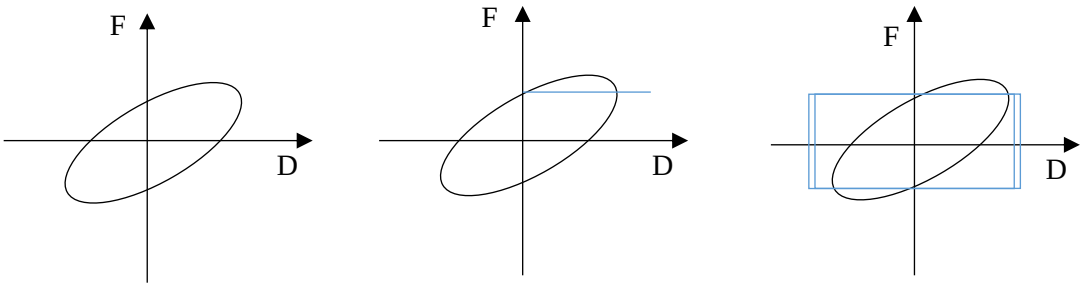

(b) Hysteretic characteristic of the visco-plastic damper
(VPD: Visco-Plastic Damper)

Fig. 3.1 Ideal visco-plastic damper model and hysteresis graph

Combination	Visco-plastic damper classification and application configuration
• Viscoelastic & Friction devices (VPD)	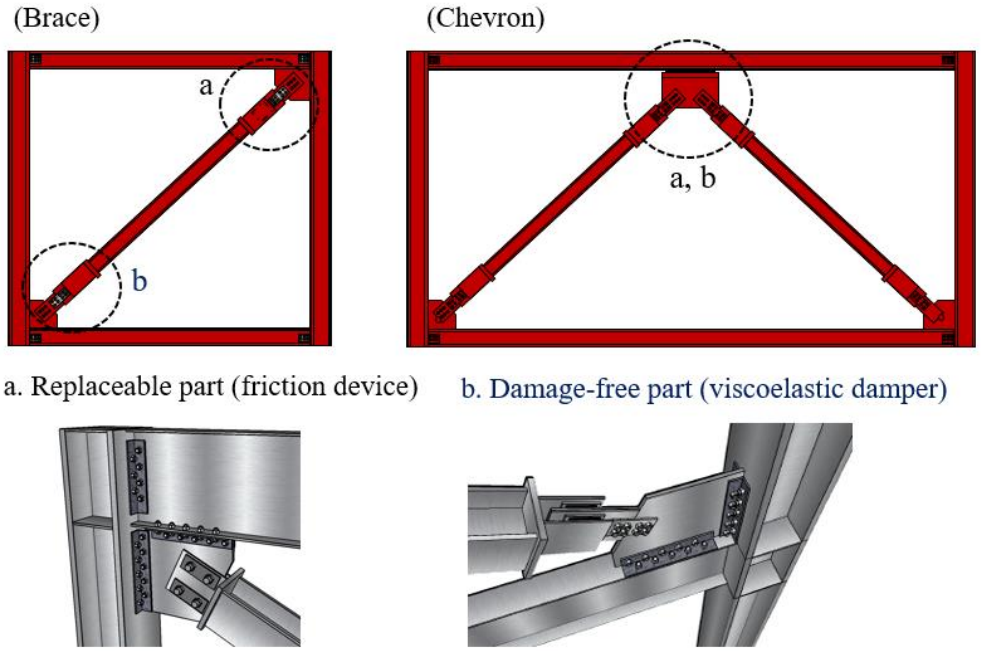

Fig. 3.2 Visco-plastic damper classification and application configuration

Fig.3.2 shows visco-plastic damper classification and application configuration. The visco-plastic damper can apply to braced or chevron types based on different site conditions. For the braced type, one of the interesting characteristics is that it intentionally separates from the viscoelastic (damage-free) part and the friction or steel part (replaceable part), allowing easy replacement after a large-scale earthquake (Fig. 3.2)

3.2.1 VPD (Visco-plastic damper) (brace type)

Fig. 3.3 illustrates the on-site application of a virtual VPD (brace type). Combining the capacity of a viscoelastic damper that activates at a lesser frequency of vibration and the friction peak force control function of the friction devices can, in turn, reduce unintentionally induced axial force caused by the use of a velocity dependent damper (e.g. viscous, viscoelastic, and elastomeric dampers). This reduced peak force ultimately results in the reduction of the foundation reinforcement that is directly related to the project cost. It can efficiently achieve advanced seismic performance by reducing the base shear.

Moreover, VPD can cover an entire range of amplitudes of vibration; from small and medium size-vibrations caused by wind, to vibrations as strong as those caused by earthquakes. In cases of wind and small-to-moderate earthquake induced vibrations, the response characteristic of the visco-plastic damper is similar to that of the viscoelastic damper due to a high-damping rubber shear strain under small amplitudes of deformation. In cases of massive earthquake induced vibration, the induced force exceeds the holding capacity of the viscoelastic damper so that the damper starts to activate under large amplitudes of deformation. Unlike other types of damper, it is not only affordable, it also has superior field applicability.

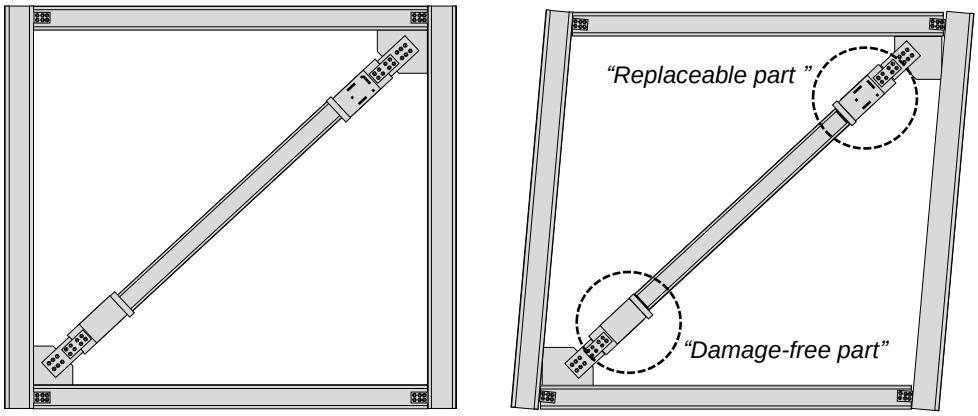

Fig. 3.3 VPD application and behaviour under dynamic loading

3.2.2 VPD (Visco-plastic damper) (chevron type)

Fig. 3.4 shows a steel MRF equipped with visco-plastic dampers and the expected force (F)-deformation (D) hysteresis of the visco-plastic damper under earthquake loading. The peak force of the visco-plastic damper is equal to the activation force of the friction device. The steel MRF has full-strength moment-resisting beam-column connections. However, the presence of the gusset plate will further stiffen the joint region, causing a high probability of the beam to yield (in the area outside the gusset plate) under strong earthquakes. A removable bolted fuse in the beam outside the gusset plate area, such as the one used in the dual frame proposed by Baiguera et al. (2016), may be used to facilitate beam reparability.

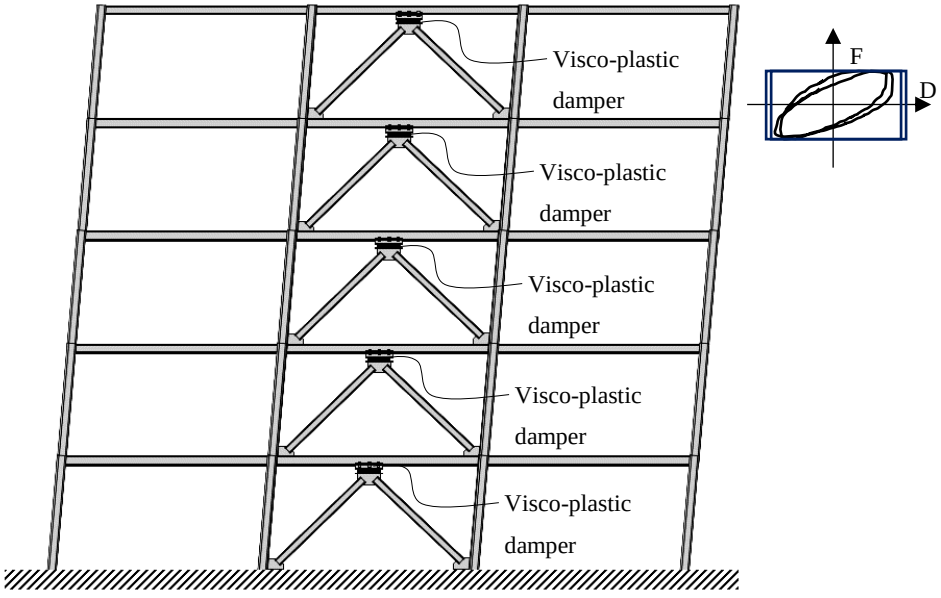

Fig. 3.4 Visco-plastic damper application (chevron type) and behaviour

3.3 Practical structural details for the VPD

3.3.1 VPD (Viscoelastic with friction device system)

3.3.1.1 Braced type

Fig. 3.5(a) shows a tentative configuration of the VPD that can be divided into two parts: the damage-free part (bottom right) that consists of the viscoelastic, and replaceable parts (upper left) that consist of friction devices with a friction pad bonded on the gusset plates that can be fabricated using bolt connection to the frames, as shown in Fig. 3.5(b). For the viscoelastic part, standard configuration details of viscoelastic damper used and viscoelastic damper consists of two viscoelastic pads bonded within two steel plates that are welded to the plates bonded to the i-beam. This part can be welded to the plates since it is damage-free, therefore it sustains elastic status regardless of the size of the amplitudes.

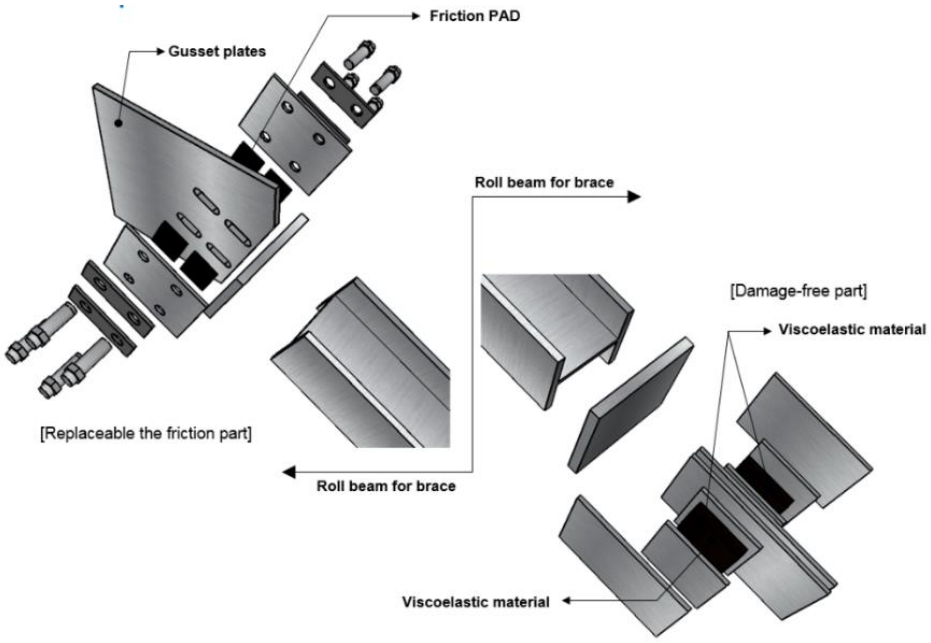

(a)

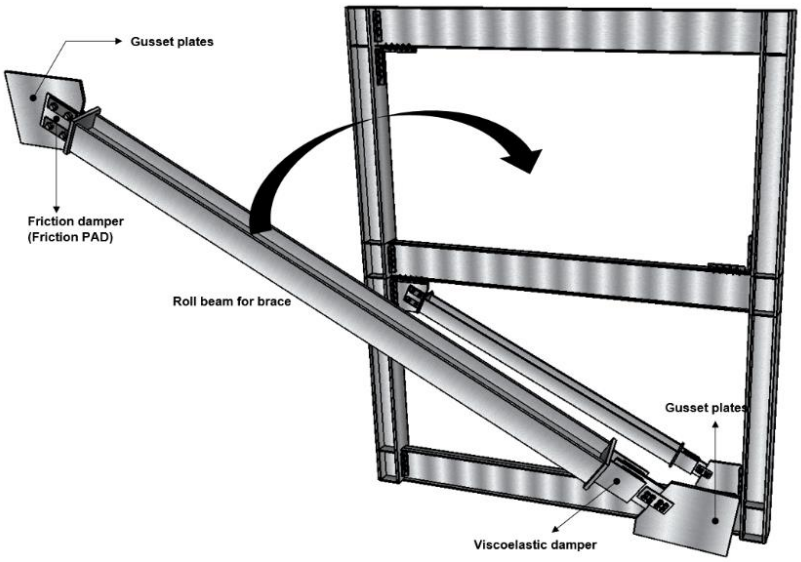

(b)

Fig. 3.5 VPD (brace type) tentative configuration and site application

3.3.1.2 Chevron type

The main components of the visco-plastic damper are the viscoelastic damper and the friction device, which are connected in series. The viscoelastic damper has a standard configuration of an elastomeric material bonded within two steel plates. It is supported by strong braces through a bolted gusset plate-brace connection. The friction device on the other hand is realised at the bottom flange of the beam by using two additional steel plates and two brass plates. Long slotted holes are drilled on the bottom flange of the beam to provide the required travel path for the bolts, which are pre-tensioned to tune the activation force of the friction device (Fig. 3.6).

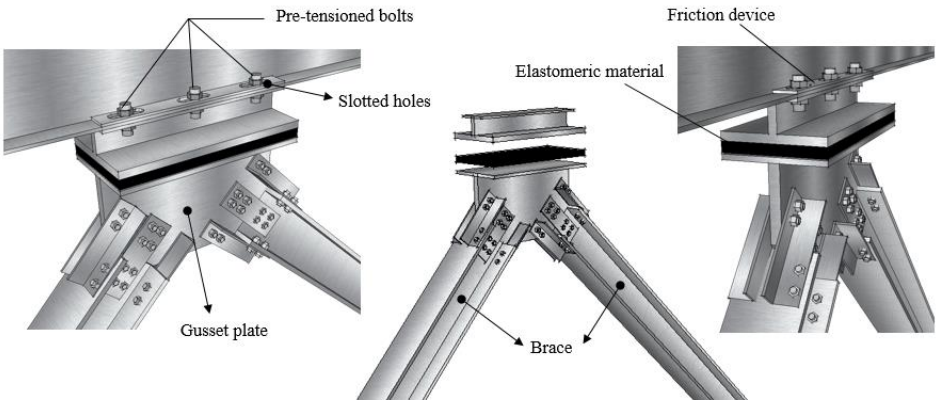

Fig. 3.6 Tentative configuration of the visco-plastic damper and its supporting braces

3.4 Simplified design procedure

In terms of the design procedure of the visco-plastic damper, the design should be completed in advance. Viscoelastic dampers are designed for the high ductility steel MRF presented in Chapter 2 (Fig. 3.7). The design is performed following the procedure of Lee et al. (2005), which involves the following steps (five storey with visco-elastic damper):

(Step 1): Define the performance objectives. A target θmax equal to 1.2% under the DBE is defined for the steel MRF with viscoelastic dampers, i.e. significantly lower than the 1.76% of the high ductility steel MRF.

(Step 2): Define the β factor, which is equal to Ki/Ko,i, where Ki is the viscoelastic damper stiffness and Ko,i is the horizontal stiffness of Storey i. The Ko,i of each storey of the steel MRF is calculated as the ratio of the inter-storey displacement over the total shear force of the storey on the basis of a simple static analysis for an inverted triangular height-wise distribution of lateral forces. A β factor equal to 0.3 is selected in this study.

(Step 3): The fundamental period of vibration of the steel MRF with dampers is obtained on the basis of modal analysis. In this analysis, the dampers are represented by springs with stiffness equal to Ki. The dampers are assumed to be supported by stiff braces (as shown in Fig. 3.8) with horizontal stiffness equal to 10 Ko,i. The period of vibration of the steel MRF with viscoelastic dampers was equal to 1.13 s. in this study.

(Step 4): The required area of the viscoelastic material is calculated as Ai=(ki×ti)/G′, where ti is the thickness of the viscoelastic material (set equal to 4 cm for all storeys) and G' is the storage shear modulus, which depends on frequency and temperature. In this work, the viscoelastic material used in Karavasilis et al. (2011) is adopted, which for a period of vibration equal to 1.13 s, has G′ equal to 1.5 MPa. If the calculated areas Ai are too large for

practical application, the designer should revert to Step 2 and select a smaller value for the β factor.

(Step 5): In this step, the loss shear modulus of the viscoelastic material is calculated as G´´= G´× η, where η is the loss factor, which for the viscoelastic material adopted herein (Karavasilis et al., 2011), has a value equal to 1.0 for a broad range of frequencies. Then the damping coefficient of the viscoelastic damper can be calculated as Ci = G´´×A_i/(ω_1×t_i), where ω_1=2π/T_1.

(Step 6): The supplemental equivalent damping ratio provided by the viscoelastic dampers is calculated as (Whittaker et al., 2003):

$$\zeta_{eq} = \frac{T_1}{4\pi} \times \frac{\sum_i C_i (\phi_i - \phi_{i-1})^2}{\sum_i m_i \times \phi_i^2} \quad (3\text{-}1)$$

where mi and φi are the mass and mode shape displacement at Floor i. This supplemental damping is added to the inherent damping ratio of the steel MRF (i.e. 3%) to calculate the total damping ratio ζtot. This damping ratio is used to calculate the damping reduction factor (Whitaker et al., 2003), which can be then used to reduce the elastic design spectrum of Eurocode 8. For this spectrum, a standard response spectrum analysis can be conducted to estimate the drifts of the steel MRF fitted with viscoelastic dampers.

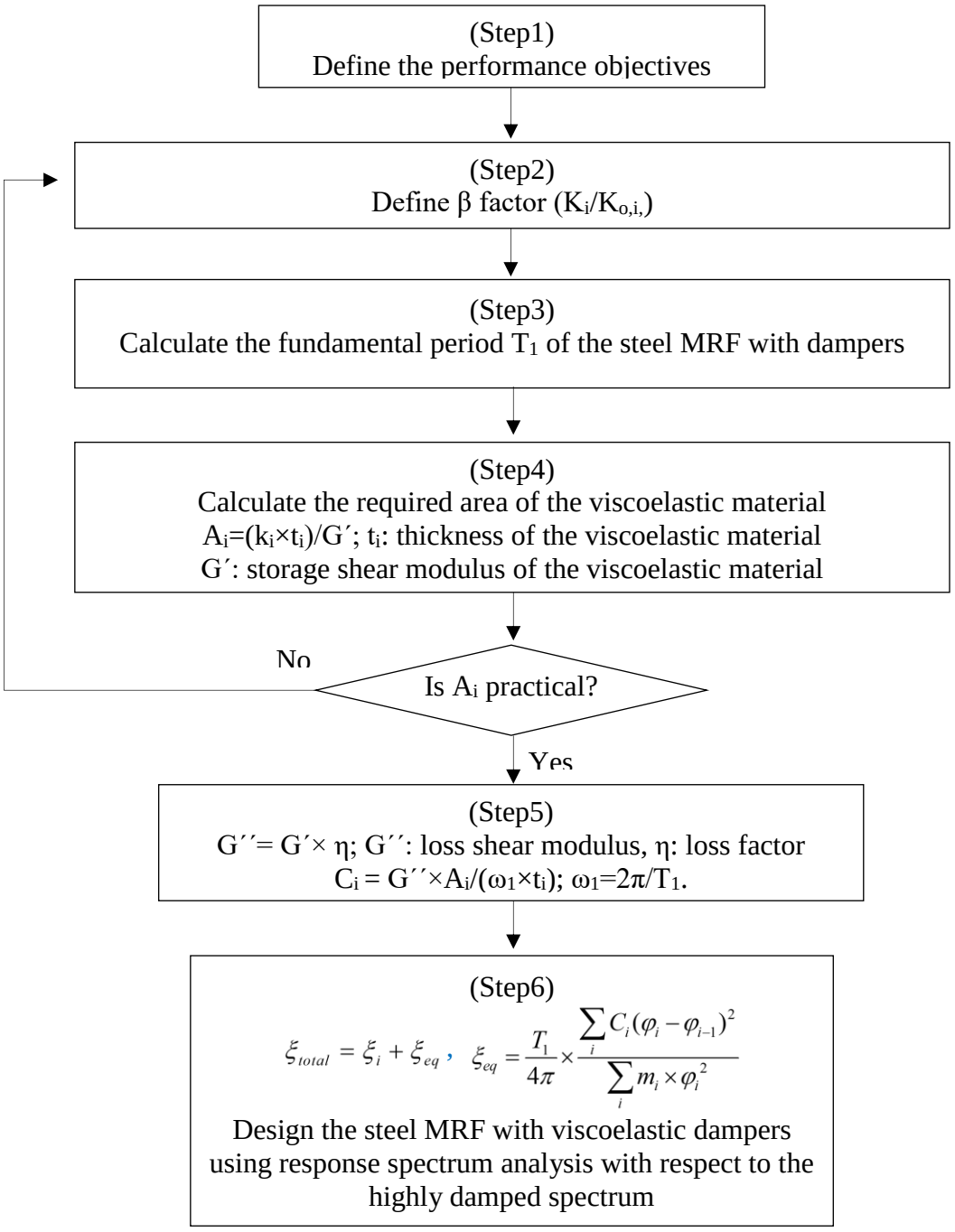

Fig. 3.7 Viscoelastic damper design procedure steps (Lee et al., 2005)

3.5 Optimisation procedure using Lambda value

The steel MRF with visco-plastic dampers can be designed by adding one additional step to the design procedure presented in Chapter 3.4. In this step, a pushover analysis is conducted on the steel MRF with viscoelastic dampers, and the force in the damper of each storey at the point of the expected drift of the steel MRF under the DBE, F_i* is extracted. Then, the activation force of the friction device at each storey is calculated as $F_{y,i}= \lambda F_i$*, where λ is a multiplier that takes values equal or lower than unity. The suitable value of λ is unknown, and is the primary parameter of investigation. In particular, parametric designs of visco-plastic dampers with λ equal to 1.0, 0.8, 0.6, 0.4 and 0.2 are carried out to investigate the effect of the activation force of the friction device on the seismic response of steel MRFs with visco-plastic dampers. Fig. 3.8 shows schematically the design process for the visco-plastic dampers given a completed design for the MRF with viscoelastic dampers.

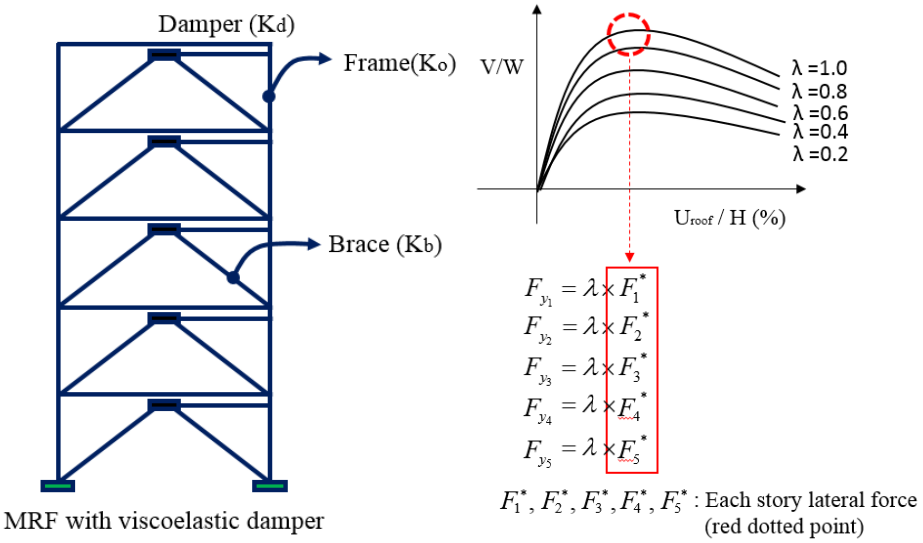

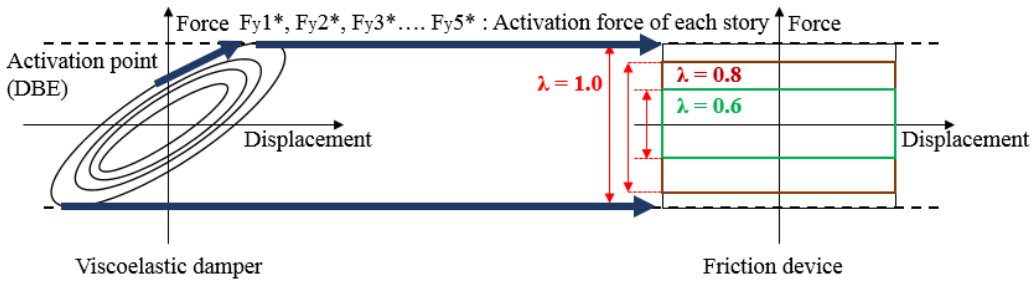

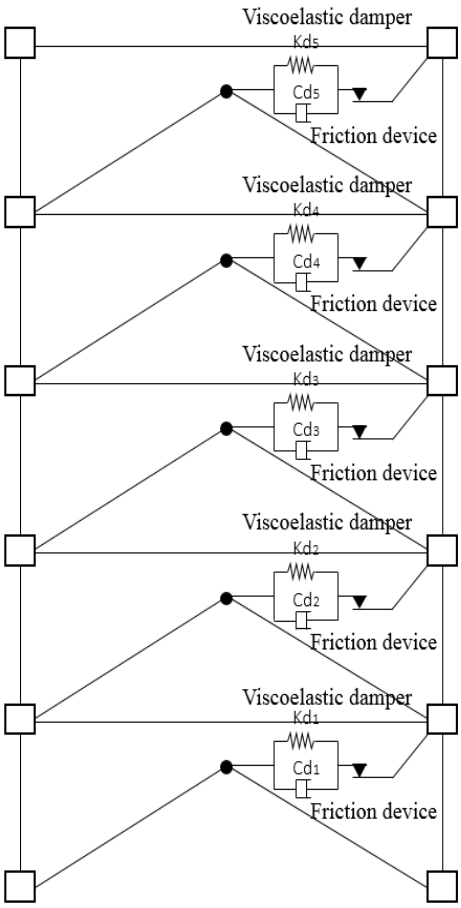

Fig. 3.8 Design procedure of steel MRF with visco-plastic dampers given a completed design of the same steel MRF with viscoelastic dampers

3.6 Summary

In this chapter, the visco-plastic damper (VPD) was described. The basic model of the visco-plastic damper is a combination of viscoelastic and friction devices. The schematic of the behaviour under dynamic loading and application configuration were explained. Then, practical structural details were explored. Lastly, a simplified design procedure for steel MRFs with visco-plastic dampers was developed and the need for research to identify the optimum value of the so-called Lambda parameter involved in the design process was identified.

Chapter 4.

Comparison of the seismic performance of buildings using viscoelastic and visco-plastic dampers

4.1 Introduction

This chapter compares the seismic performance of 5, 10, and 20-storey buildings fitted with viscoelastic and visco-plastic dampers. After following the design procedures of the viscoelastic damper, the results of pushover analysis are presented as a technique of designing the visco-plastic damper. Then, a scaling procedure for non-linear time history analysis utilising 20 far field seismic records is described. A comparison of the results of the MRFs, MRFs with viscous dampers, and MRFs with viscoelastic dampers in terms of peak drifts, residual drifts, as well as peak base shear is then provided. Finally, optimum λ factors based on seismic performance under the design and maximum considered earthquake intensities are suggested.

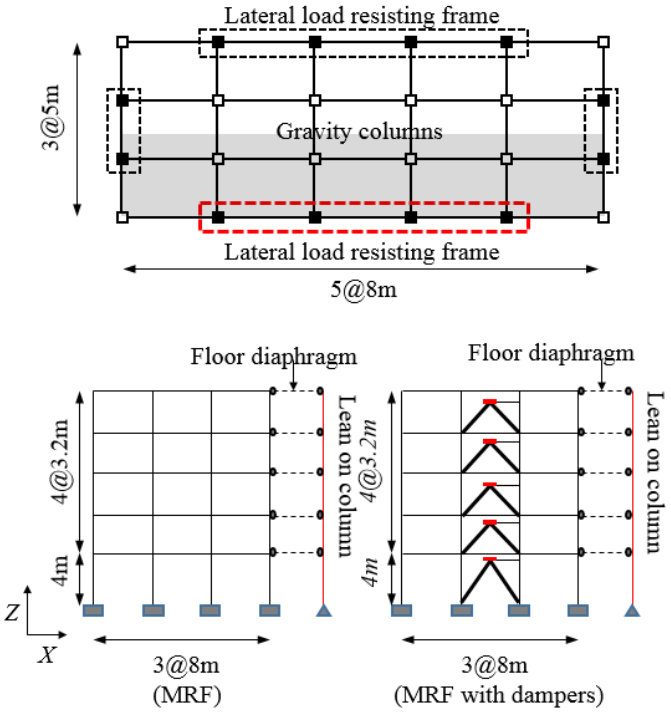

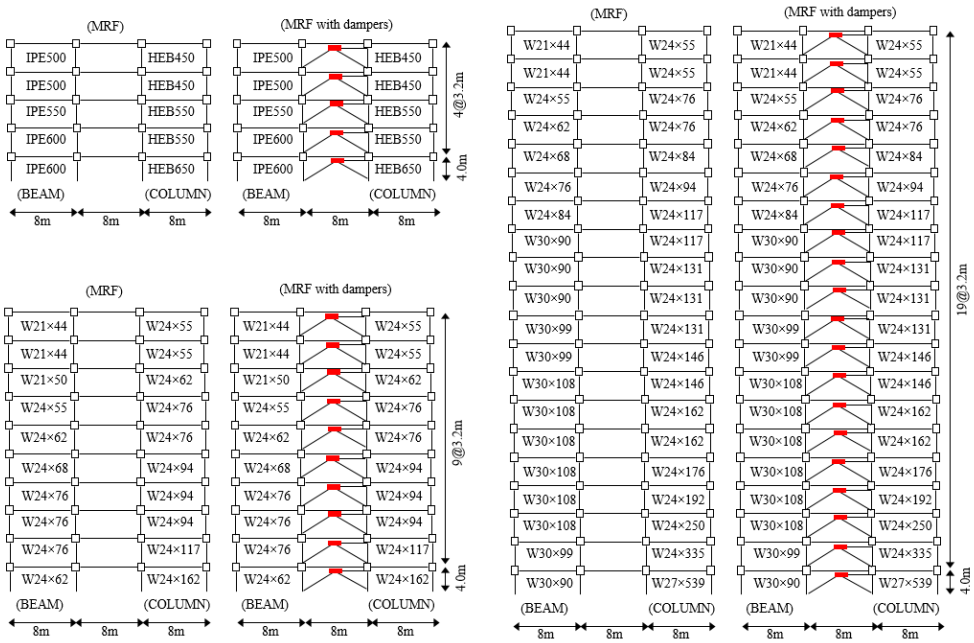

Fig. 4.1 Prototype building (elevation and plan)

The 5, 10, and 20-storey prototype office buildings considered in this thesis comprise two perimeter lateral-load resisting frames in the longitudinal x direction, as shown in Fig 4.1. The design focuses on one of the two perimeter frames. This frame consists of three bays with a width equal to 8.0 m. The height of all stories is equal to 3.2 m, with the exception of the first storey, which has a height equal to 4.0 m. Beams and columns are constructed from S275 and S355 steel grade, respectively. The frame is first designed as a high ductility steel MRF per Eurocode 8. The Design Basis Earthquake (DBE) is represented by the elastic design response spectrum for peak ground acceleration equal to 0.35g, important factor II, soil type B, and a 3.0% inherent damping ratio. Dead (G) and live (Q) loads are representative of those used in European steel design practice. A lean-on column is used to account for the P-Δ effects of the weight supported by the internal gravity columns. Fig. 4.1 shows the cross-sections of the columns and beams. The cross-sectional area and the flexural stiffness of the lean-on column are considered as the sum of the gravity columns corresponding to half of the total plan, and the base of the lean-on column is regarded as the pin and the other columns' base as completely fixed to the ground. SAP2000 software has been used for the designs presented in this thesis. For the design of a brace, α

value (the ratio of brace stiffness to the total storey MRF lateral stiffness) is assumed as equal to ten following the two criteria of Lin and Chopra (2003). Typical α value range is 5< α <10. A value of 10 is recommended by Kasai et al. (2008).

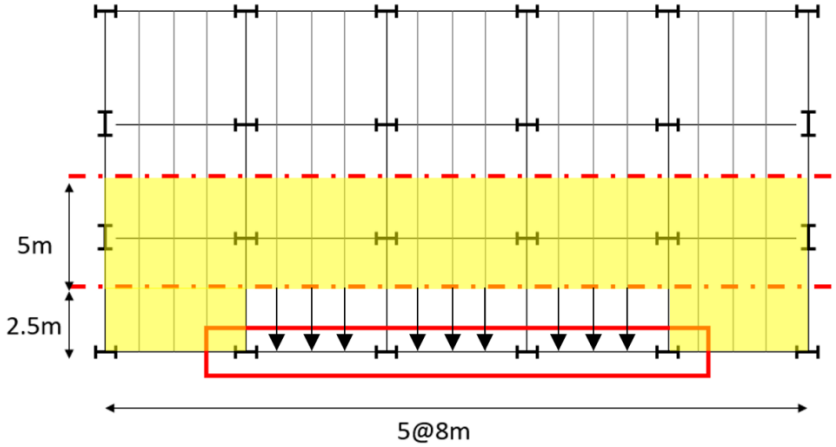

Fig. 4.2 Loading plan

4.2 Loading

As can be seen from Fig. 4.2, the red box perimeter lateral-load resisting frame considered in this study should sustain half of the seismic loading of the plan. Table 4.1 and Table 4.2 show the loads used in the prototype model. All loads are placed on each column as a type of nodal load. Distributed loading for the external columns is 4m × 2.5m × 5.9 kN/m^2 (G+0.3Q value from the Table 1) = 59kN and 8m × 2.5m × 5.9 kN/m^2= 118kN for the internal column. External glass weight for the first level is 14.5m (2.5m+12m) × 4.0m (first floor height) × 2.1 kN/m^2 =121.8kN for the external columns, and 8m ×4.0m (first floor height) ×2.1kN/m^2= 67.2kN for the internal columns. The external glass weights for the other levels are 14.5m (2.5m+12m) ×3.2m (other floor height) × 2.1kN/m^2=97.44kN for the external columns, and 8m ×3.2m (other floor height) ×2.1kN/m^2 = 53.76kN for the internal columns. Regarding areas outside the selected frame (yellow area), gravity load without self-weight is 5.0m × 40m + (2.5m×8m×2EA)) ×5.9kN/m^2 =1416.7kN. In terms of the self-weight of columns, these are calculated separately between the inner columns and the exterior columns, since the tributary area of each column is different. For the first storey column, the column weight of 36kN (4.5kN/ea × 8ea) is

calculated as 78.5kN/m3 (steel density) ×4m (column height) × 0.0145 m2 (column section area supposed as W24× 76), and for other storey columns, 78.5kN/ m3 (steel density) × 3.2m (column height) ×0.0145 m2 (column section area) = 29.12kN (3.64kN/ea ×8ea). Also, claddings for the yellow area, 10m × 4m (storey height) × 2.1 kN/m^2 = 84kN for the first storey and 10m × 3,2m (storey height) × 2.1 kN/m^2 = 67.2kN for the other stories where seismic load combination E + G + 0.3 × Q is used.

Table 4. 1 Gravity loads considered in the design example

Load	Type	Value (kN/m^2)
Composite slab	G	2.5
Internal light partitions	G	0.5
Girders	G	0.3
Mechanical/electrical	G	0.5
External glasses	G	2.1*
Cover	G	1.2
Column, beam	G	**
Office	Q	3

(1F)

Load	Internal column nodal load	External column nodal load
1. Gravity load*	1536kN	
2. Distributed load	118kN	59kN
3. External glasses	67.2kN	121.8kN
Total load	2268kN	
Total mass	2268 / 9.81 = 231.19	

(Other storey)

Load	Internal column nodal load	External column nodal load
1. Gravity load*	1512.2kN	
2. Distributed load	118kN	59kN
3. External glasses	53.7kN	97.4kN
Total load	2168kN	
Total mass	2168.6 / 9.81 = 221.06	

Table 4.2 Vertical loads due to seismic combination (G+0.3Q)

*including column weights

4.3 Non-linear model description

Non-linear models for the steel MRF with viscoelastic or visco-plastic dampers were developed in OpenSees. For the column, the steel MRF models include fiber beam column elements to capture axial force-bending moment interaction (Fig. 4.3(a), (b)). In the beam, concentrated plasticity rotational springs are used at the end of the beams to simulate strength and stiffness deterioration (Fig. 4.4). The rotation of the beam is conducted at the plastic hinges at both ends of the beam, which is expressed as a bilinear backbone curve whose equation is adapted from the Lignos deterioration model. The cyclic deterioration of beam strength can be expressed regarding the occurrence of beam rotations.

For the panel zone, twelve nodes and eight elastic beam-column elements are strongly connected to creates a 'rigid zone' to resist the shear force caused by the opposite moment between beam and column interaction (Fig 4.3(a)). A lean-on column is used to account for P-Δ effects, and a Rayleigh matrix representation for the 3.0% damping. More details of these modelling techniques can be found in Karavasilis (2016). Viscoelastic dampers are modeled using a simple Kelvin model, i.e. a spring and dashpot in parallel with values equal to those calculated during the design phase (Section 3.2). The visco-plastic dampers are modeled by connecting in series a bilinear elastic perfectly plastic spring with an initial stiffness 1000 times (to simulate the nearly rigid behaviour of the friction device before sliding) the stiffness of the viscoelastic damper, and a yield force equal to the activation force of the friction device in the previously mentioned Kelvin model (Fig. 4.3(b)).

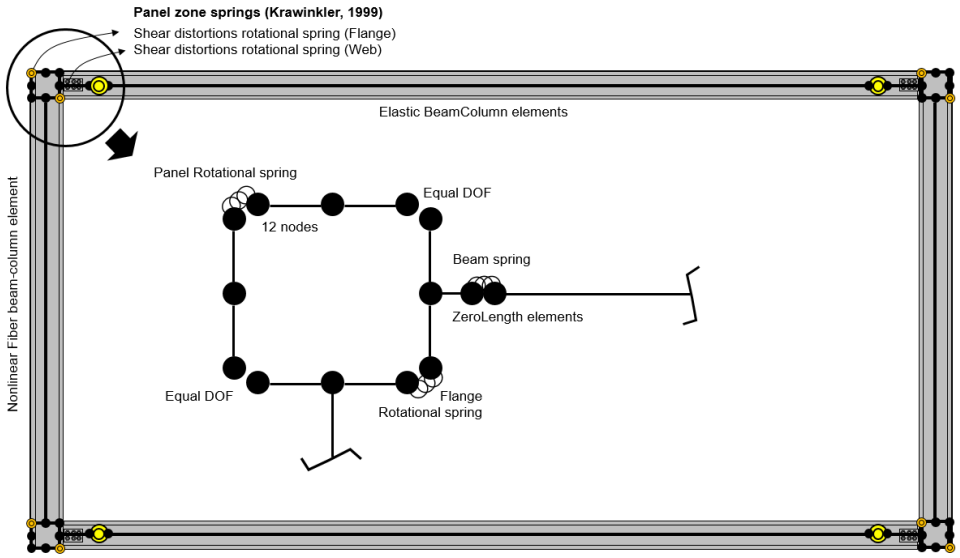

(a) Non-linear modelling details

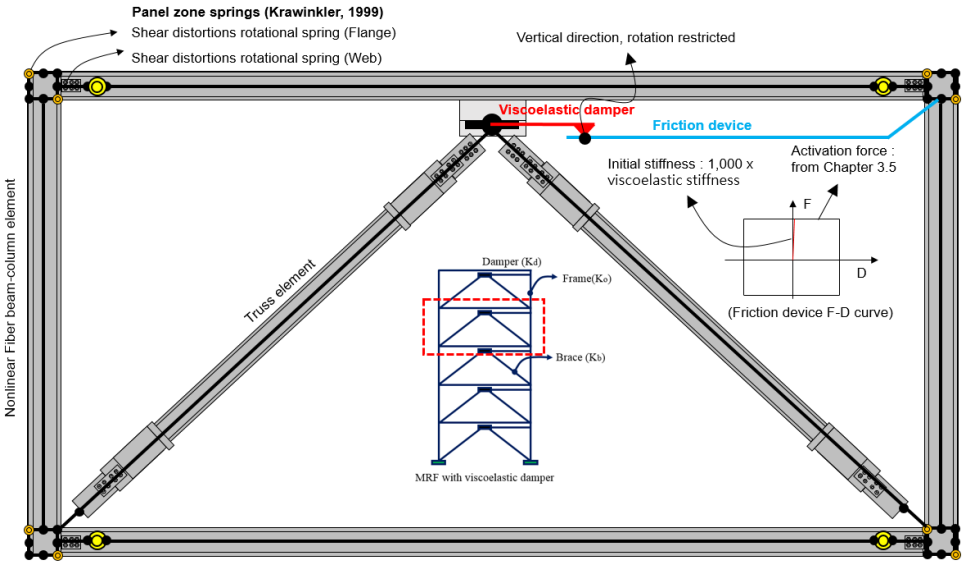

(b) Visco-plastic damper modelling details

Fig. 4.3 OpenSees modelling details

4.3.1 Beam spring deterioration model

Reliable deterioration beam spring models are calibrated throughout more than 300 experiments that consider the different variations of the steel wide flange beams (Lignos and Krawinkler, 2011). Fig. 4.4 (a), (b) shows the monotonic backbone curve and cyclic deterioration model that was used in the thesis.

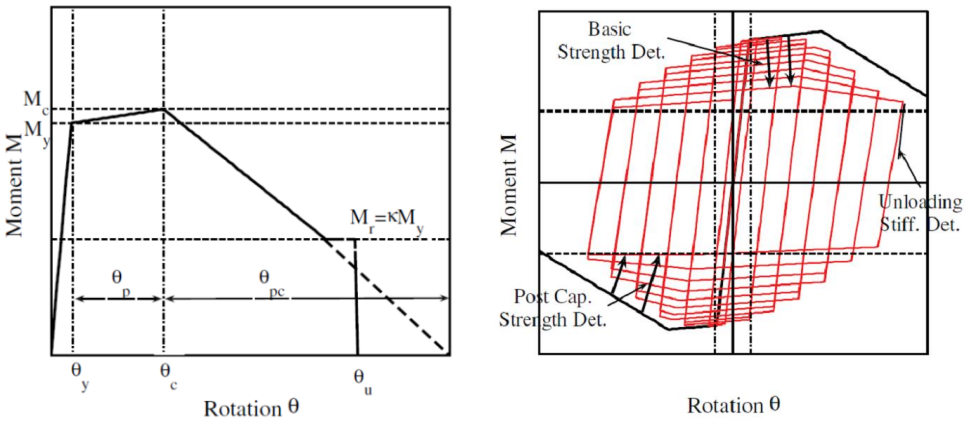

(a) Monotonic backbone curve (b) Cyclic loading deterioration model

Fig. 4.4 Modified deterioration model adopted from Lignos and Krawinkler, 2011

According to the Losnos and Krawinkler (2011), for beam spring modeling, the plastic rotation of the beam used differs according to the size of the beam.

When depth of the beam d<533mm

$$\theta_{\mathrm{p}} = 0.0865 \cdot \left(\frac{h}{t_{\mathrm{w}}}\right)^{-0.365} \cdot \left(\frac{b_{\mathrm{f}}}{2 \cdot t_{\mathrm{f}}}\right)^{-0.140} \cdot \left(\frac{L}{d}\right)^{0.340} \cdot \left(\frac{d}{533}\right)^{-0.721} \cdot \left(\frac{F_{\mathrm{y}}}{355}\right)^{-0.230} \quad (4\text{-}1)$$

$$\theta_{\mathrm{pc}} = 5.63 \cdot \left(\frac{h}{t_{\mathrm{w}}}\right)^{-0.565} \cdot \left(\frac{b_{\mathrm{f}}}{2 \cdot t_{\mathrm{f}}}\right)^{-0.800} \cdot \left(\frac{d}{533}\right)^{-0.280} \cdot \left(\frac{F_{\mathrm{y}}}{355}\right)^{-0.430} \quad (4\text{-}2)$$

Where, depth of the beam d≧533mm

$$\theta_{\mathrm{p}} = 0.318 \cdot \left(\frac{h}{t_{\mathrm{w}}}\right)^{-0.550} \cdot \left(\frac{b_{\mathrm{f}}}{2 \cdot t_{\mathrm{f}}}\right)^{-0.345} \cdot \left(\frac{L_b}{r_y}\right)^{-0.0230} \cdot \left(\frac{L}{d}\right)^{0.090} \cdot \left(\frac{d}{533}\right)^{-0.330} \cdot \left(\frac{F_{\mathrm{y}}}{355}\right)^{-0.130}$$

(4-3)

$$\theta_{\mathrm{pc}} = 7.50 \cdot \left(\frac{h}{t_{\mathrm{w}}}\right)^{-0.610} \cdot \left(\frac{b_{\mathrm{f}}}{2 \cdot t_{\mathrm{f}}}\right)^{-0.710} \cdot \left(\frac{L_{\mathrm{b}}}{r_{\mathrm{y}}}\right)^{-0.110} \cdot \left(\frac{d}{533}\right)^{-0.161} \cdot \left(\frac{F_{\mathrm{y}}}{355}\right)^{-0.320} \quad (4\text{-}4)$$

where

d: beam depth

h: depth of web

t_w: thickness of web

b_f: width of flange

t_f: thickness of flange

L: shear length

F_y: yield strength

L_b: lateral bracing length

r_y: radius of gyration about weak axis

Cyclic deterioration rate is defined by the parameter of reference cumulative plastic rotation (Λ), and can also be divided into two functions.

When depth of the beam d<533mm

$$\Lambda = 495 \cdot \left(\frac{h}{t_w}\right)^{-1,340} \cdot \left(\frac{b_f}{2 \cdot t_f}\right)^{-0.595} \cdot \left(\frac{F_y}{355}\right)^{-0.360} \quad (4\text{-}5)$$

Where, depth of the beam d≧533mm

$$\Lambda = 536 \cdot \left(\frac{h}{t_w}\right)^{-1,260} \cdot \left(\frac{b_f}{2 \cdot t_f}\right)^{-0.525} \cdot \left(\frac{L_b}{r_y}\right)^{-0.130} \cdot \left(\frac{F_y}{355}\right)^{-0.291} \quad (4\text{-}6)$$

4.3.2 Panel zone spring model

Fig. 4.5 shows the typical beam-column connections and the contribution of the moment-rotation relationships that consist of the panel component and flange components, as can be seen from Fig. 4.6.

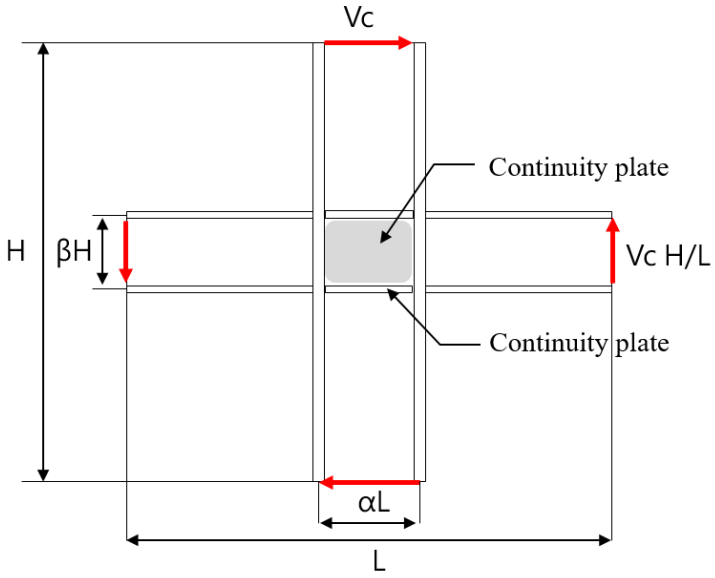

Fig. 4.5 typical beam-column connection (FEMA 451B)

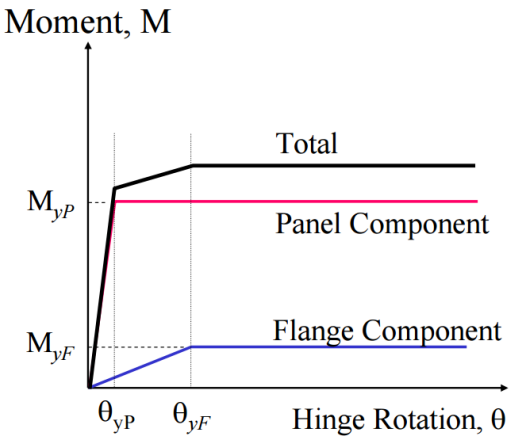

Fig. 4.6 Krawinkler moment-rotation relationships (FEMA 451B)

For the required properties for the panel component,

$$M_{\mathrm{yP,K}} = 0.6 \cdot F_{\mathrm{y}} \cdot a \cdot L \cdot \beta \cdot H \cdot \left(t_{\mathrm{wc}} + t_{\mathrm{d}}\right) \quad (4.7)$$

$$\theta_{\mathrm{yP,K}} = \frac{0.6 \cdot F_{\mathrm{y}}}{\mathrm{G}} \quad (4.8)$$

where $M_{\mathrm{yP,K}}$: panel component yield moment

F_{y} : column and double plate yield strength

$a \cdot L$: distance between the centre of column flanges (Fig. 4.5)

$\beta \cdot H$: distance between the centre of beam flanges (Fig. 4.5)

t_{wc} : column web thickness

t_{d} : doubler plate thickness

$\theta_{\mathrm{yP,K}}$: panel component yield rotation

G : steel shear modulus

For the required properties for the flange component,

$$M_{\mathrm{yF,K}} = 1.8 \cdot F_{\mathrm{y}} \cdot b_{\mathrm{cf}} \cdot t_{\mathrm{cf}}^2 \quad (4.9)$$

$$\theta_{\mathrm{yF,K}} = 4 \cdot \theta_{\mathrm{yP,K}} \quad (4.10)$$

where $M_{\mathrm{yF,K}}$: column flange yield moment

b_{cf} : column flange width

t_{cf} : column flange thickness

$\theta_{\mathrm{yF,K}}$: column flange yield rotation

Opensees non-linear spring models for beam and panel zone rotational spring values were compared with the result of hand calculation values using equations (4.3) to (4.10).

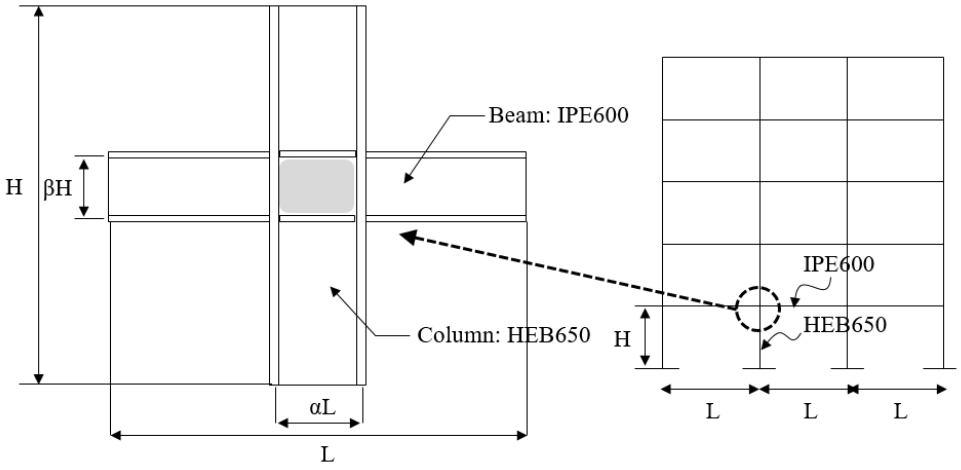

Fig. 4.7 Opensees modeling beam column detail

(For instance 1st story beam-column connections)

Since the depth of the beam of the opensees modeling is d≧533mm;

(From equation 4.3)

$$\theta_{\mathrm{p}} = 0.318 \cdot \left(\frac{h}{t_{\mathrm{w}}}\right)^{-0.550} \cdot \left(\frac{b_{\mathrm{f}}}{2 \cdot t_{\mathrm{f}}}\right)^{-0.345} \cdot \left(\frac{L_b}{r_y}\right)^{-0.0230} \cdot \left(\frac{L}{d}\right)^{0.090} \cdot \left(\frac{d}{533}\right)^{-0.330} \cdot \left(\frac{F_{\mathrm{y}}}{355}\right)^{-0.130}$$

$$= 0.318 \times \left(\frac{0.6 - 2 \times 0.019}{0.012}\right)^{-0.550} \cdot \left(\frac{0.22}{2 \cdot 0.019}\right)^{-0.345} \cdot \left(\frac{7.35}{0.0466}\right)^{-0.0230}$$

$$\cdot \left(\frac{7.35}{0.6}\right)^{0.090} \cdot \left(\frac{0.6}{533}\right)^{-0.330} \cdot \left(\frac{275}{355}\right)^{-0.130} = 0.02319 rad$$

(From equation 4.4)

$$\theta_{\mathrm{pc}} = 7.50 \cdot \left(\frac{h}{t_{\mathrm{w}}}\right)^{-0.610} \cdot \left(\frac{b_{\mathrm{f}}}{2 \cdot t_{\mathrm{f}}}\right)^{-0.710} \cdot \left(\frac{L_{\mathrm{b}}}{r_{\mathrm{y}}}\right)^{-0.110} \cdot \left(\frac{d}{533}\right)^{-0.161} \cdot \left(\frac{F_{\mathrm{y}}}{355}\right)^{-0.320}$$

$$= 7.50 \cdot \left(\frac{0.6 - 2 \times 0.019}{0.012}\right)^{-0.610} \cdot \left(\frac{0.22}{2 \cdot 0.019}\right)^{-0.710} \cdot \left(\frac{7.35}{0.0466}\right)^{-0.110} \cdot \left(\frac{0.6}{533}\right)^{-0.161} \cdot \left(\frac{275}{355}\right)^{-0.320}$$

$$= 0.12588 rad$$

(From equation 4.6)

$$\Lambda = 536 \cdot \left(\frac{h}{t_w}\right)^{-1,260} \cdot \left(\frac{b_f}{2 \cdot t_f}\right)^{-0.525} \cdot \left(\frac{L_b}{r_y}\right)^{-0.130} \cdot \left(\frac{F_y}{355}\right)^{-0.291}$$

$$= 536 \cdot \left(\frac{0.6 - 2 \times 0.019}{0.012}\right)^{-1,260} \cdot \left(\frac{0.22}{2 \cdot 0.019}\right)^{-0.525} \cdot \left(\frac{7.35}{0.0466}\right)^{-0.130} \cdot \left(\frac{275}{355}\right)^{-0.291} = 0.93416 rad$$

In the Fig. 4.7, the value of α equals to 0.77375 and β equals to 0.14525 since L is equals to 8m, H is equals to 4.0m. the required properties for the panel zone are used (Fig. 4.7)

(From equation 4.7)

$$M_{yP,K} = 0.6 \cdot F_y \cdot a \cdot L \cdot \beta \cdot H \cdot (t_{wc} + t_d)$$

$$= 0.6 \cdot 355000 \cdot (0.7735 \cdot 0.8) \cdot 0.581 \cdot (0.016 + 0.032) = 3679.9 \text{ kN} \cdot \text{m}$$

(From equation 4.8)

$$\theta_{yP,K} = \frac{0.6 \cdot F_y}{G} = \frac{0.6 \cdot 355000}{80769230.8} = 0.00264 \text{ rad}$$

(From equation 4.9)

$$M_{yF,K} = 1.8 \cdot F_y \cdot b_{cf} \cdot t_{cf}^2 = 1.8 \cdot 355000 \cdot 0.30 \cdot 0.031^2 = 184.2 \text{ kN} \cdot \text{m}$$

(From equation 4.10)

$$\theta_{yF,K} = 4 \cdot \theta_{yP,K} = 4 \cdot 0.00264 = 0.01055 \text{ rad}$$

4.4 Simplified design procedure of MRFs with viscoelastic dampers

The viscoelastic damper design procedure is given in Chapter 3.4. as follows:.

(Step1) Define the performance objective

In this step, performance targets for 5, 10, and 20-storey MRF with viscoelastic dampers are set at 1.2%, 1.0%, and 0.6%, respectively, using respond spectrum analysis, which corresponds to 20% effective damping (e.g. reduced target drift using Bs,1 factor in Table 4.3 is 1.5 for a 5-storey building). Damping coefficient B corresponds to the value of the total damping ratio β.

$$S_a(T,\beta) = \frac{S_a(T,5\%)}{B(\beta)} \qquad (4.1)$$

Effective damping β	Ramirez et al. (2000)	
	$B_{s,1}$	$B_{s,2}$
<0.02	0.80	0.80
0.05	1.00	1.00
0.10	1.20	1.20
0.20	**1.50**	**1.50**
0.30	1.70	1.70
0.40	1.90	1.90
0.50	2.20	2.20
0.60	2.30	2.60
0.70	2.35	2.90
0.80	2.40	3.30
0.90	2.45	3.70
1.00	2.50	4.00

Table 4.3 Values of the total damping ratio, *β adapted by* Ramirez et al. (2000)

Seismic performance were checked by story drift values throughout the respond spectrum analysis under DBE levels where SAP2000 commercial software used. Before conducting the analysis, SAP2000 and Opensees models were firstly check with having the same fundamental periods and member property and same size member for both models.

Table 4.4 Opensees and SAP2000 model comparions

Contents		Comparisons	
		Opensees model	SAP2000 model
Fundamental periods (sec)	(5story)	1.28	1.28
	(10story)	2.68	2.68
	(20story)	3.87	3.87

Fig. 4.8 shows the result of respond spectrum analysis using SAP2000 showing the peak storey drift θmax (%) under DBE. The red-dotted graph is a target drift for the MRF with viscoelastic dampers using B in Table 4.3 (e.g. 1.2% is calculated as 1.76%/1.5 corresponding to 20% effective damping).

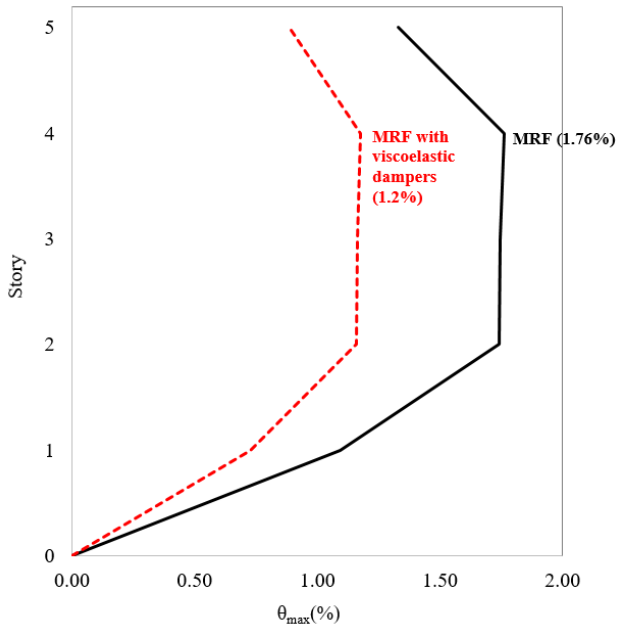

(DBE)

(a) 5-storey peak storey drift θ_{max}(%) for MRF and MRF with viscoelastic dampers

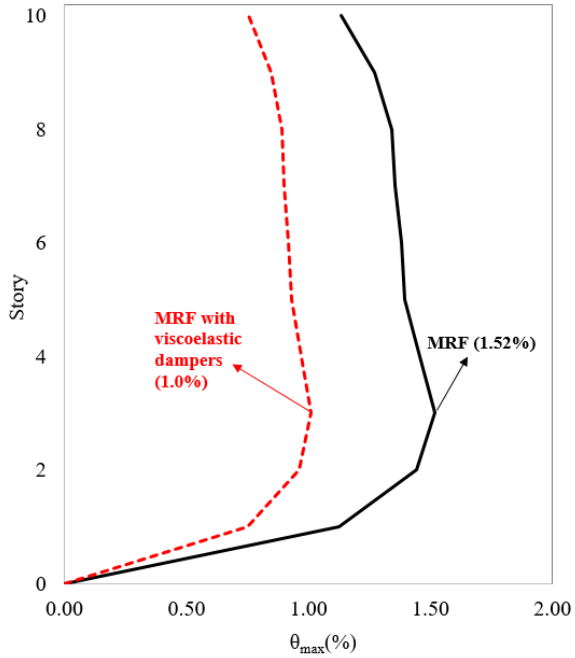

(DBE)

(b) 10-storey peak storey drift θ_{max} (%) for MRF and MRF with viscoelastic dampers

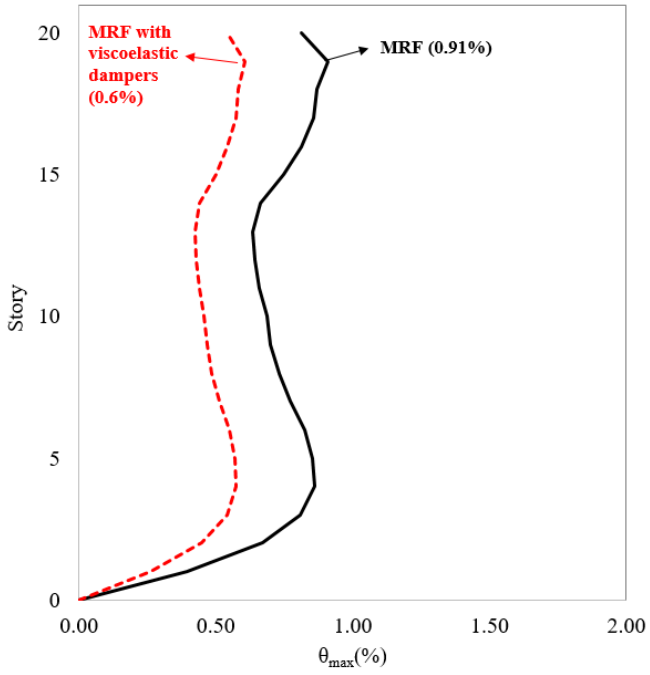

(DBE)

(c) 20-storey peak storey drift θ_{max}(%) for MRF and MRF with viscoelastic dampers

Fig. 4.8 The results of the θ_{max}(%) under DBE using respond spectrum analysis

(Step 2): Define the β factor

As can be seen in the table below, β factor (β = Ki / Ko) is considered equal to 0.3 for 5-storey, equal to 0.43 for 10-storey, and equal to 0.42 for 20-storey buildings to match with the target drift.

(Step 3) Using modal analysis for the MRFs with viscoelastic dampers, the reduced fundamental period (T_1) for 5-storey, 10-storey, and 20-storey is 1.13s, 2.25s, and 3.32s, respectively. Table 4.5 shows the comparison of design data for the MRF and the MRF with viscoelastic dampers as well as the properties of viscoelastic dampers.

Table 4.5. Comparison of design data for MRF and MRF with viscoelastic dampers

Storey	T_1 (sec)	ζ_{tot} (%)	θ_{max} (%), DBE
MRF	1.28	3	1.76
MRF with viscoelastic dampers	1.13	15	1.2

(a) 5-storey building

Storey	T_1 (sec)	ζ_{tot} (%)	θ_{max} (%), DBE
MRF	2.68	3	1.52
MRF with viscoelastic dampers	2.25	18	1.0

(b) 10-storey building

Storey	T_1 (sec)	ζ_{tot} (%)	θ_{max} (%), DBE
MRF	3.87	3	0.91
MRF with viscoelastic dampers	3.32	19	0.6

(c) 20-storey building

Table 4.6 Properties of viscoelastic dampers (5-storey, 10-storey, 20-storey)

Storey	Ko (kN/m)	Ki (kN/m)	Ai (m²)	ti (m)	C, kN-s/m
5	32684.8	9805.4	0.26	0.04	1763.5
4	42398.9	12719.7	0.34	0.04	2287.6
3	56983.2	17095.0	0.46	0.04	3074.4
2	69364.2	20809.2	0.55	0.04	3742.4
1	98859.3	29657.8	0.79	0.04	5333.8

(a) 5 storey (β =0.3)

Storey	Ko (kN/m)	Ki (kN/m)	Ai (m²)	ti (m)	C, kN-s/m
10	17634.4	7582.8	0.36	0.04	2715.4
9	27048.1	11630.7	0.55	0.04	4164.9
8	33598.2	14447.2	0.68	0.04	5173.5
7	40172.2	17274.0	0.81	0.04	6185.8

6	45897.1	19735.7	0.93	0.04	7067.3
5	52046.2	22379.9	0.26	0.04	8014.2
4	56842.8	24442.4	0.34	0.04	8752.8
3	61935.5	26632.3	0.46	0.04	9537.0
2	72639.2	31234.9	0.55	0.04	11185.2
1	79930.5	34370.1	0.79	0.04	12307.9

(b) 10 storey (β =0.43)

Storey	Ko (kN/m)	Ki (kN/m)	Ai (m²)	ti (m)	C, kN-s/m
20	16560.2	6955.3	0.56	0.04	3675.1
19	25059.5	10525.0	0.84	0.04	5561.3
18	33106.4	13904.7	1.11	0.04	7347.2
17	38628.7	16224.0	1.30	0.04	8572.7
16	44709.8	18778.1	1.50	0.04	9922.3
15	51982.9	21832.8	1.75	0.04	11536.3
14	62859.9	26401.2	2.11	0.04	13950.2
13	71312.2	29951.1	2.40	0.04	15826.0
12	77037.0	32355.6	2.59	0.04	17096.5
11	81290.3	34141.9	2.73	0.04	18040.4
10	85750.8	36015.3	2.88	0.04	19030.3
9	92007.8	38643.3	3.09	0.04	20418.9
8	96878.6	40689.0	3.26	0.04	21499.8
7	102003.6	42841.5	3.43	0.04	22637.2
6	106106.1	44564.6	3.57	0.04	23547.7
5	112396.7	47206.6	3.78	0.04	24943.7
4	123797.1	51994.8	4.16	0.04	27473.8
3	144214.8	60570.2	4.85	0.04	32005.0
2	184814.9	77622.3	6.21	0.04	41015.2
1	263198.2	110543.2	8.84	0.04	58410.4

(c) 20 storey (β =0.42)

(Step 4~5): For instance, in the case of the 5-storey building, using modal analysis, the fundamental period of vibration of the steel MRF with dampers, where T_1 is 1.13s and frequency is 5.56 (rad/s), storage shear modulus G' is equal to 1.5Mpa, η equal to 1.0, and loss shear modulus is G'', =1.5 (Fig. 4.9).

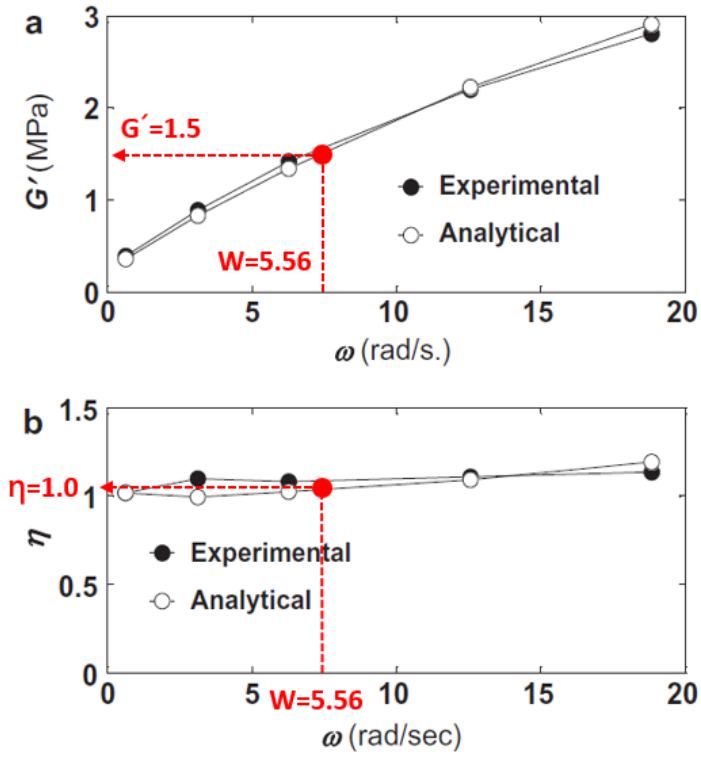

(a) 5-storey

(b)

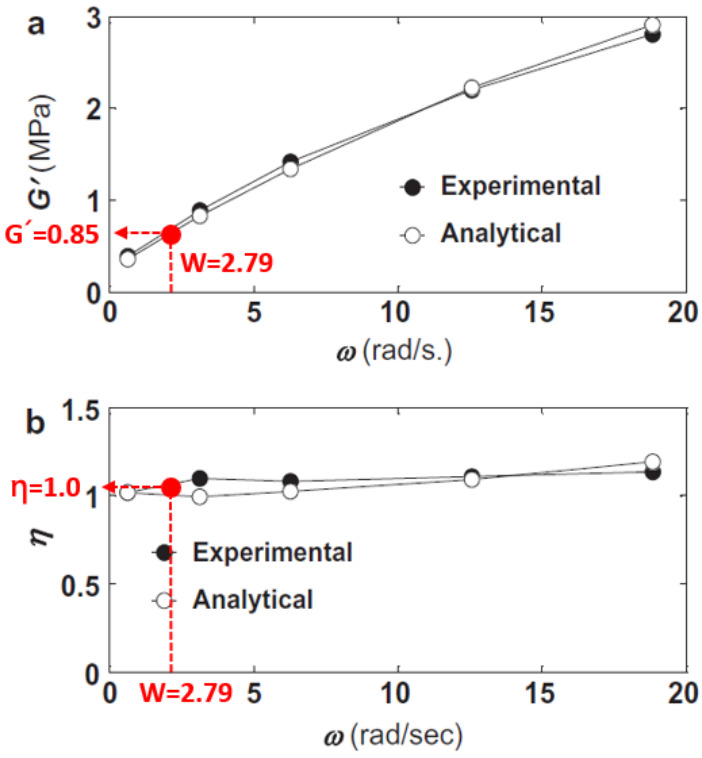

(b) 10-storey

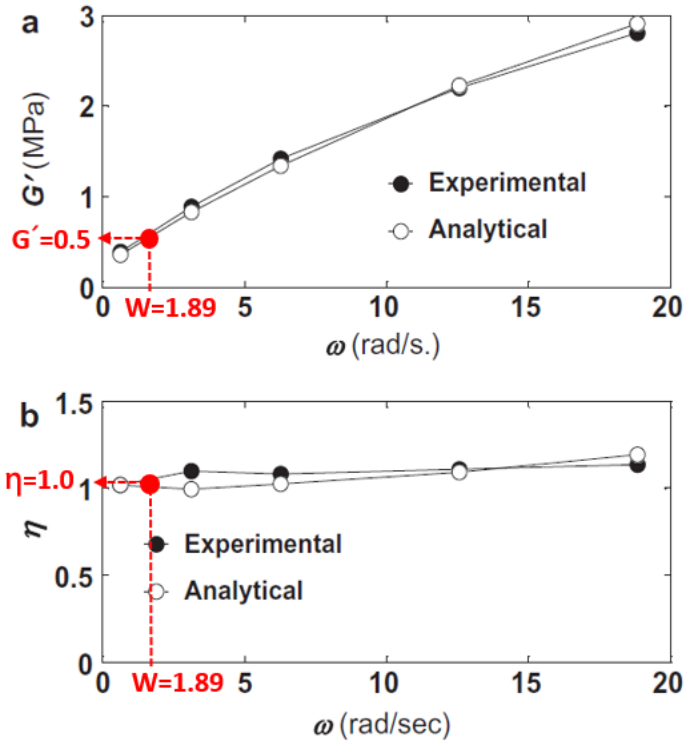

(c) 20-storey

Fig. 4.9 G´ and η based on the natural frequency of MRF with viscoelastic dampers (from Karavasilis et al., 2011)

For the 10 and 20-storey buildings, the fundamental period of vibration of the steel MRF with dampers, where T_1 is 2.25s and 3.32s, is 2.79 (rad/s) and 1.89 (rad/s), respectively. Therefore, storage shear modulus G´ is equal to 0.85Mpa and 0.5Mpa, η values are both equal to 1.0, and loss shear modulus is G´´=0.85 for 10-storey and G´´=0.5 for a 20-storey buildings.

(Step 6): Total damping and damping coefficient of the MRF with viscoelastic damper is stated in Table A (Appendix Chapter).

4.5 Visco-plastic damper design procedure using pushover analysis

Following the instructions given in Chapter 3.5, a pushover analysis is carried out for the steel MRF with viscoelastic dampers, and the force at the damper of each storey at the point of the expected drift of the steel MRF under the DBE, Fi* is extracted. Before conducting the MRF with visco-plastic design procedure, a pushover analysis is carried out to determine the point at which the viscoelastic damper shows full capacity. Fig. 4.10 shows the reduced activation peak force based on the reduction of λ value from 1.0 to 0.2.

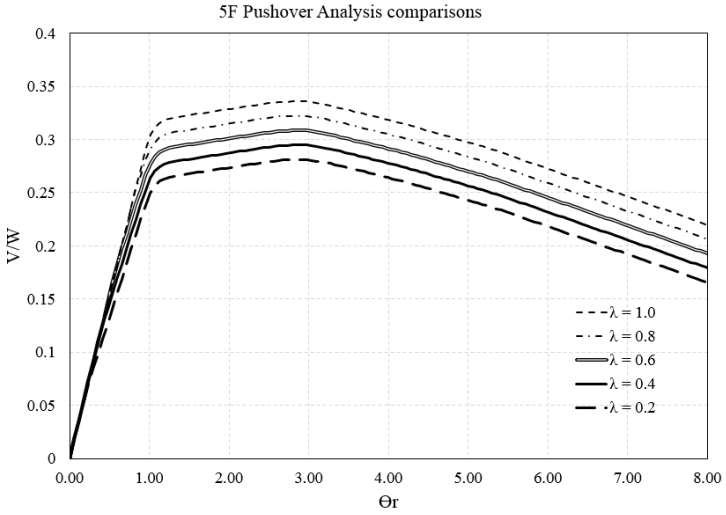

Fig. 4.10 Storey pushover analysis for MRFs with visco-plastic dampers

Table 4.7 5-storey visco-plastic damper stiffness and activation force

Storey	K=β (=0.3)	K[1](1000*Kn)	Fy(kN) (λ=1.0)	Fy(kN) (λ=0.8)	Fy(kN) (λ=0.6)	Fy(kN) (λ=0.4)	Fy(kN) (λ=0.2)
5	9805	9805447	144	115	86	57	29
4	12720	12719665	243	194	146	97	49
3	17095	17094972	336	269	201	134	67
2	20809	20809249	385	308	231	154	77
1	29658	29657795	419	335	251	168	84

[1] Stiffness of the friction devices

4.1.4 10-storey with visco-plastic dampers

The same procedure is conducted for the 10-storey building with viscoelastic dampers.

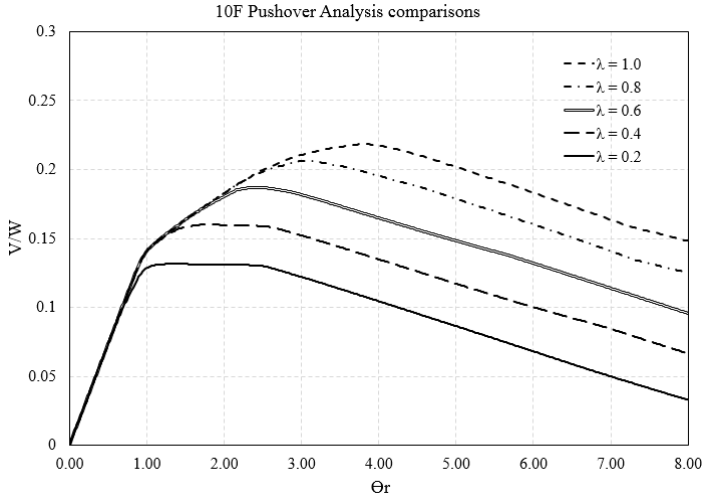

Fig. 4.11 Storey pushover analysis for MRFs with visco-plastic dampers

Table 4.8 10-storey visco-plastic damper stiffness and activation force

storey	K=β (=0.43)	K[1](1000*Kn)	Fy(kN) (λ=1.0)	Fy(kN) (λ=0.8)	Fy(kN) (λ=0.6)	Fy(kN) (λ=0.4)	Fy(kN) (λ=0.2)
10	7583	7582796	427	341.6	256.2	170.8	85.4
9	11631	11630689	872	697.6	523.2	348.8	174.4
8	14447	14447219	1372.5	1098	823.5	549	274.5
7	17274	17274032	1372.5	1098	823.5	549	274.5
6	19736	19735744	1847.6	1478.1	1108.6	739.1	369.5
5	22380	22379853	2630.1	2104.1	1578.1	1052	526
4	24442	24442422	2871.3	2297	1722.8	1148.5	574.3
3	26632	26632258	3090.9	2472.8	1854.6	1236.4	618.2
2	31235	31234867	3458	2766.4	2074.8	1383.2	691.6
1	34370	34370113	4396.6	3517.3	2638	1758.7	879.3

[1] Stiffness of the friction devices

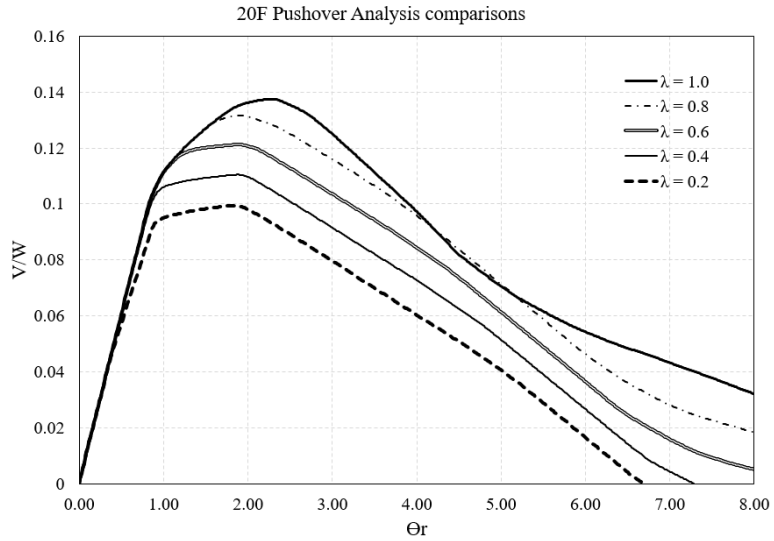

Fig. 4.12 20 Storey pushover analysis for MRFs with visco-plastic dampers

Table 4.9 20-storey visco-plastic damper stiffness and activation force

Storey	K=β (=0.42)	K (1000*Kn)	Fy(kN) (λ=1.0)	Fy(kN) (λ=0.8)	Fy(kN) (λ=0.6)	Fy(kN) (λ=0.4)	Fy(kN) (λ=0.2)
20	6955	6955277	149.2	119.4	89.5	59.7	29.8
19	10525	10524980	274.2	219.3	164.5	109.7	54.8
18	13905	13904694	448.2	358.5	268.9	179.3	89.6
17	16224	16224046	632.9	506.3	379.7	253.2	126.6
16	18778	18778135	849.5	679.6	509.7	339.8	169.9
15	21833	21832825	1094.6	875.7	656.8	437.8	218.9
14	26401	26401171	1414.2	1131.4	848.5	565.7	282.8
13	29951	29951106	1684.3	1347.4	1010.6	673.7	336.9
12	32356	32355556	1922	1537.6	1153.2	768.8	384.4
11	34142	34141935	2096.1	1676.9	1257.6	838.4	419.2
10	36015	36015335	2254.8	1803.8	1352.9	901.9	451
9	38643	38643275	2384.4	1907.5	1430.6	953.7	476.9
8	40689	40689001	2489.8	1991.9	1493.9	995.9	498
7	42842	42841530	2559.4	2047.5	1535.6	1023.8	511.9
6	44565	44564565	2598.5	2078.8	1559.1	1039.4	519.7
5	47207	47206612	2591.2	2072.9	1554.7	1036.5	518.2
4	51995	51994798	2536.1	2028.9	1521.6	1014.4	507.2
3	60570	60570211	2314.7	1851.7	1388.8	925.9	462.9
2	77622	77622264	2037.7	1630.2	1222.6	815.1	407.5
1	110543	110543229	1708.6	1366.9	1025.1	683.4	341.7

4.6 Scaling procedure for non-linear time history analysis

A set of 20 recorded far-fault ground motions (Karavasilis, 2016) are used for non-linear dynamic analyses. These ground motions were recorded on stiff soil, do not exhibit pulse-type near-fault characteristics, and were scaled at the DBE and maximum considered earthquake (MCE) intensities; where the seismic intensity is represented by 5% spectral acceleration. Sa, at T_1. Fig. 4.13 to 15 shows the spectra of these ground motions when scaled to the DBE at T_1=1.13 s in 5-storey, T_1=2.25 s in 10-storey, and T_1=3.32 s in 20-storey buildings. The MCE is assumed to have an intensity 1.5 times that of the DBE.

Table 4.10 Far-fault ground motions and scaling for 5-storey buildings

No	Ground Motion	Station	Location	PGA (g)	DBE S.F.	MCE S.F.
1	Manjil 1990	Abbar	Iran	0.51	0.22	0.33
2	Manjil 1990	Abbar	Iran	0.50	0.10	0.15
3	Kocaeli 1999	Arcelik	Turkey	0.22	0.39	0.59
4	Kocaeli 1999	Arcelik	Turkey	0.15	0.39	0.59
5	Friuli 1976	Tolmezzo	Italy	0.35	0.22	0.33
6	Friuli 1976	Tolmezzo	Italy	0.31	0.17	0.25
7	Superstition Hills 1987	El Centro Imp. Co.	USA	0.36	0.11	0.16
8	Superstition Hills 1987	El Centro Imp. Co.	USA	0.26	0.14	0.21
9	Duzce 1999	Bolu	Turkey	0.73	0.09	0.13
10	Duzce 1999	Bolu	Turkey	0.82	0.05	0.07
11	Superstition Hills 1987	Poe Road (temp)	USA	0.45	0.10	0.15
12	Superstition Hills 1987	Poe Road (temp)	USA	0.30	0.13	0.20
13	Loma Prieta 1989	Capitola	USA	0.53	0.08	0.12
14	Loma Prieta 1989	Capitola	USA	0.44	0.14	0.21
15	Chi-Chi 1999	CHY101	Taiwan	0.35	0.12	0.18
16	Chi-Chi 1999	CHY101	Taiwan	0.44	0.07	0.10
17	Landers 1992	Coolwater	USA	0.28	0.20	0.30
18	Landers 1992	Coolwater	USA	0.42	0.12	0.17
19	Kocaeli 1999	Duzce	Turkey	0.31	0.13	0.20
20	Kocaeli 1999	Duzce	Turkey	0.36	0.07	0.10

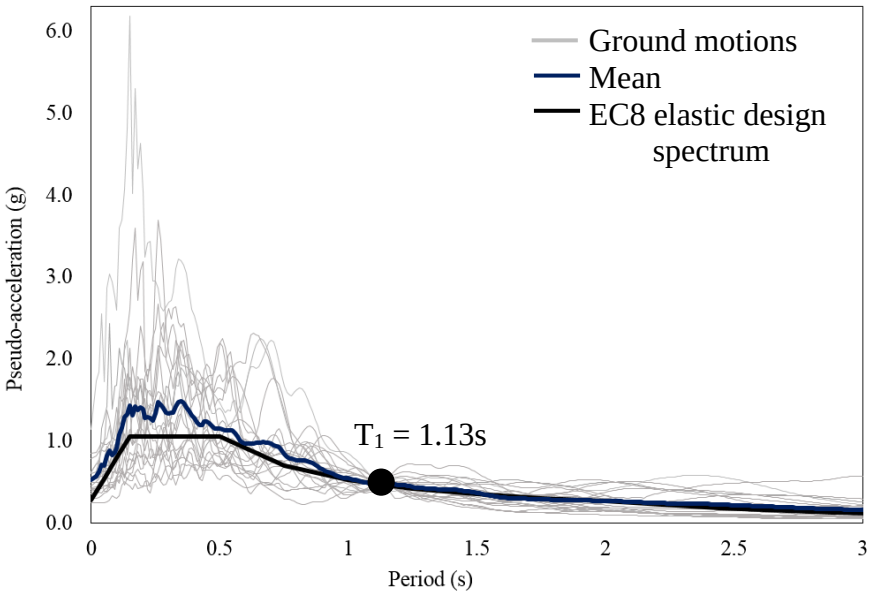

Fig. 4.13 Response spectra of the scaled (at DBE for 5-storey T_1=1.13 s) ground motions used for non-linear dynamic analysis along with the design spectrum of Eurocode 8

Table 4.11 Far-fault ground motions and scaling for 10-storey buildings

No	Ground Motion	Station	Location	PGA (g)	DBE S.F.	MCE S.F.
1	Manjil 1990	Abbar	Iran	0.51	0.09	0.13
2	Manjil 1990	Abbar	Iran	0.50	0.05	0.08
3	Kocaeli 1999	Arcelik	Turkey	0.22	0.61	0.92
4	Kocaeli 1999	Arcelik	Turkey	0.15	0.33	0.50
5	Friuli 1976	Tolmezzo	Italy	0.35	0.41	0.62
6	Friuli 1976	Tolmezzo	Italy	0.31	0.46	0.70
7	Superstition Hills 1987	El Centro Imp. Co.	USA	0.36	0.13	0.19
8	Superstition Hills 1987	El Centro Imp. Co.	USA	0.26	0.07	0.11
9	Duzce 1999	Bolu	Turkey	0.73	0.09	0.14
10	Duzce 1999	Bolu	Turkey	0.82	0.11	0.16
11	Superstition Hills 1987	Poe Road (temp)	USA	0.45	0.12	0.18
12	Superstition Hills 1987	Poe Road (temp)	USA	0.30	0.11	0.17
13	Loma Prieta 1989	Capitola	USA	0.53	0.17	0.25
14	Loma Prieta 1989	Capitola	USA	0.44	0.34	0.51
15	Chi-Chi 1999	CHY101	Taiwan	0.35	0.07	0.10
16	Chi-Chi 1999	CHY101	Taiwan	0.44	0.04	0.06
17	Landers 1992	Coolwater	USA	0.28	0.40	0.60
18	Landers 1992	Coolwater	USA	0.42	0.23	0.34

19	Kocaeli 1999	Duzce	Turkey	0.31	0.06	0.09
20	Kocaeli 1999	Duzce	Turkey	0.36	0.07	0.10

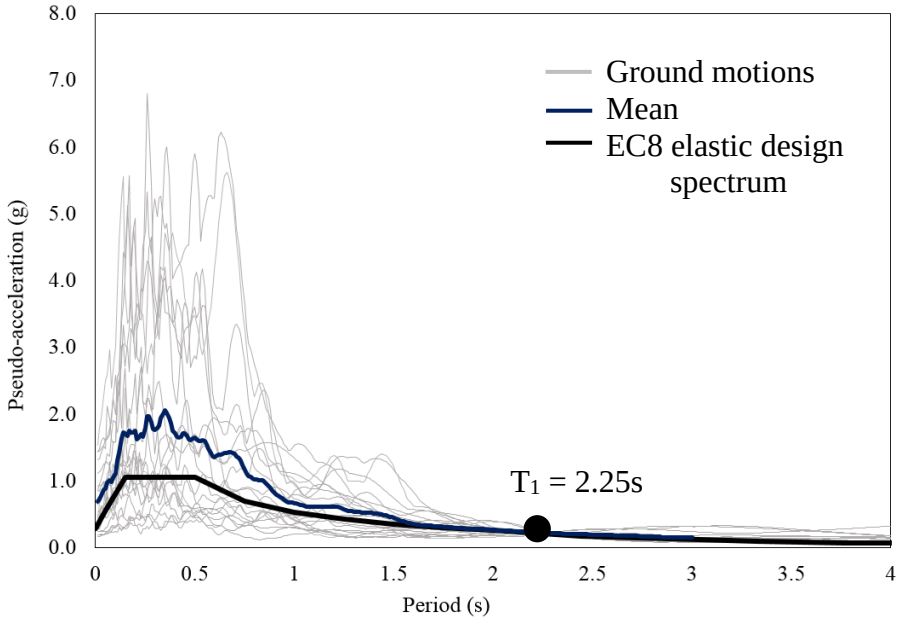

Fig. 4.14 Response spectra of the scaled (at DBE for 10-storey T_1=2.25 s) ground motions used for non-linear dynamic analysis along with the design spectrum of Eurocode 8

.

Table 4.12 Far-fault ground motions and scaling for 20-storey buildings

No	Ground Motion	Station	Location	PGA (g)	DBE S.F.	MCE S.F.
1	Manjil 1990	Abbar	Iran	0.51	0.11	0.16
2	Manjil 1990	Abbar	Iran	0.50	0.06	0.08
3	Kocaeli 1999	Arcelik	Turkey	0.22	0.18	0.27
4	Kocaeli 1999	Arcelik	Turkey	0.15	0.14	0.21
5	Friuli 1976	Tolmezzo	Italy	0.35	0.37	0.55
6	Friuli 1976	Tolmezzo	Italy	0.31	0.31	0.47
7	Superstition Hills 1987	El Centro Imp. Co.	USA	0.36	0.12	0.19
8	Superstition Hills 1987	El Centro Imp. Co.	USA	0.26	0.09	0.13
9	Duzce 1999	Bolu	Turkey	0.73	0.06	0.09
10	Duzce 1999	Bolu	Turkey	0.82	0.09	0.13
11	Superstition Hills 1987	Poe Road (temp)	USA	0.45	0.09	0.14
12	Superstition Hills 1987	Poe Road (temp)	USA	0.30	0.07	0.10
13	Loma Prieta 1989	Capitola	USA	0.53	0.19	0.28

14	Loma Prieta 1989	Capitola	USA	0.44	0.26	0.38
15	Chi-Chi 1999	CHY101	Taiwan	0.35	0.02	0.03
16	Chi-Chi 1999	CHY101	Taiwan	0.44	0.03	0.05
17	Landers 1992	Coolwater	USA	0.28	0.20	0.30
18	Landers 1992	Coolwater	USA	0.42	0.25	0.38
19	Kocaeli 1999	Duzce	Turkey	0.31	0.04	0.06
20	Kocaeli 1999	Duzce	Turkey	0.36	0.09	0.13

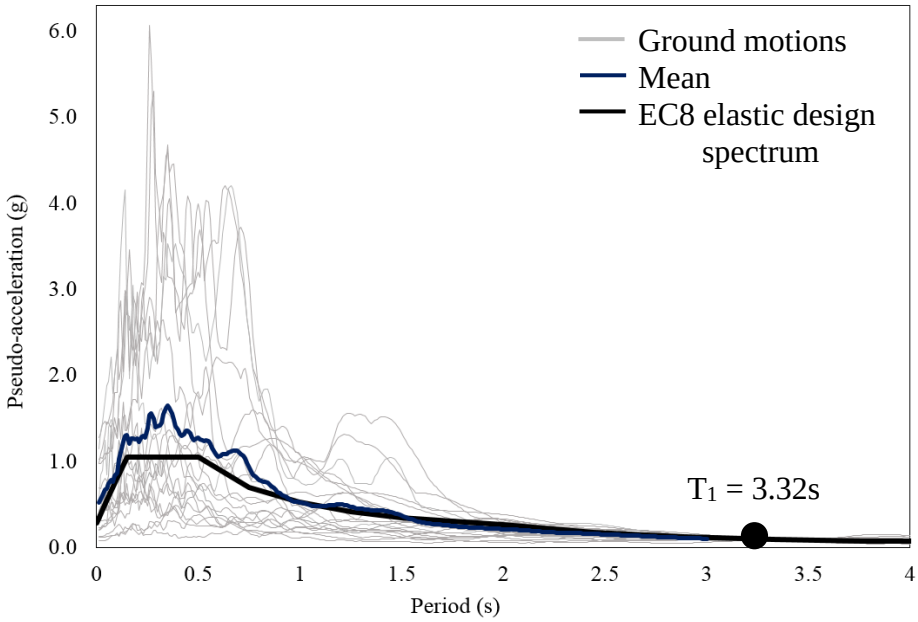

Fig. 4.15 Response spectra of the scaled (at DBE for 20-storey T_1=3.32 s) ground motions used for non-linear dynamic analysis along with the design spectrum of Eurocode 8

4.7 Comparison of the non-linear time history analysis results for MRFs with viscoelastic and MRFs with visco-plastic dampers

4.7.1 Peak storey drift mean value

Fig 4.16 shows the mean value of the peak storey drift, θmax, of the MRF with viscoelastic and visco-plastic dampers (λ equal to 1.0, 0.8, 0.6, 0.4, and 0.2) under the DBE and MCE. For the MRF with viscoelastic dampers, for the 5-storey, θ_{max} is 0.96% under the DBE and 1.42% under the MCE. For the MRF with visco-plastic dampers, θ_{max} is 1.0% (λ=1.0), 1.05% (λ=0.8), 1.13% (λ=0.6), 1.27% (λ=0.4), and 1.47% (λ=0.2) under the DBE, while θ_{max} is 1.61% (λ=1.0), 1.70% (λ=0.8), 1.83% (λ=0.6), 2.02% (λ=0.4), and 2.2% (λ=0.2) under the MCE. The target design of θ_{max} under the DBE is equal to 1.2% (Step 1 of the design procedure in Section 3.2). Therefore, the analysis results show that it is possible to use λ values in the range of 0.4 - 0.6 and still satisfy the design drift requirements under the DBE.

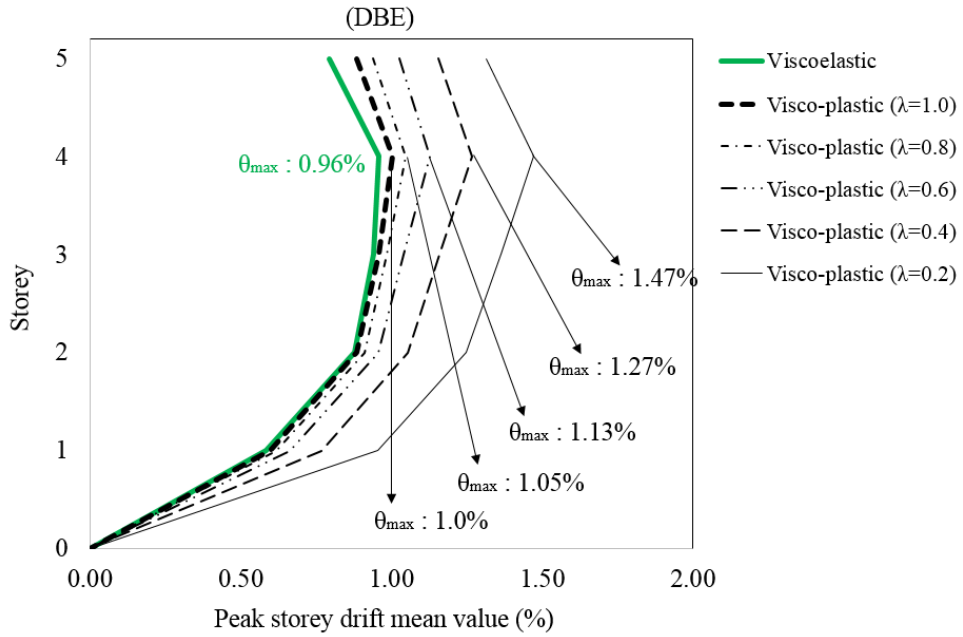

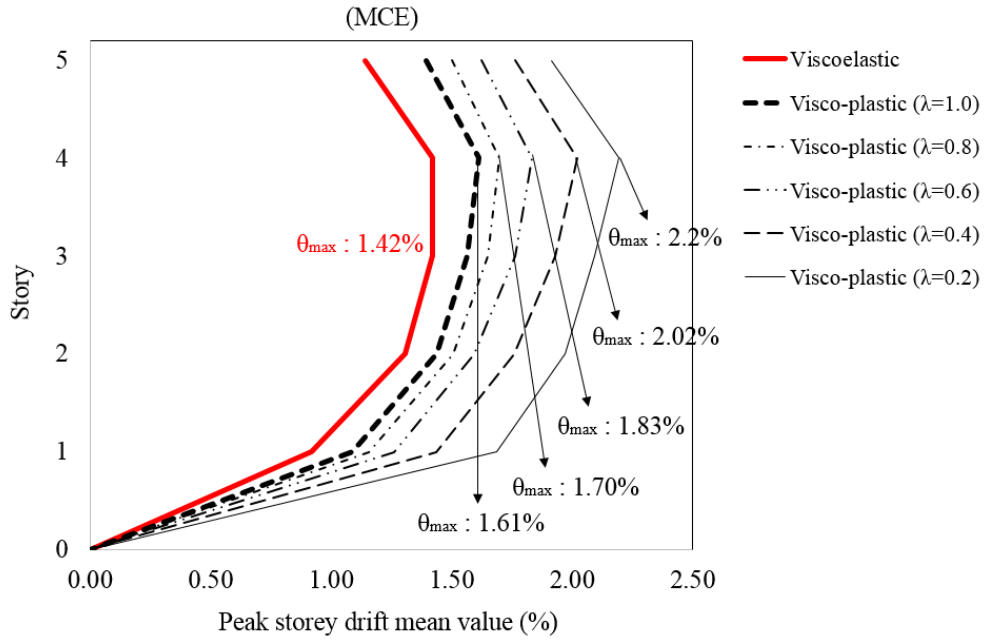

Fig. 4.16 Mean value of the peak storey drift (DBE and MCE) for 5-storey buildings

For the 10-storey building, as can be seen from Fig. 4.17, θ_{max} is 0.93% under the DBE and 1.32% under the MCE for the MRF with viscoelastic dampers. For the MRF with visco-plastic dampers, θ_{max} is 0.93% (λ=1.0), 0.93% (λ=0.8), 0.95% (λ=0.6), 1.05% (λ=0.4), and 1.26% (λ=0.2) under the DBE, while θmax is 1.37% (λ=1.0), 1.39% (λ=0.8), 1.45% (λ=0.6), 1.54% (λ=0.4), and 1.77% (λ=0.2) under the MCE. The target design of θ_{max} under the DBE is equal to 1.0% (Step 1 of the design procedure in Section 3.2). Therefore, the analysis results show that it is possible to use λ values in the range of 0.4 – 1.0 and still satisfy the design drift requirements under the DBE.

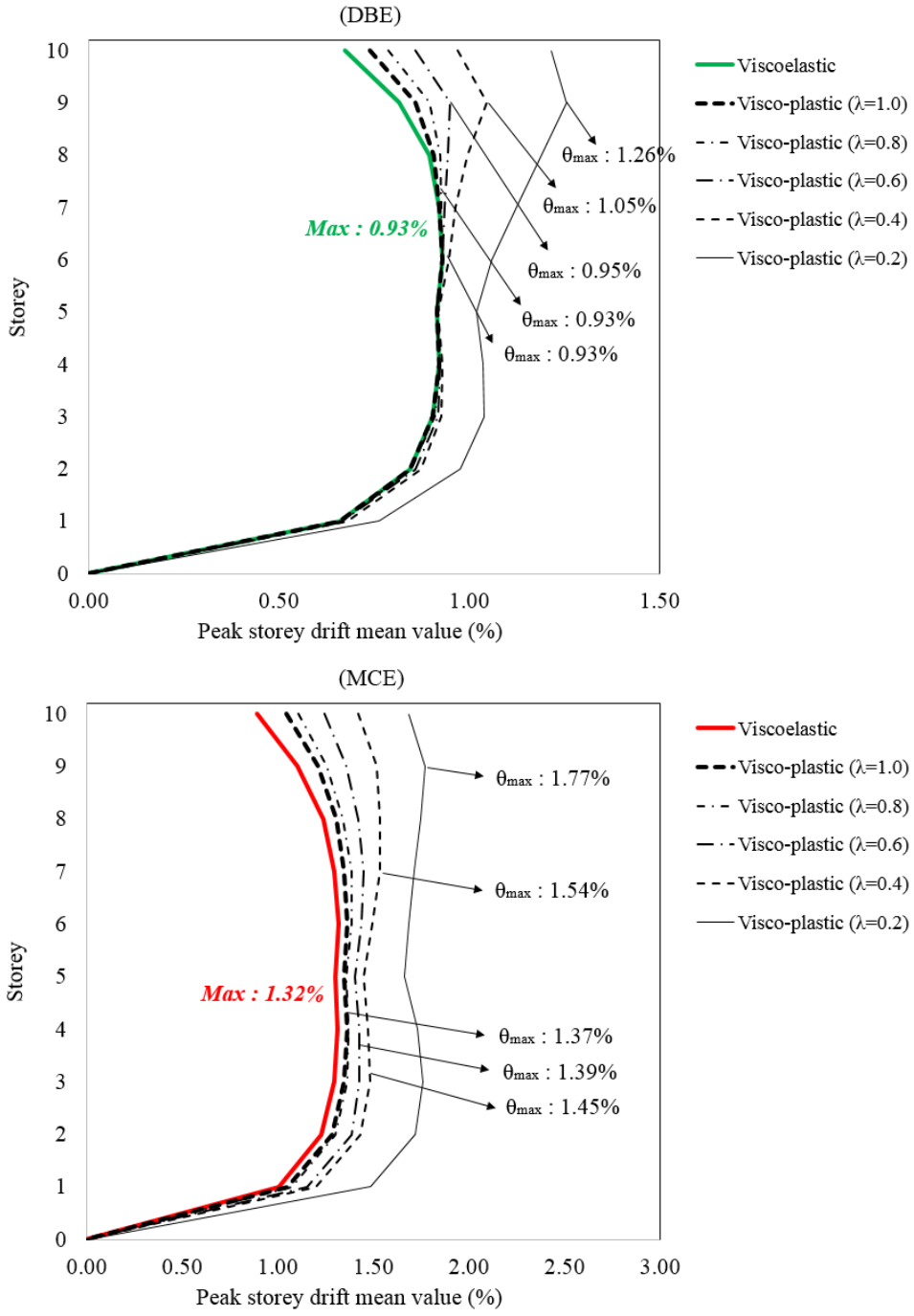

Fig. 4.17 Mean value of the peak storey drift (DBE and MCE) for 10-storey buildings

For the 20-storey building, as can be seen from Fig. 4.18, θ_{max} is 0.62% under the DBE and 0.92% under the MCE for the MRF with viscoelastic damper. For the MRF with visco-plastic dampers, θ_{max} is 0.66% (λ=1.0), 0.69% (λ=0.8), 0.73% (λ=0.6), 0.83% (λ=0.4), and 1.02% (λ=0.2) under the DBE, while θ_{max} is 1.06% (λ=1.0), 1.11% (λ=0.8), 1.19% (λ=0.6), 1.31% (λ=0.4),

and 1.57% (λ=0.2) under the MCE. The target design of θ_{max} under the DBE is equal to 0.6% (Step 1 of the design procedure in Section 3.2). Therefore, the analysis results show that it is possible to use λ values in the range of 0.8 -1.0 and still satisfy the design drift requirements under the DBE.

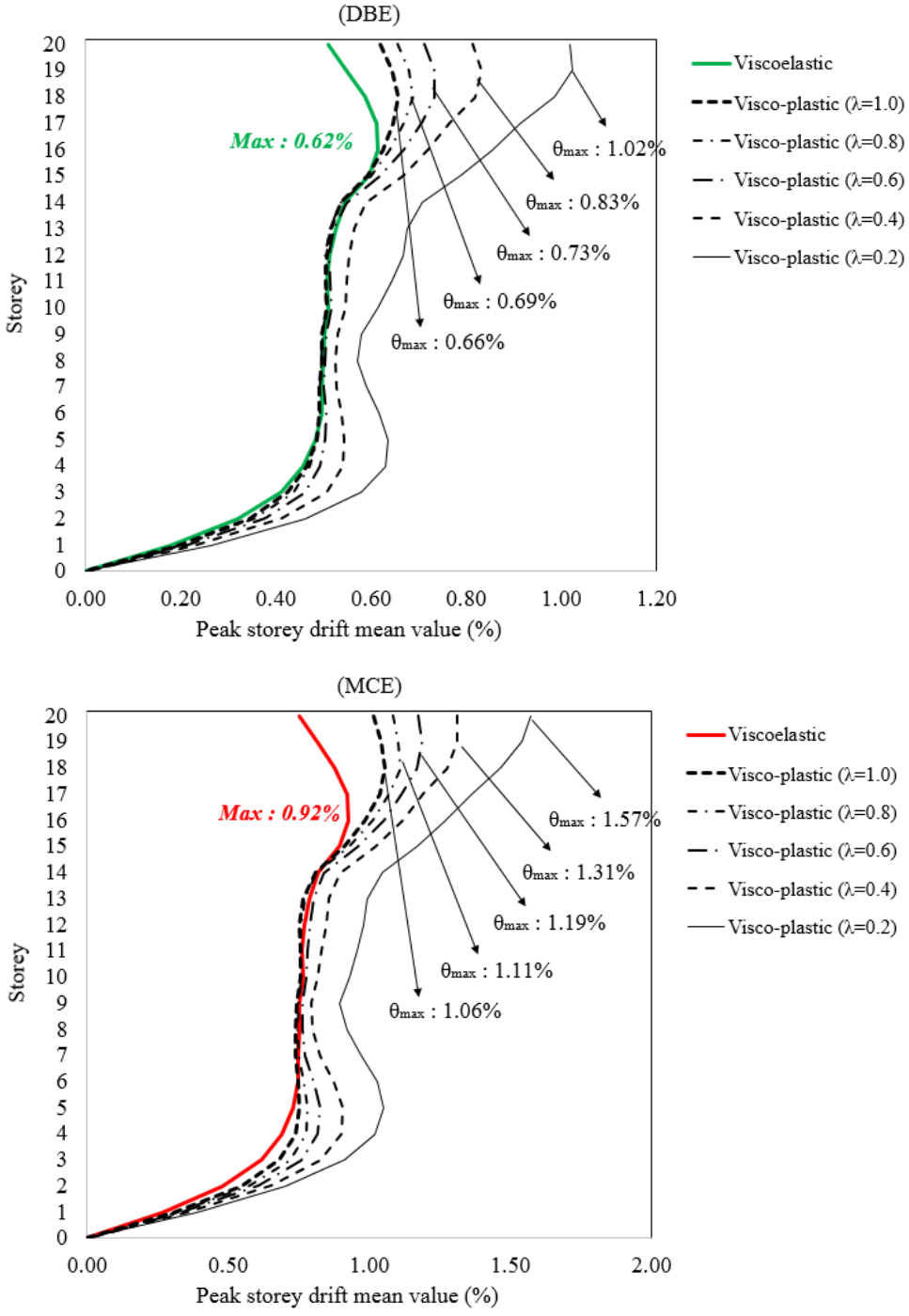

Fig. 4.18 Mean value of the peak storey drift (DBE and MCE) for 20-storey buildings

4.7.2 Base shear

For the 5-storey building, Fig.4.19 shows the base shear mean value for the MRF with viscoelastic and visco-plastic dampers under the DBE and MCE. The results show that there is no significant benefit in terms of reducing the base shear force under the DBE. However, appreciable reductions can be achieved under the MCE. In particular, visco-plastic dampers designed for λ in the range of 0.4-0.6 offer reductions in the peak shear force equal to 17%. On the basis of the results presented in this section, λ values within the range of 0.4-0.6 seem appropriate in terms of reducing drift while also controlling the base shear force.

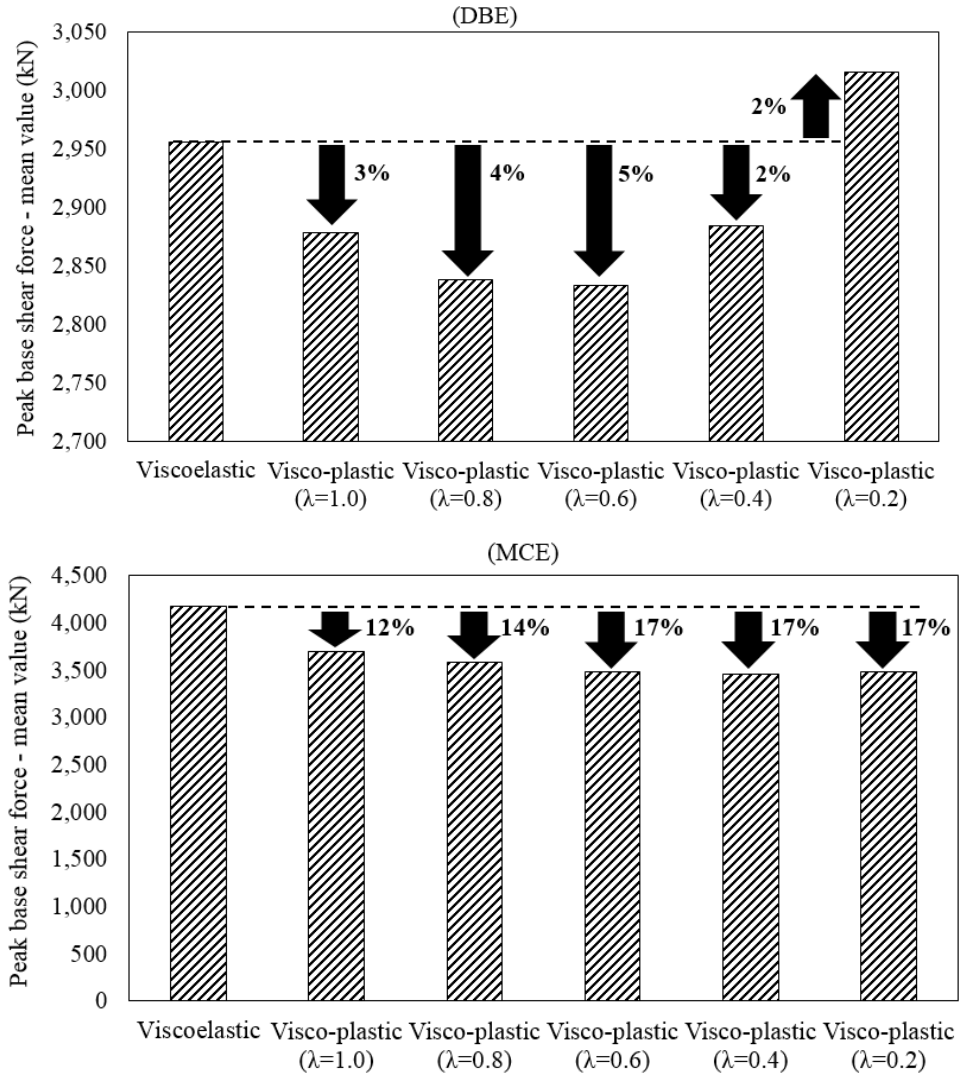

Fig. 4.19 Mean value of the peak base shear force (DBE and MCE) for 5-storey buildings

For the 10-storey building, as can be seen from Fig. 4.20, visco-plastic dampers designed for λ in the range of 0.4-0.6 offer reductions in the peak shear force equal to 18% and 11%, respectively. On the basis of the results presented in this section, λ values within the range of 0.4-0.6 seem suitable in terms of reducing drift while also controlling the base shear force.

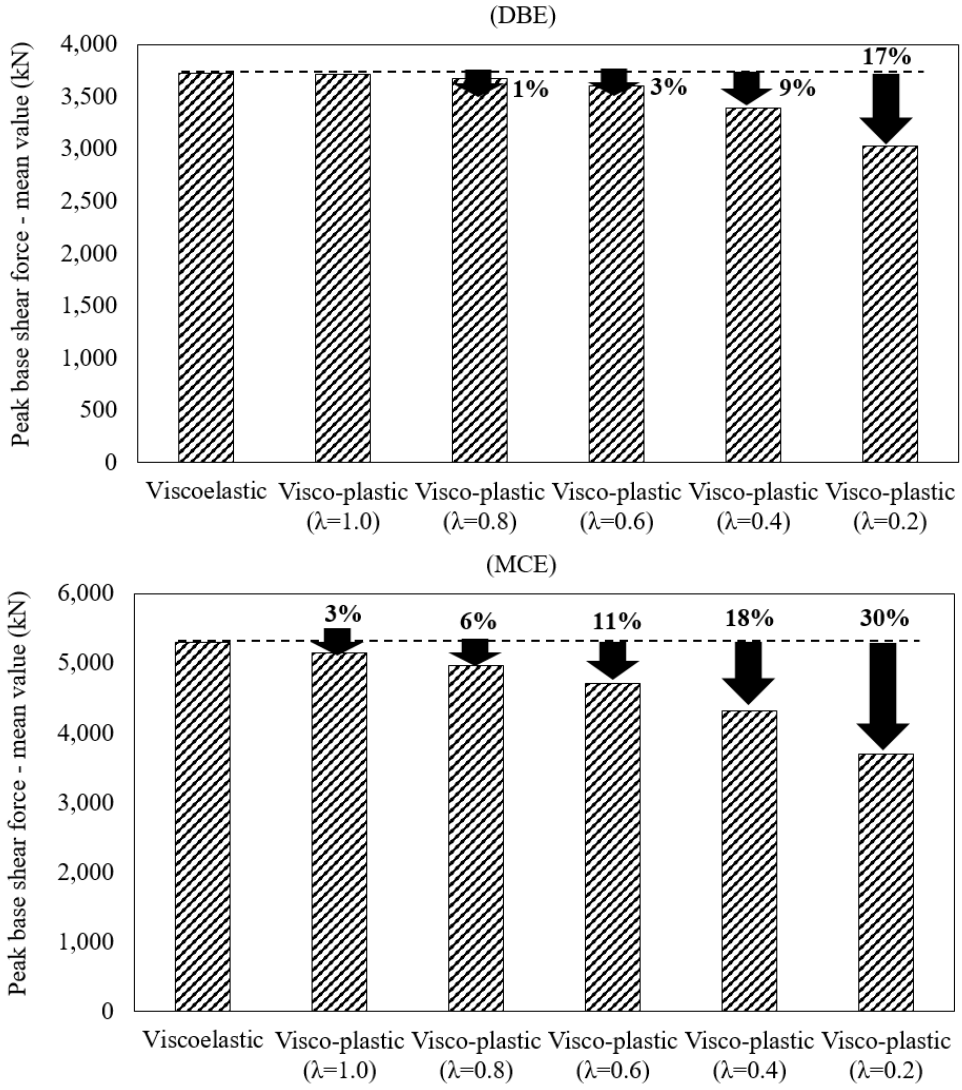

Fig. 4.20 Mean value of the peak base shear force (DBE and MCE) for 10-storey buildings

For the 20-storey building, as can be seen from Fig. 4.21, visco-plastic dampers designed for λ in the range of 0.8-1.0 offer reductions in the peak shear force equal to 15% and 13%, respectively. On the basis of the results presented in this section, λ values within the range of 0.8-1.0 seem appropriate in terms of reducing drift while also controlling the base shear force.

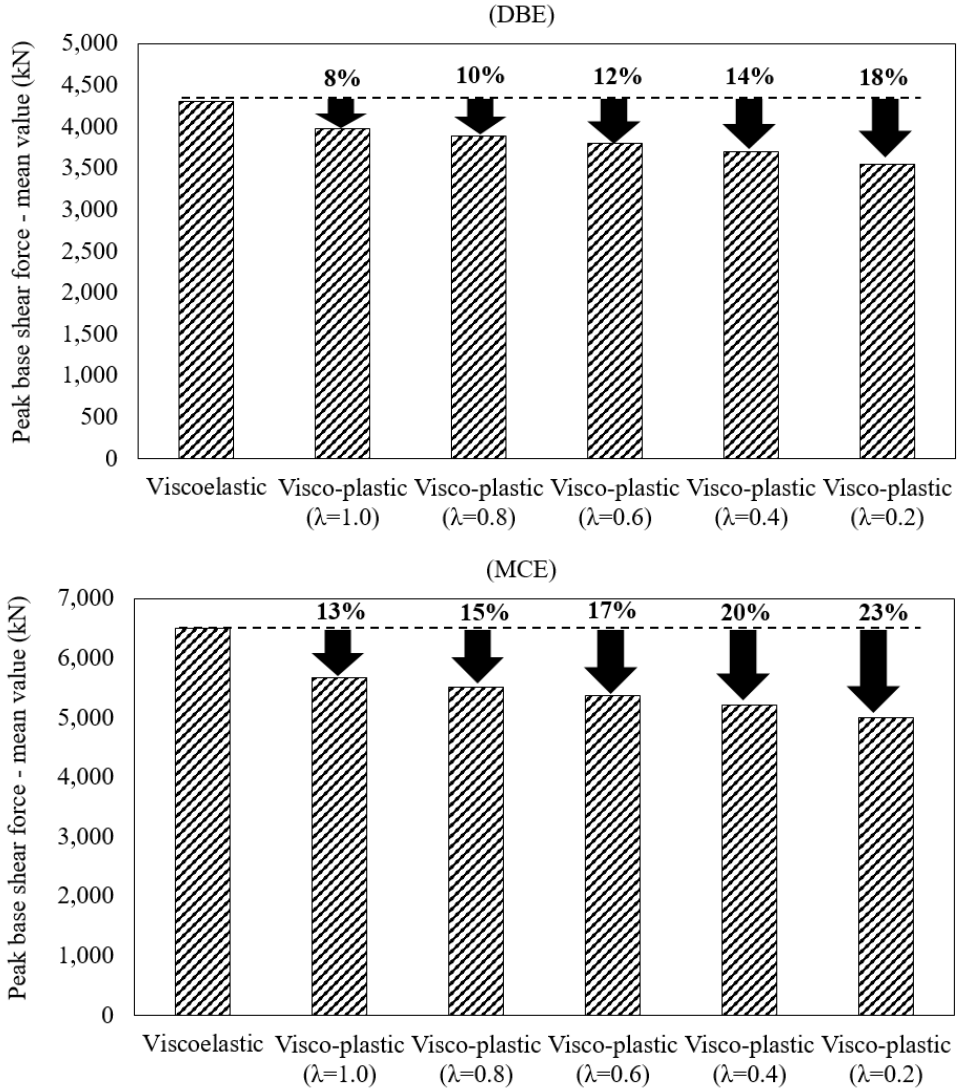

Fig. 4.21 Mean value of the peak base shear force (DBE and MCE) for 20-storey buildings

4.7.3 Hysteresis of the visco-plastic damper

Fig. 4.22 shows the hysteresis of the viscoelastic and friction components of the visco-plastic damper under an earthquake ground motion scaled at the DBE. Overall damper behaviour is governed by the friction device after activation of the friction damper. Also observable here is, as λ decreases (e.g., from λ=1.0 to λ=0.2), the activation force can be reduced, meaning the activation force can be controlled intentionally. The hysteresis of the visco-plastic damper shows a similar result in 10 and 20-storey buildings.

(λ=1.0)

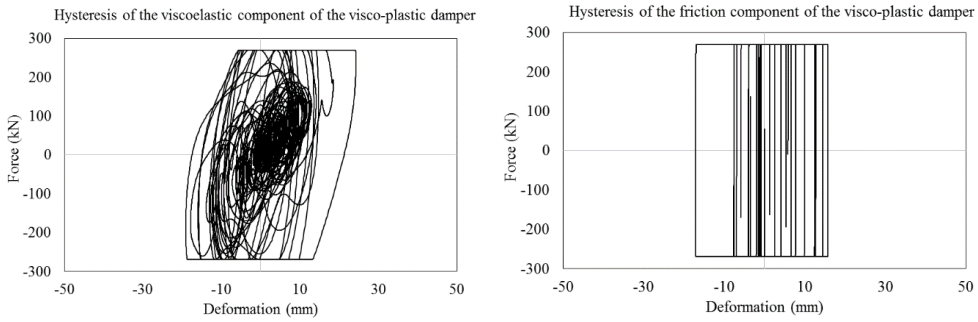

(λ=0.8)

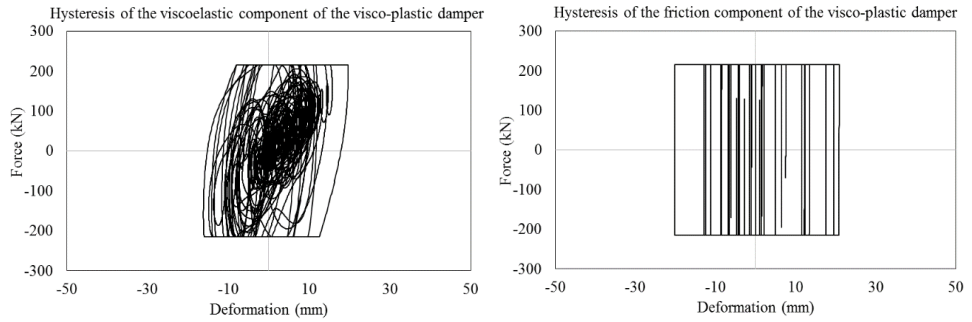

(λ=0.6)

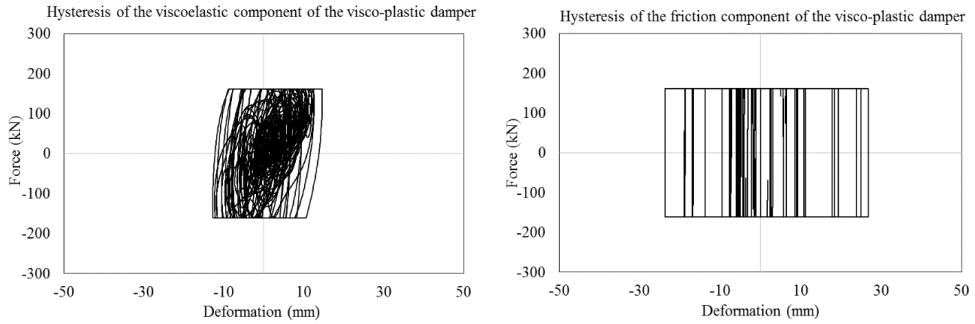

(λ=0.4)

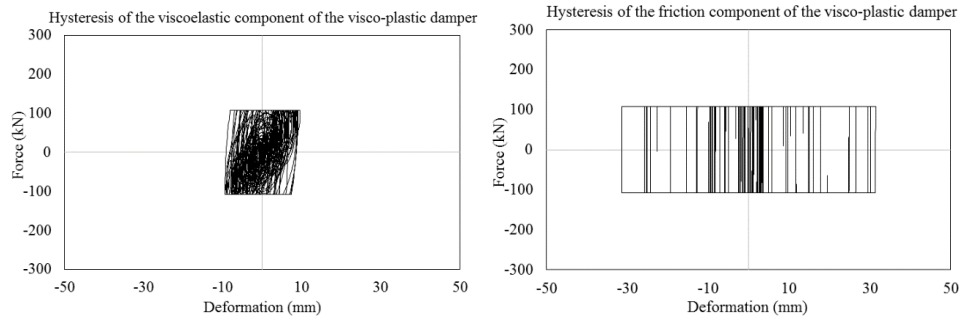

(λ=0.2)

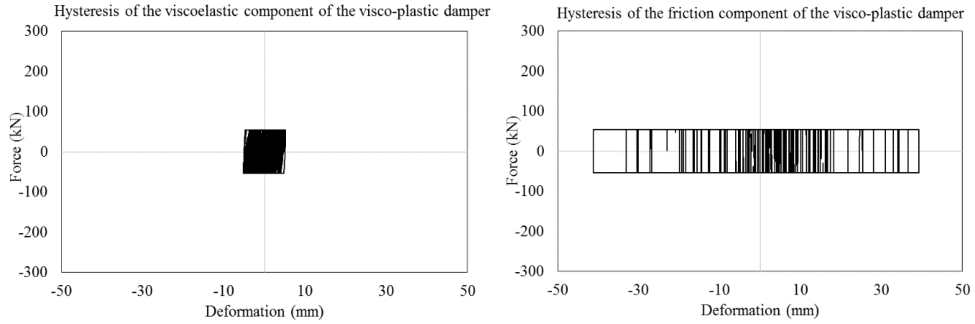

Fig. 4.22 Hysteresis of the viscoelastic and friction components of the visco-plastic damper

4.7.4 Residual drift

Table 4.13 and Table 4.14 compare the median values of the residual storey drift, θr, obtained from non-linear dynamic time history analysis for each storey under the 20 ground motions scaled to the DBE and MCE levels. Even though the θr of the MRFs with visco-plastic dampers are higher than those of the MRF with viscoelastic dampers, they still have very small values under the DBE (lower than 0.17% for λ=1.0 to λ=0.2).

Table 4.13 Median values of the residual drift (%, DBE)

Storey	Viscoelastic	Visco-plastic (λ=1.0)	Visco-plastic (λ=0.8)	Visco-plastic (λ=0.6)	Visco-plastic (λ=0.4)	Visco-plastic (λ=0.2)
5	0.0024	0.0278	0.0334	0.0355	0.0556	0.1218
4	0.0045	0.0265	0.0373	0.0399	0.0671	0.1601
3	0.0055	0.0202	0.0281	0.0296	0.0593	0.1566

2	0.0054	0.0207	0.0237	0.0229	0.0542	0.1410
1	0.0070	0.0208	0.0236	0.0283	0.0691	0.1573

Table 4.14 Median values of the residual drift (%, MCE)

Storey	Viscoelastic	Visco-plastic (λ=1.0)	Visco-plastic (λ=0.8)	Visco-plastic (λ=0.6)	Visco-plastic (λ=0.4)	Visco-plastic (λ=0.2)
5	0.0565	0.1727	0.1999	0.2678	0.3534	0.4124
4	0.0946	0.2446	0.2882	0.3652	0.4552	0.4999
3	0.1101	0.2912	0.3415	0.4144	0.4855	0.5388
2	0.0996	0.2917	0.3377	0.3998	0.4728	0.5555
1	0.1128	0.3009	0.3478	0.3979	0.4690	0.5872

For the use of visco-plastic dampers in 10 and 20-storey buildings, the trend is similar to that of the 5-storey equivalent. As can be seen from Table 4.15 to Table 4.18, the θr of the MRFs with visco-plastic dampers is higher than that of the MRF with viscoelastic dampers, however, values under the DBE are very small, i.e. lower than 0.19% for λ=1.0 to λ=0.2 in the 10-storey building, and lower than 0.14% for λ=1.0 to λ=0.2 in the 20-storey building.

Table 4.15 Median values of the residual drift (%, DBE)

Storey	Viscoelastic	Visco-plastic (λ=1.0)	Visco-plastic (λ=0.8)	Visco-plastic (λ=0.6)	Visco-plastic (λ=0.4)	Visco-plastic (λ=0.2)
10	0.0103	0.0285	0.0535	0.0830	0.1121	0.1908
9	0.0156	0.0323	0.0559	0.0841	0.1086	0.1900
8	0.0238	0.0330	0.0513	0.0743	0.0948	0.1672
7	0.0297	0.0280	0.0408	0.0550	0.0731	0.1386
6	0.0295	0.0290	0.0306	0.0384	0.0520	0.1167
5	0.0281	0.0280	0.0301	0.0349	0.0401	0.1051
4	0.0282	0.0285	0.0315	0.0365	0.0389	0.0994
3	0.0279	0.0286	0.0325	0.0388	0.0403	0.1026
2	0.0329	0.0339	0.0385	0.0466	0.0477	0.1137
1	0.0384	0.0390	0.0436	0.0520	0.0521	0.1192

Table 4.16 Median values of the residual drift (%, MCE)

Storey	Viscoelastic	Visco-plastic (λ=1.0)	Visco-plastic (λ=0.8)	Visco-plastic (λ=0.6)	Visco-plastic (λ=0.4)	Visco-plastic (λ=0.2)
10	0.0659	0.1352	0.1708	0.2399	0.3093	0.3482
9	0.0923	0.1459	0.1925	0.2542	0.3268	0.3808
8	0.1180	0.1463	0.2017	0.2577	0.3282	0.4136
7	0.1323	0.1464	0.1940	0.2487	0.3248	0.4240
6	0.1368	0.1471	0.1809	0.2347	0.3219	0.4237
5	0.1385	0.1493	0.1784	0.2201	0.3138	0.4220
4	0.1426	0.1570	0.1865	0.2224	0.3182	0.4503
3	0.1448	0.1652	0.1977	0.2352	0.3318	0.4764
2	0.1478	0.1725	0.2093	0.2506	0.3478	0.5077
1	0.1552	0.1787	0.2163	0.2593	0.3504	0.5085

Table 4.17 Median values of the residual drift (%, DBE)

Storey	Viscoelastic	Visco-plastic (λ=1.0)	Visco-plastic (λ=0.8)	Visco-plastic (λ=0.6)	Visco-plastic (λ=0.4)	Visco-plastic (λ=0.2)
20	0.0016	0.0215	0.0329	0.0483	0.0397	0.1463
19	0.0018	0.0229	0.0330	0.0462	0.0383	0.1400
18	0.0023	0.0228	0.0312	0.0409	0.0325	0.1212
17	0.0027	0.0193	0.0257	0.0320	0.0251	0.0838
16	0.0032	0.0142	0.0197	0.0241	0.0212	0.0581
15	0.0037	0.0090	0.0136	0.0185	0.0163	0.0538
14	0.0040	0.0057	0.0086	0.0134	0.0136	0.0480
13	0.0045	0.0049	0.0067	0.0105	0.0138	0.0450
12	0.0050	0.0050	0.0064	0.0091	0.0143	0.0410
11	0.0055	0.0053	0.0067	0.0088	0.0144	0.0332
10	0.0060	0.0060	0.0074	0.0098	0.0143	0.0250
9	0.0065	0.0069	0.0083	0.0114	0.0145	0.0187
8	0.0071	0.0081	0.0100	0.0130	0.0160	0.0161
7	0.0076	0.0097	0.0121	0.0140	0.0184	0.0183
6	0.0080	0.0121	0.0142	0.0151	0.0211	0.0258
5	0.0084	0.0146	0.0150	0.0170	0.0235	0.0335
4	0.0086	0.0157	0.0160	0.0193	0.0236	0.0364
3	0.0079	0.0150	0.0166	0.0199	0.0192	0.0302
2	0.0049	0.0119	0.0127	0.0151	0.0113	0.0171
1	0.0047	0.0081	0.0078	0.0078	0.0063	0.0082

Table 4.18 Median values of the residual drift (%, MCE)

Storey	Viscoelastic	Visco-plastic (λ=1.0)	Visco-plastic (λ=0.8)	Visco-plastic (λ=0.6)	Visco-plastic (λ=0.4)	Visco-plastic (λ=0.2)
20	0.0174	0.1373	0.1614	0.2016	0.2702	0.3026
19	0.0200	0.1338	0.1576	0.1942	0.2599	0.2900
18	0.0245	0.1224	0.1444	0.1759	0.2339	0.2653
17	0.0285	0.0973	0.1145	0.1376	0.1812	0.2183
16	0.0308	0.0692	0.0812	0.0951	0.1229	0.1601
15	0.0296	0.0503	0.0588	0.0724	0.0922	0.1287
14	0.0267	0.0327	0.0406	0.0544	0.0710	0.1064
13	0.0233	0.0208	0.0288	0.0432	0.0573	0.0904
12	0.0198	0.0134	0.0214	0.0377	0.0527	0.0787
11	0.0156	0.0090	0.0158	0.0319	0.0468	0.0645
10	0.0130	0.0081	0.0107	0.0240	0.0383	0.0587
9	0.0112	0.0120	0.0167	0.0279	0.0390	0.0606
8	0.0127	0.0201	0.0265	0.0416	0.0504	0.0796
7	0.0168	0.0313	0.0390	0.0595	0.0699	0.1088
6	0.0204	0.0443	0.0571	0.0803	0.0936	0.1326
5	0.0224	0.0581	0.0762	0.0988	0.1064	0.1376
4	0.0216	0.0704	0.0868	0.1029	0.1023	0.1221
3	0.0170	0.0687	0.0796	0.0859	0.0824	0.0882
2	0.0087	0.0510	0.0551	0.0546	0.0501	0.0460
1	0.0047	0.0238	0.0236	0.0222	0.0172	0.0289

4.8 Optimum lambda factors based on the seismic performance under the design and maximum considered earthquake intensities

Optimisation will propose a suitable λ factor that achieves the target seismic performance by different parameter study and simultaneously reduce the base shear. In this thesis, five parameter studies of λ equal to 1.0, 0.8, 0.6, 0.4 and 0.2 were conducted for purposes of optimisation. Numerical analysis results showed λ values within the range of 0.4-0.6 for the 5-storey building, which seems appropriate in terms of reducing drift while also controlling the base shear force. For the visco-plastic dampers used in the 10-storey building, λ

values were within the range of 0.4-0.6, and in the 20-storey building activation force λ values were within the range of 0.8-1.0.

The interesting finding here is that when visco-plastic dampers are used in the MRF, there is small decrease in the reduction of base shear under DBE, however, if the seismic intensity is greater, for example at a strong earthquake level such as MCE, it shows a significant reduction in the base shear.

When the visco-plastic damper is applied to low storey buildings (5 and 10-storey), the appropriate activation points of the friction device at a load of 40 to 60% of the viscoelastic damper are advantageous in reducing the base shear force whilst still achieving the overall performance target.
On the other hand, when the visco-plastic damper is applied to higher storey structures (20-storey), the activation force of the friction devices suggests a larger value (e.g. 80-100% of the viscoelastic damper peak force under DBE).

4.9 Summary

In this chapter, parametric designs of visco-plastic dampers with different activation forces for their friction devices were carried out and compared with the results of viscoelastic damper performance tests for 5, 10, and 20-storey buildings. The activation force of the friction device was designed on the basis of the λ factor, which reflects the ratio of the peak force of the visco-plastic damper to the peak force of a viscoelastic damper under the DBE. A non-linear dynamic analysis for a set of 20 earthquake ground motions scaled to the DBE and MCE was carried out in OpenSees. This was based on the results of the simplified design procedure and non-linear seismic response analyses under both the design basis earthquake and the maximum considered earthquake. The following conclusions were drawn:

1) The 5-storey building results highlight the advantages of the visco-plastic damper. From the results presented in this thesis, it was identified that appropriate values of the λ factor might be within 0.4 to 0.6. In particular, visco-plastic dampers designed for λ within 0.4

to 0.6 were found to satisfy the strict peak storey drift under the DBE, while achieving a reduction in the peak base shear force equal to 17%. Regarding residual drift, θr, the visco-plastic damper shows values below 0.1% from λ=1.0 to λ=0.2, under DBE intensity level. These values are below the 0.5% limitation for economically replaceable residual drift. The median values of the residual drift gradually increase under MCE intensity level. However, they remain under 0.5% until λ=0.4. These results imply that MRFs fitted with visco-plastic dampers are an economical means of improving resilience performance.

2) For the 10 and 20-storey buildings, the proper values of the λ factor may be within 0.4 to 0.6 for 10-storey, and 0.8 to 1.0 for 20-storey buildings, respectively. In particular, visco-plastic dampers designed for λ within 0.4 to 0.6 were found to satisfy the strict peak storey drift under the DBE, while achieving a reduction in the peak base shear force equal to 11~18% in 10-storey buildings, and λ within 0.8 to 1.0 were found to satisfy the strict peak storey drift under the DBE while achieving a reduction in the peak base shear force equal to 13~15% in 20-storey buildings. Regarding residual drift, θr, the visco-plastic damper shows values below 0.19% for λ=1.0 to λ=0.2 in 10-storey buildings, and lower than 0.14% for λ=1.0 to λ=0.2 in 20-storey buildings. These values are below the 0.5% limitation for economically replaceable residual drift. The median values of the residual drift gradually increase under MCE intensity level. However, they remain under 0.5% until λ=0.2 in 10-storey buildings, and under 0.4% until λ=0.2 in 20-storey buildings. These results suggest that MRFs fitted with visco-plastic dampers also offer benefit in terms of economical means for improving resilience performance, even in tall buildings (10 and 20-storey).

Chapter 5.

Collapse assessment of a building fitted with visco-plastic dampers

---

5.1 Introduction

In this chapter, incremental dynamic analyses up to point of collapse are conducted for 5-storey MRFs with visco-plastic or viscoelastic dampers. The response databank is used to develop the collapse fragility curves of the two MRFs and draw conclusions relevant to the effect of the visco-plastic damper on the probability of collapse..

5.2 Collapse evaluation using Incremental Dynamic Analysis

To evaluate vulnerability to collapse, IDA (Incremental Dynamic Analysis) was carried out on the MRFs with viscoelastic and with visco-plastic dampers using a set of 20 far-field seismic records. The IDA results for all steel MRFs with viscoelastic and visco-plastic dampers (from λ=1.0 to λ=0.2) are shown in Fig. 5.1, where it can be seen that Sa(T_1) increases gradually until the IDA curve flattens out at certain Sa (T_1) level, which represents dynamic instability and a loss of lateral resistance. This procedure is employed to estimate collapse at a specific seismic intensity, Sa(T_1), under a particular ground motion.

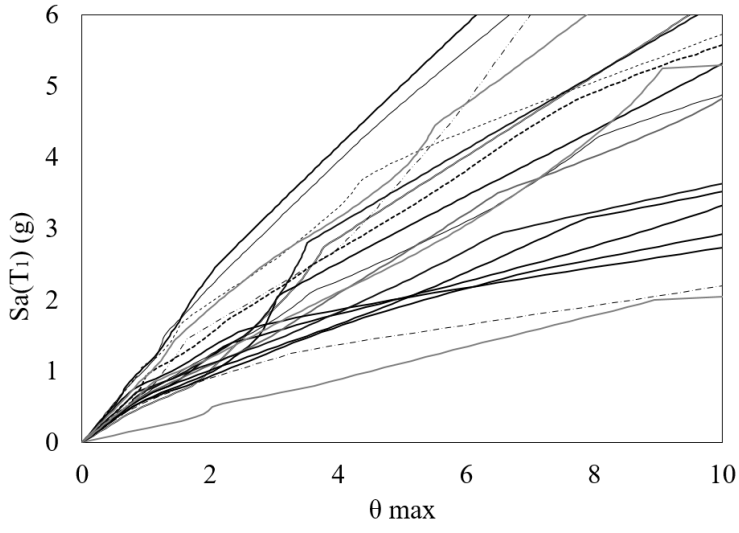

(Viscoelastic)

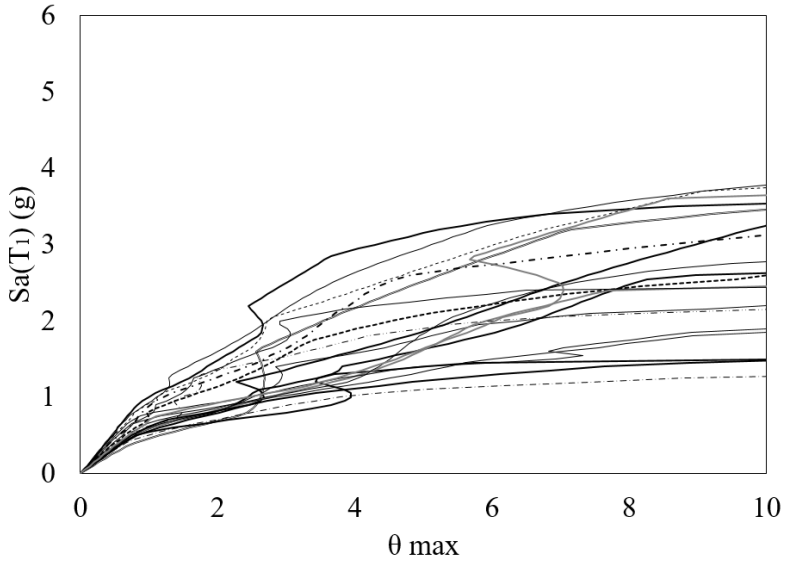

(λ=1.0)

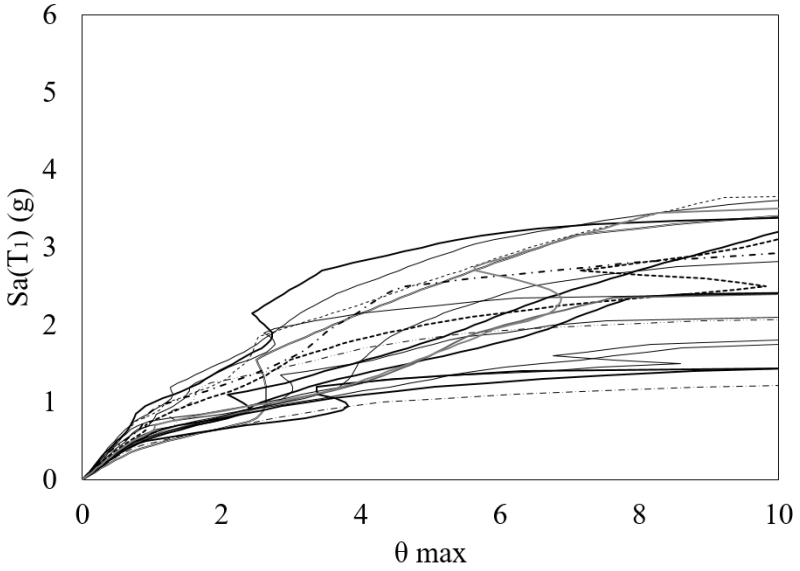

(λ=0.8)

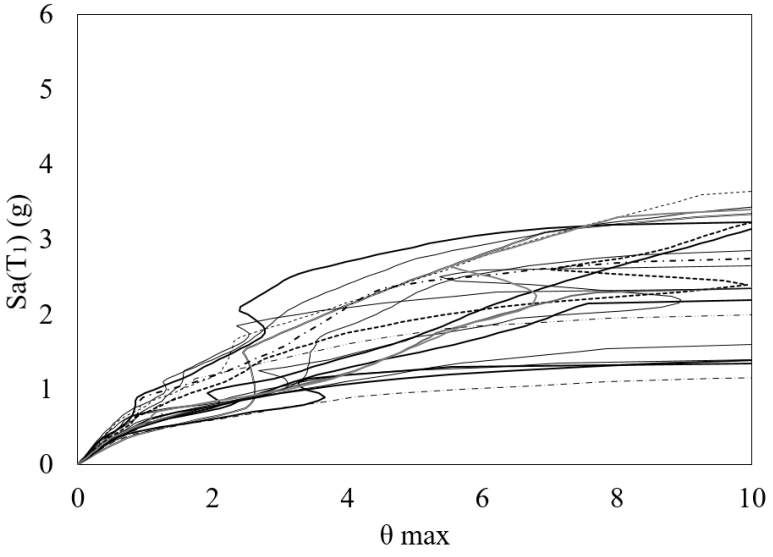

(λ=0.6)

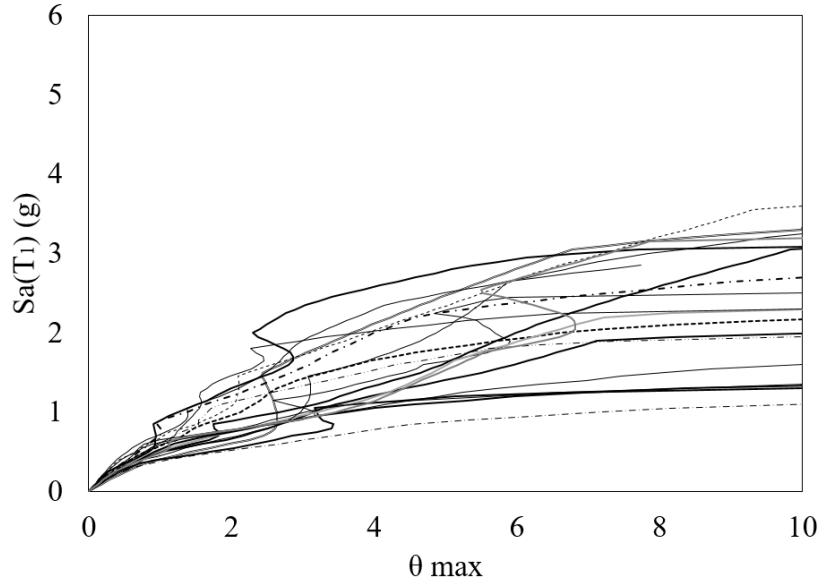

(λ=0.4)

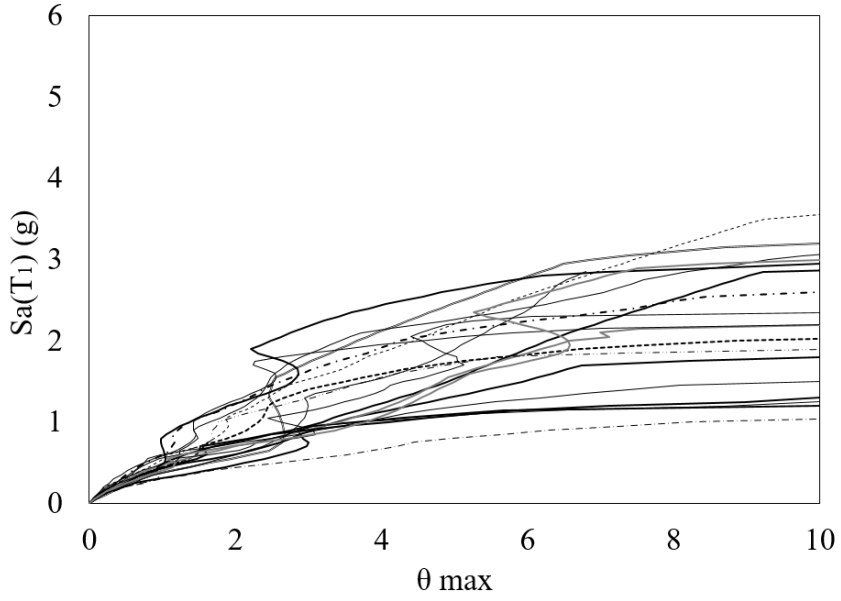

(λ=0.2)

Fig. 5. 1 IDA analysis result for 5-storey MRFs with viscoelastic and visco-plastic dampers.

An interesting finding from the IDA results is that MRFs with viscoelastic dampers have higher θmax values than MRFs with visco-plastic dampers (from λ=1.0 to λ=0.2) at the $Sa(T_1)$ value at which collapse occurs (e.g. the $Sa(T_1)$ mean value for each system causing collapse using a set of 20 pairs of ground motions is, respectively, 5.5% for MRFs with viscoelastic dampers, 2.9% for λ=1.0, 2.8% for λ=0.8, 2.7% for λ=0.6, 2.6% for λ=0.4, and 2.5% for λ=0.2.)

5.3 Effect of λ factor on collapse fragility

The collapse probability curve can be estimated from the result of the IDA analysis (Baker, 2011). Baker indicate that collapse probability function is rewarded as effective technique in estimating the collapse likelihood of the structural response using dynamic structural analysis at a specific period. It is scaling up seismic intensity until spectral acceleration cause the building collapse.

As can be seen from Fig. 5.2,

the probability function is used as follow;

$$P(C \mid Sa = x) = \Phi\left(\frac{\ln x - \mu}{\beta}\right) \quad (5\text{-}1)$$

Where, $P(C \mid Sa = x)$ is collapse probability at Sa=x.

$\Phi(\,)$ = normal cumulative distribution function

μ = mean value of Sa

β = standard deviation of logSa which represents dispersion of Sa.

$$\hat{\mu} = \frac{1}{n}\sum_{i=1}^{n} \ln Sa_i \quad (5\text{-}2)$$

$$\hat{\beta} = \sqrt{\frac{1}{n-1}\sum_{i=1}^{n}\left(\ln Sa_i - \hat{\mu}\right)^2} \quad (5\text{-}3)$$

Where,

n = ground motions number,

Sai = Sa when the structure collapse starts to begin under specific i-th ground motion

$\hat{\mu}$ =mean value of the lognormal Sa making the building collapse.

$\hat{\beta}$ = standard deviation of the lognormal Sa making the building collapse.

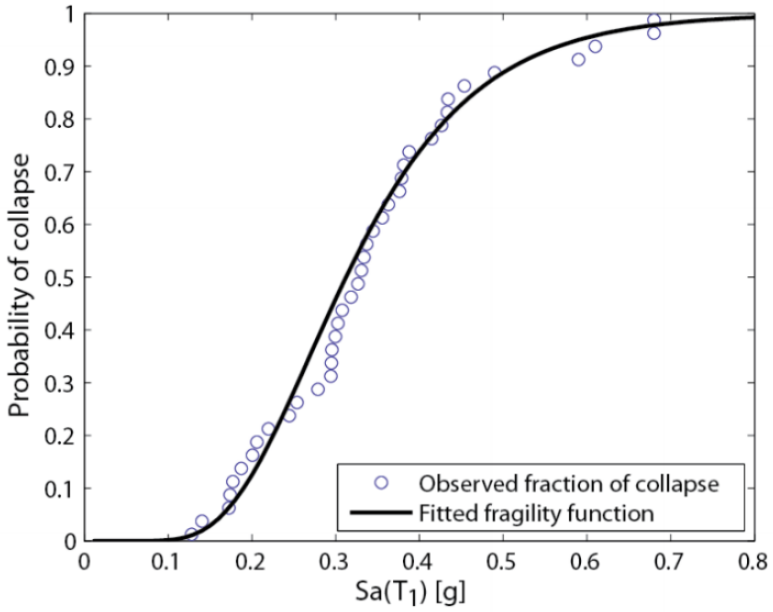

Fig. 5. 2 Fitted fragility curve adopted from Baker, 2011

Using the spectral acceleration values Sa1, Sa2 and Sa3, which lead to the collapse of the structure, as normalized by using the acceleration at the MCE level (Sa,Mce) as X_2, Arrange the values in ascending order. (Y_2) (e.g., in this paper, a total of 20 seismic loads are used, and Sa1 and Sa2 are sorted in ascending order, and then the value of Sa, which causes the smallest collapse in Y2 column, The 1/20 of Y2 column means that the probability of earthquake load collapse is 5% for a building with a total of 20 earthquake ground motions. This means 100% collapse probability. Fig. 5.3 (λ=1.0 to λ=0.2) shows fitted dot data of the fragility curve of MRFs with visco-plastic dampers.

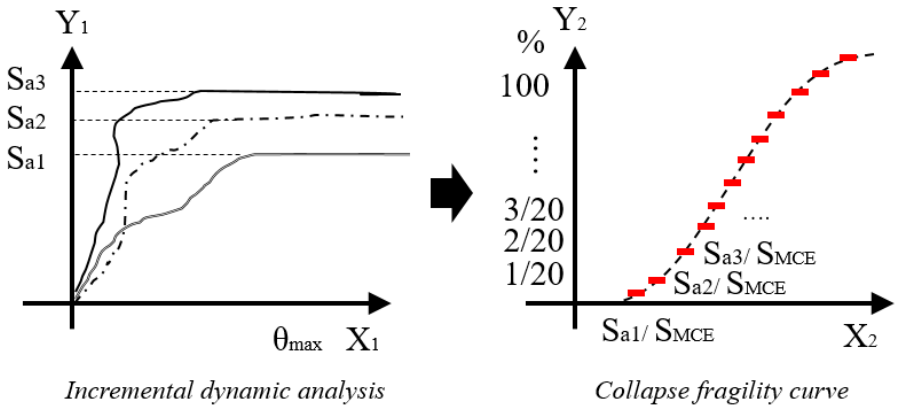

Fig. 5. 3 Fitted dot data of the fragility curve from IDA results

From this procedures, Fig 5.4 shows the fitted dot data of the fragility curve of MRFs with visco-plastic damper from λ=1.0 to λ=0.2

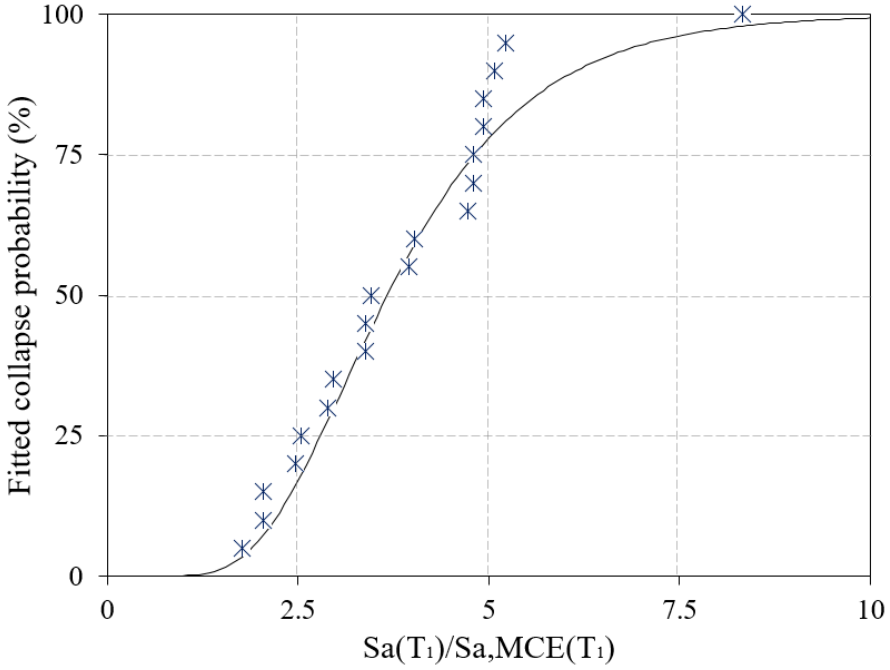

(λ=1.0)

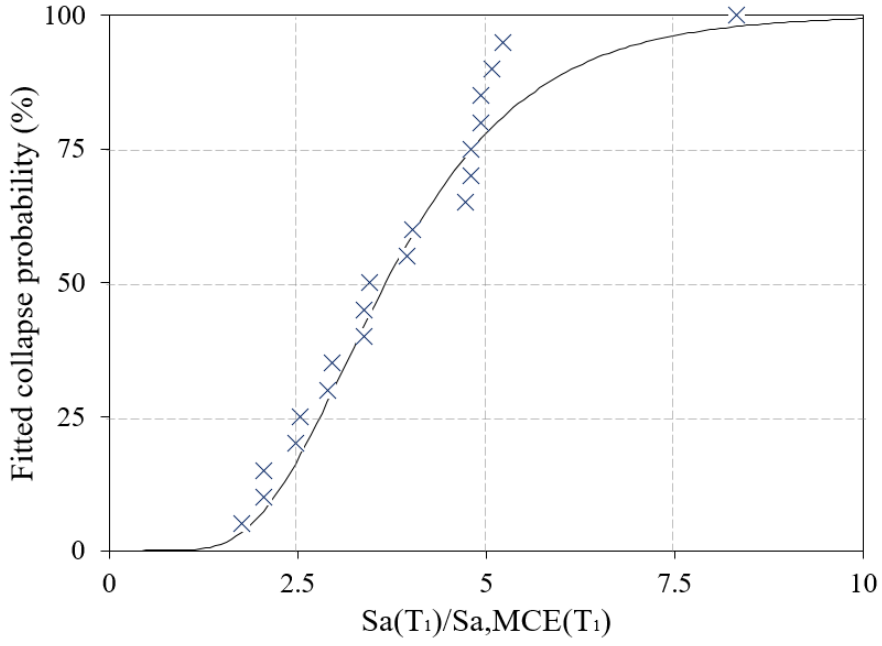

(λ=0.8)

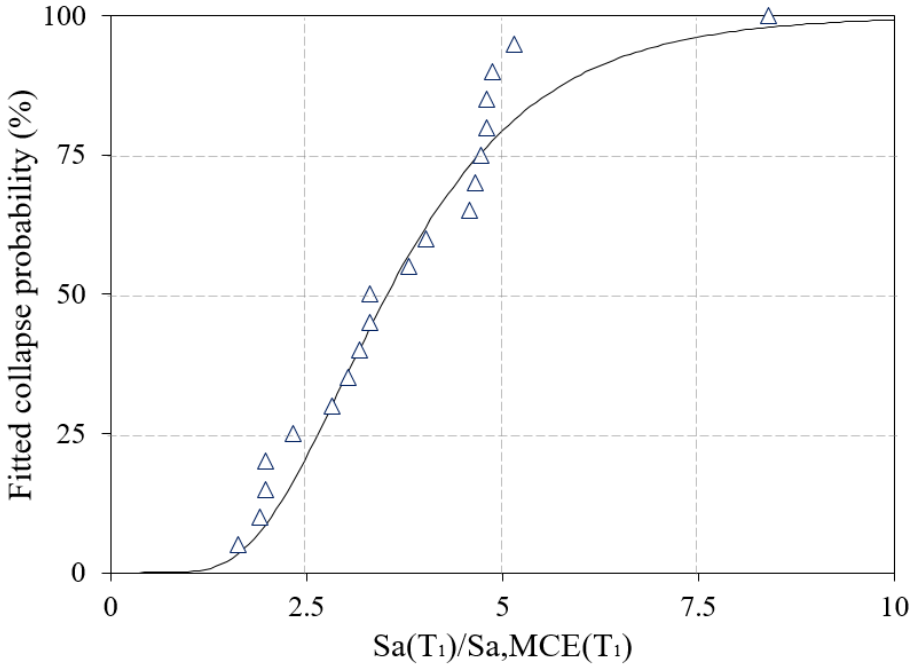
100
75
50
25
0
Fitted collapse probability (%)
0
2.5
5
7.5
10
Sa(T1)/Sa,MCE(T1)

(λ=0.6)

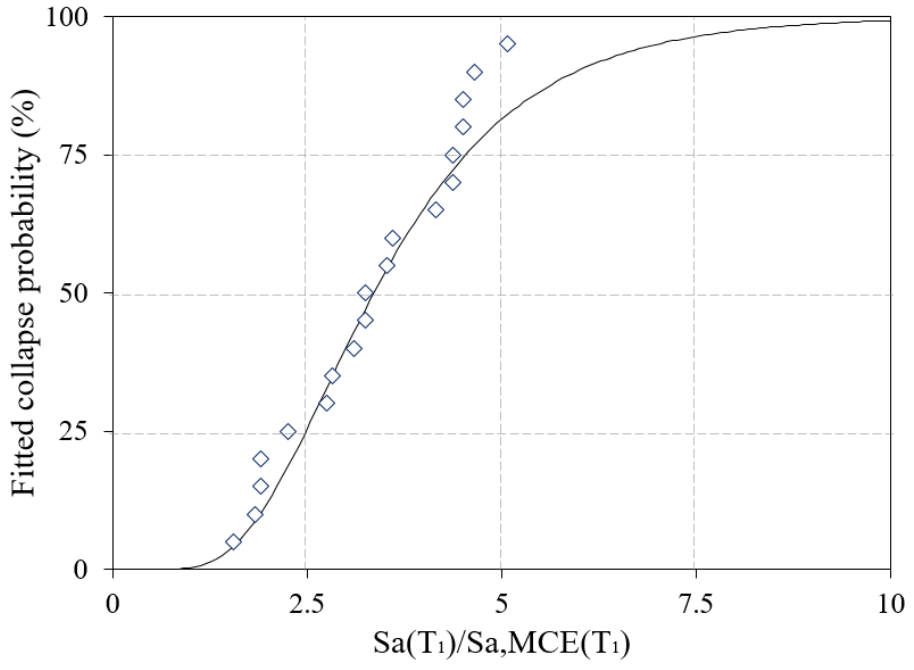
100
75
50
25
0
Fitted collapse probability (%)
0
2.5
5
7.5
10
Sa(T1)/Sa,MCE(T1)

(λ=0.4)

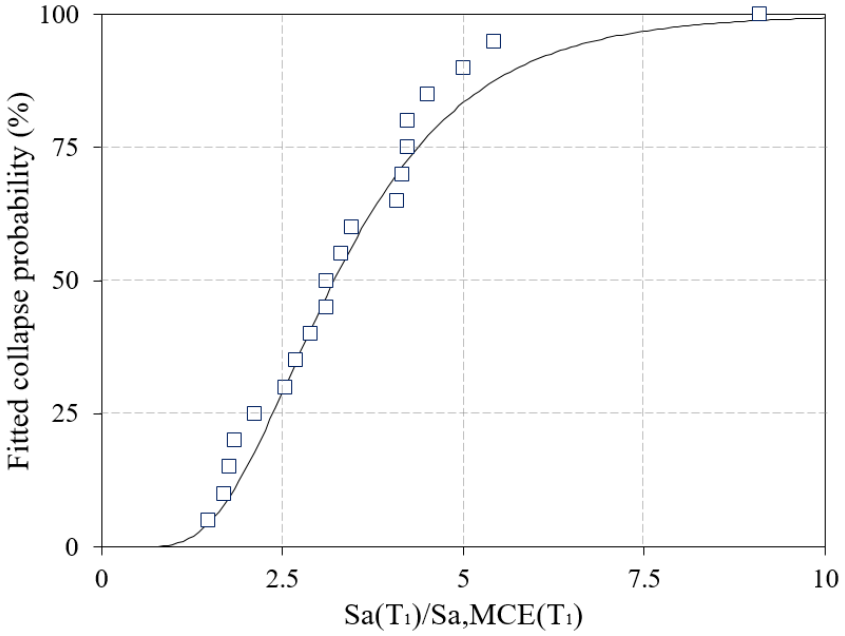

(λ=0.2)

Fig. 5. 4 Fitted dot data of the fragility curve of MRFs with visco-plastic dampers (λ=1.0 to λ=0.2)

Fig. 5.5 shows collapse fragility curve of MRFs with viscoelastic and visco-plastic dampers. As can be seen from Fig. 5.5, the $Sa(T_1)$ value corresponding to 50% probability of collapse is 5.7·Sa, $MCE(T_1)$ for the steel MRFs with viscoelastic dampers, 3.8·Sa,MCE(T1) for the steel MRFs with visco-plastic dampers designed for λ=1.0, 3.7·Sa, MCE(T1) for the steel MRFs with visco-plastic dampers designed for λ=0.8, 3.6·Sa, $MCE(T_1)$ for the steel MRFs with visco-plastic dampers designed for λ=0.6, 3.4·Sa, $MCE(T_1)$ for the steel MRFs with visco-plastic dampers designed for λ=0.4, and 3.2·Sa, and $MCE(T_1)$ for the steel MRFs with visco-plastic dampers designed for λ=0.2. The aforementioned values clearly indicate that as λ decreases, the 50% collapse resistance of the steel MRF decreases. Moreover, the viscoelastic dampers clearly provide higher collapse resistance than that achieved by the visco-plastic dampers for the whole range of seismic intensities. It should be pointed out, however, that for seismic intensities equal to or lower than 2.5 times the intensity of the MCE, the probability of collapse of the steel MRFs with the visco-plastic dampers is very small (i.e. less than 5%) for all the examined values of λ. Therefore, from a design point of view, the visco-

plastic damper can be used without any concern for the collapse resistance of steel MRFs.

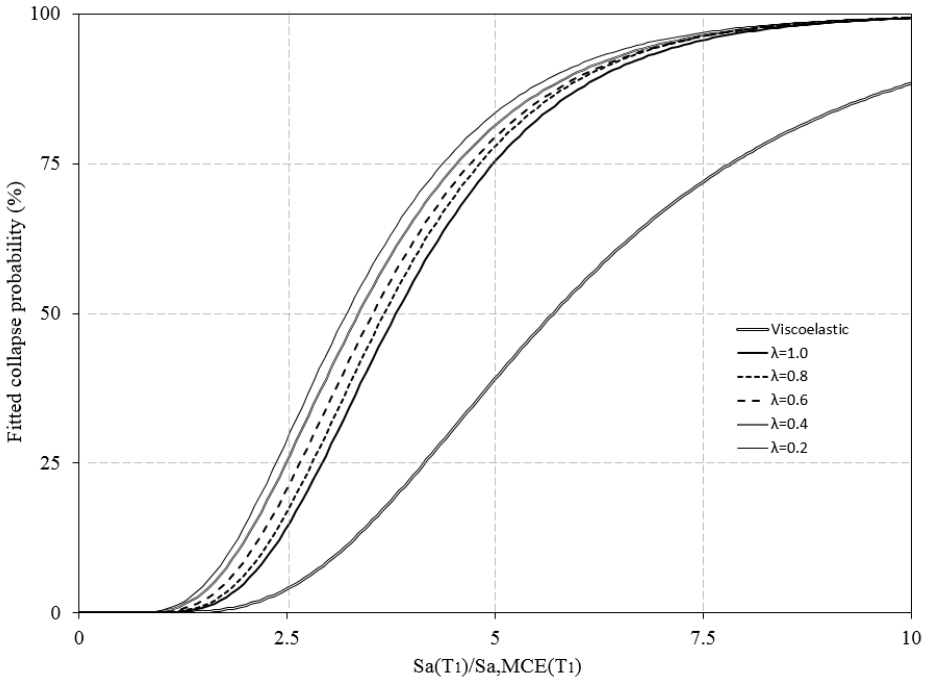

Fig. 5. 5 Collapse fragility curve of MRFs with viscoelastic and visco-plastic dampers.

5.4 Summary

In this chapter, IDA (Incremental Dynamic Analysis) was carried out on 5-storey steel MRFs with viscoelastic and visco-plastic dampers to determine their collapse resistance under 20 far-field seismic records. Sa(T_1) increases gradually until the MRFs with viscoelastic or visco-plastic dampers become dynamically unstable and lose lateral resistance. The results reveal that the MRFs with viscoelastic dampers have higher θ_{max} values than MRFs with visco-plastic dampers (from λ=1.0 to λ=0.2) at the Sa (T_1) value that leads to collapse.

In addition, the collapse fragility curve for MRFs with viscoelastic and visco-plastic dampers was shown to estimate the probability of collapse when fitting a normalised cumulative distribution as function of Sa(T_1) associated with collapse using 20 seismic ground motions. The results show that collapse resistance drops as λ value decreases from λ=1.0 to λ=0.2, indicating that the probability of collapse increases as the λ value decreases.

Chapter 6.

Conclusions and limitations, recommendations for the future research

6.1 Conclusions

According to current seismic design standards, the main purpose of a building is to ensure life safety in the occurrence of a strong earthquake (ASCE/SEI 7-10, 2010). Earthquake resilience is a secondary consideration. Direct losses due to restoration costs and business downtime caused by earthquake-induced disruption are increasing, hence, many researchers are focused on improving seismic structural systems towards low-damage performance, repairability, and earthquake resilience. Rate-dependent passive dampers, such as viscous, viscoelastic, and elastomeric, are now a mature and readily available technology for resilience-based seismic design (Christopoulos et al., 2006). Prior numerical and experimental research has shown that rate-dependent dampers are highly effective in reducing plastic deformations, drifts, residual drifts, and the probability of collapse of steel moment-resisting frames (MRFs) (Karavasilis et al., 2011; Karavasilis et al., 2012; Seo et al., 2014). Despite their significant advantages, rate-dependent dampers produce forces that increase with inter-storey velocities, and, therefore, may induce high axial forces to the columns (Logotheti et al., 2018).

This thesis introduces an approach to overcome the shortcomings of viscoelastic dampers and presents a new hybrid system as an effective means of increasing earthquake resilience.

Chapter 1 describes the restrictions of traditional design standards and introduces the performance-based design approach needed to improve structural resilience performance. Also, research objectives and the thesis outline are briefly described. To date, several studies have demonstrated that velocity-dependent dampers (e.g., viscous, viscoelastic, and elastomeric) perform exceptionally well in improving seismic resilience when used within MRF. However, the characteristics of the velocity damper are dependent on

inter-storey velocity, and, therefore, may induce high axial forces to the columns. This detrimental effect becomes more pronounced when steel MRF experiences plastic deformation that leads to increased base shear of the structure, escalating project costs.

To alleviate this unfavourable outcome, one solution is to use the modified capacity rule for MRF with velocity dampers to limit the occurrence of the plastic hinges on the columns so that happening plastic mechanism similar to existing MRF buildings occurs (Kariniotakis and Karavasilis, 2017). Another method is to utilise a hybrid damper system that imposes a limit on the peak force that is exerted on the structural members it is attached to.

The thesis focuses on the latter method, specifically a state-of- the-art hybrid visco-plastic damper, and evaluates the seismic performance of steel frames equipped with such dampers. Prior to proposing the development of a hybrid damper, Chapter 2 looks into several supplementary passive dampers of different characteristics and their application and effectiveness in seismic design and/or retrofit. Furthermore, seismic design methods for buildings with viscous or viscoelastic dampers are also discussed.

Chapter 3 focuses on practical details of the visco-plastic damper (VPD). The visco-plastic damper is described as an in-series combination of a viscoelastic damper and a friction device. The basic visco-plastic damper model is a combination of viscoelastic and friction devices. Its schematic behaviour under dynamic loading and its practical application configuration are explained, and practical structural details are explored. Lastly, a simplified design procedure for steel MRFs with visco-plastic dampers is introduced and the need for research to identify the optimum value of the so-called Lambda parameter involved in the design process is identified.

Chapter 4 presents a numerical design and assessment study on steel MRFs with visco-plastic dampers and their direct comparison with steel MRFs with viscoelastic dampers. The visco-plastic damper is realised by the in-series combination of a viscoelastic damper and a friction device. Such

configuration allows a viscoelastic damping output under small amplitudes of deformation and a friction damping output under large amplitudes of deformation. The optimum level of activation force for the friction device of the visco-plastic damper was considered as an unknown and was the primary parameter of investigation where the activation force of the friction device is determined on the basis of the λ factor, which reflects the ratio of the peak force of the visco-plastic damper to the peak force of a viscoelastic damper under the DBE. A prototype steel building was designed as a high ductility steel MRF. This MRF was then equipped with viscoelastic dampers or visco-plastic dampers to achieve high seismic performance, i.e. a design peak storey drift under the design earthquake (475 year return period) equal to 1.2% for 5-storey, 1.0% for 10-storey and 0.6% for 20-storey buildings. Parametric designs were carried out by designing visco-plastic dampers with different friction device activation forces. Non-linear dynamic analyses for a set of 20 earthquake ground motions scaled to the design and maximum considered earthquake intensities were carried out in OpenSees.

In addition, in Chapter 5, Incremental Dynamic Analyses (IDA) were carried out up to collapse, and a FEMA P-58 fragility curve was drawn to evaluate the collapse probability of MRFs with viscoelastic and visco-plastic dampers, respectively.

The following conclusions were reached:

1) The main goal of the visco-plastic damper for resilience-based seismic design is the reduction of storey drifts without increasing the base shear force - a design objective that is difficult to achieve with conventional viscous or viscoelastic dampers.

2) The design of the viscoelastic damper was in accordance with that presented in Seo et al. (2014).Viscoelastic dampers are first designed for the high ductility steel MRF. Then, it is necessary to define the performance objectives and the β factor that is the ratio between the viscoelastic damper stiffness and the horizontal stiffness of each

storey. After that, the required area of the viscoelastic material and the damping coefficient of the viscoelastic damper that is used as total damping ratio, including inherent damping which is used to reduce the elastic design spectrum, are calculated. For this spectrum, a standard response spectrum analysis can be conducted to estimate the drifts of the steel MRF with viscoelastic dampers.

3) For the design of the visco-plastic damper, the steel MRF with visco-plastic dampers can be designed by adding one additional step to the design procedure of the viscoelastic damper. The pushover analysis on the steel MRF with viscoelastic dampers carried out on the steel MRF with viscoelastic dampers and the force in the damper of each storey at the point of the expected drift of the steel MRF under the DBE, F_i* is extracted. Then, the activation force of the friction device at each storey is calculated as $F_{y,i}= \lambda F_i$*, where λ is a multiplier that takes values equal or lower than unity. The response results helped to identify the range of activation force values for the friction device of the visco-plastic damper that allow drift reduction, residual drift reduction, control of the peak base shear force, and adequate seismic collapse resistance to be simultaneously achieved.

4) The non-linear dynamic analysis results highlight the advantages of the visco-plastic damper. Optimisation will propose a suitable λ factor that achieves the target seismic performance of different parameter studies and simultaneously reduces base shear. In this thesis, five parameter studies of λ equal to 1.0, 0.8, 0.6, 0.4 and 0.2 were conducted for purposes of optimisation. Numerical analysis showed λ values within the range of 0.4-0.6 for the 5-storey building, which seems appropriate in terms of reducing drift, while also controlling the base shear force. For the visco-plastic dampers used in the 10-storey building, λ values were within the 0.4-0.6 range, and in the 20-storey building, activation force λ values were within the 0.8-1.0 range.

In other words, when the visco-plastic damper is applied to low storey buildings (5 to 10-storey), friction device activation points at 40 to 60% of viscoelastic damper load are advantageous in reducing base shear force whilst still achieving the overall performance target. On the other hand, when the visco-plastic damper is applied to higher storey structures (20-storey), the activation at a higher load of the friction devices is more appropriate. (e.g. 80-100% of the viscoelastic damper peak force under DBE).

5) When visco-plastic dampers are used in the MRF, there is a small decrease in the reduction of base shear under the seismic intensity of DBE level intensity, however, if the seismic intensity is greater, for example during a strong earthquake such as an MCE, it shows a significant reduction in base shear.

6) For the 5-storey building, the results highlight the advantages of the visco-plastic damper. From the results presented in this thesis, appropriate λ factor values were identified to be within 0.4 to 0.6. In particular, visco-plastic dampers designed for λ within 0.4 to 0.6 were found to satisfy the strict peak storey drift under the DBE whilst also achieving a reduction in peak base shear force equal to 17%.

7) For 10 and 20-storey buildings, proper λ factor values were found to be within 0.4 to 0.6 for the 10-storey, and 0.8 to 1.0 for 20-storey buildings. In particular, visco-plastic dampers designed for λ within 0.4 to 0.6 were found to satisfy strict peak storey drift under the DBE, while achieving a reduction in peak base shear force equal to 11 to18% in 10-storey buildings, and λ factor values within 0.8 to 1.0 were found to satisfy strict peak storey drift under the DBE whilst also achieving a reduction in peak base shear force equal to 13-15% in 20-storey buildings.

8) Residual drift is crucial for achieving earthquake resilience. Regarding 5-storey residual drift, θr, the visco-plastic damper shows values below 0.1% from λ=1.0 to λ=0.2 under DBE intensity level. The median values of the residual drift gradually increase in line with an increase in seismic intensity level. However, they remain under 0.5% until λ=0.4. These results imply that MRFs fitted with visco-plastic dampers are an economical means of improving resilience performance. Regarding 10 to 20-storey building residual drift, θr, the visco-plastic damper shows values below 0.19% for λ=1.0 to λ=0.2 in 10-storey buildings, and lower than 0.14% for λ=1.0 to λ=0.2 in 20-storey buildings. These values are below the 0.5% limitation for economically replaceable residual drift. The median values of as above the residual drift gradually increase under MCE intensity level. However, they remain under 0.5% until λ=0.2 in 10-storey buildings, and under 0.4% until λ=0.2 in 20-storey buildings. These results suggest that MRFs fitted with visco-plastic dampers are also beneficial in terms of economical means of improving resilience performance, even in medium to tall buildings (10 to 20-storey).

9) IDA (Incremental Dynamic Analysis) was carried out for viscoelastic and visco-plastic dampers to determine earthquake resilience using 20 far-field seismic records. The results show that Sa(T_1) increases gradually until each system becomes dynamically unstable and loses lateral resistance. The results also reveal that MRF with viscoelastic dampers has higher θ_{max} values than MRF with visco-plastic dampers (from λ=1.0 to λ=0.2) at the Sa (T_1) value that leads to collapse.

10) The collapse fragility curve for the MRF with viscoelastic and visco-plastic dampers was shown to estimate the probability of collapse when fitting a normalised cumulative distribution as the function of Sa(T1) associated with collapse using 20 seismic ground motions. The results show that collapse resistance drops as λ value decreases from λ=1.0 to λ=0.2, indicating that the probability of collapse increases as the λ value decreases The results indicate that as λ decreases, the 50% collapse resistance of the steel MRF decreases. Moreover, the viscoelastic dampers clearly provide higher collapse resistance than that achieved by the visco-plastic dampers for the entire range of seismic intensities. It should be pointed out, however, that for seismic intensities equal to or lower than 2.5 times the intensity of the MCE, the probability of collapse of the steel MRFs with visco-plastic dampers is very small (i.e. less than 5%) for all examined values of λ. Therefore, from a design point of view, the visco-plastic damper can be used without any concern for the collapse resistance of steel MRFs.

6.2 Limitation of the study and the future research work

1) Parameter study was conducted using different values of Lambda factor. However, it has a limitation for applying proposed Lambda factor to other different height buildings with having different structural systems. It is needed to explore more parameter study with more specified Lambda factor.

2) In the nonlinear dynamic analysis, the ground motions are only considered far-fault pulse and it is necessary to verify the seismic performance for the visco-plastic damper using near-fault pulse ground motions.

3) For the visco-plastic damper component, FEM analysis for the details of the visco-plastic damper and experimental seismic performance are required to understand more the behavior of the visco-plastic damper.

References

ASCE (2010)Minimum design loads for buildings and other structures, ASCE/SEI standard ASCE 7-10. ASCE, Reston

Aiken, I. D. (1990). The application of viscoelastic dampers to seismically resistant structures. In Proc. 4th US Conf. Earthquake Eng. (pp. 459-468).

Akiyama, H. (1985). Earthquake-resistant limit-state design for buildings. *Univ of Tokyo Pr*

Allahvirdizadeh, Y., Mohamadian, M., & HaghiFam, M. R. (2017). A comparative study of energy control strategies for a standalone PV/WT/FC hybrid renewable system. *International Journal of Renewable Energy Research (IJRER)*, 7(3), 1463-1475.

Applied Technology Council (ATC). (2006). Next-generation performance-based seismic design guidelines: Program plan for new and existing buildings (*FEMA-445*).

Applied Technology Council. (2009). Quantification of building seismic performance factors. US Department of Homeland Security, *FEMA*.

Apostolakis, G., & Dargush, G. F. (2010). Optimal seismic design of moment-resisting steel frames with hysteretic passive devices. *Earthquake Engineering & Structural Dynamics*, 39(4), 355-376.

Baker, J. W. (2011). Fitting fragility functions to structural analysis data using maximum likelihood estimation. Technical note, Stanford University.

Balut, N., & Gioncu, V. (2003). Suggestion for an improved 'dog-bone'solution. Proc., Stessa, 129-134.

Baiguera, M., Vasdravellis, G., & Karavasilis, T. L. (2016). Dual seismic-resistant steel frame with high post-yield stiffness energy-dissipative braces for residual drift reduction. *Journal of Constructional Steel Research*, 122, 198-212.

Basim, M. C., & Estekanchi, H. E. (2015). Application of endurance time method in performance-based optimum design of structures. *Structural Safety*, 56, 52-67.

Bardar, A., Abdollahzadeh, G., Jamnani , H. (2015) Visco-plastic damper effects on behavior of steel frames subjected to blast loading. *1st International Conference on Human, Architecture, Civil Engineering and City*

Benedetti, A., Landi, L., & Merenda, D. G. (2014). Displacement-based design of an energy dissipating system for seismic upgrading of existing masonry structures. *Journal of Earthquake Engineering*, 18(4), 477-501.

Building Seismic Safety Council (US), & Applied Technology Council. (1997). NEHRP guidelines for the seismic rehabilitation of buildings (Vol. 1). *Federal Emergency Management Agency*.

Cavallaro, G. F., Latour, M., Francavilla, A. B., Piluso, V., & Rizzano, G. (2018). Standardised friction damper bolt assemblies time-related relaxation and installed tension variability. *Journal of Constructional Steel Research*, 141, 145-155.

Charney, F. A., & Ibrahim, Y. E. (2004, August). New visco-plastic passive energy device. *In Proc. of 13th World Conference on Earthquake Engineering*.

Chen, G., & Wu, J. (2003). Experimental study on multiple tuned mass dampers to reduce seismic responses of a three-storey building structure. *Earthquake engineering & structural dynamics*, 32(5), 793-810.

Christopoulos, C., & Montgomery, M. (2013). Viscoelastic coupling dampers (VCDs) for enhanced wind and seismic performance of high-rise buildings. *Earthquake Engineering & Structural Dynamics*, 42(15), 2217-2233.

Christopoulos, C., Filiatrault, A., & Bertero, V. V. (2006). Principles of passive supplemental damping and seismic isolation. *Iuss press*.

Christopoulos, C., & Montgomery, M. (2013). Viscoelastic coupling dampers (VCDs) for enhanced wind and seismic performance of high-rise buildings. *Earthquake Engineering & Structural Dynamics*, 42(15), 2217-2233.

Cherry, S., & Filiatrault, A. (1993). Seismic response control of buildings using friction dampers. *Earthquake Spectra*, 9(3), 447-466.

Chen, G., Mu, H., & Bothe, E. R. (2001). Metallic dampers for seismic design and retrofit of bridges.

Christopoulos, C., & Montgomery, M. (2013). Viscoelastic coupling dampers (VCDs) for enhanced wind and seismic performance of high-rise buildings. *Earthquake Engineering & Structural Dynamics*, 42(15), 2217-2233.

Chang, K. C., Lai, M. L., Soong, T. T., Hao, D. S., & Yeh, Y. C. (1993). Seismic behavior and design guidelines for steel frame structures with added viscoelastic dampers, *MCEER Technical Reports (public)*

Cimellaro, G. P. (2016). Urban resilience for emergency response and recovery. New York: *Springer*.

Constantinou, M. C., & Symans, M. D. (1993). Experimental study of seismic response of buildings with supplemental fluid dampers. *The Structural Design of Tall Buildings*, 2(2), 93-132.

Connor, J., Lauflamme, S. (2014) *Structural Motion Engineering USA*. Massachusetts Institute of Technology Cambridge

Deierlein, G. G., Krawinkler, H., & Cornell, C. A. (2003, February). A framework for performance-based earthquake engineering. *In Pacific conference on earthquake engineering* (pp. 1-8).

Dimopoulos, A. I., Tzimas, A. S., Karavasilis, T. L., & Vamvatsikos, D. (2016). Probabilistic economic seismic loss estimation in steel buildings using post-tensioned moment-resisting frames and viscous dampers. *Earthquake Engineering & Structural Dynamics*, 45(11), 1725-1741.

Eurocode 8 (2013) ‘Design of Structures for Earthquake Resistance’

FEMA (1997) NEHRP guidelines for the seismic rehabilitation of buildings. FEMA report 273,Washington, DC

FEMA (2009) Quantification of building seismic performance factors. FEMA P695, Washington,DC

FEMA (2012a) Guidelines for seismic performance assessment of buildings. FEMA P58/Pre-Release, Aug 2012, Washington, DC

Feng, Y., Wu, J., Chong, X., & Meng, S. (2018). Seismic lateral displacement analysis and design of an earthquake-resilient dual wall-frame system. *Engineering Structures*, 177, 85-102.

Filiatrault, A., & Cherry, S. (1990). Seismic design spectra for friction-damped structures. *Journal of Structural Engineering*, 116(5), 1334-1355.

Filiatrault, A., Tremblay, R., & Kar, R. (2000). Performance evaluation of friction spring seismic damper. *Journal of Structural Engineering*, 126(4), 491-499.

Fischinger, M. (Ed.). (2014). Performance-based seismic engineering: Vision for an earthquake resilient society (Vol. 32). Dordrecht, *The Netherlands: Springer*.

Fu, Y., & Kasai, K. (1998). Comparative study of frames using viscoelastic and viscous dampers. *Journal of Structural Engineering*, 124(5), 513-522.

Fu, Y., & Cherry, S. (2000). Design of friction damped structures using lateral force procedure. *Earthquake engineering & structural dynamics*, 29(7), 989-1010.

Ghobarah, A. (2001). Performance-based design in earthquake engineering: state of development. *Engineering structures*, 23(8), 878-884.

Guo, T., Xu, J., Xu, W., & Di, Z. (2014). Seismic Upgrade of Existing Buildings with Fluid Viscous Dampers: Design Methodologies and Case Study. *Journal of Performance of Constructed Facilities*, 29(6), 04014175.

Hashemi, A., Zarnani, P., Masoudnia, R., & Quenneville, P. (2017). Seismic resilient lateral load resisting system for timber structures. *Construction and Building Materials*, 149, 432-443.

Hashemi, A., Zarnani, P., Masoudnia, R., & Quenneville, P. (2017). Seismic resistant rocking coupled walls with innovative Resilient Slip Friction (RSF) joints. *Journal of Constructional Steel Research*, 129, 215-226.

Hamidia, M., Filiatrault, A., & Aref, A. (2014). Seismic Collapse Capacity–Based Evaluation and Design of Frame Buildings with Viscous Dampers Using Pushover Analysis. *Journal of Structural Engineering*, 141(6), 04014153.

Heysami, A. (2015). Types of dampers and their seismic performance during an earthquake. *Current world environment*, 10, 1002-1015.

Hussain, S., Lee, D., & Retamal, E. (1998). Viscous damping for base isolated structures.

Ibrahim, Y. E., Marshall, J., & Charney, F. A. (2007). A visco-plastic device for seismic protection of structures. *Journal of Constructional Steel Research*, 63(11), 1515-1528.

Kamperidis, V. C., Karavasilis, T. L., & Vasdravellis, G. (2018). Self-centering steel column base with metallic energy dissipation devices. *Journal of Constructional Steel Research*, 149, 14-30.

Karavasilis, T. L., Blakeborough, T., & Williams, M. S. (2011). Development of nonlinear analytical model and seismic analyses of a steel frame with self-centering devices and viscoelastic dampers. *Computers & Structures*, 89(11-12), 1232-1240.

Karavasilis, T. L., Kerawala, S., & Hale, E. (2012). Hysteretic model for steel energy dissipation devices and evaluation of a minimal-damage seismic design approach for steel buildings. *Journal of Constructional Steel Research*, 70, 358-367.

Karavasilis, T. L., Sause, R., & Ricles, J. M. (2012). Seismic design and evaluation of steel moment-resisting frames with compressed elastomer dampers. *Earthquake Engineering & Structural Dynamics*, 41(3), 411-429.

Karavasilis, T. L. (2016). Assessment of capacity design of columns in steel moment resisting frames with viscous dampers. *Soil Dynamics and Earthquake Engineering*, 88, 215-222.

Kariniotakis, K., & Karavasilis, T. L. (2018). Modified capacity design rule for columns in tall steel MRFs with linear viscous dampers within the framework of Eurocode 8. *Bulletin of Earthquake Engineering*, 16(2), 917-932.

Kasai, K., Fu, Y., & Watanabe, A. (1998). Passive control systems for seismic damage mitigation. *Journal of Structural Engineering*, 124(5), 501-512.

Khazaei, M. (2013). Investigation on dynamics nonlinear analysis of steel frames with steel dampers. Procedia Engineering, 54, 401-412.

Khoo, H. H., Clifton, C., MacRae, G., Zhou, H., & Ramhormozian, S. (2015). Proposed design models for the asymmetric friction connection. *Earthquake Engineering & Structural Dynamics*, 44(8), 1309-1324.

Kibayashi, M., Kasai, K., Tsuji, Y., Kikuchi, M., Kimura, Y., Kobayashi, T., ... & Matsuba, Y. (2004, August). JSSI manual for building passive control technology. PART-2 Criteria for implementation of energy dissipation devices. *In 13th World Conference on Earthquake Engineering*. Vancouver, BC, Canada:[sn].

Kim, J. and Shin, H. (2017) 'Seismic loss assessment of a structure retrofitted with slit-friction hybrid dampers', *Engineering Structures*, 130, pp.336-350.

Kim, Y. J., Ahn, T. S., Bae, J. H., & Oh, S. H. (2016). Experimental study of using cantilever type steel plates for passive energy dissipation. International *Journal of Steel Structures*, 16(3), 959-974.

Krawinkler, H., & Deierlein, G. G. (2014). Challenges towards achieving earthquake resilience through performance-based earthquake engineering. In

Performance-based seismic engineering: Vision for an earthquake resilient society (pp. 3-23). *Springer, Dordrecht*.

Lee, K. S., Fan, C. P., Sause, R., & Ricles, J. (2005). Simplified design procedure for frame buildings with viscoelastic or elastomeric structural dampers. *Earthquake engineering & structural dynamics*, 34(10), 1271-1284.

Lee, C. H., Woo, S. K., Ju, Y. K., Lee, D. W., & Kim, S. D. (2014). Modified fatigue model for hourglass-shaped steel strip damper subjected to cyclic loadings. *Journal of Structural Engineering*, 141(8), 04014206.

Lee, C. H., Ju, Y. K., Min, J. K., Lho, S. H., & Kim, S. D. (2015). Non-uniform steel strip dampers subjected to cyclic loadings. *Engineering Structures*, 99, 192-204.

Lee, C. H., Kim, J., Kim, D. H., Ryu, J., & Ju, Y. K. (2016). Numerical and experimental analysis of combined behavior of shear-type friction damper and non-uniform strip damper for multi-level seismic protection. *Engineering Structures*, 114, 75-92.

Lee, J., Kang, H., & Kim, J. (2017). Seismic performance of steel plate slit-friction hybrid dampers. *Journal of Constructional Steel Research*, 136, 128-139.

Lin, K. Y., & Sung, Y. (1991). Analysis of interlaminar stresses in viscoelastic composites. *International Journal of Solids and Structures*, 27(7), 929-945.

Lin, T. K., Chen, C. C., Chang, K. C., Lin, C. C. J., & Hwang, J. S. (2009). Mitigation of micro vibration by viscous dampers. *Earthquake Engineering and Engineering Vibration*, 8(4), 569-582.

Lin, W. H., & Chopra, A. K. (2003). Earthquake response of elastic single-degree-of-freedom systems with nonlinear viscoelastic dampers. *Journal of Engineering Mechanics*, 129(6), 597-606.

Liu, Z., Atamturktur, S., & Juang, C. H. (2013). Performance based robust design optimization of steel moment resisting frames. *Journal of Constructional Steel Research*, 89, 165-174.

Lobo, R. F., Bracci, J. M., Shen, K. L., Reinhorn, A. M., & Soong, T. T. (1993). Inelastic response of R/C structures with viscoelastic braces. *Earthquake Spectra*, 9(3), 419-446.

Longarini, N., Cabras, L., Zucca, M., Chapain, S., & Aly, A. M. (2017). Structural Improvements for Tall Buildings under Wind Loads: *Comparative Study*. *Shock and Vibration*, 2017.

Lu, Z., Chen, X., Zhang, D., & Dai, K. (2017). Experimental and analytical study on the performance of particle tuned mass dampers under seismic excitation. *Earthquake Engineering & Structural Dynamics*, 46(5), 697-714.

Mahmoodi, P., & Keel, C. J. (1989). Analysis and the Design of Multi-Layer Viscoelastic (VE) Dampers for Tall Structures. *In Structural Design, Analysis and Testing (pp. 451-489). ASCE*

Marshall, J. D., & Charney, F. A. (2010). A hybrid passive control device for steel structures, I: Development and analysis. *Journal of Constructional Steel Research*, 66(10), 1278-1286.

Miyamoto, H. K., & Gilani, A. S. (2013). Response of structures with viscous dampers subjected to large earthquakes. *In Structures Congress 2013*: Bridging Your Passion with Your Profession (pp. 2118-2127).

Moehle, J., & Deierlein, G. G. (2004, August). A framework methodology for performance-based earthquake engineering. *In 13th world conference on earthquake engineering* (Vol. 679).

Moon, K. H., Han, S. W., & Lee, C. S. (2017). Seismic retrofit design method using friction damping systems for old low-and mid-rise regular reinforced concrete buildings. *Engineering Structures*, 146, 105-117.

National Research Council. (2011). National earthquake resilience: Research, implementation, and outreach. *National Academies Press*.

NIST (2015) Community resilience planning guide for buildings and infrastructure systems, *National Institute of Standards and Technology*

Ng, C. L., & Xu, Y. L. (2006). Seismic response control of a building complex utilizing passive friction damper: experimental investigation. *Earthquake engineering & structural dynamics*, 35(6), 657-677.

Nikoukalam, M. T., Mirghaderi, S. R., & Dolatshahi, K. M. (2015). Analytical study of moment-resisting frames retrofitted with shear slotted bolted connection. *Journal of Structural Engineering*, 141(11), 04015019.

Oh, S. H., Kim, Y. J., & Ryu, H. S. (2009). Seismic performance of steel structures with slit dampers. *Engineering structures*, 31(9), 1997-200

Pinto, P. E., Giannini, R., & Franchin, P. (2004). Seismic reliability analysis of structures.

Rawlinson, T. A., & Marshall, J. D. (2014). Single-Degree-of-Freedom Characterization of Multi-Phase Passive Control Systems. *Journal of Earthquake Engineering*, 18(4), 589-610.

SANWA TEKKI COORPORATION MR damper (2017). https://www.tekki.co.jp/en/products/list/dampers/product_building04/ (Accessed 12 July 2018).

Samali, B., & Kwok, K. C. S. (1995). Use of viscoelastic dampers in reducing wind-and earthquake-induced motion of building structures. *Engineering Structures*, 17(9), 639-654.

Seo, C. Y., Karavasilis, T. L., Ricles, J. M., & Sause, R. (2014). Seismic performance and probabilistic collapse resistance assessment of steel moment resisting frames with fluid viscous dampers. *Earthquake Engineering & Structural Dynamics*, 43(14), 2135-2154.

Share, M., Ghalehnovi, M., & Shabakhti, N. (2009). Evaluation of Capacity Spectrum Method for Estimate of Seismic Performance in Buckling-Restrained Braced Frame. *In Structures Congress 2009*: Don't Mess with Structural Engineers: Expanding Our Role (pp. 1-10).

Shi, G., Hu, F., & Shi, Y. (2016). Comparison of seismic design for steel moment frames in Europe, the United States, Japan and China. *Journal of Constructional Steel Research*, 127, 41-53.

Shen, K. L., & Soong, T. T. (1995). Modeling of viscoelastic dampers for structural applications. Journal of Engineering Mechanics, 121(6), 694-701.

Sheikholeslami, A., Behnamfar , F. (2012) Seismic behaviour of new visco plastic device equipped with steel cores and viscoelastic solid. *15th World Conference on Earthquake Engineering*

Siahpolo, N., Gerami, M., Vahdani, R. (2013) Performance evaluation of mid-height steel moment resisting frames rehabilitatetd by visco–plastic dampers using nonlinear linear time history analysis. Journal of Basic and Applied Scientific Research, Vol. 3(1), 376-388

Silwal, B., Ozbulut, O. E., & Michael, R. J. (2016). Seismic collapse evaluation of steel moment resisting frames with superelastic viscous damper. *Journal of Constructional Steel Research*, 126, 26-36.

Silwal, B., Ozbulut, O. E., & Michael, R. J. (2016). Seismic collapse evaluation of steel moment resisting frames with superelastic viscous damper. *Journal of Constructional Steel Research*, 126, 26-36.

Soulages, J. (1995). Performance based seismic engineering of buildings (Vol. 1). *Structural Engineers Association of California*.

Symans, M. D., Charney, F. A., Whittaker, A. S., Constantinou, M. C., Kircher, C. A., Johnson, M. W., & McNamara, R. J. (2008). Energy dissipation systems for seismic applications: current practice and recent developments. *Journal of structural engineering*, 134(1), 3-21.

Tsai, C. S., & Lee, H. H. (1993). Applications of viscoelastic dampers to high-rise buildings. *Journal of structural engineering*, 119(4), 1222-1233.

Tanake, Y., Kawaguchi, S., Sukagawa, M., Masaki, N., Sera, S., Washiyama, Y., Mitsusaka, Y. (2004) Jssi manual for building passive control technology part-4 performance and quality control of viscous dampers. *13th World Conference on Earthquake Engineering*, 1387

Taylordevices.[Online]. Available: http://www. taylordevices. com/Tech-Paper-archives/literature-pdf/36-ViscousDamping. pdf.

Tse, K. T., Kwok, K. C., & Tamura, Y. (2012). Performance and cost evaluation of a smart tuned mass damper for suppressing wind-induced lateral-torsional motion of tall structures. *Journal of Structural Engineering*, 138(4), 514-525.

Uang, C. M. (1991). Establishing R (or R w) and C d factors for building seismic provisions. *Journal of structural Engineering*, 117(1), 19-28.

Uang, C. M., & Bertero, V. V. (1991). UBC seismic serviceability regulations: critical review. *Journal of Structural Engineering*, 117(7), 2055-2068.

Uang, C. M., & Bruneau, M. (2018). State-of-the-Art Review on Seismic Design of Steel Structures (Doctoral dissertation, *American Society of Civil Engineers*).

Vasdravellis, G., Karavasilis, T. L., & Uy, B. (2014). Design rules, experimental evaluation, and fracture models for high-strength and stainless-steel hourglass shape energy dissipation devices. *Journal of Structural Engineering*, 140(11), 04014087.

Vamvatsikos, D., Kazantzi, A. K., & Aschheim, M. A. (2015). Performance-based seismic design: Avant-garde and code-compatible approaches. *ASCE-ASME Journal of Risk and Uncertainty in Engineering Systems*, Part A: Civil Engineering, 2(2), C4015008.

Vision, S. E. A. O. C. (2000). Committee.(1995). Performance based seismic engineering of buildings, part, 2.

Wada, A., Qu, Z., Motoyui, S., & Sakata, H. (2010). Integrity, Strength and Deformability in Seismic Design of Multi-Story Structures. Tokyo Institute of Technology.

Wakahara, T., Ohyama, T., & Fujii, K. (1992). Suppression of wind-induced vibration of a tall building using tuned liquid damper. *Journal of Wind Engineering and Industrial Aerodynamics*, 43(1-3), 1895-1906.

Wasti, S. T., & Ozcebe, G. (Eds.). (2006). Advances in earthquake engineering for urban risk reduction (Vol. 66). *Springer*.

Whittaker, A. S., Constantinou, M. C., Ramirez, O. M., Johnson, M. W., & Chrysostomou, C. Z. (2003). Equivalent lateral force and modal analysis procedures of the 2000 NEHRP Provisions for buildings with damping systems. *Earthquake Spectra*, 19(4), 959-980.

Zhang, R. H., & Soong, T. T. (1992). Seismic design of viscoelastic dampers for structural applications. *Journal of Structural Engineering*, 118(5), 1375-1392.

Zemp Qin, X., & Sheldon, C. (2008). Study on semi-active control of mega-sub controlled structure by MR damper subject to random wind loads. *Earthquake Engineering and Engineering Vibration*, 7(3), 285.

Appendix

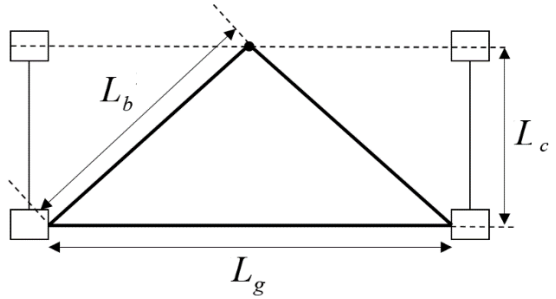

Table A.1 5-storey brace section design

Storey	L_b(m)	L_c(m)	L_g(m) [1]	Section	Area(㎡)	K_b [2]	α [3]
5	5.0	3.2	7.55	HEB180	0.0065	320993.9	9.8
4	5.0	3.2	7.55	HEB220	0.0091	449391.4	10.6
3	5.0	3.2	7.45	HEB260	0.0118	580678.9	10.2
2	5.0	3.2	7.45	HEB300	0.0149	733230.2	10.6
1	5.5	4	7.35	HEB700	0.0306	1082999.3	11.0

1 Net length (m) from column to column

2 Brace stiffness

3 the ratio of brace stiffness to the total story MRF lateral stiffness

Table A.2 10-storey brace section design

Storey	L_b(m)	L_c(m)	L_g(m) [1]	Section	Area (m^2)	K_b [2]	α [3]
10	5.1	3.2	8	w10x19	0.003626	183690.4	10.4
9	5.1	3.2	8	w10x30	0.005703	288909.7	10.7
8	5.1	3.2	8	w10x39	0.007419	375841.0	11.2
7	5.1	3.2	8	w16x45	0.008581	434707.0	10.8
6	5.1	3.2	8	w16x50	0.009484	480452.3	10.5
5	5.1	3.2	8	w18x60	0.0114	577515.4	11.1
4	5.1	3.2	8	w21x68	0.0129	653504.3	11.5
3	5.1	3.2	8	w21x73	0.0139	704163.6	11.4
2	5.1	3.2	8	w21x83	0.0157	795350.2	10.9
1	5.4	4	8	w24x117	0.0222	947416.6	11.9

1 Net length (m) from column to column

2 Brace stiffness

3 the ratio of brace stiffness to the total story MRF lateral stiffness

Table A.3 20-storey brace section design

Storey	L_b(m)	L_c(m)	L_g(m) [1]	Section	A	K_b [2]	α [3]
20	5.1	3.2	8	w12x19	0.003594	182069.3	11.0
19	5.1	3.2	8	w12x26	0.004935	250003.4	10.0
18	5.1	3.2	8	w14x38	0.007226	366063.7	11.1
17	5.1	3.2	8	w16x45	0.008581	434707.0	11.3
16	5.1	3.2	8	w18x50	0.009484	480452.3	10.7
15	5.1	3.2	8	w24x55	0.011	557251.7	10.7
14	5.1	3.2	8	w24x68	0.013	658570.2	10.5
13	5.1	3.2	8	w24x76	0.0145	734559.1	10.3
12	5.1	3.2	8	w24x84	0.0159	805482.1	10.5
11	5.1	3.2	8	w24x94	0.0179	906800.6	11.2
10	5.1	3.2	8	w24x94	0.0179	906800.6	10.6
9	5.1	3.2	8	w24x103	0.0195	987855.3	10.7
8	5.1	3.2	8	w24x103	0.0195	987855.3	10.2
7	5.1	3.2	8	w24x117	0.0222	1124635.3	11.0
6	5.1	3.2	8	w24x117	0.0222	1124635.3	10.6
5	5.1	3.2	8	w24x117	0.0222	1124635.3	10.0
4	5.1	3.2	8	w24x131	0.0248	1256349.4	10.1
3	5.1	3.2	8	w24x162	0.0308	1560304.9	10.8
2	5.1	3.2	8	w24x207	0.0392	1985842.5	10.7
1	5.4	4	8	w24x370	0.0703	3000152.4	11.4

1 Net length (m) from column to column

2 Brace stiffness

3 the ratio of brace stiffness to the total story MRF lateral stiffness

Table A.4 5-storey damping coefficient

Storey	Disp. (mm)	*(φ)i	Δi	Wx (kN)	hx (m)	∑Δi X hi	Fx(kN)	K (kN/m)	C,kN/m	(φ i-φ i-1)^2	C × (φ i-φ i-1)^2	*(φ)i^2	mi (ton)	mi × (φ h)	mi × (φ h)i^2
Total						0.03					647.48			652.16	488.36
5	3.17	1.00	0.001	2168.60	16.80	0.01	16.80	32684.8	1763.5	0.0264	46.51	1.00	216.86	216.86	216.86
4	2.65	0.84	0.001	2168.60	13.60	0.01	13.60	42398.9	2287.6	0.0513	117.40	0.70	216.86	181.64	152.14
3	1.93	0.61	0.001	2168.60	10.40	0.01	10.40	56983.2	3074.4	0.0512	157.34	0.37	216.86	132.51	80.97
2	1.22	0.38	0.001	2168.60	7.20	0.00	7.20	69364.2	3742.4	0.0478	178.90	0.15	216.86	83.46	32.12
1	0.53	0.17	0.001	2268.00	4.0	0.00	4.00	98859.3	5333.8	0.0276	147.32	0.03	226.80	37.69	6.26

Table A.5 10-storey damping coefficient

Storey	Disp. (mm)	*(φ)i	Δi	Wx (kN)	hx (m)	∑Δi X hi	Fx(kN)	K (kN/m)	C,kN/m	(φ i-φ i-1)^2	C × (φ i-φ i-1)^2	*(φ)i^2	mi (ton)	mi × (φ h)	mi × (φ h)i^2
Total						0.03					782.62			1219.29	879.85
10	25.76	1.00	0.002	2168.60	32.80	0.06	32.80	17634.4	2715.4	0.0052	14.16	1.00	216.86	216.86	216.86
9	23.90	0.93	0.002	2168.60	29.60	0.07	29.60	27048.1	4164.9	0.0080	33.41	0.86	216.86	201.20	186.67
8	21.59	0.84	0.003	2168.60	26.40	0.07	26.40	33598.2	5173.5	0.0105	54.46	0.70	216.86	181.78	152.37
7	18.95	0.74	0.003	2168.60	23.20	0.06	23.20	40172.2	6185.8	0.0117	72.46	0.54	216.86	159.53	117.36
6	16.16	0.63	0.003	2168.60	20.0	0.06	20.00	45897.1	7067.3	0.0125	88.09	0.39	216.86	136.06	85.36
5	13.29	0.52	0.003	2168.60	16.80	0.05	16.80	52046.2	8014.2	0.0123	98.72	0.27	216.86	111.85	57.69
4	10.43	0.40	0.003	2168.60	13.60	0.04	13.60	56842.8	8752.8	0.0123	107.67	0.16	216.86	87.78	35.53
3	7.57	0.29	0.003	2168.60	10.40	0.03	10.40	61935.5	9537.0	0.0117	111.87	0.09	216.86	63.73	18.73
2	4.78	0.19	0.002	2168.60	7.20	0.02	7.20	72639.2	11185.2	0.0093	103.50	0.03	216.86	40.24	7.47
1	2.30	0.09	0.002	2268.00	4.0	0.01	4.00	79930.5	12307.9	0.0080	98.29	0.01	226.80	20.27	1.81

Table A.6 20-storey damping coefficient

Storey	Disp. (mm)	*(φ)i	Δi	Wx (kN)	hx (m)	∑Δi X hi	Fx(kN)	K (kN/m)	C,kN/m	(φ i-φ i-1)^2	C × (φ i-φ i-1)^2	*(φ)i^2	mi (ton)	mi × (φ h)	mi × (φ h)i^2
Total						3.96					924.56			2194.68	1528.32
20	111.04	1.00	0.004	2168.60	64.80	0.25	64.80	16560.2	3675.1	0.0012	4.56	1.00	216.86	216.86	216.86
19	107.13	0.96	0.005	2168.60	61.60	0.31	61.60	25059.5	5561.3	0.0021	11.48	0.93	216.86	209.22	201.85
18	102.08	0.92	0.006	2168.60	58.40	0.33	58.40	33106.4	7347.2	0.0025	18.57	0.85	216.86	199.37	183.29
17	96.50	0.87	0.006	2168.60	55.20	0.34	55.20	38628.7	8572.7	0.0031	26.84	0.76	216.86	188.47	163.79
16	90.29	0.81	0.007	2168.60	52.0	0.34	52.00	44709.8	9922.3	0.0035	34.32	0.66	216.86	176.33	143.38
15	83.76	0.75	0.007	2168.60	48.80	0.32	48.80	51982.9	11536.3	0.0035	40.21	0.57	216.86	163.58	123.39
14	77.20	0.70	0.006	2168.60	45.60	0.28	45.60	62859.9	13950.2	0.0031	42.75	0.48	216.86	150.77	104.83
13	71.06	0.64	0.006	2168.60	42.40	0.25	42.40	71312.2	15826.0	0.0029	46.41	0.41	216.86	138.77	88.80
12	65.04	0.59	0.006	2168.60	39.20	0.24	39.20	77037.0	17096.5	0.0030	51.17	0.34	216.86	127.03	74.40
11	58.97	0.53	0.006	2168.60	36.0	0.22	36.00	81290.3	18040.4	0.0031	56.24	0.28	216.86	115.16	61.15
10	52.77	0.48	0.006	2168.60	32.80	0.21	32.80	85750.8	19030.3	0.0032	60.48	0.23	216.86	103.05	48.97
9	46.51	0.42	0.006	2168.60	29.60	0.18	29.60	92007.8	20418.9	0.0031	62.76	0.18	216.86	90.83	38.04
8	40.35	0.36	0.006	2168.60	26.40	0.16	26.40	96878.6	21499.8	0.0030	65.29	0.13	216.86	78.80	28.64
7	34.23	0.31	0.006	2168.60	23.20	0.14	23.20	102003.6	22637.2	0.0030	66.96	0.10	216.86	66.85	20.61
6	28.19	0.25	0.006	2168.60	20.0	0.12	20.00	106106.1	23547.7	0.0029	68.61	0.06	216.86	55.06	13.98
5	22.20	0.20	0.006	2168.60	16.80	0.10	16.80	112396.7	24943.7	0.0027	68.24	0.04	216.86	43.35	8.67
4	16.39	0.15	0.005	2168.60	13.60	0.07	13.60	123797.1	27473.8	0.0024	64.57	0.02	216.86	32.01	4.73
3	11.01	0.10	0.005	2168.60	10.40	0.05	10.40	144214.8	32005.0	0.0018	57.17	0.01	216.86	21.50	2.13
2	6.32	0.06	0.004	2168.60	7.20	0.03	7.20	184814.9	41015.2	0.0011	45.56	0.00	216.86	12.33	0.70
1	2.61	0.02	0.003	2268.00	4.0	0.01	4.00	263198.2	58410.4	0.0006	32.37	0.00	226.80	5.34	0.13

Table A.7 5-storey visco-plastic damper stiffness and activation force

Storey	β[1] (=0.3)	K[2](1000*K_n)	Fy (λ=1.0) (kN)	Fy (λ=0.8) (kN)	Fy (λ=0.6) (kN)	Fy (λ=0.4) (kN)	Fy (λ=0.2) (kN)
5	9805	9805447	144	115	86	57	29
4	12720	12719665	243	194	146	97	49
3	17095	17094972	336	269	201	134	67
2	20809	20809249	385	308	231	154	77
1	29658	29657795	419	335	251	168	84

[1] $\beta=K_i/K_{o,i}$, where K_i is the viscoelastic damper stiffness and $K_{o,i}$ is the horizontal stiffness of storey i

[2] Stiffness of the friction devices = initial stiffness 1,000 times that of the viscoelastic damper.

Table A.8 10-storey visco-plastic damper stiffness and activation force

Storey	β[1] (=0.43)	K[2] (1000*Kn)	Fy (λ=1.0) (kN)	Fy (λ=0.8) (kN)	Fy (λ=0.6) (kN)	Fy (λ=0.4) (kN)	Fy (λ=0.2) (kN)
10	7583	7582796	427.0	341.6	256.2	170.8	85.4
9	11631	11630689	872.0	697.6	523.2	348.8	174.4
8	14447	14447219	1372.5	1098.0	823.5	549.0	274.5
7	17274	17274032	1372.5	1098.0	823.5	549.0	274.5
6	19736	19735744	1847.6	1478.1	1108.6	739.1	369.5
5	22380	22379853	2630.1	2104.1	1578.1	1052.0	526.0
4	24442	24442422	2871.3	2297.0	1722.8	1148.5	574.3
3	26632	26632258	3090.9	2472.8	1854.6	1236.4	618.2
2	31235	31234867	3458.0	2766.4	2074.8	1383.2	691.6
1	34370	34370113	4396.6	3517.3	2638.0	1758.7	879.3

[1] $\beta=K_i/K_{o,i}$, where K_i is the viscoelastic damper stiffness and $K_{o,i}$ is the horizontal stiffness of storey i

[2] Stiffness of the friction devices = initial stiffness 1,000 times that of the viscoelastic damper.

Table A.9 20-storey visco-plastic damper stiffness and activation force

Storey	β[1] (=0.3)	K[2] (1000*Kn)	Fy (λ=1.0) (kN)	Fy1 (λ=0.8) (kN)	Fy1 (λ=0.6) (kN)	Fy1 (λ=0.4) (kN)	Fy1 (λ=0.2) (kN)
20	6955	6955277	149.2	119.4	89.5	59.7	29.8
19	10525	10524980	274.2	219.3	164.5	109.7	54.8
18	13905	13904694	448.2	358.5	268.9	179.3	89.6
17	16224	16224046	632.9	506.3	379.7	253.2	126.6
16	18778	18778135	849.5	679.6	509.7	339.8	169.9
15	21833	21832825	1094.6	875.7	656.8	437.8	218.9
14	26401	26401171	1414.2	1131.4	848.5	565.7	282.8
13	29951	29951106	1684.3	1347.4	1010.6	673.7	336.9
12	32356	32355556	1922.0	1537.6	1153.2	768.8	384.4
11	34142	34141935	2096.1	1676.9	1257.6	838.4	419.2
10	36015	36015335	2254.8	1803.8	1352.9	901.9	451.0
9	38643	38643275	2384.4	1907.5	1430.6	953.7	476.9
8	40689	40689001	2489.8	1991.9	1493.9	995.9	498.0
7	42842	42841530	2559.4	2047.5	1535.6	1023.8	511.9
6	44565	44564565	2598.5	2078.8	1559.1	1039.4	519.7
5	47207	47206612	2591.2	2072.9	1554.7	1036.5	518.2
4	51995	51994798	2536.1	2028.9	1521.6	1014.4	507.2
3	60570	60570211	2314.7	1851.7	1388.8	925.9	462.9
2	77622	77622264	2037.7	1630.2	1222.6	815.1	407.5
1	110543	110543229	1708.6	1366.9	1025.1	683.4	341.7

[1] $\beta=K_i/K_{o,i}$, where K_i is the viscoelastic damper stiffness and $K_{o,i}$ is the horizontal stiffness of storey i

[2] Stiffness of the friction devices = initial stiffness 1,000 times that of the viscoelastic damper.

Table A.10 5-storey base shear (DBE)

	Mean value	Q1 (kN)	Q2 (kN)	Q3 (kN)	Q4 (kN)	Q5 (kN)	Q6 (kN)	Q7 (kN)	Q8 (kN)	Q9 (kN)	Q10 (kN)	Q11 (kN)	Q12 (kN)	Q13 (kN)	Q14 (kN)	Q15 (kN)	Q16 (kN)	Q17 (kN)	Q18 (kN)	Q19 (kN)	Q20 (kN)
Viscoelastic	2956.1	3706	3492	2958	3792	4231	2462	3267	3018	3169	2739	2396	2334	2657	2282	2276	2455	2639	3251	3121	2877
Visco-plastic (λ=1.0)	2878.4	3442	3072	2940	3679	3800	2413	3204	3040	3193	2678	2395	2329	2653	2233	2274	2436	2671	3188	3109	2819
Visco-plastic (λ=0.8)	2838.0	3473	2874	2838	3607	3683	2326	3180	3064	3159	2896	2413	2245	2615	2289	2197	2401	2571	3213	3009	2707
Visco-plastic (λ=0.6)	2833.1	3625	2847	2764	3565	3560	2353	3116	3007	3156	3020	2331	2147	2754	2343	2146	2313	2539	3247	2901	2928
Visco-plastic (λ=0.4)	2884.5	3657	2864	2702	3477	3399	2705	2981	3008	3113	3087	2327	2389	3171	2418	2167	2152	2618	3290	3110	3055
Visco-plastic (λ=0.2)	3016.2	3612	2895	3077	3376	3236	3177	2817	2978	3180	2992	2751	3030	3040	3068	2629	2414	2704	3201	3221	2925

Table A.11 5-storey viscoelastic drift summary (DBE)

Storey	Mean value (%)	Q1 (%)	Q2 (%)	Q3 (%)	Q4 (%)	Q5 (%)	Q6 (%)	Q7 (%)	Q8 (%)	Q9 (%)	Q10 (%)	Q11 (%)	Q12 (%)	Q13 (%)	Q14 (%)	Q15 (%)	Q16 (%)	Q17 (%)	Q18 (%)	Q19 (%)	Q20 (%)
Max	0.96	1.26	1.08	0.81	1.02	1.10	1.02	1.14	0.92	1.02	0.98	0.67	0.78	0.88	0.94	0.81	1.03	0.89	1.16	1.13	1.00
5	0.79	1	0.77	0.66	0.68	0.87	0.93	0.93	0.65	0.84	0.75	0.56	0.69	0.71	0.82	0.64	0.86	0.72	1	1	0.79
4	0.96	1.26	1.02	0.75	0.86	1.02	1.02	1.14	0.85	1.02	0.96	0.67	0.78	0.88	0.94	0.81	1.03	0.89	1.16	1.13	0.99
3	0.94	1.25	1.08	0.81	0.97	1.07	0.85	1.14	0.92	0.98	0.98	0.65	0.71	0.88	0.82	0.81	0.98	0.87	1.06	0.98	1
2	0.88	1.14	1.02	0.77	1.02	1.1	0.67	1.05	0.91	0.94	0.91	0.63	0.63	0.81	0.75	0.73	0.87	0.76	0.98	0.91	0.92
1	0.58	0.75	0.67	0.52	0.75	0.81	0.41	0.7	0.63	0.64	0.58	0.44	0.41	0.54	0.49	0.47	0.54	0.47	0.63	0.64	0.6

Table A.12 5-storey visco-plastic (λ=1.0) drift summary (DBE)

Storey	Mean value (%)	Q1 (%)	Q2 (%)	Q3 (%)	Q4 (%)	Q5 (%)	Q6 (%)	Q7 (%)	Q8 (%)	Q9 (%)	Q10 (%)	Q11 (%)	Q12 (%)	Q13 (%)	Q14 (%)	Q15 (%)	Q16 (%)	Q17 (%)	Q18 (%)	Q19 (%)	Q20 (%)
Max	1.00	1.21	1.11	0.82	1.04	1.16	1.16	1.24	0.92	1.08	1.01	0.67	0.81	0.90	1.05	0.82	1.12	0.93	1.29	1.30	1.02
5	0.89	1.08	0.84	0.71	0.71	0.97	1.16	1.06	0.65	0.9	0.8	0.57	0.76	0.75	0.98	0.65	1	0.77	1.23	1.28	0.84
4	1.00	1.19	1.06	0.78	0.85	0.99	1.13	1.24	0.85	1.08	1.01	0.67	0.81	0.9	1.05	0.82	1.12	0.93	1.29	1.3	1.02
3	0.96	1.21	1.11	0.82	0.97	1.08	0.87	1.18	0.92	1	1.01	0.65	0.72	0.88	0.84	0.81	1.02	0.89	1.12	1.02	1.02
2	0.89	1.13	1.05	0.78	1.04	1.16	0.66	1.08	0.91	0.98	0.92	0.63	0.64	0.82	0.73	0.73	0.87	0.76	0.98	0.92	0.93
1	0.60	0.74	0.67	0.55	0.8	0.92	0.41	0.72	0.63	0.68	0.58	0.44	0.42	0.55	0.47	0.47	0.53	0.46	0.66	0.64	0.61

Table A.13 5-storey visco-plastic (λ=0.8) drift summary (DBE)

Storey	Mean value (%)	Q1 (%)	Q2 (%)	Q3 (%)	Q4 (%)	Q5 (%)	Q6 (%)	Q7 (%)	Q8 (%)	Q9 (%)	Q10 (%)	Q11 (%)	Q12 (%)	Q13 (%)	Q14 (%)	Q15 (%)	Q16 (%)	Q17 (%)	Q18 (%)	Q19 (%)	Q20 (%)
Max	1.05	1.19	1.17	0.87	1.09	1.20	1.23	1.32	0.95	1.09	1.05	0.67	0.85	0.96	1.11	0.85	1.18	0.97	1.41	1.35	1.11
5	0.94	1.12	0.88	0.71	0.77	1.02	1.23	1.13	0.73	0.9	0.81	0.6	0.82	0.82	1.07	0.68	1.07	0.8	1.36	1.35	0.94
4	1.05	1.16	1.12	0.81	0.88	1.02	1.17	1.32	0.87	1.09	1.03	0.67	0.85	0.96	1.11	0.85	1.18	0.97	1.41	1.34	1.11
3	0.98	1.19	1.17	0.87	1	1.11	0.89	1.23	0.95	1.01	1.05	0.65	0.74	0.89	0.87	0.83	1.06	0.92	1.19	1.01	1.06
2	0.91	1.14	1.1	0.79	1.09	1.2	0.68	1.11	0.95	1.01	0.96	0.63	0.66	0.84	0.75	0.72	0.9	0.77	1.01	0.96	0.96
1	0.62	0.75	0.68	0.56	0.87	0.96	0.43	0.74	0.67	0.71	0.61	0.45	0.43	0.56	0.48	0.47	0.55	0.48	0.69	0.66	0.62

Table A.14 5-storey visco-plastic (λ=0.6) drift summary (DBE)

Storey	Mean value (%)	Q1 (%)	Q2 (%)	Q3 (%)	Q4 (%)	Q5 (%)	Q6 (%)	Q7 (%)	Q8 (%)	Q9 (%)	Q10 (%)	Q11 (%)	Q12 (%)	Q13 (%)	Q14 (%)	Q15 (%)	Q16 (%)	Q17 (%)	Q18 (%)	Q19 (%)	Q20 (%)
Max	1.13	1.21	1.26	0.97	1.19	1.27	1.31	1.42	1.04	1.13	1.10	0.73	0.94	1.04	1.21	0.88	1.26	0.96	1.67	1.43	1.24
5	1.03	1.15	0.96	0.75	0.87	1.09	1.31	1.19	0.91	1.01	0.84	0.71	0.91	0.91	1.18	0.73	1.14	0.84	1.59	1.43	1.04
4	1.13	1.17	1.22	0.93	0.98	1.1	1.23	1.42	0.96	1.13	1.07	0.73	0.94	1.04	1.21	0.88	1.26	0.96	1.67	1.41	1.24
3	1.04	1.21	1.26	0.97	1.08	1.15	0.91	1.31	1.04	1.05	1.1	0.67	0.78	0.92	0.92	0.85	1.12	0.93	1.32	1.04	1.17
2	0.96	1.18	1.15	0.82	1.19	1.27	0.69	1.14	1.01	1.06	1	0.65	0.69	0.89	0.79	0.73	0.93	0.77	1.11	1.03	1.04
1	0.66	0.82	0.7	0.59	1.01	1.02	0.45	0.77	0.7	0.76	0.67	0.46	0.45	0.62	0.52	0.49	0.56	0.52	0.74	0.69	0.7

Table A.15 5-storey visco-plastic (λ=0.4) drift summary (DBE)

Storey	Mean value (%)	Q1 (%)	Q2 (%)	Q3 (%)	Q4 (%)	Q5 (%)	Q6 (%)	Q7 (%)	Q8 (%)	Q9 (%)	Q10 (%)	Q11 (%)	Q12 (%)	Q13 (%)	Q14 (%)	Q15 (%)	Q16 (%)	Q17 (%)	Q18 (%)	Q19 (%)	Q20 (%)
Max	1.27	1.30	1.34	1.14	1.44	1.36	1.40	1.60	1.24	1.19	1.15	0.91	1.09	1.25	1.33	0.94	1.33	1.02	2.04	1.50	1.43
5	1.15	1.26	1.04	0.92	1.05	1.15	1.4	1.29	1.21	1.14	0.88	0.88	1.04	1.09	1.3	0.78	1.19	0.96	1.85	1.5	1.16
4	1.27	1.26	1.32	1.12	1.16	1.22	1.28	1.6	1.24	1.19	1.12	0.91	1.09	1.25	1.33	0.94	1.33	1.02	2.04	1.49	1.43
3	1.16	1.3	1.34	1.14	1.27	1.22	0.98	1.49	1.18	1.1	1.15	0.76	0.9	1.18	1.05	0.89	1.18	0.93	1.64	1.13	1.37
2	1.06	1.3	1.17	0.89	1.44	1.36	0.78	1.23	1.15	1.12	1.04	0.71	0.68	1.19	0.95	0.76	0.96	0.79	1.25	1.12	1.22
1	0.77	1.1	0.76	0.61	1.3	1.11	0.61	0.82	0.8	0.82	0.75	0.5	0.52	0.88	0.61	0.51	0.58	0.58	0.88	0.76	0.85

Table A.16 5-storey visco-plastic (λ=0.2) drift summary (DBE)

Storey	Mean value (%)	Q1 (%)	Q2 (%)	Q3 (%)	Q4 (%)	Q5 (%)	Q6 (%)	Q7 (%)	Q8 (%)	Q9 (%)	Q10 (%)	Q11 (%)	Q12 (%)	Q13 (%)	Q14 (%)	Q15 (%)	Q16 (%)	Q17 (%)	Q18 (%)	Q19 (%)	Q20 (%)
Max	1.47	1.73	1.37	1.47	1.88	1.51	1.50	1.93	1.51	1.29	1.16	1.24	1.24	1.59	1.47	1.14	1.31	1.34	2.46	1.56	1.72
5	1.31	1.41	1.07	1.16	1.35	1.23	1.5	1.52	1.36	1.29	0.91	1.18	1.07	1.33	1.41	1.01	1.18	1.23	2.12	1.56	1.38
4	1.47	1.44	1.36	1.47	1.56	1.38	1.37	1.93	1.51	1.22	1.14	1.24	1.24	1.59	1.47	1.14	1.31	1.34	2.46	1.55	1.72
3	1.36	1.56	1.37	1.41	1.69	1.32	1.06	1.84	1.44	1.17	1.16	1	1.13	1.41	1.22	1.12	1.17	1.09	2.18	1.24	1.69
2	1.25	1.73	1.18	1.16	1.88	1.51	1	1.47	1.35	1.19	1.11	0.88	1	1.34	1.11	0.98	0.99	0.86	1.56	1.23	1.45
1	0.96	1.64	0.77	0.89	1.76	1.28	0.83	0.94	0.97	0.94	0.82	0.65	0.77	0.97	0.82	0.66	0.65	0.64	1.16	0.88	1.06

Table A.17 5-storey base shear (MCE)

	Mean value	Q1 (kN)	Q2 (kN)	Q3 (kN)	Q4 (kN)	Q5 (kN)	Q6 (kN)	Q7 (kN)	Q8 (kN)	Q9 (kN)	Q10 (kN)	Q11 (kN)	Q12 (kN)	Q13 (kN)	Q14 (kN)	Q15 (kN)	Q16 (kN)	Q17 (kN)	Q18 (kN)	Q19 (kN)	Q20 (kN)
Viscoelastic	4178.2	5203	4596	4344	4924	5507	3692	4561	4195	4387	3856	3589	3500	3850	3386	3406	3722	3955	4692	4203	3996
Visco-plastic (λ=1.0)	3697.7	4395	3636	3765	4068	4199	3386	3749	3790	3828	3697	3488	3281	3692	3384	3174	3493	3701	4026	3641	3560
Visco-plastic (λ=0.8)	3577.8	4280	3593	3620	3914	4038	3301	3602	3571	3705	3689	3452	3105	3485	3343	3148	3361	3594	3862	3454	3439
Visco-plastic (λ=0.6)	3481.6	4149	3507	3454	3776	3857	3361	3429	3543	3550	3620	3403	3229	3437	3215	3137	3216	3458	3694	3283	3313
Visco-plastic (λ=0.4)	3461.8	4160	3338	3545	3732	3681	3463	3282	3474	3494	3481	3413	3277	3531	3519	3160	3166	3381	3556	3355	3227
Visco-plastic (λ=0.2)	3475.7	4243	3394	3577	3713	3519	3455	3232	3489	3599	3277	3524	3365	3596	3512	3249	3152	3646	3488	3347	3137

Table A.18 5-storey viscoelastic drift summary (MCE)

Storey	Mean value (%)	Q1 (%)	Q2 (%)	Q3 (%)	Q4 (%)	Q5 (%)	Q6 (%)	Q7 (%)	Q8 (%)	Q9 (%)	Q10 (%)	Q11 (%)	Q12 (%)	Q13 (%)	Q14 (%)	Q15 (%)	Q16 (%)	Q17 (%)	Q18 (%)	Q19 (%)	Q20 (%)
Max	1.42	2.01	1.66	1.20	1.55	1.67	1.57	1.79	1.37	1.45	1.52	1.00	1.17	1.33	1.42	1.23	1.60	1.36	1.78	1.58	1.47
5	1.14	1.44	1.13	0.97	0.99	1.1	1.41	1.29	0.92	1.14	1.08	0.85	1.04	1.04	1.23	0.96	1.27	1.07	1.45	1.38	1.07
4	1.42	1.92	1.54	1.12	1.21	1.39	1.57	1.71	1.24	1.38	1.46	1	1.17	1.33	1.42	1.23	1.6	1.36	1.78	1.58	1.42
3	1.42	2.01	1.66	1.2	1.42	1.57	1.27	1.79	1.37	1.45	1.52	0.98	1.06	1.33	1.22	1.22	1.54	1.32	1.64	1.38	1.47
2	1.31	1.81	1.51	1.14	1.55	1.67	0.99	1.62	1.36	1.41	1.34	0.94	0.94	1.21	1.1	1.09	1.28	1.13	1.36	1.37	1.31
1	0.92	1.29	1.03	0.79	1.27	1.35	0.61	1.16	1.02	1.05	0.88	0.67	0.61	0.83	0.73	0.7	0.84	0.7	0.95	1.02	0.88

Table A.19 5-storey visco-plastic (λ=1.0) drift summary (MCE)

Storey	Mean value (%)	Q1 (%)	Q2 (%)	Q3 (%)	Q4 (%)	Q5 (%)	Q6 (%)	Q7 (%)	Q8 (%)	Q9 (%)	Q10 (%)	Q11 (%)	Q12 (%)	Q13 (%)	Q14 (%)	Q15 (%)	Q16 (%)	Q17 (%)	Q18 (%)	Q19 (%)	Q20 (%)
Max	1.61	2.29	1.97	1.34	1.82	1.93	2.05	2.03	1.52	1.58	1.74	1.05	1.36	1.52	1.85	1.36	2.00	1.49	2.37	1.77	1.61
5	1.40	1.6	1.39	1.06	1.24	1.12	2.05	1.47	1.11	1.23	1.22	0.99	1.32	1.25	1.79	1.06	1.7	1.21	2.08	1.77	1.25
4	1.61	1.94	1.88	1.28	1.43	1.3	1.91	1.96	1.26	1.33	1.67	1.05	1.36	1.52	1.85	1.36	2	1.49	2.37	1.71	1.61
3	1.57	2.27	1.97	1.34	1.53	1.58	1.37	2.03	1.44	1.49	1.74	0.99	1.14	1.37	1.34	1.31	1.78	1.42	2.08	1.53	1.59
2	1.44	2.29	1.68	1.17	1.82	1.93	1.03	1.83	1.52	1.58	1.47	0.96	1.02	1.25	1.08	1.11	1.38	1.13	1.69	1.5	1.35
1	1.09	1.9	1.1	0.89	1.72	1.82	0.65	1.4	1.25	1.36	0.88	0.69	0.66	0.94	0.74	0.73	0.96	0.74	1.26	1.13	0.92

Table A.20 5-storey visco-plastic (λ=0.8) drift summary (MCE)

Storey	Mean value (%)	Q1 (%)	Q2 (%)	Q3 (%)	Q4 (%)	Q5 (%)	Q6 (%)	Q7 (%)	Q8 (%)	Q9 (%)	Q10 (%)	Q11 (%)	Q12 (%)	Q13 (%)	Q14 (%)	Q15 (%)	Q16 (%)	Q17 (%)	Q18 (%)	Q19 (%)	Q20 (%)
Max	1.70	2.42	2.09	1.40	2.02	2.03	2.17	2.14	1.65	1.66	1.81	1.16	1.50	1.65	1.98	1.41	2.10	1.44	2.58	1.73	1.70
5	1.50	1.75	1.5	1.17	1.37	1.21	2.17	1.53	1.26	1.35	1.27	1.13	1.44	1.35	1.95	1.11	1.78	1.3	2.32	1.73	1.32
4	1.70	2.02	2.03	1.37	1.58	1.37	1.96	2.08	1.37	1.34	1.73	1.16	1.5	1.65	1.98	1.41	2.1	1.44	2.58	1.61	1.7
3	1.65	2.38	2.09	1.4	1.71	1.65	1.35	2.14	1.59	1.54	1.81	1.03	1.21	1.47	1.41	1.34	1.85	1.4	2.3	1.64	1.66
2	1.50	2.42	1.72	1.16	2.02	2.03	1.01	1.91	1.65	1.66	1.51	0.99	1.04	1.36	1.16	1.12	1.42	1.11	1.81	1.59	1.4
1	1.16	2.05	1.28	0.89	1.92	1.91	0.65	1.46	1.34	1.46	0.88	0.71	0.66	1.04	0.81	0.75	1.01	0.78	1.38	1.18	0.98

Table A.21 5-storey visco-plastic (λ=0.6) drift summary (MCE)

Storey	Mean value (%)	Q1 (%)	Q2 (%)	Q3 (%)	Q4 (%)	Q5 (%)	Q6 (%)	Q7 (%)	Q8 (%)	Q9 (%)	Q10 (%)	Q11 (%)	Q12 (%)	Q13 (%)	Q14 (%)	Q15 (%)	Q16 (%)	Q17 (%)	Q18 (%)	Q19 (%)	Q20 (%)
Max	1.83	2.66	2.18	1.48	2.32	2.15	2.30	2.35	1.85	1.75	1.89	1.36	1.70	1.81	2.13	1.49	2.19	1.45	2.89	1.78	1.76
5	1.62	1.91	1.58	1.31	1.56	1.31	2.3	1.68	1.37	1.48	1.32	1.31	1.6	1.47	2.12	1.19	1.84	1.4	2.66	1.64	1.38
4	1.83	2.24	2.17	1.48	1.79	1.47	2.02	2.29	1.52	1.41	1.8	1.36	1.7	1.81	2.13	1.49	2.19	1.45	2.89	1.71	1.76
3	1.76	2.63	2.18	1.42	2	1.74	1.32	2.35	1.79	1.63	1.89	1.13	1.34	1.65	1.52	1.43	1.93	1.29	2.6	1.78	1.66
2	1.59	2.66	1.74	1.16	2.32	2.15	0.98	2.05	1.85	1.75	1.55	1.06	1.02	1.5	1.29	1.17	1.49	1.06	1.94	1.7	1.4
1	1.26	2.28	1.47	0.87	2.24	2.03	0.73	1.53	1.55	1.55	0.9	0.77	0.72	1.13	0.88	0.8	1.08	0.82	1.51	1.28	1.05

Table A.22 5-storey visco-plastic (λ=0.4) drift summary (MCE)

Storey	Mean value (%)	Q1 (%)	Q2 (%)	Q3 (%)	Q4 (%)	Q5 (%)	Q6 (%)	Q7 (%)	Q8 (%)	Q9 (%)	Q10 (%)	Q11 (%)	Q12 (%)	Q13 (%)	Q14 (%)	Q15 (%)	Q16 (%)	Q17 (%)	Q18 (%)	Q19 (%)	Q20 (%)
Max	2.02	2.97	2.27	1.68	2.74	2.30	2.43	2.66	2.12	1.86	1.92	1.63	1.83	1.95	2.33	1.77	2.22	1.77	3.22	1.93	1.85
5	1.77	2.09	1.67	1.46	1.8	1.47	2.43	1.95	1.4	1.65	1.37	1.49	1.63	1.61	2.33	1.42	1.87	1.63	3.08	1.51	1.45
4	2.02	2.54	2.27	1.68	2.08	1.64	2.11	2.6	1.73	1.49	1.83	1.63	1.83	1.95	2.33	1.77	2.22	1.77	3.22	1.87	1.85
3	1.93	2.94	2.25	1.47	2.41	1.86	1.31	2.66	2.04	1.73	1.92	1.33	1.48	1.8	1.68	1.75	1.97	1.34	2.91	1.93	1.8
2	1.76	2.97	1.88	1.36	2.74	2.3	1.06	2.27	2.12	1.86	1.58	1.2	1.18	1.56	1.41	1.44	1.58	1.13	2.14	1.83	1.6
1	1.44	2.57	1.6	1.1	2.71	2.19	0.85	1.64	1.87	1.67	0.93	0.94	0.91	1.17	0.98	1.07	1.24	0.88	1.68	1.46	1.29

Table A.23 5-storey visco-plastic (λ=0.2) drift summary (MCE)

Storey	Mean value (%)	Q1 (%)	Q2 (%)	Q3 (%)	Q4 (%)	Q5 (%)	Q6 (%)	Q7 (%)	Q8 (%)	Q9 (%)	Q10 (%)	Q11 (%)	Q12 (%)	Q13 (%)	Q14 (%)	Q15 (%)	Q16 (%)	Q17 (%)	Q18 (%)	Q19 (%)	Q20 (%)
Max	2.20	3.23	2.40	1.91	3.40	2.45	2.62	2.71	2.34	2.01	1.94	1.84	1.78	2.04	2.53	2.00	2.08	2.05	3.58	2.05	2.05
5	1.92	2.37	1.83	1.63	2.09	1.66	2.62	2.07	1.42	1.86	1.38	1.63	1.57	1.72	2.48	1.52	1.79	1.87	3.58	1.65	1.58
4	2.20	2.8	2.4	1.91	2.56	1.86	2.25	2.71	2	1.65	1.84	1.84	1.78	2.04	2.53	1.98	2.08	2.05	3.54	2.04	2.05
3	2.09	3.23	2.38	1.62	3	1.95	1.35	2.7	2.29	1.87	1.94	1.59	1.48	1.88	1.89	2	1.9	1.56	3.15	2.05	2.05
2	1.97	3.2	2.15	1.61	3.38	2.45	1.09	2.19	2.34	2.01	1.63	1.39	1.48	1.54	1.45	1.92	1.74	1.37	2.58	1.91	1.96
1	1.69	2.8	1.88	1.36	3.4	2.37	0.94	1.54	2.16	1.87	1.01	1.22	1.33	1.15	1.2	1.72	1.49	0.97	2.1	1.54	1.7

Table A.24 10-storey base shear (DBE)

	Mean value	Q1 (kN)	Q2 (kN)	Q3 (kN)	Q4 (kN)	Q5 (kN)	Q6 (kN)	Q7 (kN)	Q8 (kN)	Q9 (kN)	Q10 (kN)	Q11 (kN)	Q12 (kN)	Q13 (kN)	Q14 (kN)	Q15 (kN)	Q16 (kN)	Q17 (kN)	Q18 (kN)	Q19 (kN)	Q20 (kN)
Viscoelastic	3728	2600	2167	4291	4167	5943	7224	3512	2444	3936	3241	3256	2694	4038	5564	2982	2476	4454	4885	2055	2621
Visco-plastic (λ=1.0)	3716	2602	2169	4296	4167	5935	6965	3516	2445	3937	3240	3258	2697	4040	5564	2983	2478	4456	4886	2057	2623
Visco-plastic (λ=0.8)	3676	2602	2169	4296	4167	5893	6608	3516	2445	3937	3240	3258	2697	4040	5566	2983	2478	4456	4486	2057	2623
Visco-plastic (λ=0.6)	3602	2602	2169	4298	4167	5310	6002	3531	2445	3937	3254	3258	2697	3968	5194	2983	2478	4243	4815	2057	2623
Visco-plastic (λ=0.4)	3391	2602	2169	4003	4020	4537	5299	3557	2445	3772	3325	3149	2702	3560	4530	2983	2478	3820	4194	2057	2615
Visco-plastic (λ=0.2)	3029	2687	2061	3726	3451	3889	4643	2877	2340	3066	3165	2711	2770	2658	3736	3071	2420	3450	3483	2027	2354

Table A.25 10-storey viscoelastic drift summary (DBE)

Storey	Mean value (%)	Q1 (%)	Q2 (%)	Q3 (%)	Q4 (%)	Q5 (%)	Q6 (%)	Q7 (%)	Q8 (%)	Q9 (%)	Q10 (%)	Q11 (%)	Q12 (%)	Q13 (%)	Q14 (%)	Q15 (%)	Q16 (%)	Q17 (%)	Q18 (%)	Q19 (%)	Q20 (%)
Max	0.93	0.74	0.64	1.19	1.34	1.24	1.26	0.94	0.78	0.99	1.23	0.77	0.75	0.98	1.35	0.89	0.78	1.12	1.28	0.63	0.85
10	0.68	0.48	0.4	0.71	0.65	0.96	1.04	0.65	0.46	0.66	0.93	0.52	0.5	0.75	1.1	0.46	0.43	0.86	1	0.38	0.56
9	0.82	0.6	0.5	0.9	0.82	1.15	1.15	0.76	0.58	0.81	1.14	0.63	0.61	0.9	1.31	0.59	0.55	1.03	1.14	0.47	0.7
8	0.90	0.67	0.58	1.06	0.95	1.24	1.26	0.81	0.68	0.9	1.23	0.68	0.68	0.97	1.35	0.69	0.64	1.12	1.1	0.53	0.8
7	0.92	0.71	0.62	1.15	1.06	1.21	1.25	0.86	0.73	0.94	1.17	0.69	0.7	0.98	1.23	0.75	0.7	1.1	1.16	0.56	0.84
6	0.93	0.72	0.64	1.19	1.16	1.14	1.21	0.89	0.77	0.97	1.06	0.7	0.72	0.97	1.2	0.81	0.75	1.03	1.21	0.59	0.85
5	0.92	0.72	0.64	1.18	1.23	1.03	1.15	0.89	0.77	0.97	0.95	0.72	0.72	0.95	1.17	0.83	0.76	0.95	1.24	0.61	0.83
4	0.92	0.74	0.64	1.17	1.31	1.01	1.13	0.93	0.78	0.99	0.87	0.76	0.73	0.92	1.15	0.87	0.78	0.92	1.28	0.63	0.79
3	0.91	0.74	0.61	1.11	1.34	1.05	1.09	0.94	0.76	0.99	0.81	0.77	0.75	0.84	1.08	0.89	0.77	0.89	1.28	0.63	0.76
2	0.84	0.69	0.56	1	1.31	1.04	1	0.88	0.69	0.92	0.73	0.72	0.72	0.75	1	0.84	0.7	0.83	1.22	0.58	0.7
1	0.66	0.53	0.42	0.77	1.09	0.84	0.81	0.68	0.51	0.71	0.56	0.55	0.56	0.56	0.81	0.65	0.53	0.65	0.99	0.44	0.52

Table A.26 10-storey visco-plastic (λ=1.0) drift summary (DBE)

Storey	Mean value (%)	Q1 (%)	Q2 (%)	Q3 (%)	Q4 (%)	Q5 (%)	Q6 (%)	Q7 (%)	Q8 (%)	Q9 (%)	Q10 (%)	Q11 (%)	Q12 (%)	Q13 (%)	Q14 (%)	Q15 (%)	Q16 (%)	Q17 (%)	Q18 (%)	Q19 (%)	Q20 (%)
Max	0.93	0.74	0.64	1.20	1.34	1.25	1.57	0.94	0.78	0.99	1.23	0.77	0.75	0.98	1.54	0.89	0.78	1.12	1.36	0.63	0.85
10	0.74	0.54	0.4	0.71	0.65	1	1.57	0.65	0.46	0.66	0.95	0.52	0.5	0.75	1.45	0.46	0.43	0.86	1.28	0.38	0.56
9	0.86	0.64	0.5	0.9	0.82	1.18	1.48	0.76	0.58	0.81	1.15	0.63	0.61	0.9	1.54	0.59	0.55	1.03	1.36	0.47	0.7
8	0.91	0.69	0.58	1.06	0.95	1.25	1.29	0.82	0.68	0.9	1.23	0.68	0.68	0.97	1.41	0.69	0.64	1.12	1.19	0.53	0.8
7	0.92	0.71	0.62	1.15	1.06	1.23	1.28	0.86	0.73	0.94	1.17	0.69	0.7	0.98	1.22	0.75	0.7	1.1	1.16	0.56	0.84
6	0.93	0.72	0.64	1.2	1.16	1.15	1.21	0.89	0.77	0.97	1.06	0.7	0.72	0.98	1.18	0.81	0.75	1.03	1.21	0.59	0.85
5	0.92	0.72	0.64	1.18	1.23	1.02	1.15	0.89	0.77	0.97	0.95	0.72	0.72	0.95	1.17	0.83	0.76	0.95	1.24	0.61	0.83
4	0.92	0.74	0.64	1.17	1.31	1.01	1.13	0.93	0.78	0.99	0.87	0.76	0.73	0.92	1.15	0.87	0.78	0.92	1.28	0.63	0.79
3	0.91	0.74	0.61	1.11	1.34	1.05	1.1	0.94	0.76	0.99	0.81	0.77	0.75	0.84	1.08	0.89	0.77	0.89	1.28	0.63	0.76
2	0.85	0.69	0.56	1	1.31	1.04	1.02	0.88	0.69	0.92	0.73	0.72	0.72	0.75	1	0.84	0.7	0.83	1.22	0.58	0.7
1	0.66	0.53	0.42	0.77	1.09	0.83	0.82	0.68	0.52	0.71	0.56	0.55	0.56	0.56	0.81	0.65	0.53	0.65	0.99	0.44	0.52

Table A.27 10-storey visco-plastic (λ=0.8) drift summary (DBE)

Storey	Mean value (%)	Q1 (%)	Q2 (%)	Q3 (%)	Q4 (%)	Q5 (%)	Q6 (%)	Q7 (%)	Q8 (%)	Q9 (%)	Q10 (%)	Q11 (%)	Q12 (%)	Q13 (%)	Q14 (%)	Q15 (%)	Q16 (%)	Q17 (%)	Q18 (%)	Q19 (%)	Q20 (%)
Max	0.93	0.74	0.64	1.20	1.34	1.29	1.79	0.94	0.78	0.99	1.28	0.77	0.75	0.98	1.72	0.89	0.78	1.14	1.54	0.63	0.85
10	0.79	0.54	0.4	0.71	0.65	1.14	1.79	0.66	0.46	0.66	1.05	0.52	0.5	0.77	1.7	0.46	0.43	0.9	1.48	0.38	0.56
9	0.90	0.64	0.5	0.9	0.82	1.26	1.61	0.77	0.58	0.81	1.24	0.63	0.61	0.92	1.72	0.59	0.55	1.07	1.54	0.47	0.7
8	0.92	0.69	0.58	1.06	0.95	1.29	1.26	0.82	0.68	0.9	1.28	0.68	0.68	0.98	1.51	0.69	0.64	1.14	1.3	0.53	0.8
7	0.93	0.71	0.62	1.15	1.06	1.29	1.26	0.86	0.73	0.94	1.18	0.69	0.7	0.98	1.26	0.75	0.7	1.1	1.16	0.56	0.84
6	0.93	0.72	0.64	1.2	1.16	1.18	1.23	0.89	0.77	0.97	1.05	0.7	0.72	0.98	1.14	0.81	0.75	1.03	1.21	0.59	0.85
5	0.92	0.72	0.64	1.18	1.23	1.03	1.18	0.89	0.77	0.97	0.93	0.72	0.72	0.95	1.16	0.83	0.76	0.94	1.24	0.61	0.83
4	0.92	0.74	0.64	1.17	1.31	1.01	1.18	0.93	0.78	0.99	0.87	0.76	0.73	0.92	1.15	0.87	0.78	0.92	1.28	0.63	0.79
3	0.91	0.74	0.61	1.11	1.34	1.05	1.16	0.94	0.76	0.99	0.81	0.77	0.75	0.84	1.09	0.89	0.77	0.89	1.28	0.63	0.76
2	0.85	0.69	0.56	1	1.31	1.03	1.1	0.88	0.69	0.92	0.73	0.72	0.72	0.75	1	0.84	0.7	0.83	1.22	0.58	0.7
1	0.66	0.53	0.42	0.77	1.09	0.82	0.86	0.68	0.52	0.71	0.56	0.55	0.56	0.56	0.81	0.65	0.53	0.65	0.99	0.44	0.52

Table A.28 10-storey visco-plastic (λ=0.6) drift summary (DBE)

Storey	Mean value (%)	Q1 (%)	Q2 (%)	Q3 (%)	Q4 (%)	Q5 (%)	Q6 (%)	Q7 (%)	Q8 (%)	Q9 (%)	Q10 (%)	Q11 (%)	Q12 (%)	Q13 (%)	Q14 (%)	Q15 (%)	Q16 (%)	Q17 (%)	Q18 (%)	Q19 (%)	Q20 (%)
Max	0.95	0.74	0.64	1.20	1.34	1.39	2.03	0.95	0.78	0.99	1.44	0.77	0.75	1.04	1.89	0.89	0.78	1.22	1.76	0.63	0.85
10	0.86	0.54	0.4	0.71	0.65	1.34	2.03	0.75	0.46	0.68	1.24	0.52	0.5	0.86	1.89	0.46	0.43	1.02	1.76	0.38	0.56
9	0.95	0.64	0.5	0.9	0.82	1.39	1.78	0.84	0.58	0.81	1.44	0.63	0.61	1	1.82	0.59	0.55	1.19	1.76	0.47	0.7
8	0.94	0.69	0.58	1.06	0.95	1.31	1.23	0.82	0.68	0.9	1.43	0.68	0.68	1.04	1.51	0.69	0.64	1.22	1.42	0.53	0.8
7	0.94	0.71	0.62	1.15	1.06	1.34	1.2	0.86	0.73	0.94	1.26	0.69	0.7	1.02	1.25	0.75	0.7	1.15	1.17	0.56	0.84
6	0.93	0.72	0.64	1.2	1.16	1.22	1.17	0.89	0.77	0.97	1.07	0.7	0.72	0.97	1.16	0.81	0.75	1.03	1.21	0.59	0.85
5	0.91	0.72	0.64	1.18	1.23	1.06	1.15	0.89	0.77	0.97	0.9	0.72	0.72	0.95	1.18	0.83	0.76	0.93	1.23	0.61	0.83
4	0.92	0.74	0.64	1.17	1.31	1.07	1.16	0.93	0.78	0.99	0.84	0.76	0.73	0.91	1.19	0.87	0.78	0.92	1.28	0.63	0.79
3	0.92	0.74	0.61	1.11	1.34	1.12	1.16	0.95	0.76	0.99	0.81	0.77	0.75	0.84	1.15	0.89	0.77	0.91	1.29	0.63	0.76
2	0.86	0.69	0.56	1	1.31	1.08	1.11	0.88	0.69	0.92	0.74	0.72	0.72	0.75	1.07	0.84	0.7	0.86	1.23	0.58	0.7
1	0.67	0.53	0.42	0.77	1.09	0.84	0.89	0.68	0.52	0.71	0.56	0.55	0.56	0.56	0.84	0.65	0.53	0.66	0.99	0.44	0.52

Table A.29 10-storey visco-plastic (λ=0.4) drift summary (DBE)

Storey	Mean value (%)	Q1 (%)	Q2 (%)	Q3 (%)	Q4 (%)	Q5 (%)	Q6 (%)	Q7 (%)	Q8 (%)	Q9 (%)	Q10 (%)	Q11 (%)	Q12 (%)	Q13 (%)	Q14 (%)	Q15 (%)	Q16 (%)	Q17 (%)	Q18 (%)	Q19 (%)	Q20 (%)
Max	1.05	0.74	0.64	1.31	1.35	1.52	2.36	1.01	0.78	1.00	1.75	0.77	0.75	1.27	2.00	0.89	0.78	1.43	2.02	0.63	0.87
10	0.97	0.54	0.4	0.81	0.66	1.52	2.36	0.94	0.46	0.83	1.58	0.59	0.51	1.07	2	0.46	0.43	1.27	2.02	0.38	0.58
9	1.05	0.64	0.5	0.98	0.83	1.52	2.09	1.01	0.58	0.89	1.75	0.67	0.62	1.23	1.91	0.59	0.55	1.43	1.96	0.47	0.72
8	1.00	0.69	0.58	1.19	0.96	1.31	1.3	0.95	0.68	0.91	1.68	0.69	0.68	1.27	1.47	0.69	0.64	1.41	1.48	0.53	0.81
7	0.96	0.71	0.62	1.31	1.07	1.35	1.16	0.88	0.73	0.97	1.4	0.69	0.7	1.18	1.25	0.75	0.7	1.25	1.13	0.56	0.86
6	0.95	0.72	0.64	1.31	1.17	1.21	1.12	0.9	0.77	0.98	1.1	0.7	0.72	1.04	1.24	0.81	0.75	1.07	1.2	0.59	0.87
5	0.92	0.72	0.64	1.23	1.24	1.08	1.07	0.9	0.77	0.97	0.88	0.73	0.72	0.97	1.2	0.83	0.77	0.93	1.25	0.61	0.83
4	0.93	0.74	0.64	1.16	1.32	1.17	1.13	0.95	0.78	0.99	0.82	0.76	0.73	0.92	1.17	0.87	0.78	0.91	1.34	0.63	0.79
3	0.93	0.74	0.61	1.08	1.35	1.18	1.16	0.96	0.76	1	0.81	0.77	0.75	0.86	1.15	0.89	0.77	0.92	1.39	0.63	0.76
2	0.87	0.69	0.56	0.98	1.32	1.1	1.15	0.89	0.69	0.93	0.77	0.71	0.72	0.76	1.15	0.84	0.7	0.89	1.35	0.58	0.69
1	0.68	0.53	0.42	0.74	1.1	0.85	0.96	0.68	0.52	0.71	0.59	0.54	0.56	0.55	0.88	0.65	0.53	0.7	1.11	0.44	0.52

Table A.30 10-storey visco-plastic (λ=0.2) drift summary (DBE)

Storey	Mean value (%)	Q1 (%)	Q2 (%)	Q3 (%)	Q4 (%)	Q5 (%)	Q6 (%)	Q7 (%)	Q8 (%)	Q9 (%)	Q10 (%)	Q11 (%)	Q12 (%)	Q13 (%)	Q14 (%)	Q15 (%)	Q16 (%)	Q17 (%)	Q18 (%)	Q19 (%)	Q20 (%)
Max	1.26	0.74	0.67	1.90	1.80	1.93	2.73	1.24	0.83	1.19	2.36	0.90	0.87	1.74	2.38	1.01	0.83	1.99	2.21	0.62	1.03
10	1.21	0.54	0.46	1.22	0.77	1.93	2.73	1.2	0.55	1.09	2.23	0.84	0.71	1.41	2.38	0.53	0.51	1.8	2.21	0.46	0.72
9	1.26	0.64	0.56	1.38	0.95	1.79	2.12	1.24	0.68	1.16	2.36	0.9	0.81	1.66	2.11	0.65	0.63	1.99	2.1	0.53	0.86
8	1.19	0.69	0.62	1.71	1.07	1.43	1.63	1.08	0.78	1.13	2.13	0.84	0.83	1.74	1.66	0.76	0.72	1.89	1.56	0.59	0.97
7	1.13	0.71	0.66	1.9	1.26	1.49	1.34	0.97	0.83	1.19	1.67	0.76	0.83	1.59	1.35	0.85	0.78	1.58	1.11	0.61	1.03
6	1.06	0.72	0.67	1.81	1.48	1.27	1.24	0.99	0.83	1.17	1.17	0.78	0.82	1.26	1.21	0.9	0.83	1.21	1.24	0.59	1.01
5	1.02	0.72	0.65	1.51	1.62	1.29	1.33	0.98	0.81	1.12	0.92	0.85	0.78	1.01	1.26	0.92	0.83	0.96	1.33	0.6	0.91
4	1.04	0.74	0.63	1.28	1.74	1.26	1.47	1.08	0.82	1.14	0.92	0.9	0.84	0.96	1.27	0.98	0.83	1.02	1.43	0.62	0.81
3	1.04	0.74	0.62	1.3	1.8	1.16	1.36	1.12	0.79	1.1	0.96	0.9	0.87	0.88	1.32	1.01	0.81	1.13	1.49	0.62	0.8
2	0.98	0.69	0.57	1.32	1.8	1.13	1.18	1.03	0.71	0.98	0.88	0.8	0.82	0.76	1.22	0.96	0.73	1.18	1.46	0.57	0.72
1	0.76	0.53	0.42	1.12	1.58	0.9	0.95	0.77	0.52	0.72	0.67	0.57	0.62	0.55	0.88	0.74	0.55	0.99	1.21	0.44	0.53

Table A.31 10-storey base shear (MCE)

	Mean value	Q1 (kN)	Q2 (kN)	Q3 (kN)	Q4 (kN)	Q5 (kN)	Q6 (kN)	Q7 (kN)	Q8 (kN)	Q9 (kN)	Q10 (kN)	Q11 (kN)	Q12 (kN)	Q13 (kN)	Q14 (kN)	Q15 (kN)	Q16 (kN)	Q17 (kN)	Q18 (kN)	Q19 (kN)	Q20 (kN)
Viscoelastic	5292	3856	3241	6558	5597	7623	10050	4294	3533	5284	4670	4867	3836	5643	8191	4115	3570	6682	7505	3057	3678
Visco-plastic (λ=1.0)	5141	3858	3243	6564	5596	7355	8249	4293	3534	5284	4671	4869	3838	5643	7613	4116	3571	6403	7391	3059	3678
Visco-plastic (λ=0.8)	4967	3858	3243	6208	5477	6612	7557	4283	3534	5283	4701	4869	3838	5490	6965	4116	3571	6212	6779	3059	3678
Visco-plastic (λ=0.6)	4713	3858	3243	5556	4961	5927	6931	4273	3534	5001	4759	4717	3841	5106	6308	4116	3571	5706	6124	3059	3665
Visco-plastic (λ=0.4)	4317	3731	3240	4969	4297	5352	6275	3949	3491	4265	4362	4219	3871	4300	5483	3978	3508	5034	5431	3057	3529
Visco-plastic (λ=0.2)	3694	3199	2832	4101	3701	4724	5487	3262	2981	3689	3762	3607	3118	3448	4791	3227	3101	4166	4817	3025	2850

Table A.32 10-storey viscoelastic drift summary (MCE)

Storey	Mean value (%)	Q1 (%)	Q2 (%)	Q3 (%)	Q4 (%)	Q5 (%)	Q6 (%)	Q7 (%)	Q8 (%)	Q9 (%)	Q10 (%)	Q11 (%)	Q12 (%)	Q13 (%)	Q14 (%)	Q15 (%)	Q16 (%)	Q17 (%)	Q18 (%)	Q19 (%)	Q20 (%)
Max	1.32	1.06	0.96	1.82	2.45	1.58	1.74	1.33	1.17	1.45	1.89	1.12	1.11	1.74	1.87	1.41	1.17	1.12	1.28	0.94	0.85
10	0.89	0.7	0.6	0.95	0.94	1.11	1.32	0.89	0.68	0.87	1.38	0.77	0.74	1.19	1.42	0.68	0.65	0.86	1	0.57	0.56
9	1.10	0.86	0.75	1.26	1.25	1.34	1.6	1.04	0.85	1.09	1.72	0.93	0.91	1.49	1.7	0.85	0.82	1.03	1.14	0.71	0.7
8	1.24	0.97	0.86	1.56	1.6	1.53	1.68	1.18	1	1.23	1.89	1.01	1.01	1.7	1.77	1.01	0.95	1.12	1.1	0.8	0.8
7	1.30	1.02	0.92	1.74	1.88	1.58	1.55	1.28	1.09	1.28	1.83	1.02	1.04	1.74	1.85	1.11	1.05	1.1	1.16	0.84	0.84
6	1.32	1.04	0.96	1.82	2.11	1.55	1.47	1.33	1.15	1.34	1.63	1.03	1.07	1.67	1.87	1.2	1.12	1.03	1.21	0.88	0.85
5	1.30	1.04	0.96	1.8	2.26	1.51	1.46	1.33	1.16	1.38	1.42	1.04	1.07	1.5	1.83	1.24	1.15	0.95	1.24	0.91	0.83
4	1.31	1.06	0.95	1.75	2.39	1.52	1.56	1.33	1.17	1.44	1.3	1.1	1.06	1.34	1.8	1.35	1.17	0.92	1.28	0.94	0.79
3	1.30	1.06	0.92	1.63	2.45	1.53	1.7	1.3	1.14	1.45	1.2	1.12	1.11	1.22	1.71	1.41	1.15	0.89	1.28	0.94	0.76
2	1.23	1	0.84	1.5	2.4	1.47	1.74	1.21	1.05	1.39	1.1	1.07	1.09	1.08	1.57	1.39	1.08	0.83	1.22	0.88	0.7
1	1.01	0.78	0.64	1.31	2.14	1.23	1.54	0.97	0.81	1.14	0.88	0.83	0.89	0.83	1.3	1.17	0.86	0.65	0.99	0.68	0.52

Table A.33 10-storey visco-plastic (λ=1.0) drift summary (MCE)

Storey	Mean value (%)	Q1 (%)	Q2 (%)	Q3 (%)	Q4 (%)	Q5 (%)	Q6 (%)	Q7 (%)	Q8 (%)	Q9 (%)	Q10 (%)	Q11 (%)	Q12 (%)	Q13 (%)	Q14 (%)	Q15 (%)	Q16 (%)	Q17 (%)	Q18 (%)	Q19 (%)	Q20 (%)
Max	1.37	1.06	0.96	1.83	2.45	1.59	1.93	1.34	1.17	1.45	2.09	1.12	1.11	1.79	2.17	1.41	1.17	1.72	1.36	0.94	1.32
10	1.05	0.7	0.6	0.95	0.94	1.28	1.93	0.95	0.68	0.87	1.74	0.77	0.74	1.33	2.17	0.68	0.65	1.27	1.28	0.57	0.81
9	1.21	0.86	0.75	1.26	1.25	1.41	1.76	1.08	0.86	1.09	2.01	0.93	0.91	1.62	2.03	0.85	0.82	1.57	1.36	0.71	1.03
8	1.31	0.97	0.86	1.56	1.6	1.54	1.56	1.18	1	1.23	2.09	1.01	1.01	1.78	1.83	1.01	0.95	1.72	1.19	0.8	1.22
7	1.35	1.02	0.93	1.74	1.88	1.59	1.51	1.28	1.09	1.28	1.92	1.02	1.04	1.79	1.73	1.11	1.05	1.71	1.16	0.83	1.3
6	1.37	1.04	0.96	1.83	2.11	1.56	1.47	1.33	1.15	1.35	1.6	1.03	1.07	1.68	1.83	1.2	1.12	1.58	1.21	0.88	1.32
5	1.35	1.04	0.96	1.8	2.26	1.51	1.51	1.33	1.16	1.38	1.36	1.04	1.07	1.49	1.84	1.24	1.15	1.41	1.24	0.91	1.25
4	1.36	1.06	0.95	1.75	2.39	1.52	1.7	1.34	1.17	1.44	1.28	1.11	1.07	1.33	1.87	1.35	1.17	1.32	1.28	0.94	1.19
3	1.35	1.06	0.92	1.63	2.45	1.53	1.84	1.3	1.14	1.45	1.2	1.12	1.11	1.22	1.85	1.41	1.15	1.3	1.28	0.94	1.08
2	1.28	1	0.85	1.5	2.4	1.47	1.88	1.21	1.05	1.39	1.11	1.07	1.09	1.08	1.74	1.39	1.08	1.25	1.22	0.88	0.98
1	1.05	0.78	0.64	1.31	2.14	1.23	1.68	0.97	0.81	1.14	0.88	0.83	0.89	0.83	1.45	1.18	0.86	1.01	0.99	0.68	0.75

Table A.34 10-storey visco-plastic (λ=0.8) drift summary (MCE)

Storey	Mean value (%)	Q1 (%)	Q2 (%)	Q3 (%)	Q4 (%)	Q5 (%)	Q6 (%)	Q7 (%)	Q8 (%)	Q9 (%)	Q10 (%)	Q11 (%)	Q12 (%)	Q13 (%)	Q14 (%)	Q15 (%)	Q16 (%)	Q17 (%)	Q18 (%)	Q19 (%)	Q20 (%)
Max	1.39	1.06	0.96	1.84	2.45	1.63	2.03	1.34	1.17	1.45	2.31	1.12	1.11	2.00	2.17	1.41	1.17	1.87	1.54	0.94	1.32
10	1.11	0.7	0.6	0.98	0.94	1.38	2.03	1.06	0.68	0.88	2.14	0.78	0.74	1.55	2.13	0.68	0.65	1.42	1.48	0.57	0.81
9	1.25	0.86	0.75	1.28	1.25	1.42	1.79	1.18	0.86	1.09	2.29	0.93	0.91	1.86	1.93	0.85	0.82	1.73	1.54	0.71	1.03
8	1.34	0.97	0.86	1.58	1.6	1.58	1.6	1.18	1	1.23	2.31	1.01	1.01	2	1.75	1.01	0.95	1.87	1.3	0.8	1.22
7	1.39	1.02	0.93	1.76	1.88	1.63	1.56	1.28	1.09	1.28	2.04	1.02	1.04	1.95	1.97	1.11	1.05	1.81	1.16	0.83	1.3
6	1.39	1.04	0.96	1.84	2.1	1.57	1.49	1.33	1.15	1.34	1.62	1.03	1.07	1.74	2.06	1.2	1.12	1.65	1.21	0.88	1.32
5	1.36	1.04	0.96	1.8	2.26	1.49	1.51	1.33	1.16	1.38	1.32	1.04	1.07	1.49	2.07	1.24	1.15	1.48	1.24	0.91	1.25
4	1.37	1.06	0.95	1.74	2.39	1.51	1.64	1.34	1.17	1.44	1.23	1.11	1.07	1.31	2.14	1.35	1.17	1.38	1.28	0.94	1.19
3	1.36	1.06	0.92	1.62	2.45	1.53	1.74	1.3	1.14	1.45	1.19	1.12	1.11	1.22	2.17	1.41	1.15	1.39	1.28	0.94	1.08
2	1.30	1	0.85	1.53	2.41	1.48	1.76	1.21	1.05	1.39	1.12	1.07	1.09	1.08	2.09	1.39	1.08	1.36	1.22	0.88	0.98
1	1.07	0.78	0.64	1.35	2.15	1.24	1.55	0.97	0.81	1.14	0.9	0.83	0.89	0.83	1.81	1.18	0.86	1.13	0.99	0.68	0.75

Table A.35 10-storey visco-plastic (λ=0.6) drift summary (MCE)

Storey	Mean value (%)	Q1 (%)	Q2 (%)	Q3 (%)	Q4 (%)	Q5 (%)	Q6 (%)	Q7 (%)	Q8 (%)	Q9 (%)	Q10 (%)	Q11 (%)	Q12 (%)	Q13 (%)	Q14 (%)	Q15 (%)	Q16 (%)	Q17 (%)	Q18 (%)	Q19 (%)	Q20 (%)
Max	1.45	1.06	0.96	1.99	2.66	1.64	2.31	1.36	1.17	1.46	2.64	1.11	1.11	2.43	2.45	1.41	1.17	2.02	2.36	0.94	1.34
10	1.24	0.7	0.6	1.1	0.82	1.5	2.31	1.25	0.68	1.01	2.64	0.86	0.76	1.96	1.95	0.68	0.65	1.66	2.36	0.57	0.82
9	1.36	0.86	0.75	1.39	1.1	1.47	1.88	1.36	0.86	1.22	2.64	0.99	0.92	2.28	1.9	0.85	0.82	1.94	2.23	0.71	1.05
8	1.42	0.97	0.86	1.74	1.43	1.58	1.56	1.26	1	1.32	2.53	1.02	1.02	2.43	2.03	1.01	0.95	2.02	1.63	0.8	1.24
7	1.45	1.02	0.93	1.96	1.74	1.64	1.54	1.29	1.09	1.31	2.15	1.02	1.06	2.3	2.22	1.11	1.05	1.92	1.44	0.83	1.34
6	1.44	1.04	0.96	1.99	2.02	1.56	1.49	1.33	1.15	1.3	1.62	1.03	1.08	1.96	2.32	1.2	1.12	1.75	1.64	0.88	1.34
5	1.41	1.04	0.96	1.86	2.22	1.5	1.46	1.33	1.16	1.33	1.34	1.05	1.07	1.56	2.34	1.24	1.15	1.54	1.8	0.91	1.26
4	1.42	1.06	0.95	1.71	2.44	1.53	1.66	1.33	1.17	1.41	1.22	1.11	1.07	1.34	2.42	1.35	1.17	1.41	2.02	0.94	1.18
3	1.43	1.06	0.92	1.55	2.62	1.59	1.7	1.3	1.14	1.46	1.2	1.11	1.11	1.25	2.45	1.41	1.15	1.4	2.119	0.94	1.07
2	1.39	1	0.85	1.6	2.66	1.56	1.63	1.21	1.05	1.41	1.17	1.05	1.09	1.1	2.39	1.39	1.08	1.4	2.21	0.88	0.97
1	1.15	0.78	0.64	1.41	2.42	1.32	1.39	0.97	0.81	1.15	0.95	0.81	0.89	0.82	2.1	1.18	0.86	1.18	1.96	0.68	0.75

Table A.36 10-storey visco-plastic (λ=0.4) drift summary (MCE)

Storey	Mean value (%)	Q1 (%)	Q2 (%)	Q3 (%)	Q4 (%)	Q5 (%)	Q6 (%)	Q7 (%)	Q8 (%)	Q9 (%)	Q10 (%)	Q11 (%)	Q12 (%)	Q13 (%)	Q14 (%)	Q15 (%)	Q16 (%)	Q17 (%)	Q18 (%)	Q19 (%)	Q20 (%)
Max	1.54	1.07	0.97	2.28	3.40	1.79	2.60	1.57	1.18	1.55	3.12	1.16	1.18	2.97	2.56	1.42	1.17	2.19	2.02	0.94	1.58
10	1.42	0.8	0.61	1.32	0.93	1.79	2.6	1.5	0.72	1.26	3.12	1.07	0.93	2.51	2.3	0.71	0.69	2.02	2.02	0.6	0.94
9	1.52	0.95	0.76	1.61	1.24	1.67	2.05	1.57	0.9	1.47	3.01	1.16	1.1	2.87	2.21	0.89	0.86	2.19	1.96	0.72	1.19
8	1.54	1.04	0.87	2.03	1.61	1.55	1.74	1.37	1.05	1.55	2.67	1.11	1.18	2.97	1.98	1.06	1.01	2.16	1.48	0.81	1.46
7	1.53	1.07	0.94	2.28	1.96	1.63	1.64	1.35	1.15	1.46	2.18	1.07	1.18	2.7	2.18	1.17	1.11	2.04	1.13	0.85	1.58
6	1.50	1.07	0.97	2.22	2.33	1.6	1.57	1.4	1.18	1.31	1.72	1.08	1.16	2.19	2.34	1.24	1.16	1.81	1.2	0.87	1.52
5	1.45	1.04	0.96	1.92	2.64	1.56	1.79	1.38	1.17	1.32	1.5	1.09	1.09	1.68	2.43	1.26	1.17	1.54	1.25	0.91	1.32
4	1.47	1.06	0.95	1.77	2.98	1.62	2.07	1.37	1.17	1.45	1.39	1.15	1.1	1.46	2.53	1.35	1.17	1.41	1.34	0.94	1.16
3	1.48	1.07	0.92	1.88	3.27	1.7	2.02	1.33	1.13	1.53	1.37	1.12	1.13	1.28	2.56	1.42	1.14	1.4	1.39	0.94	1.03
2	1.43	1.01	0.84	1.93	3.4	1.71	1.82	1.24	1.04	1.49	1.32	1.06	1.1	1.12	2.45	1.41	1.07	1.46	1.35	0.88	0.94
1	1.20	0.79	0.64	1.73	3.2	1.48	1.56	0.99	0.8	1.23	1.06	0.82	0.89	0.85	2.13	1.19	0.85	1.26	1.11	0.68	0.72

Table A.37 10-storey visco-plastic (λ=0.2) drift summary (MCE)

Storey	Mean value (%)	Q1 (%)	Q2 (%)	Q3 (%)	Q4 (%)	Q5 (%)	Q6 (%)	Q7 (%)	Q8 (%)	Q9 (%)	Q10 (%)	Q11 (%)	Q12 (%)	Q13 (%)	Q14 (%)	Q15 (%)	Q16 (%)	Q17 (%)	Q18 (%)	Q19 (%)	Q20 (%)
Max	1.77	1.36	1.02	2.64	4.72	2.45	2.76	1.70	1.36	1.76	3.20	1.39	1.52	3.38	3.15	2.34	1.47	2.69	2.21	1.04	1.79
10	1.69	1.04	0.73	1.37	1.33	2.45	2.76	1.7	0.83	1.62	3.2	1.27	1.12	2.9	3.15	0.9	0.81	2.55	2.21	0.79	1.03
9	1.77	1.26	0.85	1.65	1.74	2.06	2.49	1.67	1	1.76	3.05	1.39	1.31	3.27	2.79	1.1	0.99	2.69	2.1	0.89	1.31
8	1.75	1.36	0.95	1.95	2.3	1.66	2.17	1.34	1.18	1.74	2.72	1.32	1.35	3.38	2.35	1.3	1.13	2.6	1.56	0.98	1.63
7	1.71	1.27	1.01	2.04	2.85	1.73	2.08	1.48	1.33	1.58	2.22	1.21	1.38	3.06	2.12	1.45	1.27	2.27	1.11	0.99	1.79
6	1.69	1.16	1.02	2.08	3.33	1.66	2.4	1.54	1.36	1.42	1.65	1.16	1.37	2.42	2.37	1.59	1.39	1.89	1.24	0.96	1.71
5	1.66	1.18	1.01	2.11	3.73	1.7	2.31	1.55	1.3	1.44	1.49	1.27	1.34	1.75	2.55	1.76	1.44	1.57	1.33	1	1.44
4	1.73	1.23	1.01	2.32	4.19	1.78	2.43	1.54	1.32	1.6	1.53	1.35	1.46	1.46	2.63	2.02	1.47	1.62	1.43	1.03	1.17
3	1.76	1.22	0.97	2.52	4.56	1.88	2.26	1.52	1.29	1.59	1.64	1.26	1.52	1.26	2.57	2.24	1.44	1.93	1.49	1.04	1.01
2	1.72	1.15	0.87	2.64	4.72	1.91	2.1	1.44	1.19	1.44	1.62	1.18	1.48	1.07	2.41	2.34	1.39	2.13	1.46	0.97	0.94
1	1.49	0.93	0.65	2.49	4.46	1.7	1.89	1.17	0.92	1.14	1.37	0.93	1.22	0.81	2.09	2.15	1.15	2.01	1.21	0.75	0.72

Table A.38 20-storey base shear (DBE)

	Mean value	Q1 (kN)	Q2 (kN)	Q3 (kN)	Q4 (kN)	Q5 (kN)	Q6 (kN)	Q7 (kN)	Q8 (kN)	Q9 (kN)	Q10 (kN)	Q11 (kN)	Q12 (kN)	Q13 (kN)	Q14 (kN)	Q15 (kN)	Q16 (kN)	Q17 (kN)	Q18 (kN)	Q19 (kN)	Q20 (kN)
Viscoelastic	4307	4066	2678	3305	3597	7465	8515	3565	2604	3136	4651	3347	2268	6270	6873	1594	2624	3966	9730	2292	3589
Visco-plastic (λ=1.0)	3976	3993	2680	3297	3597	6121	7186	3564	2606	3155	4766	3300	2270	5430	5909	1595	2625	3799	7833	2293	3498
Visco-plastic (λ=0.8)	3886	3823	2680	3192	3597	5990	6804	3588	2606	3083	4803	3162	2270	5161	5893	1596	2625	3640	7587	2293	3326
Visco-plastic (λ=0.6)	3797	3668	2680	3209	3593	5773	6757	3496	2605	2946	4557	2950	2270	5050	5771	1596	2625	3388	7676	2293	3026
Visco-plastic (λ=0.4)	3699	3554	2616	3055	3479	5573	6523	3554	2599	2670	4116	2709	2266	5251	5808	1596	2624	3201	7772	2298	2722
Visco-plastic (λ=0.2)	3545	3421	2284	2577	3534	5298	5778	3421	2411	2203	3669	2430	2062	6012	5975	1633	2648	3516	7385	2165	2469

Table A.39 20-storey viscoelastic drift summary (DBE)

Storey	Mean value (%)	Q1 (%)	Q2 (%)	Q3 (%)	Q4 (%)	Q5 (%)	Q6 (%)	Q7 (%)	Q8 (%)	Q9 (%)	Q10 (%)	Q11 (%)	Q12 (%)	Q13 (%)	Q14 (%)	Q15 (%)	Q16 (%)	Q17 (%)	Q18 (%)	Q19 (%)	Q20 (%)
Max	0.62	0.67	0.56	0.43	0.56	0.86	0.69	0.73	0.67	0.48	0.78	0.46	0.40	1.00	0.71	0.32	0.49	0.58	0.91	0.43	0.75
20	0.51	0.56	0.41	0.34	0.38	0.75	0.6	0.59	0.52	0.42	0.7	0.37	0.31	0.82	0.64	0.24	0.36	0.48	0.78	0.33	0.62
19	0.55	0.6	0.44	0.36	0.41	0.8	0.64	0.64	0.56	0.45	0.75	0.4	0.33	0.89	0.68	0.26	0.39	0.51	0.82	0.36	0.67
18	0.59	0.64	0.49	0.39	0.45	0.85	0.68	0.69	0.61	0.47	0.78	0.43	0.36	0.96	0.69	0.29	0.42	0.55	0.87	0.39	0.72
17	0.61	0.67	0.53	0.41	0.49	0.86	0.69	0.72	0.65	0.48	0.77	0.45	0.38	1	0.71	0.31	0.46	0.58	0.9	0.42	0.75
16	0.62	0.67	0.55	0.42	0.52	0.85	0.66	0.73	0.67	0.47	0.73	0.46	0.4	1	0.7	0.32	0.48	0.58	0.91	0.43	0.75
15	0.60	0.65	0.56	0.41	0.53	0.8	0.62	0.71	0.67	0.45	0.65	0.45	0.4	0.94	0.66	0.32	0.49	0.57	0.9	0.43	0.71
14	0.55	0.6	0.53	0.38	0.51	0.72	0.54	0.65	0.63	0.4	0.55	0.42	0.39	0.83	0.58	0.31	0.47	0.52	0.84	0.41	0.63
13	0.53	0.59	0.53	0.37	0.52	0.69	0.51	0.63	0.62	0.39	0.49	0.41	0.39	0.75	0.53	0.31	0.47	0.5	0.83	0.41	0.58
12	0.51	0.6	0.53	0.38	0.52	0.67	0.49	0.61	0.6	0.39	0.45	0.4	0.39	0.69	0.5	0.31	0.48	0.48	0.83	0.41	0.54
11	0.51	0.6	0.53	0.4	0.53	0.66	0.51	0.6	0.59	0.39	0.44	0.39	0.39	0.63	0.52	0.31	0.48	0.46	0.82	0.42	0.49
10	0.51	0.61	0.53	0.42	0.55	0.66	0.57	0.58	0.58	0.4	0.44	0.4	0.4	0.59	0.53	0.31	0.49	0.45	0.82	0.42	0.47
9	0.50	0.6	0.52	0.42	0.55	0.65	0.6	0.56	0.56	0.39	0.45	0.39	0.39	0.56	0.54	0.3	0.48	0.43	0.8	0.42	0.44
8	0.50	0.59	0.51	0.43	0.55	0.65	0.63	0.54	0.54	0.39	0.46	0.39	0.38	0.54	0.55	0.3	0.48	0.44	0.8	0.42	0.42
7	0.50	0.58	0.49	0.43	0.56	0.66	0.66	0.53	0.51	0.38	0.48	0.39	0.37	0.52	0.56	0.3	0.47	0.45	0.79	0.41	0.41
6	0.50	0.57	0.48	0.43	0.56	0.67	0.68	0.51	0.49	0.38	0.5	0.38	0.37	0.51	0.57	0.3	0.47	0.46	0.78	0.41	0.39
5	0.48	0.54	0.46	0.42	0.55	0.67	0.68	0.49	0.45	0.36	0.51	0.37	0.36	0.49	0.57	0.29	0.46	0.46	0.77	0.39	0.38
4	0.46	0.51	0.43	0.4	0.52	0.65	0.66	0.46	0.41	0.34	0.5	0.34	0.33	0.47	0.55	0.27	0.43	0.44	0.74	0.36	0.35
3	0.41	0.45	0.37	0.35	0.47	0.59	0.6	0.41	0.36	0.29	0.46	0.3	0.29	0.43	0.51	0.24	0.38	0.4	0.67	0.32	0.31
2	0.32	0.34	0.28	0.28	0.37	0.48	0.48	0.32	0.28	0.23	0.36	0.23	0.22	0.34	0.41	0.18	0.3	0.31	0.53	0.25	0.24
1	0.18	0.19	0.16	0.15	0.2	0.27	0.27	0.18	0.15	0.12	0.21	0.12	0.12	0.19	0.24	0.1	0.16	0.18	0.3	0.13	0.13

Table A.40 20-storey visco-plastic (λ=1.0) drift summary (DBE)

Storey	Mean value (%)	Q1 (%)	Q2 (%)	Q3 (%)	Q4 (%)	Q5 (%)	Q6 (%)	Q7 (%)	Q8 (%)	Q9 (%)	Q10 (%)	Q11 (%)	Q12 (%)	Q13 (%)	Q14 (%)	Q15 (%)	Q16 (%)	Q17 (%)	Q18 (%)	Q19 (%)	Q20 (%)
Max	0.66	0.68	0.56	0.43	0.56	0.96	0.83	0.72	0.67	0.48	1.06	0.46	0.40	1.24	0.99	0.32	0.49	0.59	1.35	0.43	0.77
20	0.62	0.6	0.41	0.34	0.38	0.96	0.83	0.65	0.52	0.45	1.05	0.38	0.31	1.06	0.99	0.24	0.36	0.49	1.35	0.33	0.7
19	0.64	0.63	0.44	0.36	0.41	0.96	0.83	0.68	0.56	0.47	1.06	0.4	0.33	1.16	0.97	0.26	0.39	0.52	1.35	0.36	0.74
18	0.66	0.66	0.49	0.39	0.45	0.94	0.8	0.71	0.61	0.48	1.01	0.43	0.36	1.24	0.89	0.29	0.42	0.56	1.25	0.39	0.77
17	0.65	0.68	0.53	0.41	0.49	0.89	0.75	0.72	0.65	0.48	0.91	0.45	0.38	1.23	0.78	0.31	0.46	0.58	1.03	0.42	0.77
16	0.63	0.67	0.55	0.42	0.52	0.83	0.67	0.72	0.67	0.47	0.77	0.46	0.4	1.14	0.74	0.32	0.48	0.59	0.91	0.43	0.75
15	0.59	0.65	0.56	0.41	0.53	0.76	0.59	0.7	0.67	0.44	0.62	0.45	0.4	0.99	0.68	0.32	0.49	0.57	0.88	0.43	0.7
14	0.54	0.59	0.53	0.38	0.51	0.69	0.52	0.65	0.63	0.4	0.48	0.42	0.39	0.81	0.58	0.31	0.47	0.52	0.82	0.41	0.62
13	0.52	0.59	0.53	0.37	0.52	0.67	0.49	0.63	0.62	0.39	0.43	0.41	0.39	0.7	0.52	0.31	0.47	0.5	0.81	0.41	0.57
12	0.51	0.6	0.53	0.38	0.52	0.66	0.47	0.61	0.61	0.39	0.44	0.4	0.39	0.62	0.52	0.31	0.48	0.48	0.81	0.41	0.53
11	0.50	0.6	0.53	0.4	0.53	0.65	0.49	0.6	0.59	0.39	0.44	0.39	0.39	0.59	0.53	0.31	0.48	0.46	0.81	0.42	0.49
10	0.51	0.61	0.53	0.42	0.55	0.65	0.54	0.58	0.58	0.4	0.45	0.4	0.4	0.57	0.54	0.31	0.49	0.45	0.8	0.42	0.47
9	0.50	0.59	0.52	0.42	0.55	0.64	0.56	0.56	0.56	0.39	0.46	0.39	0.39	0.54	0.54	0.3	0.48	0.43	0.78	0.42	0.44
8	0.50	0.59	0.51	0.43	0.55	0.64	0.58	0.54	0.54	0.39	0.48	0.39	0.38	0.52	0.54	0.3	0.48	0.44	0.77	0.42	0.42
7	0.49	0.58	0.49	0.43	0.56	0.64	0.61	0.53	0.51	0.38	0.49	0.39	0.37	0.5	0.54	0.3	0.47	0.45	0.77	0.41	0.41
6	0.49	0.56	0.48	0.43	0.56	0.65	0.63	0.51	0.49	0.38	0.51	0.38	0.37	0.5	0.54	0.3	0.47	0.46	0.81	0.41	0.4
5	0.49	0.54	0.46	0.42	0.55	0.67	0.66	0.49	0.45	0.36	0.52	0.37	0.36	0.49	0.55	0.29	0.46	0.46	0.83	0.39	0.38
4	0.47	0.51	0.43	0.4	0.52	0.68	0.67	0.46	0.41	0.34	0.52	0.34	0.33	0.47	0.57	0.27	0.43	0.44	0.81	0.36	0.35
3	0.42	0.44	0.37	0.35	0.47	0.66	0.66	0.41	0.36	0.29	0.49	0.3	0.29	0.44	0.56	0.24	0.38	0.39	0.75	0.32	0.31
2	0.35	0.34	0.28	0.28	0.37	0.55	0.58	0.32	0.28	0.23	0.41	0.23	0.22	0.39	0.48	0.18	0.3	0.3	0.67	0.25	0.24
1	0.20	0.18	0.16	0.15	0.2	0.32	0.35	0.18	0.15	0.12	0.24	0.12	0.12	0.24	0.29	0.1	0.16	0.17	0.4	0.13	0.13

Table A.41 20-storey visco-plastic (λ=0.8) drift summary (DBE)

Storey	Mean value (%)	Q1 (%)	Q2 (%)	Q3 (%)	Q4 (%)	Q5 (%)	Q6 (%)	Q7 (%)	Q8 (%)	Q9 (%)	Q10 (%)	Q11 (%)	Q12 (%)	Q13 (%)	Q14 (%)	Q15 (%)	Q16 (%)	Q17 (%)	Q18 (%)	Q19 (%)	Q20 (%)
Max	0.69	0.69	0.56	0.43	0.56	1.00	0.89	0.75	0.67	0.49	1.14	0.46	0.40	1.35	1.03	0.32	0.49	0.59	1.54	0.43	0.83
20	0.66	0.64	0.41	0.34	0.38	1	0.89	0.69	0.53	0.48	1.13	0.39	0.31	1.14	1.03	0.24	0.36	0.52	1.54	0.33	0.77
19	0.68	0.67	0.45	0.36	0.41	1	0.89	0.72	0.57	0.49	1.14	0.41	0.33	1.25	1	0.26	0.39	0.55	1.53	0.36	0.81
18	0.69	0.69	0.49	0.39	0.45	0.96	0.86	0.75	0.62	0.49	1.09	0.44	0.36	1.35	0.91	0.29	0.42	0.58	1.4	0.39	0.83
17	0.67	0.69	0.53	0.41	0.49	0.9	0.8	0.75	0.65	0.48	0.97	0.45	0.38	1.34	0.83	0.31	0.46	0.59	1.11	0.42	0.83
16	0.64	0.68	0.55	0.42	0.52	0.84	0.71	0.73	0.67	0.46	0.82	0.46	0.4	1.22	0.78	0.32	0.48	0.59	0.95	0.43	0.79
15	0.60	0.64	0.56	0.41	0.53	0.77	0.6	0.7	0.67	0.43	0.64	0.45	0.4	1.04	0.7	0.32	0.49	0.57	0.92	0.43	0.72
14	0.54	0.6	0.53	0.38	0.51	0.68	0.5	0.64	0.63	0.39	0.47	0.42	0.39	0.82	0.59	0.31	0.47	0.52	0.85	0.41	0.62
13	0.51	0.6	0.53	0.37	0.52	0.64	0.49	0.62	0.62	0.39	0.42	0.41	0.39	0.69	0.52	0.31	0.47	0.49	0.83	0.41	0.56
12	0.50	0.6	0.53	0.38	0.52	0.64	0.48	0.61	0.6	0.39	0.42	0.4	0.39	0.6	0.52	0.31	0.48	0.47	0.82	0.41	0.51
11	0.50	0.6	0.53	0.4	0.53	0.64	0.48	0.6	0.59	0.39	0.44	0.39	0.39	0.58	0.54	0.31	0.48	0.46	0.81	0.42	0.48
10	0.51	0.6	0.53	0.42	0.55	0.64	0.53	0.58	0.58	0.4	0.46	0.4	0.4	0.56	0.56	0.31	0.49	0.44	0.8	0.42	0.47
9	0.50	0.59	0.52	0.42	0.55	0.63	0.56	0.56	0.56	0.39	0.46	0.39	0.39	0.53	0.55	0.3	0.48	0.42	0.78	0.42	0.44
8	0.50	0.58	0.51	0.43	0.55	0.63	0.59	0.54	0.54	0.39	0.48	0.39	0.38	0.5	0.55	0.3	0.48	0.44	0.78	0.42	0.42
7	0.49	0.57	0.5	0.43	0.56	0.65	0.61	0.53	0.51	0.38	0.5	0.39	0.37	0.49	0.55	0.29	0.47	0.45	0.8	0.41	0.41
6	0.49	0.56	0.48	0.43	0.56	0.67	0.64	0.51	0.49	0.38	0.52	0.38	0.37	0.48	0.56	0.29	0.47	0.45	0.83	0.41	0.4
5	0.49	0.54	0.46	0.42	0.55	0.7	0.67	0.49	0.45	0.36	0.54	0.37	0.36	0.48	0.58	0.27	0.46	0.45	0.83	0.39	0.38
4	0.47	0.5	0.43	0.4	0.52	0.72	0.73	0.46	0.41	0.34	0.56	0.34	0.33	0.48	0.59	0.25	0.43	0.43	0.81	0.36	0.35
3	0.44	0.44	0.37	0.36	0.47	0.69	0.74	0.41	0.36	0.3	0.54	0.3	0.29	0.47	0.59	0.22	0.38	0.39	0.79	0.32	0.31
2	0.36	0.34	0.28	0.28	0.37	0.58	0.64	0.32	0.28	0.23	0.46	0.23	0.22	0.41	0.51	0.17	0.3	0.3	0.7	0.25	0.25
1	0.20	0.19	0.16	0.16	0.2	0.34	0.38	0.18	0.15	0.12	0.27	0.13	0.12	0.26	0.31	0.09	0.16	0.17	0.42	0.13	0.14

Table A.42 20-storey visco-plastic (λ=0.6) drift summary (DBE)

Storey	Mean value (%)	Q1 (%)	Q2 (%)	Q3 (%)	Q4 (%)	Q5 (%)	Q6 (%)	Q7 (%)	Q8 (%)	Q9 (%)	Q10 (%)	Q11 (%)	Q12 (%)	Q13 (%)	Q14 (%)	Q15 (%)	Q16 (%)	Q17 (%)	Q18 (%)	Q19 (%)	Q20 (%)
Max	0.73	0.73	0.56	0.43	0.56	1.06	0.99	0.79	0.68	0.52	1.21	0.47	0.40	1.50	1.10	0.32	0.49	0.63	1.90	0.43	0.92
20	0.71	0.68	0.42	0.34	0.38	1.06	0.99	0.74	0.57	0.51	1.2	0.42	0.31	1.29	1.1	0.24	0.36	0.57	1.9	0.33	0.85
19	0.73	0.71	0.46	0.37	0.41	1.05	0.98	0.77	0.61	0.52	1.21	0.44	0.33	1.4	1.06	0.26	0.39	0.6	1.86	0.36	0.89
18	0.73	0.73	0.5	0.39	0.45	0.98	0.94	0.79	0.65	0.51	1.15	0.46	0.36	1.5	0.96	0.29	0.42	0.63	1.67	0.39	0.92
17	0.71	0.72	0.53	0.41	0.49	0.9	0.86	0.78	0.67	0.48	1.02	0.46	0.38	1.48	0.93	0.31	0.46	0.63	1.3	0.42	0.91
16	0.67	0.7	0.56	0.42	0.52	0.87	0.76	0.76	0.68	0.45	0.85	0.47	0.4	1.33	0.86	0.32	0.48	0.61	1.05	0.43	0.87
15	0.62	0.66	0.56	0.41	0.53	0.8	0.64	0.71	0.67	0.41	0.67	0.46	0.4	1.1	0.76	0.32	0.49	0.57	1.02	0.43	0.78
14	0.55	0.61	0.54	0.38	0.51	0.69	0.53	0.64	0.63	0.39	0.48	0.42	0.39	0.84	0.63	0.31	0.47	0.52	0.96	0.41	0.65
13	0.52	0.6	0.53	0.37	0.52	0.65	0.51	0.61	0.61	0.39	0.42	0.41	0.39	0.68	0.57	0.31	0.47	0.49	0.94	0.41	0.56
12	0.51	0.6	0.53	0.38	0.52	0.64	0.49	0.6	0.6	0.39	0.41	0.4	0.39	0.6	0.6	0.31	0.48	0.46	0.92	0.41	0.49
11	0.51	0.6	0.53	0.4	0.54	0.64	0.54	0.59	0.59	0.39	0.43	0.39	0.39	0.57	0.63	0.31	0.48	0.45	0.89	0.42	0.48
10	0.52	0.6	0.53	0.42	0.55	0.65	0.59	0.58	0.58	0.4	0.46	0.4	0.4	0.53	0.64	0.31	0.49	0.44	0.87	0.42	0.46
9	0.51	0.59	0.52	0.42	0.55	0.65	0.6	0.56	0.55	0.39	0.48	0.39	0.39	0.5	0.62	0.3	0.48	0.42	0.83	0.42	0.44
8	0.50	0.58	0.51	0.43	0.55	0.67	0.62	0.54	0.53	0.39	0.51	0.39	0.38	0.49	0.61	0.3	0.48	0.43	0.81	0.42	0.43
7	0.50	0.57	0.49	0.43	0.56	0.69	0.62	0.53	0.51	0.38	0.54	0.39	0.37	0.49	0.59	0.29	0.47	0.44	0.82	0.41	0.41
6	0.51	0.56	0.48	0.43	0.56	0.73	0.69	0.51	0.49	0.38	0.58	0.38	0.37	0.5	0.6	0.29	0.47	0.45	0.84	0.41	0.4
5	0.50	0.54	0.46	0.43	0.55	0.76	0.77	0.5	0.45	0.36	0.61	0.37	0.36	0.5	0.61	0.27	0.46	0.45	0.86	0.39	0.38
4	0.49	0.51	0.43	0.41	0.53	0.77	0.84	0.47	0.41	0.34	0.62	0.34	0.33	0.52	0.64	0.25	0.43	0.43	0.87	0.36	0.35
3	0.46	0.46	0.37	0.37	0.47	0.74	0.84	0.43	0.36	0.3	0.59	0.31	0.29	0.52	0.64	0.22	0.38	0.4	0.89	0.32	0.32
2	0.38	0.37	0.29	0.3	0.37	0.61	0.71	0.35	0.28	0.24	0.49	0.24	0.22	0.45	0.56	0.17	0.3	0.32	0.77	0.25	0.25
1	0.22	0.21	0.16	0.17	0.2	0.35	0.41	0.2	0.15	0.14	0.28	0.14	0.12	0.27	0.33	0.09	0.16	0.19	0.45	0.13	0.15

Table A.43 20-storey visco-plastic (λ=0.4) drift summary (DBE)

Storey	Mean value (%)	Q1 (%)	Q2 (%)	Q3 (%)	Q4 (%)	Q5 (%)	Q6 (%)	Q7 (%)	Q8 (%)	Q9 (%)	Q10 (%)	Q11 (%)	Q12 (%)	Q13 (%)	Q14 (%)	Q15 (%)	Q16 (%)	Q17 (%)	Q18 (%)	Q19 (%)	Q20 (%)
Max	0.83	0.76	0.57	0.43	0.57	1.22	1.26	0.76	0.73	0.55	1.34	0.50	0.40	1.90	1.47	0.32	0.49	0.69	2.11	0.43	1.04
20	0.82	0.71	0.48	0.38	0.4	1.22	1.26	0.71	0.63	0.54	1.34	0.46	0.31	1.74	1.47	0.24	0.36	0.63	2.11	0.35	0.96
19	0.83	0.74	0.49	0.4	0.43	1.2	1.21	0.74	0.67	0.55	1.34	0.48	0.33	1.85	1.46	0.26	0.39	0.67	2.06	0.37	1.01
18	0.82	0.76	0.5	0.42	0.46	1.09	1.08	0.76	0.71	0.54	1.26	0.49	0.36	1.9	1.31	0.29	0.43	0.69	1.88	0.4	1.04
17	0.77	0.75	0.54	0.43	0.5	0.93	0.93	0.75	0.73	0.51	1.07	0.5	0.38	1.81	1.12	0.31	0.46	0.69	1.45	0.42	1.04
16	0.72	0.72	0.56	0.43	0.52	0.93	0.84	0.72	0.73	0.46	0.87	0.49	0.39	1.56	0.99	0.32	0.48	0.66	1.33	0.43	0.99
15	0.67	0.69	0.57	0.41	0.53	0.88	0.75	0.69	0.71	0.41	0.7	0.47	0.4	1.2	0.86	0.32	0.49	0.61	1.33	0.43	0.89
14	0.59	0.65	0.54	0.38	0.51	0.76	0.63	0.65	0.65	0.39	0.52	0.43	0.38	0.89	0.72	0.31	0.47	0.53	1.24	0.41	0.74
13	0.56	0.63	0.53	0.36	0.52	0.73	0.61	0.63	0.62	0.39	0.43	0.41	0.38	0.79	0.74	0.31	0.47	0.49	1.21	0.41	0.62
12	0.55	0.62	0.53	0.37	0.53	0.71	0.67	0.62	0.59	0.39	0.44	0.39	0.39	0.72	0.79	0.31	0.48	0.46	1.14	0.41	0.51
11	0.55	0.62	0.53	0.39	0.54	0.71	0.73	0.62	0.57	0.4	0.48	0.39	0.39	0.63	0.82	0.31	0.48	0.44	1.04	0.42	0.46
10	0.55	0.62	0.53	0.41	0.55	0.72	0.75	0.62	0.56	0.4	0.52	0.4	0.39	0.54	0.81	0.31	0.49	0.43	0.99	0.42	0.45
9	0.53	0.6	0.51	0.41	0.55	0.72	0.71	0.6	0.53	0.4	0.55	0.39	0.39	0.52	0.75	0.3	0.48	0.41	0.93	0.42	0.43
8	0.53	0.6	0.5	0.42	0.56	0.74	0.68	0.6	0.51	0.4	0.58	0.39	0.38	0.52	0.7	0.3	0.48	0.42	0.89	0.42	0.42
7	0.53	0.59	0.49	0.43	0.56	0.77	0.74	0.59	0.49	0.39	0.62	0.39	0.38	0.51	0.67	0.3	0.47	0.44	0.88	0.41	0.41
6	0.54	0.59	0.48	0.43	0.57	0.8	0.86	0.59	0.47	0.39	0.65	0.39	0.37	0.56	0.67	0.3	0.47	0.45	0.89	0.41	0.4
5	0.54	0.58	0.46	0.43	0.56	0.83	0.97	0.58	0.44	0.38	0.67	0.38	0.36	0.63	0.69	0.29	0.46	0.46	0.93	0.39	0.38
4	0.54	0.56	0.43	0.42	0.54	0.83	1.03	0.56	0.41	0.36	0.66	0.35	0.34	0.7	0.73	0.27	0.43	0.46	1.02	0.37	0.36
3	0.51	0.52	0.38	0.4	0.49	0.79	0.99	0.52	0.37	0.31	0.61	0.31	0.31	0.71	0.73	0.24	0.38	0.43	1.02	0.32	0.32
2	0.41	0.42	0.3	0.32	0.4	0.65	0.79	0.42	0.29	0.24	0.49	0.25	0.24	0.61	0.63	0.18	0.3	0.35	0.85	0.25	0.26
1	0.23	0.24	0.17	0.18	0.22	0.37	0.44	0.24	0.16	0.14	0.28	0.15	0.13	0.36	0.37	0.1	0.16	0.2	0.49	0.14	0.15

Table A.44 20-storey visco-plastic (λ=0.2) drift summary (DBE)

Storey	Mean value (%)	Q1 (%)	Q2 (%)	Q3 (%)	Q4 (%)	Q5 (%)	Q6 (%)	Q7 (%)	Q8 (%)	Q9 (%)	Q10 (%)	Q11 (%)	Q12 (%)	Q13 (%)	Q14 (%)	Q15 (%)	Q16 (%)	Q17 (%)	Q18 (%)	Q19 (%)	Q20 (%)
Max	1.02	0.94	0.58	0.50	0.68	1.56	1.73	0.94	0.76	0.61	1.73	0.63	0.41	2.68	2.30	0.33	0.52	0.83	2.02	0.50	1.22
20	1.02	0.91	0.5	0.43	0.55	1.56	1.73	0.91	0.64	0.61	1.73	0.58	0.31	2.61	2.3	0.26	0.43	0.78	2.02	0.47	1.06
19	1.02	0.94	0.51	0.45	0.58	1.54	1.64	0.94	0.67	0.61	1.72	0.6	0.33	2.67	2.08	0.28	0.46	0.82	1.99	0.49	1.15
18	0.99	0.94	0.52	0.47	0.62	1.4	1.43	0.94	0.71	0.59	1.63	0.62	0.35	2.68	1.71	0.3	0.48	0.83	1.81	0.5	1.22
17	0.92	0.91	0.54	0.49	0.65	1.17	1.16	0.91	0.74	0.54	1.38	0.63	0.37	2.5	1.35	0.32	0.49	0.82	1.61	0.5	1.22
16	0.85	0.86	0.57	0.5	0.66	1.03	1.01	0.86	0.76	0.51	1.05	0.61	0.38	2.13	1.14	0.33	0.51	0.79	1.73	0.5	1.16
15	0.79	0.84	0.58	0.48	0.64	1.02	0.96	0.84	0.75	0.45	0.75	0.56	0.38	1.6	1.04	0.33	0.52	0.72	1.79	0.49	1.05
14	0.71	0.8	0.55	0.43	0.61	0.91	0.91	0.8	0.68	0.4	0.56	0.48	0.37	1.17	1	0.31	0.5	0.61	1.72	0.47	0.87
13	0.68	0.78	0.54	0.39	0.61	0.85	0.88	0.78	0.65	0.39	0.47	0.42	0.38	1.1	1.15	0.3	0.5	0.57	1.64	0.43	0.71
12	0.67	0.76	0.53	0.41	0.62	0.84	0.98	0.76	0.61	0.4	0.54	0.42	0.39	0.98	1.26	0.3	0.51	0.54	1.51	0.43	0.57
11	0.64	0.73	0.52	0.43	0.63	0.83	0.97	0.73	0.59	0.4	0.58	0.42	0.4	0.84	1.22	0.3	0.51	0.51	1.32	0.43	0.51
10	0.61	0.7	0.51	0.45	0.64	0.84	0.91	0.7	0.57	0.41	0.6	0.41	0.41	0.66	1.07	0.31	0.52	0.49	1.17	0.43	0.49
9	0.58	0.66	0.49	0.46	0.65	0.83	0.83	0.66	0.54	0.4	0.62	0.4	0.41	0.59	0.87	0.3	0.51	0.46	1.03	0.44	0.47
8	0.57	0.66	0.47	0.47	0.67	0.85	0.84	0.66	0.5	0.4	0.67	0.4	0.4	0.58	0.74	0.3	0.51	0.48	0.95	0.44	0.46
7	0.59	0.66	0.47	0.48	0.67	0.87	1.04	0.66	0.46	0.4	0.7	0.41	0.4	0.69	0.7	0.3	0.5	0.5	0.98	0.45	0.45
6	0.62	0.66	0.48	0.49	0.68	0.9	1.19	0.66	0.46	0.39	0.72	0.42	0.4	0.81	0.77	0.3	0.51	0.52	1.11	0.45	0.44
5	0.64	0.66	0.47	0.48	0.68	0.92	1.21	0.66	0.47	0.38	0.73	0.42	0.39	0.93	0.88	0.3	0.51	0.52	1.24	0.45	0.43
4	0.63	0.64	0.45	0.46	0.66	0.91	1.12	0.64	0.46	0.36	0.7	0.41	0.37	1	0.97	0.29	0.49	0.53	1.32	0.42	0.41
3	0.58	0.64	0.4	0.41	0.59	0.84	0.96	0.58	0.42	0.32	0.63	0.37	0.34	0.94	0.95	0.26	0.45	0.51	1.26	0.38	0.37
2	0.46	0.58	0.31	0.32	0.47	0.68	0.73	0.46	0.33	0.26	0.49	0.3	0.26	0.74	0.76	0.21	0.36	0.43	0.99	0.29	0.29
1	0.26	0.46	0.17	0.18	0.26	0.38	0.41	0.26	0.18	0.15	0.27	0.16	0.15	0.41	0.42	0.12	0.2	0.24	0.54	0.16	0.17

Table A.45. 20-storey base shear (MCE)

	Mean value	Q1 (kN)	Q2 (kN)	Q3 (kN)	Q4 (kN)	Q5 (kN)	Q6 (kN)	Q7 (kN)	Q8 (kN)	Q9 (kN)	Q10 (kN)	Q11 (kN)	Q12 (kN)	Q13 (kN)	Q14 (kN)	Q15 (kN)	Q16 (kN)	Q17 (kN)	Q18 (kN)	Q19 (kN)	Q20 (kN)
Viscoelastic	6499	6099	4018	4958	5396	11344	12773	5347	3906	4705	6977	5020	3403	9404	10384	2391	3937	5949	15197	3438	5326
Visco-plastic (λ=1.0)	5668	5607	4020	4815	5397	8428	9527	5341	3907	4487	7016	4560	3405	7601	8607	2393	3938	5217	11000	3440	4644
Visco-plastic (λ=0.8)	5518	5374	4018	4749	5309	8183	9142	5205	3912	4304	6635	4290	3406	7585	8409	2393	3938	5014	10806	3440	4254
Visco-plastic (λ=0.6)	5367	5331	3923	4579	5217	7845	8897	4989	3895	4005	6175	4067	3399	7674	8251	2393	3936	4801	10648	3448	3874
Visco-plastic (λ=0.4)	5217	5187	3765	4113	5280	7756	8650	4787	3720	3530	5628	3820	3294	8039	7973	2402	3967	4947	10257	3385	3846
Visco-plastic (λ=0.2)	4996	5395	3180	3643	5383	7549	8422	4734	3315	3061	5413	3492	2709	8313	7236	2329	4222	5349	9612	3052	3512

Table A.46 20-storey viscoelastic drift summary (MCE)

Storey	Mean value (%)	Q1 (%)	Q2 (%)	Q3 (%)	Q4 (%)	Q5 (%)	Q6 (%)	Q7 (%)	Q8 (%)	Q9 (%)	Q10 (%)	Q11 (%)	Q12 (%)	Q13 (%)	Q14 (%)	Q15 (%)	Q16 (%)	Q17 (%)	Q18 (%)	Q19 (%)	Q20 (%)
Max	0.92	1.00	0.84	0.65	0.84	1.27	1.03	1.10	1.01	0.73	1.19	0.68	0.60	1.60	1.09	0.49	0.74	0.88	1.30	0.65	1.14
20	0.75	0.83	0.61	0.51	0.57	1.06	0.9	0.87	0.78	0.63	1.06	0.56	0.46	1.26	0.95	0.36	0.53	0.72	0.98	0.49	0.92
19	0.82	0.89	0.67	0.55	0.62	1.15	0.96	0.95	0.85	0.67	1.14	0.6	0.5	1.39	1.01	0.4	0.58	0.77	1.07	0.53	1
18	0.88	0.96	0.73	0.59	0.68	1.23	1.02	1.03	0.92	0.71	1.19	0.64	0.54	1.53	1.05	0.43	0.64	0.83	1.18	0.58	1.09
17	0.92	1	0.79	0.62	0.74	1.27	1.03	1.09	0.98	0.73	1.18	0.67	0.57	1.6	1.09	0.46	0.69	0.87	1.26	0.62	1.14
16	0.92	1	0.83	0.63	0.78	1.25	1	1.1	1.01	0.71	1.1	0.68	0.59	1.58	1.07	0.48	0.72	0.88	1.3	0.65	1.13
15	0.89	0.97	0.84	0.62	0.79	1.18	0.92	1.07	1.01	0.67	0.97	0.67	0.6	1.47	1	0.49	0.74	0.85	1.29	0.65	1.07
14	0.82	0.89	0.8	0.57	0.77	1.07	0.81	0.98	0.95	0.6	0.82	0.63	0.58	1.28	0.88	0.46	0.71	0.78	1.24	0.62	0.95
13	0.79	0.88	0.8	0.55	0.78	1.02	0.76	0.94	0.93	0.59	0.73	0.61	0.58	1.15	0.8	0.46	0.71	0.75	1.24	0.61	0.87
12	0.77	0.89	0.8	0.58	0.79	1	0.72	0.91	0.91	0.59	0.67	0.59	0.58	1.03	0.75	0.46	0.72	0.72	1.24	0.62	0.8
11	0.76	0.9	0.8	0.6	0.8	0.99	0.74	0.89	0.89	0.59	0.65	0.59	0.59	0.92	0.77	0.46	0.72	0.7	1.24	0.63	0.74
10	0.77	0.91	0.8	0.63	0.82	0.99	0.82	0.87	0.88	0.6	0.66	0.6	0.59	0.88	0.8	0.46	0.73	0.68	1.24	0.64	0.7
9	0.75	0.89	0.78	0.64	0.82	0.97	0.87	0.83	0.84	0.59	0.67	0.59	0.58	0.84	0.8	0.46	0.72	0.64	1.21	0.63	0.67
8	0.75	0.88	0.77	0.65	0.83	0.98	0.94	0.81	0.81	0.59	0.69	0.59	0.57	0.81	0.83	0.45	0.72	0.65	1.21	0.63	0.64
7	0.75	0.86	0.75	0.65	0.84	1	0.99	0.78	0.77	0.58	0.72	0.58	0.56	0.78	0.84	0.45	0.71	0.67	1.2	0.62	0.62
6	0.75	0.85	0.73	0.65	0.84	1.02	1.02	0.77	0.73	0.57	0.74	0.58	0.55	0.77	0.86	0.44	0.71	0.68	1.21	0.61	0.6
5	0.73	0.81	0.69	0.64	0.83	1.02	1.03	0.74	0.68	0.55	0.76	0.55	0.53	0.75	0.86	0.43	0.69	0.68	1.19	0.59	0.57
4	0.69	0.76	0.64	0.6	0.79	0.99	0.99	0.69	0.61	0.51	0.74	0.52	0.5	0.71	0.84	0.4	0.65	0.66	1.14	0.55	0.53
3	0.62	0.66	0.56	0.53	0.71	0.9	0.9	0.61	0.54	0.45	0.68	0.45	0.44	0.64	0.77	0.36	0.58	0.59	1.02	0.48	0.46
2	0.48	0.51	0.42	0.42	0.55	0.72	0.7	0.48	0.42	0.34	0.54	0.35	0.33	0.51	0.62	0.27	0.45	0.47	0.79	0.37	0.36
1	0.27	0.28	0.23	0.23	0.3	0.4	0.4	0.27	0.23	0.18	0.31	0.19	0.18	0.29	0.36	0.15	0.24	0.26	0.45	0.2	0.19

Table A.47 20-storey visco-plastic (λ=1.0) drift summary (MCE)

Storey	Mean value (%)	Q1 (%)	Q2 (%)	Q3 (%)	Q4 (%)	Q5 (%)	Q6 (%)	Q7 (%)	Q8 (%)	Q9 (%)	Q10 (%)	Q11 (%)	Q12 (%)	Q13 (%)	Q14 (%)	Q15 (%)	Q16 (%)	Q17 (%)	Q18 (%)	Q19 (%)	Q20 (%)
Max	1.06	1.07	0.84	0.66	0.84	1.27	1.43	1.18	1.02	0.76	2.00	0.69	0.60	2.48	1.64	0.49	0.74	0.92	1.79	0.65	1.39
20	1.02	1	0.63	0.51	0.57	1.06	1.43	1.07	0.83	0.75	2	0.61	0.46	2.48	1.64	0.37	0.53	0.83	1.79	0.49	1.25
19	1.04	1.04	0.68	0.55	0.62	1.15	1.41	1.14	0.88	0.76	1.95	0.64	0.5	2.48	1.59	0.4	0.58	0.88	1.72	0.53	1.33
18	1.06	1.07	0.74	0.59	0.68	1.23	1.34	1.18	0.95	0.76	1.8	0.67	0.54	2.48	1.62	0.43	0.64	0.91	1.52	0.58	1.39
17	1.04	1.07	0.8	0.62	0.74	1.27	1.22	1.16	1	0.73	1.55	0.69	0.57	2.35	1.54	0.46	0.69	0.92	1.41	0.62	1.37
16	0.99	1.03	0.83	0.63	0.78	1.25	1.06	1.12	1.02	0.68	1.22	0.69	0.57	2.08	1.37	0.48	0.69	0.9	1.37	0.65	1.28
15	0.91	0.97	0.84	0.62	0.8	1.18	0.91	1.05	1.01	0.63	0.93	0.68	0.59	1.66	1.16	0.49	0.72	0.86	1.35	0.65	1.13
14	0.81	0.9	0.8	0.58	0.77	1.07	0.75	0.95	0.94	0.59	0.69	0.63	0.6	1.19	0.93	0.46	0.74	0.78	1.26	0.62	0.94
13	0.77	0.9	0.8	0.55	0.78	1.02	0.67	0.92	0.92	0.59	0.64	0.61	0.58	0.96	0.8	0.46	0.71	0.73	1.23	0.61	0.83
12	0.75	0.9	0.8	0.57	0.79	1	0.65	0.9	0.9	0.59	0.62	0.59	0.58	0.89	0.8	0.46	0.71	0.7	1.2	0.62	0.75
11	0.76	0.9	0.8	0.6	0.81	0.99	0.72	0.89	0.89	0.59	0.65	0.59	0.59	0.86	0.84	0.46	0.72	0.68	1.17	0.63	0.72
10	0.76	0.9	0.8	0.63	0.82	0.99	0.77	0.87	0.88	0.6	0.68	0.6	0.59	0.82	0.87	0.47	0.73	0.66	1.15	0.64	0.7
9	0.74	0.88	0.78	0.64	0.82	0.97	0.78	0.83	0.84	0.59	0.69	0.59	0.58	0.77	0.85	0.46	0.72	0.63	1.12	0.63	0.67
8	0.74	0.87	0.77	0.65	0.83	0.98	0.81	0.81	0.81	0.59	0.72	0.59	0.57	0.74	0.84	0.45	0.72	0.65	1.12	0.63	0.64
7	0.74	0.85	0.75	0.65	0.84	1	0.85	0.79	0.77	0.58	0.76	0.58	0.56	0.72	0.83	0.45	0.71	0.66	1.22	0.62	0.62
6	0.75	0.83	0.73	0.66	0.84	1.02	0.92	0.77	0.73	0.57	0.82	0.58	0.55	0.73	0.86	0.44	0.71	0.67	1.36	0.61	0.6
5	0.75	0.8	0.7	0.64	0.83	1.02	1.11	0.74	0.68	0.55	0.87	0.55	0.53	0.73	0.9	0.43	0.69	0.67	1.47	0.59	0.57
4	0.74	0.75	0.64	0.61	0.79	0.99	1.27	0.7	0.61	0.51	0.91	0.51	0.5	0.76	0.95	0.41	0.65	0.64	1.52	0.55	0.53
3	0.68	0.67	0.56	0.55	0.71	0.9	1.28	0.63	0.54	0.45	0.87	0.45	0.44	0.75	0.96	0.36	0.58	0.58	1.44	0.48	0.46
2	0.55	0.53	0.43	0.44	0.55	0.72	1.07	0.5	0.42	0.35	0.72	0.35	0.33	0.65	0.82	0.27	0.45	0.47	1.14	0.37	0.37
1	0.31	0.3	0.23	0.24	0.3	0.4	0.59	0.29	0.23	0.2	0.41	0.2	0.18	0.4	0.48	0.15	0.24	0.27	0.62	0.2	0.21

Table A.48 20-storey visco-plastic (λ=0.8) drift summary (MCE)

Storey	Mean value (%)	Q1 (%)	Q2 (%)	Q3 (%)	Q4 (%)	Q5 (%)	Q6 (%)	Q7 (%)	Q8 (%)	Q9 (%)	Q10 (%)	Q11 (%)	Q12 (%)	Q13 (%)	Q14 (%)	Q15 (%)	Q16 (%)	Q17 (%)	Q18 (%)	Q19 (%)	Q20 (%)
Max	1.11	1.12	0.84	0.65	0.85	1.38	1.54	1.23	1.05	0.79	2.09	0.71	0.60	2.75	1.73	0.49	0.74	0.97	1.87	0.65	1.53
20	1.08	1.04	0.65	0.52	0.57	1.38	1.54	1.13	0.89	0.77	2.09	0.64	0.46	2.75	1.7	0.37	0.53	0.89	1.87	0.5	1.39
19	1.10	1.09	0.69	0.56	0.62	1.37	1.49	1.19	0.95	0.79	2.02	0.67	0.5	2.72	1.69	0.4	0.58	0.94	1.81	0.54	1.46
18	1.11	1.12	0.75	0.6	0.68	1.33	1.4	1.23	1	0.77	1.84	0.7	0.54	2.67	1.73	0.43	0.64	0.97	1.69	0.59	1.53
17	1.07	1.1	0.81	0.62	0.74	1.26	1.27	1.21	1.04	0.73	1.56	0.71	0.57	2.47	1.65	0.46	0.69	0.97	1.45	0.63	1.51
16	1.01	1.05	0.84	0.63	0.78	1.19	1.11	1.16	1.05	0.67	1.23	0.71	0.59	2.13	1.46	0.48	0.72	0.93	1.48	0.65	1.41
15	0.93	0.99	0.84	0.62	0.8	1.08	0.95	1.08	1.02	0.62	0.95	0.69	0.6	1.65	1.21	0.49	0.74	0.87	1.46	0.65	1.22
14	0.81	0.92	0.8	0.57	0.77	0.94	0.78	0.96	0.95	0.59	0.7	0.63	0.58	1.15	0.96	0.46	0.71	0.78	1.38	0.62	0.99
13	0.77	0.91	0.8	0.55	0.78	0.89	0.68	0.91	0.92	0.59	0.65	0.61	0.58	1.01	0.84	0.46	0.71	0.73	1.33	0.61	0.85
12	0.76	0.91	0.8	0.57	0.79	0.86	0.72	0.88	0.9	0.59	0.64	0.59	0.58	0.93	0.89	0.46	0.72	0.7	1.29	0.62	0.73
11	0.76	0.9	0.8	0.6	0.81	0.87	0.78	0.87	0.88	0.59	0.64	0.59	0.59	0.85	0.94	0.46	0.72	0.67	1.23	0.63	0.71
10	0.76	0.9	0.8	0.62	0.82	0.89	0.82	0.86	0.86	0.6	0.69	0.6	0.59	0.78	0.96	0.47	0.73	0.65	1.21	0.64	0.69
9	0.75	0.88	0.78	0.63	0.83	0.9	0.82	0.83	0.83	0.59	0.73	0.6	0.58	0.76	0.92	0.46	0.72	0.63	1.18	0.63	0.66
8	0.75	0.86	0.77	0.65	0.84	0.95	0.82	0.81	0.8	0.58	0.78	0.59	0.57	0.76	0.89	0.45	0.72	0.64	1.18	0.63	0.64
7	0.75	0.85	0.75	0.65	0.84	1.01	0.84	0.78	0.76	0.58	0.83	0.59	0.56	0.76	0.87	0.45	0.71	0.66	1.29	0.62	0.62
6	0.77	0.83	0.73	0.65	0.85	1.12	0.99	0.77	0.73	0.57	0.89	0.57	0.55	0.77	0.89	0.44	0.71	0.67	1.42	0.61	0.6
5	0.78	0.81	0.69	0.64	0.83	1.21	1.2	0.75	0.68	0.55	0.95	0.55	0.53	0.78	0.94	0.43	0.69	0.67	1.53	0.59	0.57
4	0.78	0.77	0.64	0.62	0.79	1.27	1.34	0.72	0.61	0.52	0.97	0.52	0.5	0.84	1.01	0.41	0.65	0.65	1.59	0.55	0.53
3	0.72	0.7	0.56	0.56	0.71	1.21	1.34	0.66	0.54	0.46	0.91	0.46	0.44	0.83	1.02	0.36	0.58	0.6	1.48	0.48	0.47
2	0.57	0.57	0.43	0.46	0.56	0.97	1.09	0.54	0.41	0.36	0.73	0.35	0.34	0.7	0.86	0.27	0.45	0.5	1.15	0.37	0.37
1	0.32	0.32	0.23	0.26	0.31	0.53	0.6	0.31	0.23	0.2	0.42	0.21	0.19	0.42	0.5	0.15	0.24	0.29	0.62	0.2	0.21

Table A.49 20-storey visco-plastic (λ=0.6) drift summary (MCE)

Storey	Mean value (%)	Q1 (%)	Q2 (%)	Q3 (%)	Q4 (%)	Q5 (%)	Q6 (%)	Q7 (%)	Q8 (%)	Q9 (%)	Q10 (%)	Q11 (%)	Q12 (%)	Q13 (%)	Q14 (%)	Q15 (%)	Q16 (%)	Q17 (%)	Q18 (%)	Q19 (%)	Q20 (%)
Max	1.19	1.14	0.85	0.65	0.85	1.52	1.75	1.23	1.10	0.82	2.23	0.75	0.59	3.08	1.94	0.49	0.74	1.04	2.01	0.65	1.70
20	1.18	1.06	0.72	0.57	0.6	1.52	1.75	1.13	0.95	0.81	2.23	0.69	0.47	3.08	1.94	0.37	0.54	0.95	2.01	0.52	1.59
19	1.19	1.11	0.74	0.6	0.64	1.47	1.64	1.18	1.01	0.82	2.15	0.72	0.5	3.05	1.88	0.4	0.58	1.01	2	0.56	1.65
18	1.17	1.14	0.76	0.63	0.69	1.31	1.45	1.2	1.07	0.81	1.93	0.74	0.53	2.94	1.88	0.43	0.64	1.04	1.86	0.6	1.7
17	1.12	1.12	0.81	0.65	0.75	1.23	1.26	1.23	1.1	0.76	1.59	0.75	0.56	2.66	1.77	0.46	0.69	1.04	1.55	0.63	1.69
16	1.05	1.08	0.85	0.65	0.79	1.22	1.15	1.22	1.1	0.69	1.23	0.74	0.58	2.21	1.55	0.48	0.72	0.99	1.61	0.65	1.57
15	0.96	1.04	0.85	0.62	0.8	1.1	1.02	1.13	1.07	0.62	0.98	0.71	0.59	1.63	1.27	0.49	0.74	0.91	1.62	0.65	1.35
14	0.84	0.97	0.81	0.57	0.77	0.97	0.84	1.01	0.97	0.59	0.72	0.64	0.57	1.19	0.99	0.46	0.71	0.8	1.55	0.62	1.07
13	0.80	0.95	0.8	0.54	0.78	0.92	0.76	0.95	0.93	0.59	0.67	0.61	0.57	1.14	0.96	0.46	0.71	0.74	1.51	0.61	0.89
12	0.79	0.93	0.8	0.56	0.79	0.9	0.83	0.9	0.89	0.59	0.67	0.59	0.58	1.03	1.05	0.46	0.72	0.69	1.44	0.62	0.75
11	0.78	0.93	0.79	0.59	0.81	0.9	0.9	0.88	0.86	0.6	0.69	0.59	0.58	0.89	1.09	0.46	0.72	0.66	1.36	0.63	0.69
10	0.78	0.92	0.79	0.62	0.83	0.93	0.92	0.86	0.84	0.6	0.74	0.6	0.59	0.82	1	0.47	0.73	0.65	1.33	0.64	0.68
9	0.76	0.9	0.77	0.62	0.83	0.94	0.87	0.84	0.8	0.6	0.78	0.6	0.57	0.8	0.93	0.46	0.72	0.63	1.3	0.63	0.65
8	0.77	0.89	0.76	0.64	0.84	1.01	0.86	0.83	0.77	0.6	0.84	0.59	0.57	0.79	0.91	0.45	0.72	0.63	1.33	0.63	0.64
7	0.77	0.88	0.74	0.64	0.85	1.1	0.92	0.81	0.74	0.59	0.91	0.58	0.56	0.79	0.95	0.45	0.71	0.65	1.37	0.62	0.62
6	0.80	0.87	0.72	0.65	0.85	1.22	1.14	0.81	0.71	0.59	0.97	0.57	0.55	0.87	1.03	0.44	0.71	0.67	1.48	0.61	0.6
5	0.83	0.86	0.69	0.65	0.84	1.32	1.34	0.79	0.67	0.58	1.02	0.56	0.54	0.98	1.11	0.43	0.69	0.69	1.6	0.59	0.58
4	0.82	0.83	0.64	0.64	0.81	1.35	1.45	0.77	0.61	0.54	1.01	0.52	0.51	1.08	1.11	0.41	0.65	0.69	1.67	0.55	0.54
3	0.76	0.77	0.57	0.6	0.74	1.27	1.39	0.71	0.54	0.47	0.93	0.45	0.45	1.07	1.11	0.36	0.58	0.64	1.58	0.48	0.49
2	0.61	0.62	0.44	0.49	0.6	1	1.1	0.57	0.43	0.36	0.73	0.37	0.35	0.86	0.93	0.27	0.45	0.52	1.25	0.38	0.39
1	0.34	0.35	0.25	0.27	0.33	0.54	0.59	0.32	0.24	0.21	0.41	0.22	0.2	0.48	0.53	0.15	0.24	0.3	0.69	0.21	0.22

Table A.50 20-storey visco-plastic (λ=0.4) drift summary (MCE)

Storey	Mean value (%)	Q1 (%)	Q2 (%)	Q3 (%)	Q4 (%)	Q5 (%)	Q6 (%)	Q7 (%)	Q8 (%)	Q9 (%)	Q10 (%)	Q11 (%)	Q12 (%)	Q13 (%)	Q14 (%)	Q15 (%)	Q16 (%)	Q17 (%)	Q18 (%)	Q19 (%)	Q20 (%)
Max	1.31	1.30	0.86	0.71	0.96	1.76	2.01	1.29	1.15	0.88	2.54	0.86	0.59	3.45	2.30	0.49	0.75	1.17	2.30	0.67	1.82
20	1.31	1.23	0.76	0.63	0.67	1.76	2.01	1.22	0.92	0.87	2.54	0.78	0.45	3.45	2.3	0.38	0.58	1.08	2.3	0.58	1.76
19	1.31	1.29	0.78	0.66	0.72	1.69	1.88	1.26	0.98	0.88	2.43	0.81	0.48	3.45	2.09	0.4	0.62	1.13	2.25	0.62	1.79
18	1.27	1.3	0.79	0.69	0.78	1.48	1.62	1.26	1.04	0.86	2.17	0.84	0.51	3.34	1.98	0.44	0.67	1.17	2.07	0.65	1.82
17	1.19	1.26	0.82	0.71	0.83	1.23	1.3	1.24	1.11	0.8	1.75	0.86	0.53	3.03	1.84	0.47	0.72	1.15	1.69	0.67	1.81
16	1.12	1.2	0.84	0.71	0.85	1.25	1.13	1.29	1.15	0.74	1.28	0.84	0.55	2.53	1.61	0.48	0.75	1.1	1.71	0.67	1.73
15	1.02	1.15	0.86	0.67	0.83	1.15	1.07	1.24	1.13	0.65	0.96	0.78	0.56	1.86	1.32	0.49	0.75	1	1.81	0.66	1.5
14	0.90	1.07	0.82	0.6	0.78	1.01	0.93	1.09	1.04	0.59	0.74	0.68	0.54	1.3	1.12	0.46	0.72	0.85	1.79	0.61	1.16
13	0.86	1.04	0.81	0.56	0.79	0.98	0.95	1.03	0.98	0.59	0.63	0.61	0.55	1.25	1.15	0.46	0.71	0.76	1.77	0.6	0.94
12	0.85	1	0.8	0.56	0.8	0.96	1.03	0.98	0.92	0.6	0.71	0.6	0.56	1.1	1.3	0.46	0.72	0.71	1.7	0.61	0.8
11	0.83	0.97	0.79	0.59	0.82	0.97	1.02	0.94	0.88	0.61	0.75	0.6	0.58	0.93	1.34	0.46	0.72	0.69	1.59	0.62	0.72
10	0.82	0.95	0.78	0.62	0.84	1	0.98	0.92	0.85	0.62	0.79	0.59	0.59	0.87	1.22	0.46	0.73	0.68	1.53	0.63	0.69
9	0.79	0.94	0.75	0.64	0.85	1.04	0.9	0.89	0.8	0.62	0.83	0.58	0.59	0.85	1.02	0.45	0.72	0.65	1.47	0.63	0.66
8	0.80	0.94	0.73	0.66	0.88	1.13	0.91	0.88	0.76	0.62	0.92	0.57	0.58	0.84	0.91	0.45	0.72	0.67	1.49	0.63	0.65
7	0.83	0.94	0.71	0.68	0.91	1.24	1.16	0.87	0.71	0.61	1	0.56	0.58	0.93	0.91	0.45	0.72	0.7	1.59	0.63	0.64
6	0.88	0.94	0.71	0.7	0.94	1.36	1.4	0.87	0.67	0.6	1.07	0.57	0.58	1.13	1.03	0.45	0.72	0.73	1.78	0.64	0.64
5	0.91	0.93	0.7	0.7	0.96	1.44	1.55	0.85	0.65	0.58	1.1	0.57	0.57	1.32	1.15	0.43	0.71	0.74	1.94	0.63	0.63
4	0.90	0.91	0.67	0.67	0.93	1.44	1.53	0.82	0.64	0.55	1.06	0.55	0.54	1.41	1.25	0.41	0.69	0.74	2.02	0.6	0.6
3	0.83	0.83	0.6	0.61	0.85	1.33	1.37	0.75	0.59	0.5	0.95	0.51	0.49	1.3	1.22	0.36	0.62	0.69	1.9	0.54	0.54
2	0.65	0.66	0.47	0.49	0.67	1.03	1.05	0.6	0.47	0.39	0.73	0.4	0.39	0.98	1	0.28	0.49	0.56	1.51	0.42	0.43
1	0.36	0.37	0.26	0.27	0.37	0.55	0.56	0.34	0.26	0.21	0.4	0.23	0.22	0.52	0.55	0.15	0.27	0.32	0.85	0.23	0.24

Table A.51 20-storey visco-plastic (λ=0.2) drift summary (MCE)

Storey	Mean value (%)	Q1 (%)	Q2 (%)	Q3 (%)	Q4 (%)	Q5 (%)	Q6 (%)	Q7 (%)	Q8 (%)	Q9 (%)	Q10 (%)	Q11 (%)	Q12 (%)	Q13 (%)	Q14 (%)	Q15 (%)	Q16 (%)	Q17 (%)	Q18 (%)	Q19 (%)	Q20 (%)
Max	1.57	1.66	0.94	0.81	1.57	2.25	2.56	1.65	1.13	1.03	2.86	1.04	0.65	3.99	2.59	0.51	0.97	1.46	2.58	0.95	2.16
20	1.57	1.56	0.84	0.72	0.95	2.25	2.56	1.5	0.95	1.03	2.86	0.97	0.52	3.99	2.59	0.43	0.84	1.33	2.58	0.86	2.16
19	1.54	1.63	0.85	0.76	1.01	2.1	2.19	1.59	1	1.03	2.67	1.02	0.55	3.85	2.23	0.46	0.9	1.41	2.47	0.91	2.16
18	1.47	1.66	0.83	0.79	1.06	1.75	1.84	1.65	1.04	0.99	2.29	1.04	0.58	3.66	1.99	0.49	0.95	1.46	2.19	0.94	2.13
17	1.36	1.58	0.87	0.8	1.09	1.44	1.56	1.64	1.11	0.88	1.78	1.04	0.62	3.45	1.77	0.51	0.97	1.43	1.73	0.95	2.05
16	1.27	1.46	0.93	0.81	1.09	1.32	1.38	1.57	1.13	0.77	1.26	1	0.65	3.01	1.48	0.51	0.96	1.34	1.96	0.92	1.88
15	1.17	1.41	0.94	0.79	1.05	1.26	1.34	1.48	1.1	0.7	0.99	0.92	0.64	2.33	1.32	0.51	0.91	1.18	2.1	0.87	1.61
14	1.05	1.32	0.88	0.7	0.96	1.12	1.28	1.34	1	0.64	0.83	0.78	0.59	1.76	1.27	0.48	0.84	1.03	2.1	0.78	1.23
13	0.99	1.28	0.84	0.7	0.92	1.12	1.37	1.22	0.95	0.64	0.79	0.68	0.6	1.39	1.3	0.47	0.86	0.97	2.1	0.74	0.94
12	0.98	1.21	0.81	0.74	0.94	1.12	1.41	1.14	0.91	0.64	0.85	0.65	0.62	1.23	1.45	0.47	0.87	0.91	2.04	0.73	0.87
11	0.96	1.12	0.78	0.77	1	1.14	1.28	1.06	0.88	0.64	0.89	0.64	0.64	1.23	1.39	0.47	0.89	0.87	1.93	0.74	0.82
10	0.93	1.04	0.76	0.79	1.11	1.2	1.05	1.01	0.85	0.64	0.91	0.64	0.65	1.19	1.15	0.47	0.9	0.83	1.86	0.75	0.79
9	0.90	1.02	0.72	0.79	1.22	1.24	0.99	0.96	0.81	0.61	0.93	0.64	0.62	1.1	0.92	0.46	0.9	0.76	1.72	0.74	0.75
8	0.92	1.06	0.71	0.8	1.37	1.33	1.12	0.94	0.75	0.6	1.04	0.65	0.6	1.11	0.98	0.47	0.91	0.81	1.68	0.75	0.74
7	0.97	1.09	0.72	0.8	1.5	1.43	1.36	0.93	0.7	0.58	1.12	0.67	0.6	1.29	1.09	0.48	0.91	0.87	1.84	0.74	0.73
6	1.03	1.13	0.72	0.79	1.57	1.53	1.54	0.94	0.72	0.57	1.14	0.69	0.6	1.51	1.25	0.49	0.92	0.92	2.1	0.74	0.71
5	1.05	1.15	0.71	0.76	1.55	1.58	1.53	0.93	0.72	0.58	1.11	0.71	0.59	1.64	1.38	0.49	0.91	0.95	2.32	0.72	0.69
4	1.02	1.12	0.67	0.71	1.43	1.55	1.4	0.9	0.7	0.57	1.02	0.69	0.56	1.66	1.42	0.47	0.87	0.93	2.39	0.67	0.66
3	0.91	1.01	0.59	0.62	1.19	1.39	1.25	0.83	0.63	0.52	0.88	0.63	0.49	1.44	1.29	0.42	0.79	0.87	2.22	0.59	0.59
2	0.70	0.77	0.45	0.48	0.85	1.06	0.99	0.65	0.48	0.42	0.69	0.5	0.37	1.07	0.96	0.33	0.62	0.7	1.76	0.45	0.46
1	0.39	0.42	0.25	0.27	0.44	0.56	0.55	0.36	0.26	0.23	0.39	0.27	0.2	0.61	0.51	0.18	0.34	0.39	1.04	0.24	0.25

Ex) storey drift mean value (DBE)

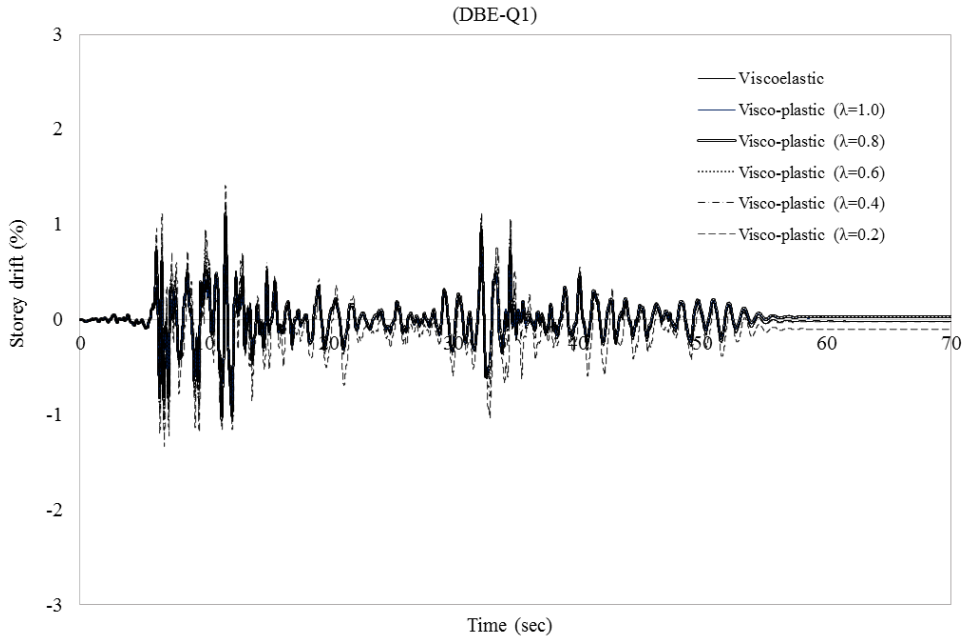

Fig. A.1 Storey drift graph for the 5-storey MRF with viscoelastic and visco-plastic damper (Q1)

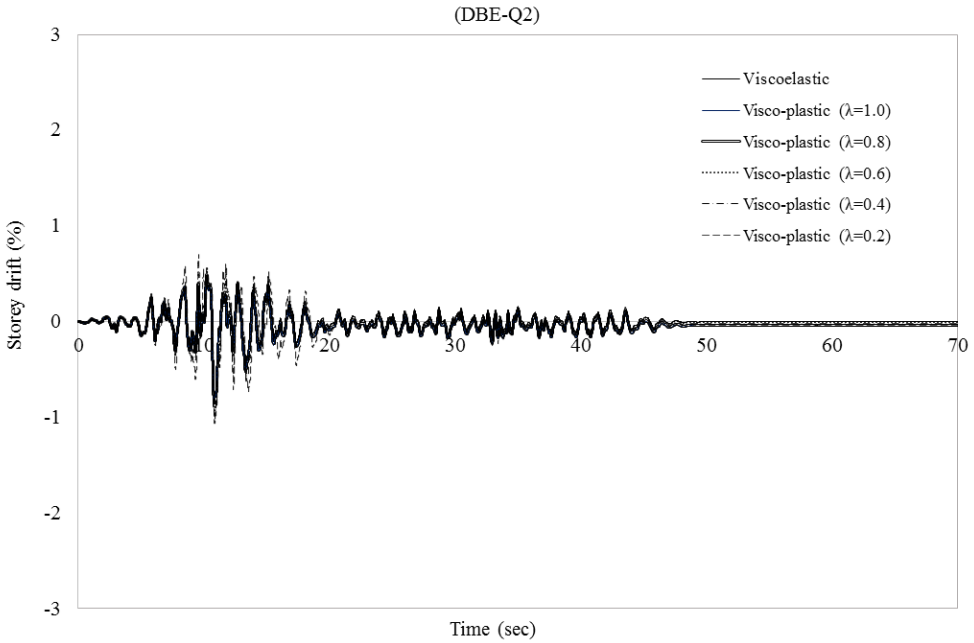

Fig. A.2 Storey drift graph for the 5-storey MRF with viscoelastic and visco-plastic damper (Q2)

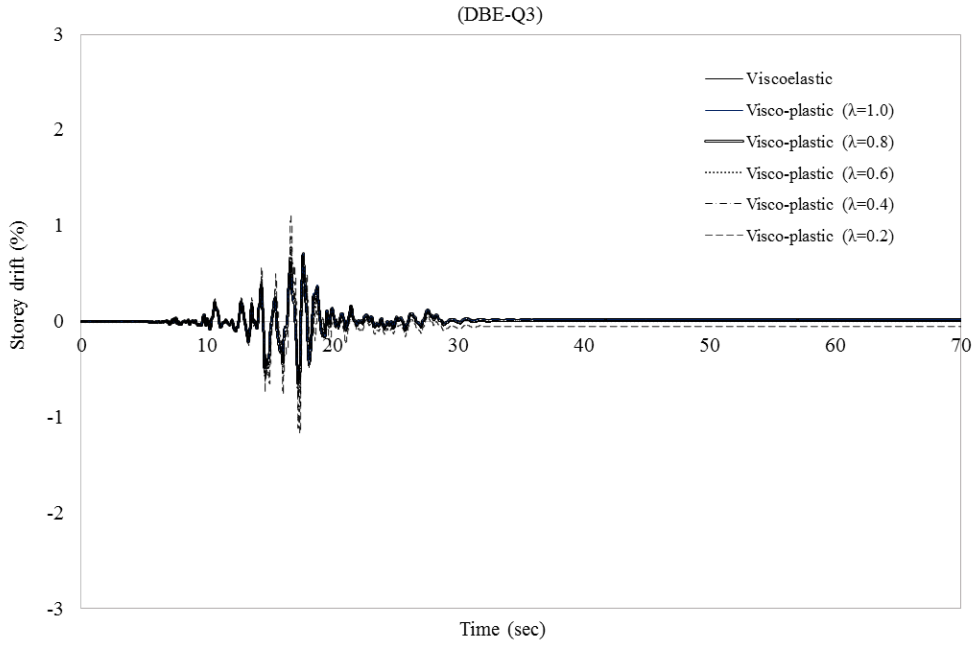

Fig. A.3 Storey drift graph for the 5-storey MRF with viscoelastic and visco-plastic damper (Q3)

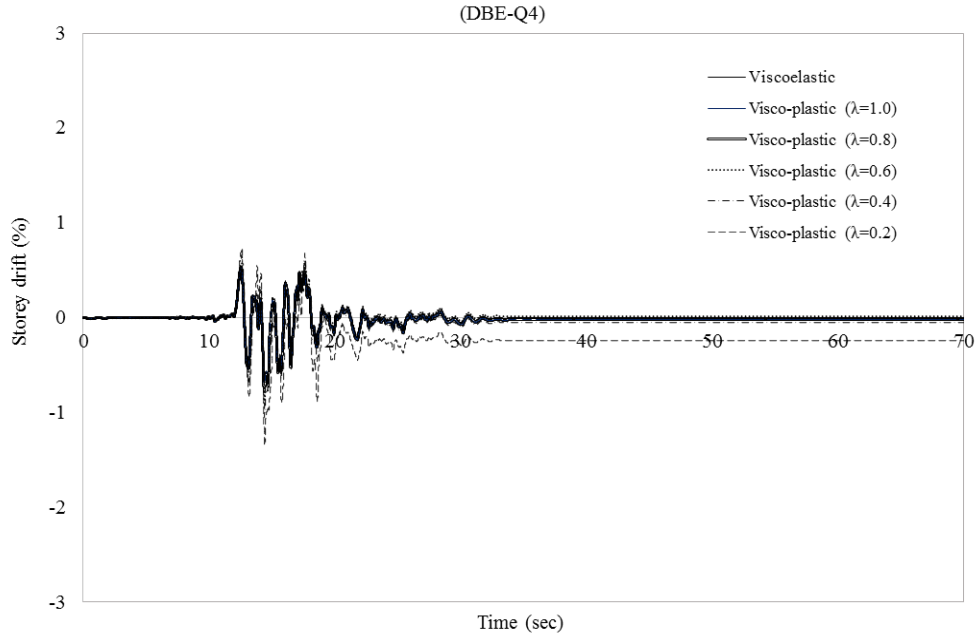

Fig. A.4 Storey drift graph for the 5-storey MRF with viscoelastic and visco-plastic damper (Q4)

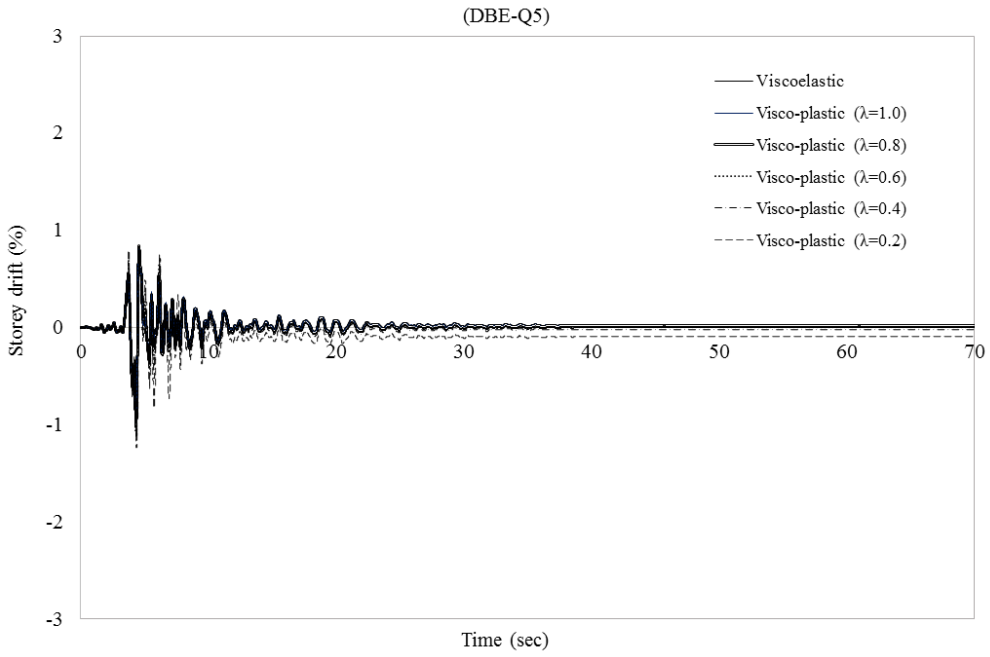

Fig. A.5 Storey drift graph for the 5-storey MRF with viscoelastic and visco-plastic damper (Q5)

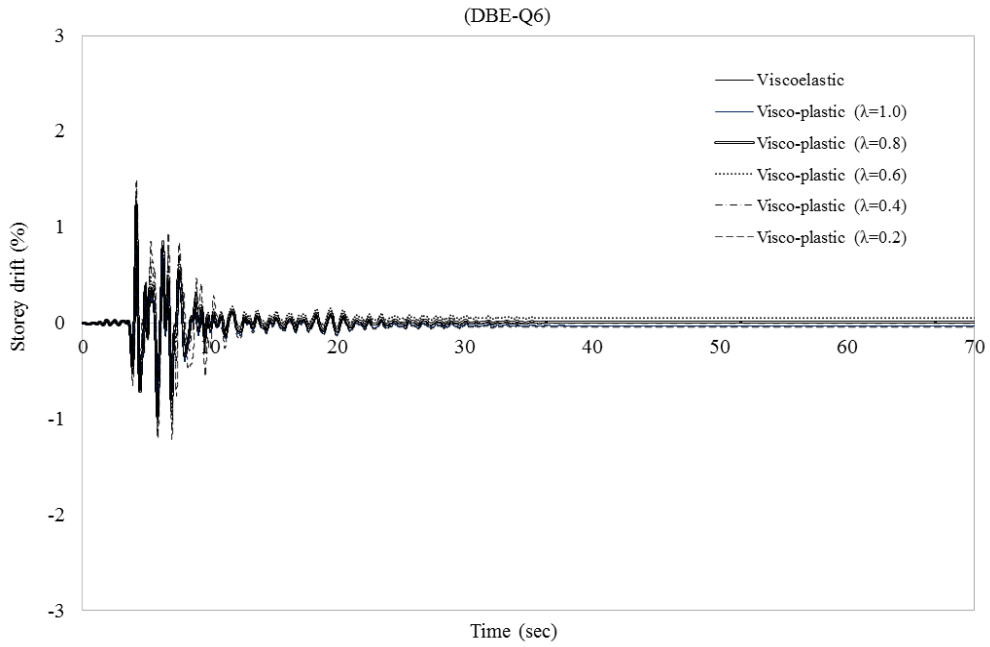

Fig. A.6 Storey drift graph for the 5-storey MRF with viscoelastic and visco-plastic damper (Q6)

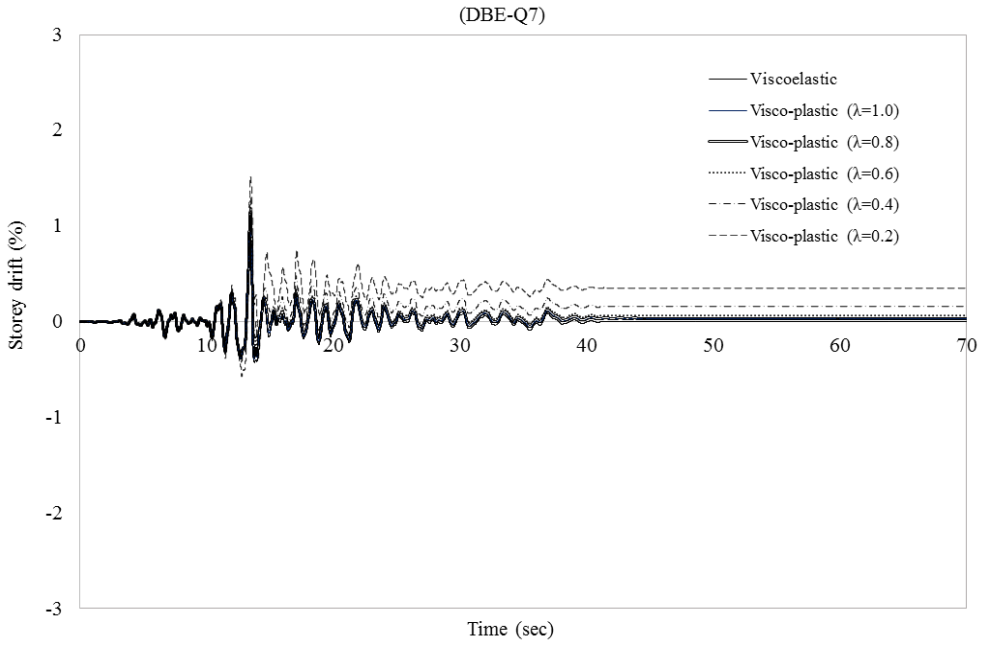

Fig. A.7 Storey drift graph for the 5-storey MRF with viscoelastic and visco-plastic damper (Q7)

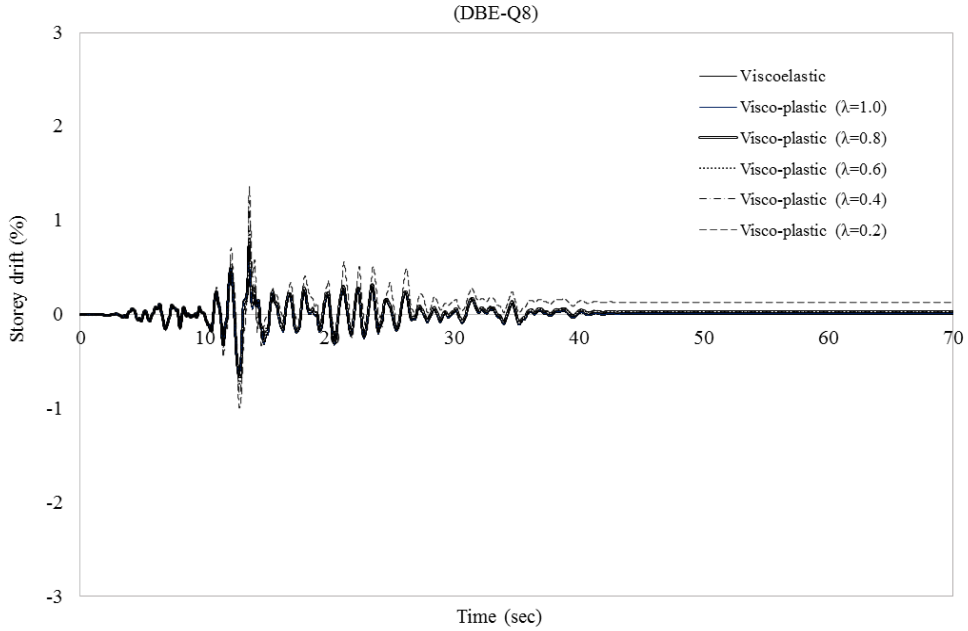

Fig. A.8 Storey drift graph for the 5-storey MRF with viscoelastic and visco-plastic damper (Q8)

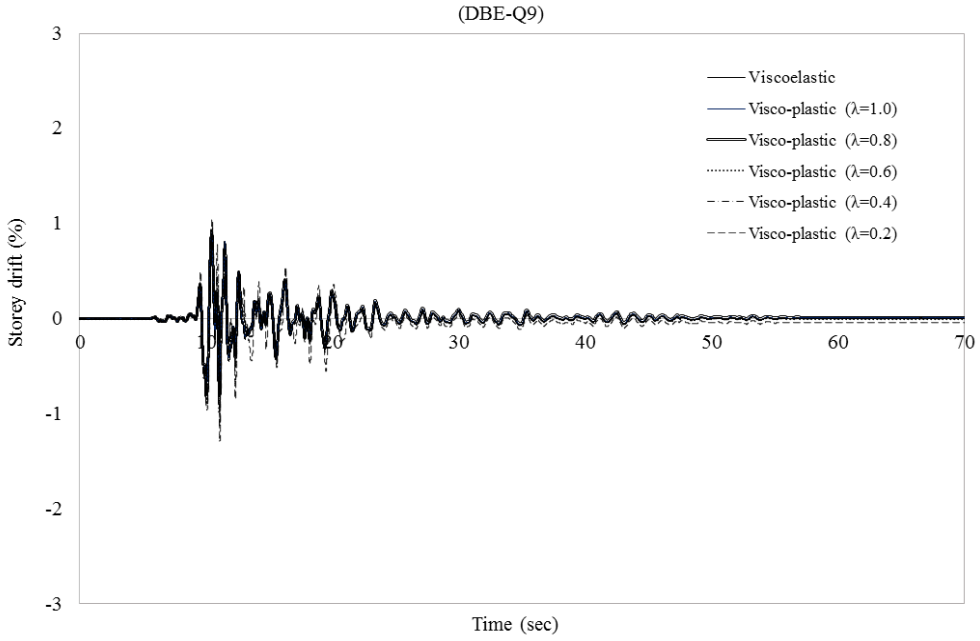

Fig. A.9 Storey drift graph for the 5-storey MRF with viscoelastic and visco-plastic damper (Q9)

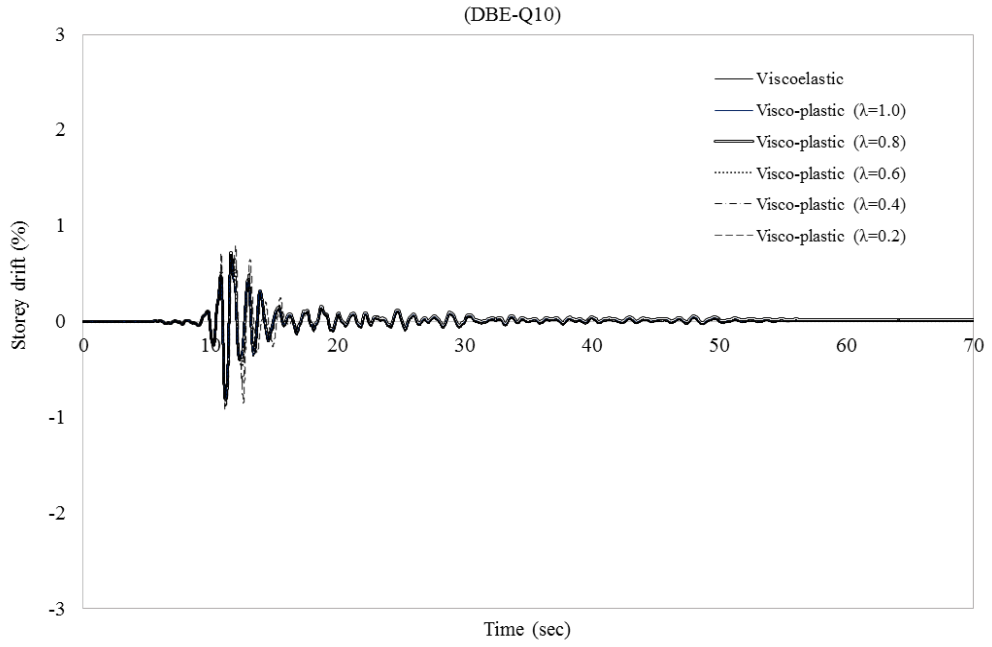

Fig. A.10 Storey drift graph for the 5-storey MRF with viscoelastic and visco-plastic damper (Q10)

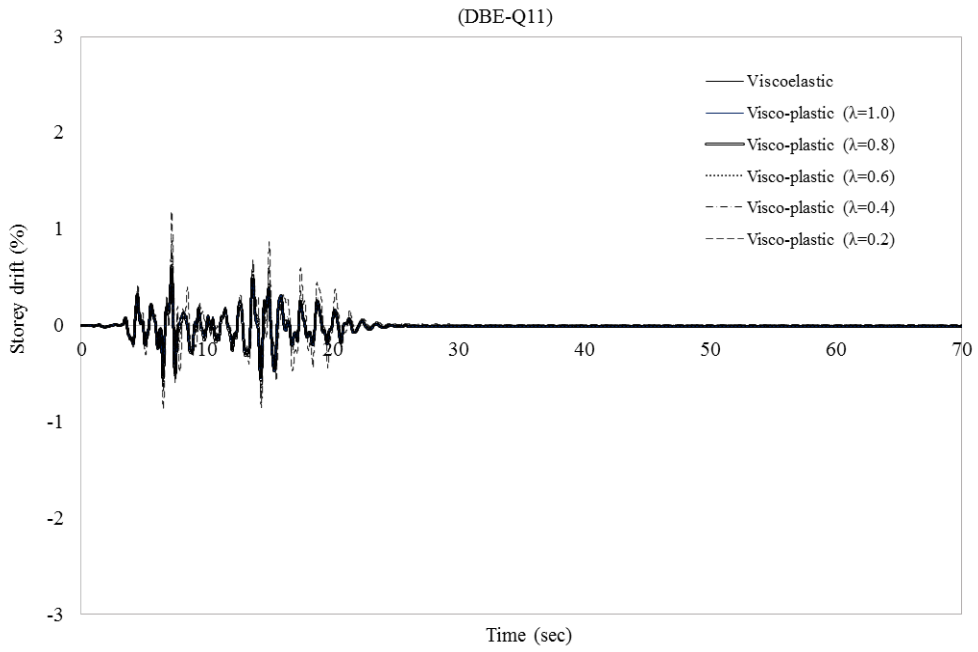

Fig. A.11 Storey drift graph for the 5-storey MRF with viscoelastic and visco-plastic damper (Q11)

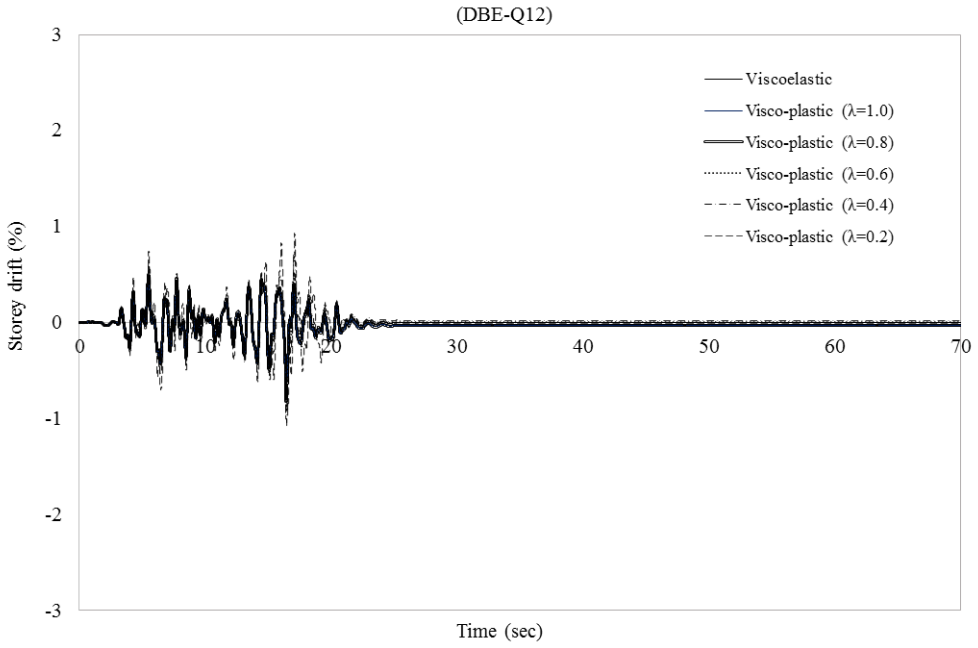

Fig. A.12 Storey drift graph for the 5-storey MRF with viscoelastic and visco-plastic damper (Q12)

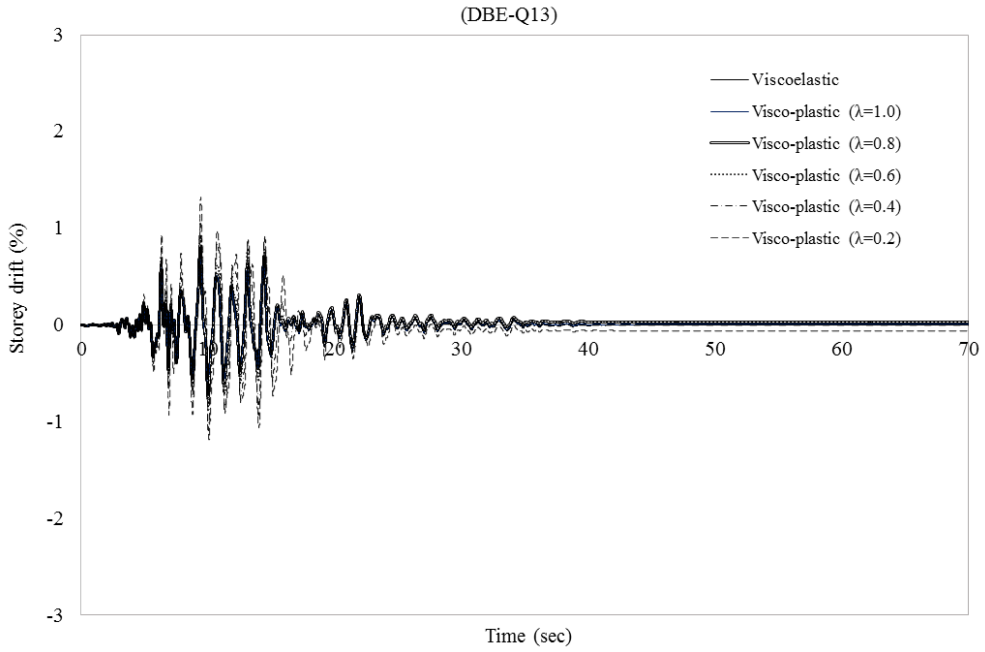

Fig. A.13 Storey drift graph for the 5-storey MRF with viscoelastic and visco-plastic damper (Q13)

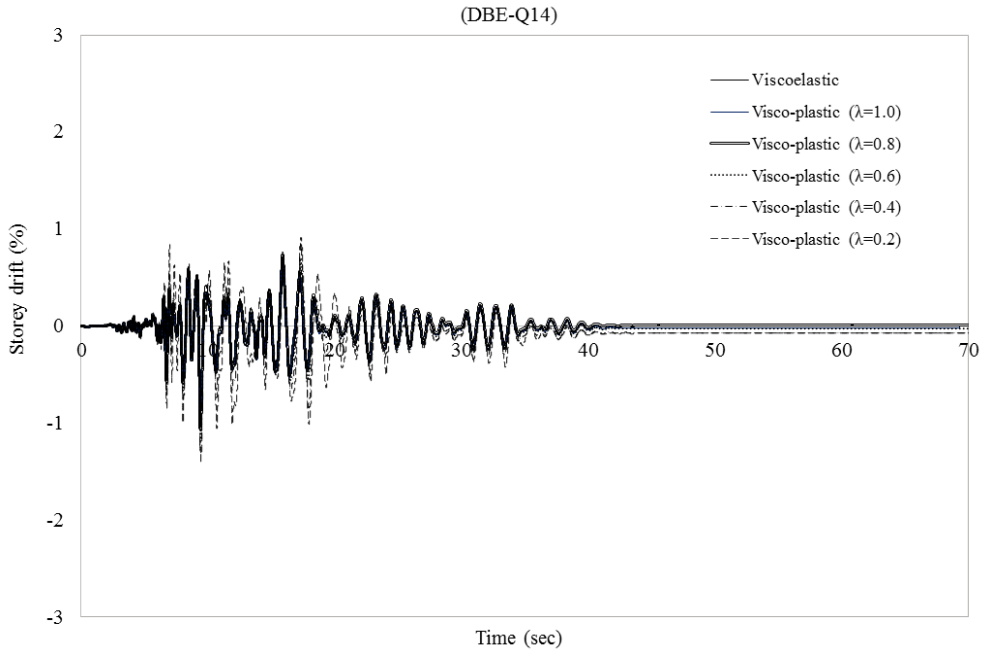

Fig. A.14 Storey drift graph for the 5-storey MRF with viscoelastic and visco-plastic damper (Q14)

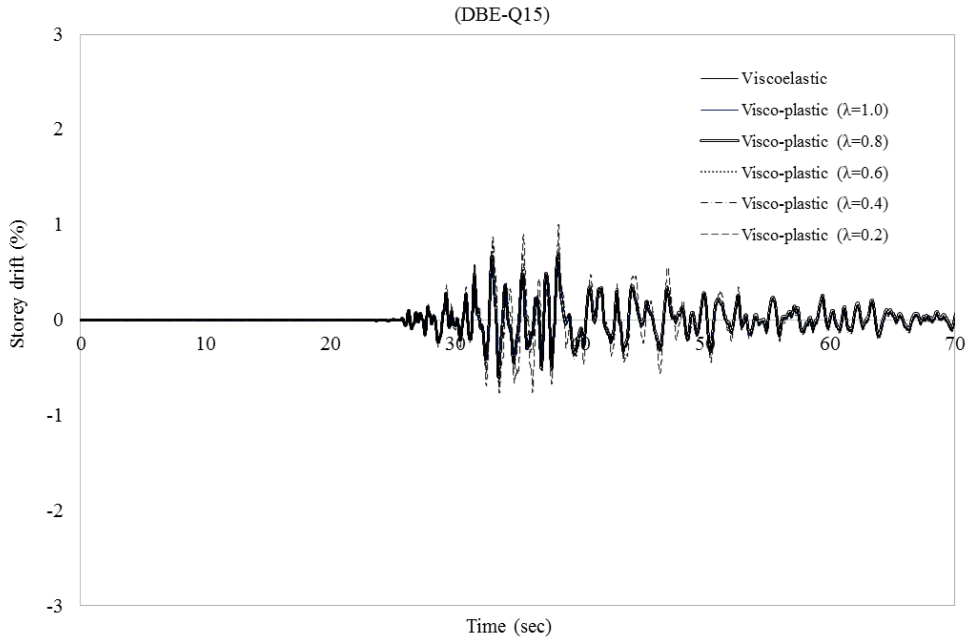

Fig. A.15 Storey drift graph for the 5story MRF with viscoelastic and visco-plastic damper (Q15)

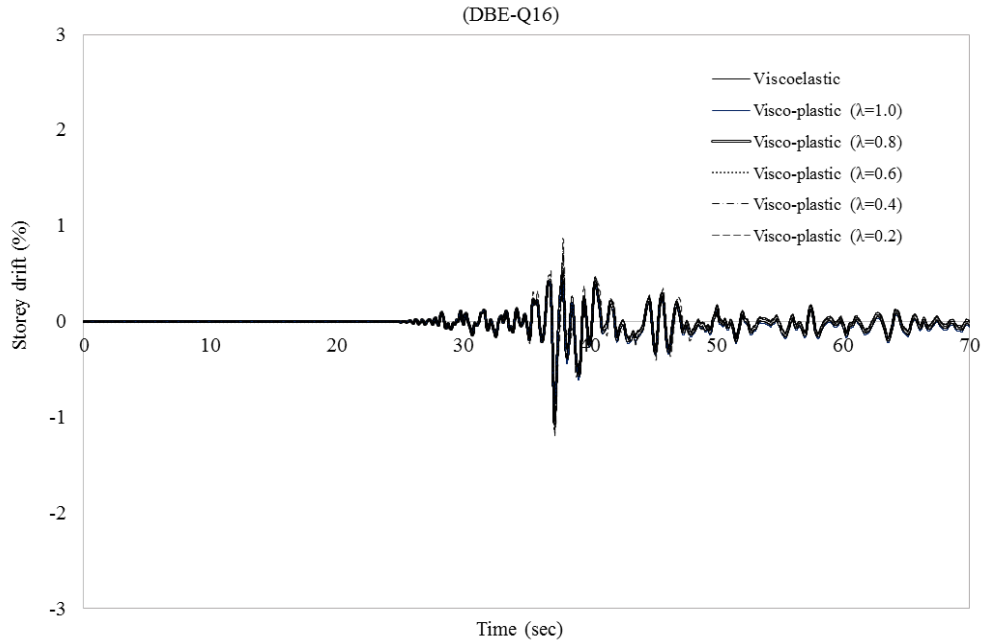

Fig. A.16 Storey drift graph for the 5-storey MRF with viscoelastic and visco-plastic damper (Q16)

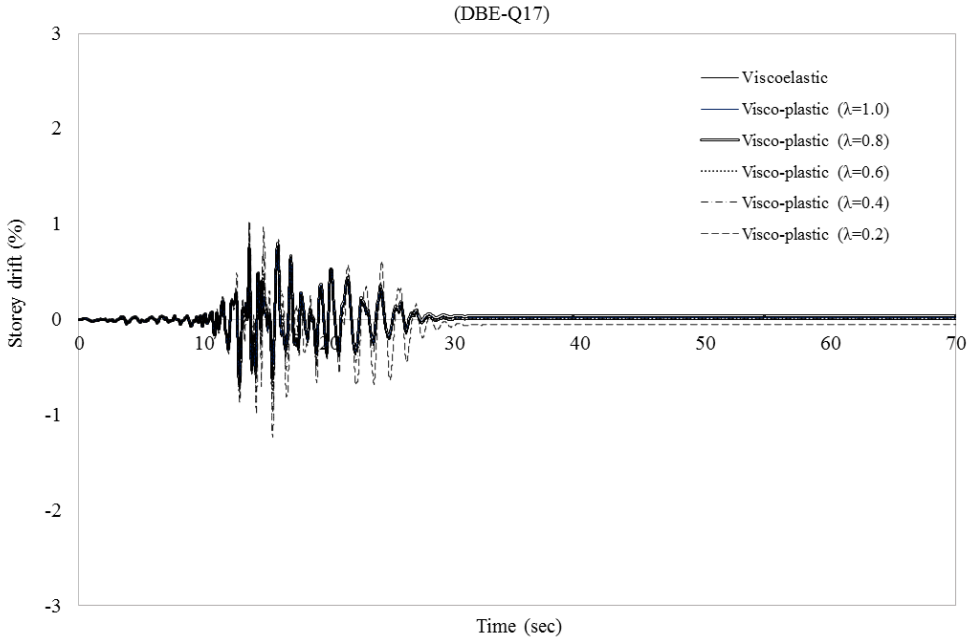

Fig. A.17 Storey drift graph for the 5-storey MRF with viscoelastic and visco-plastic damper (Q17)

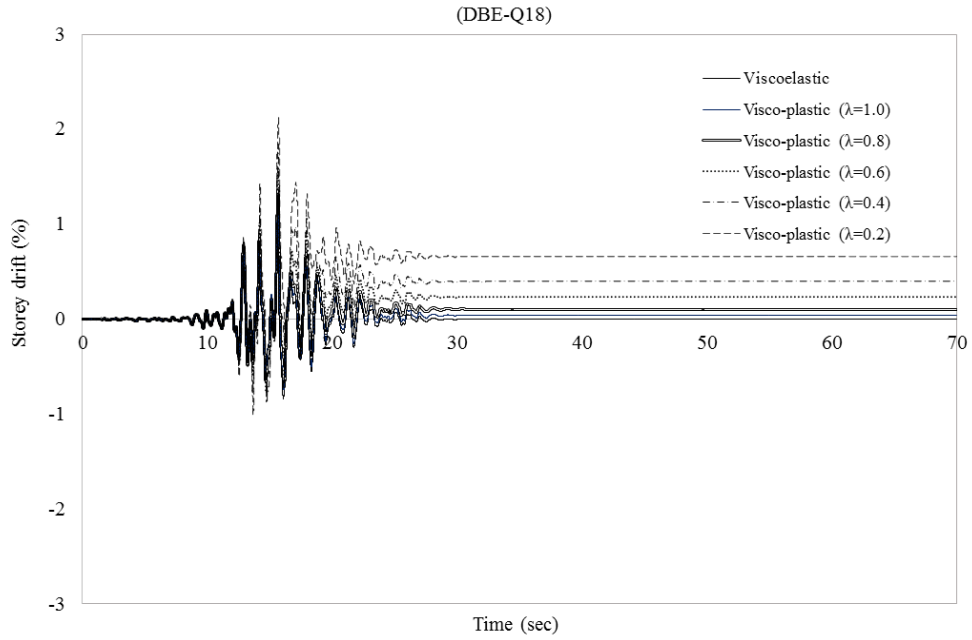

Fig. A.18 Storey drift graph for the 5-storey MRF with viscoelastic and visco-plastic damper (Q18)

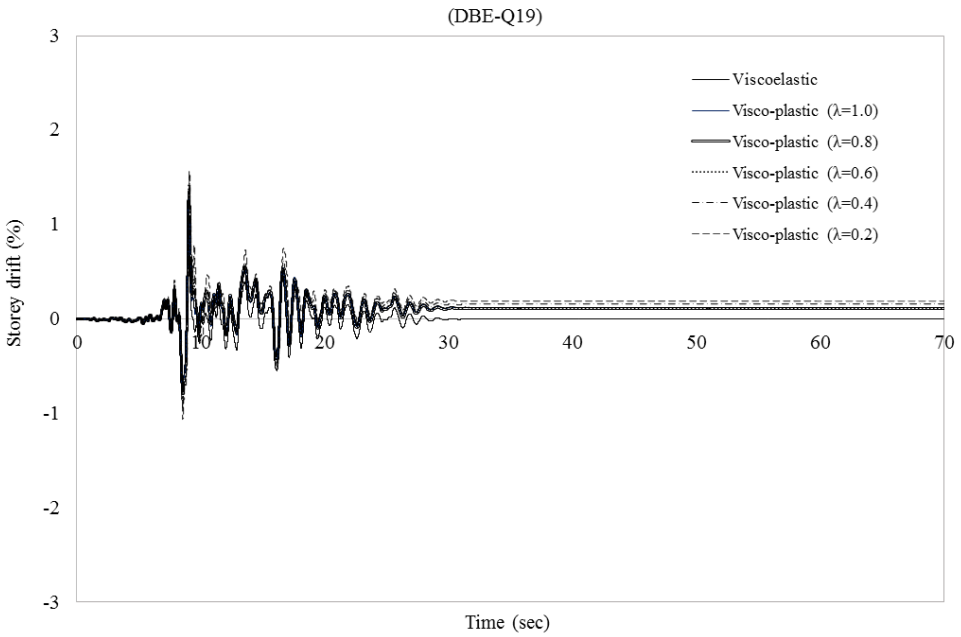

Fig. A.19 Storey drift graph for the 5-storey MRF with viscoelastic and visco-plastic damper (Q19)

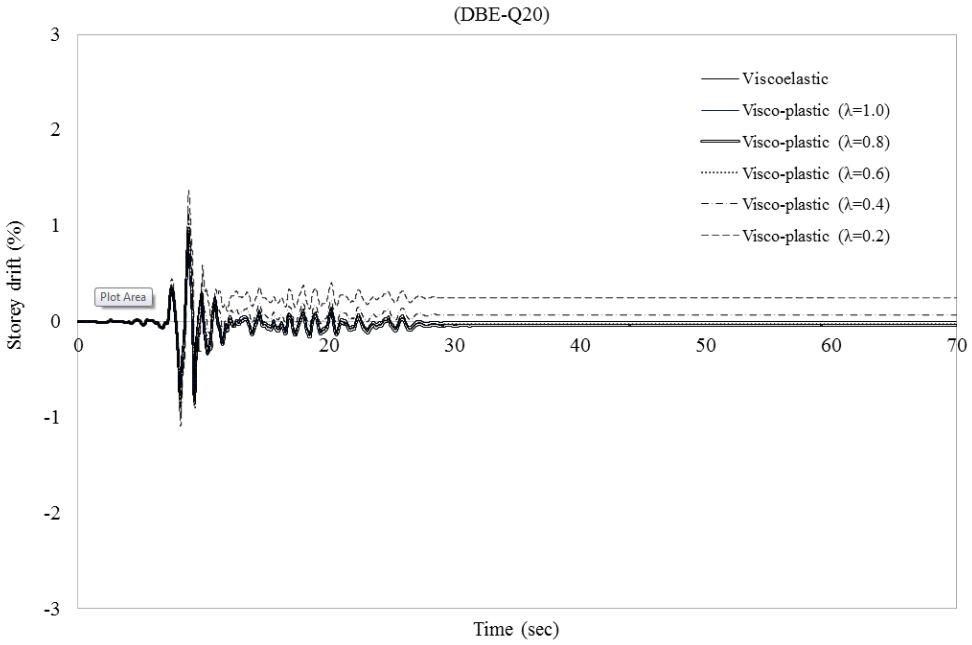

Fig. A.20 Storey drift graph for the 5-storey MRF with viscoelastic and visco-plastic damper (Q20)

Residual drift

(5story)

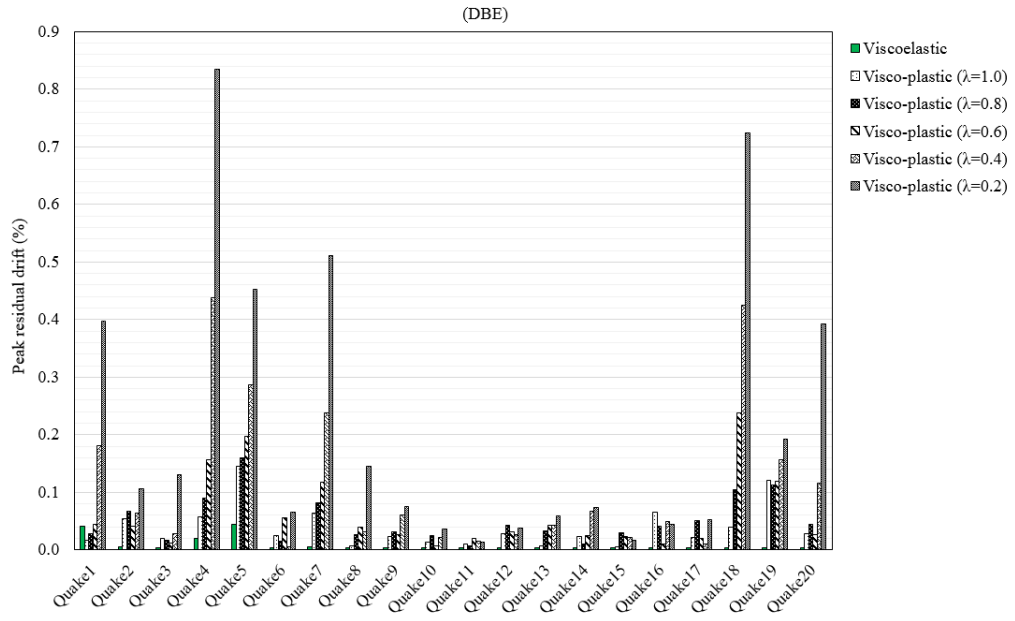

Fig. A.21 5-storey peak residual drift (%) under DBE

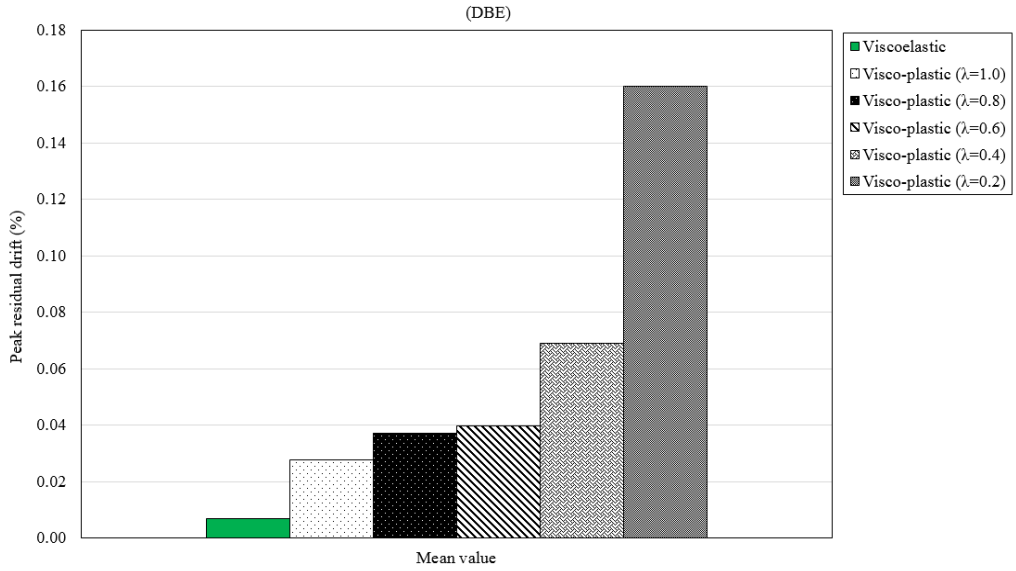

Fig. A.22 5-storey peak residual drift(%) mean value for 20 seismic records under DBE

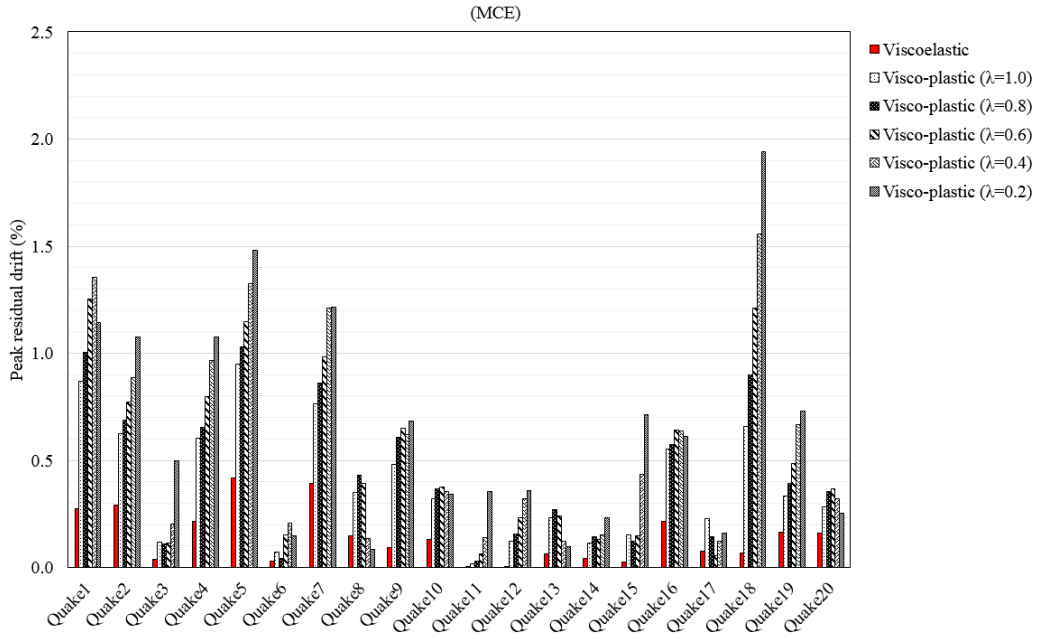

Fig. A.23 5-storey peak residual drift (%) under MCE

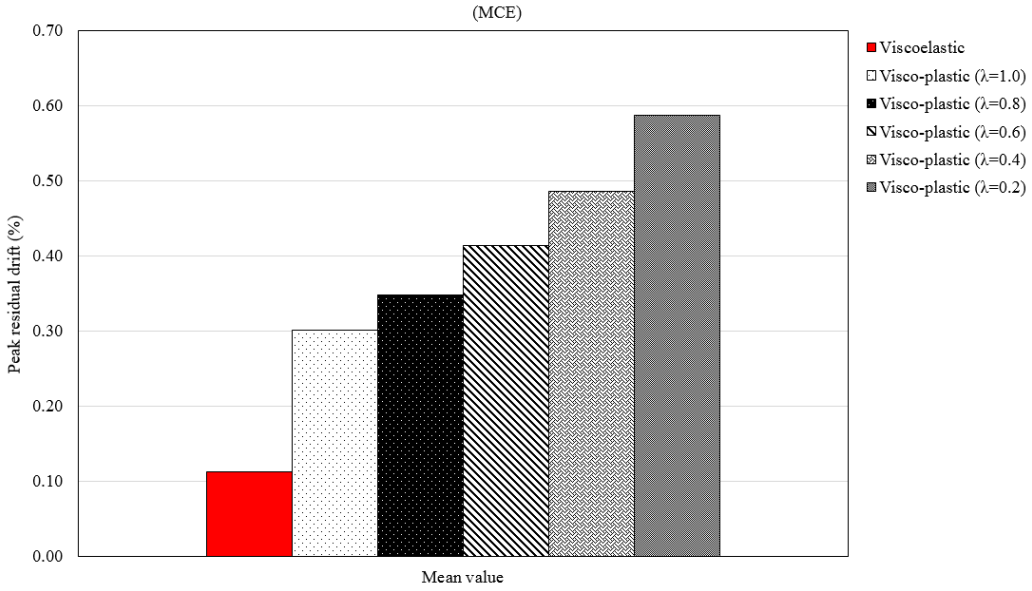

Fig. A.24 5-storey peak residual drift(%) mean value for 20 seismic records under MCE

(10story)

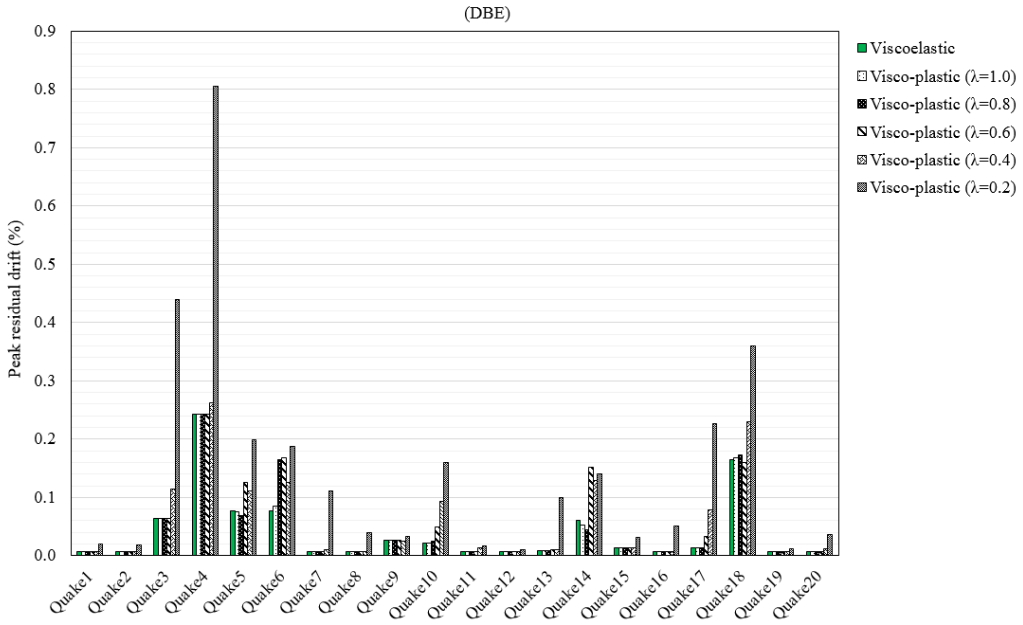

Fig. A.25 10-storey peak residual drift (%) under DBE

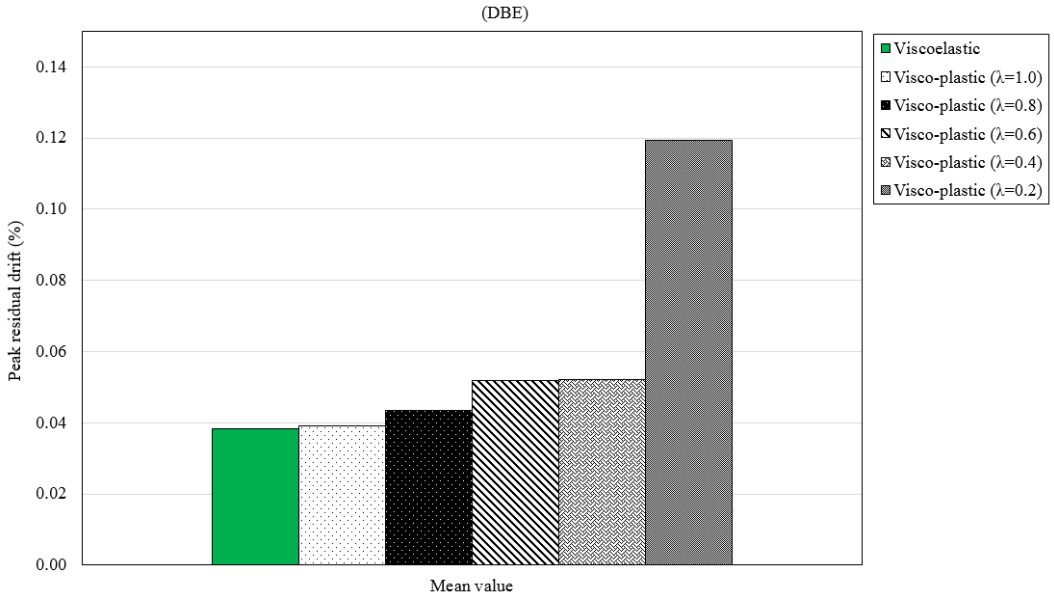

Fig. A.26 5-storey peak residual drift(%) mean value for 20 seismic records under DBE

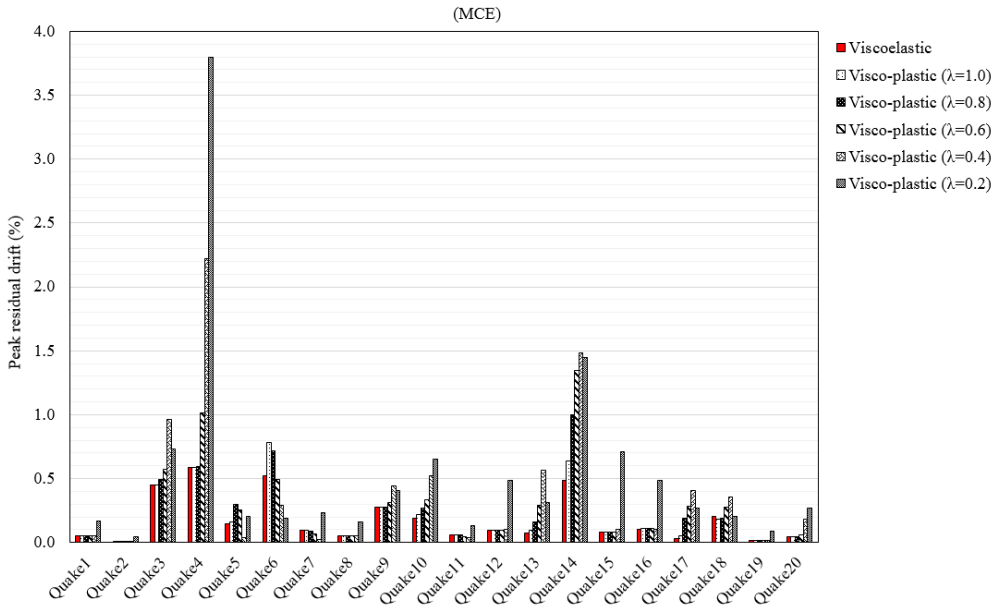

Fig. A.27 10-storey peak residual drift (%) under MCE

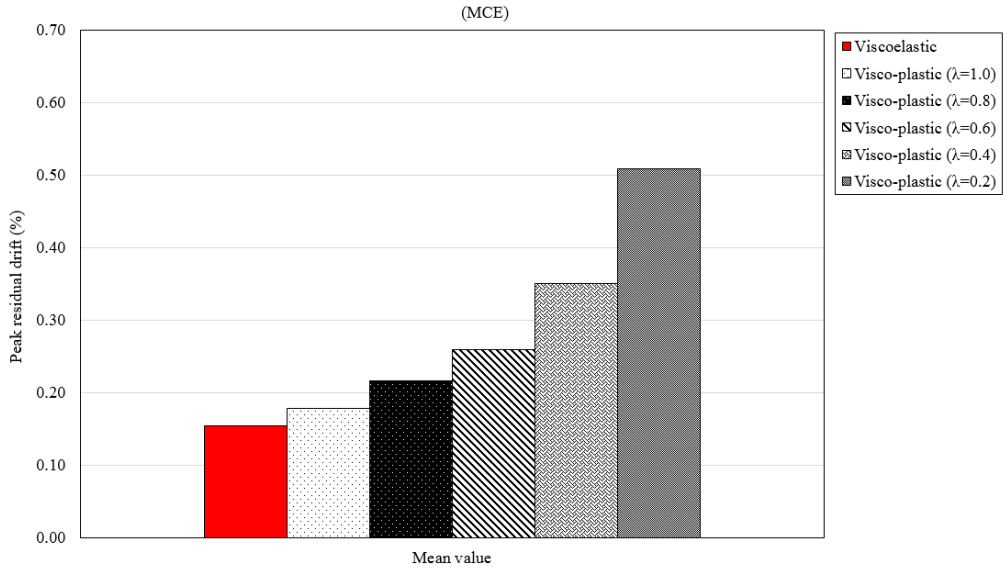

Fig. A.28 10-storey peak residual drift(%) mean value for 20 seismic records under MCE

(20story)

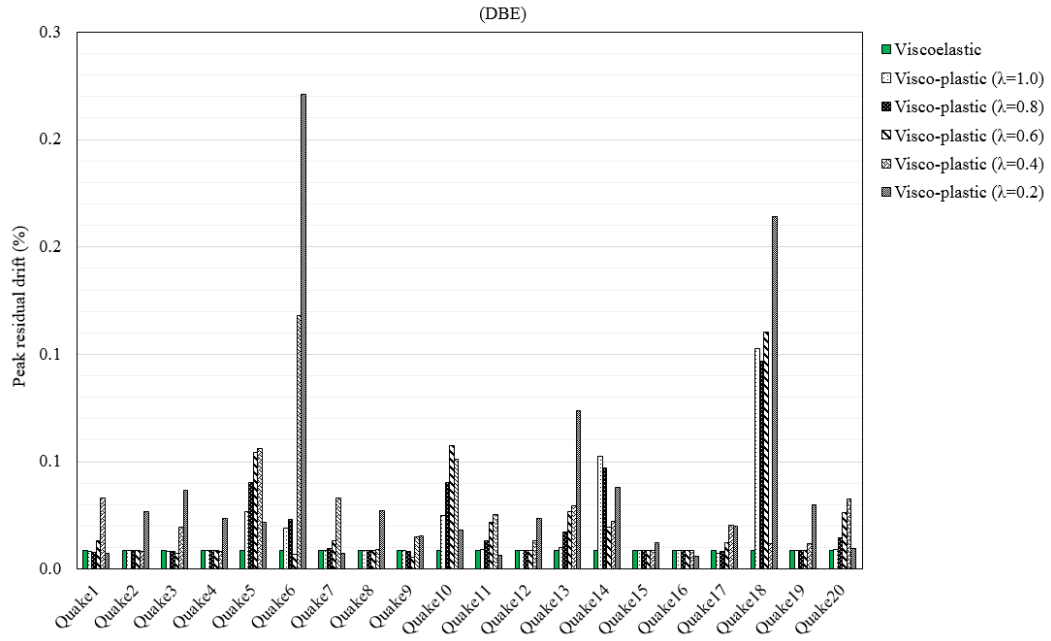

Fig. A.29 20-storey peak residual drift (%) under DBE

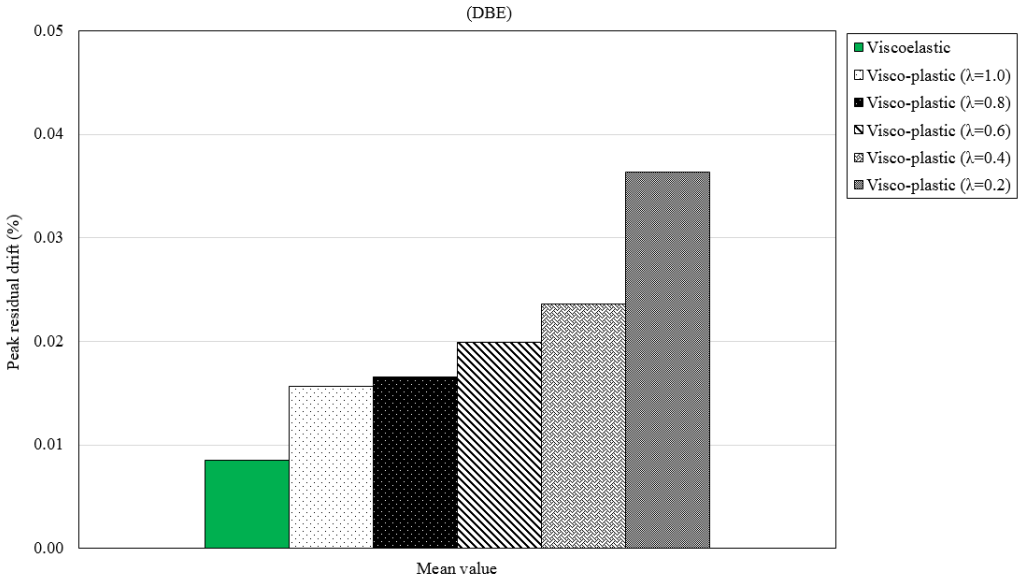

Fig. A.30 20-storey peak residual drift(%) mean value for 20 seismic records under DBE

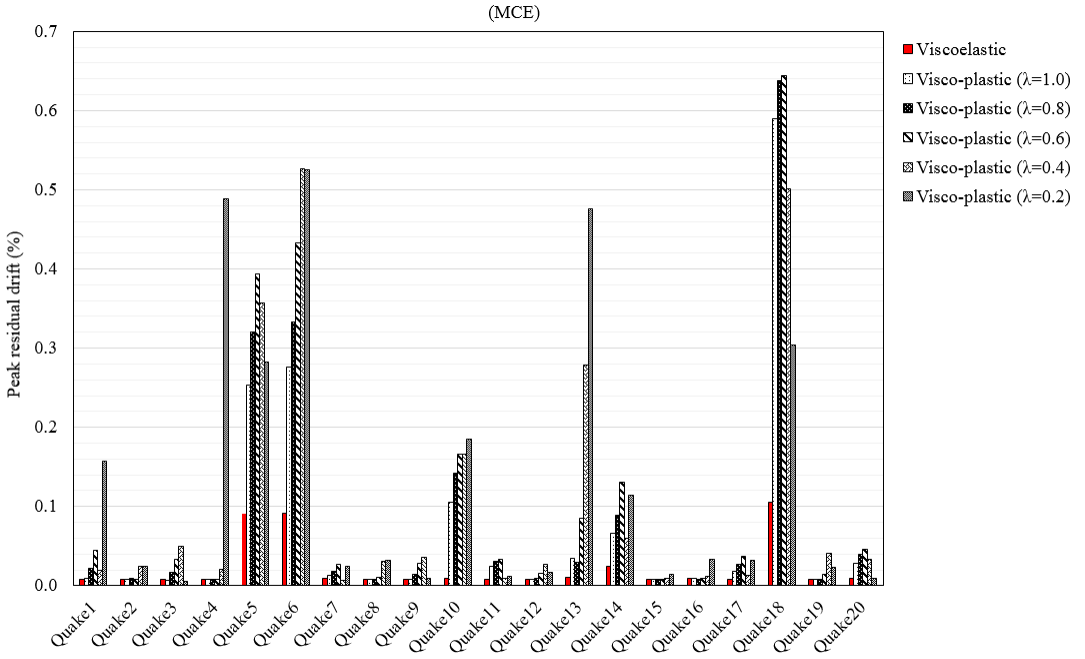

Fig. A. 31 20-storey peak residual drift (%) under MCE

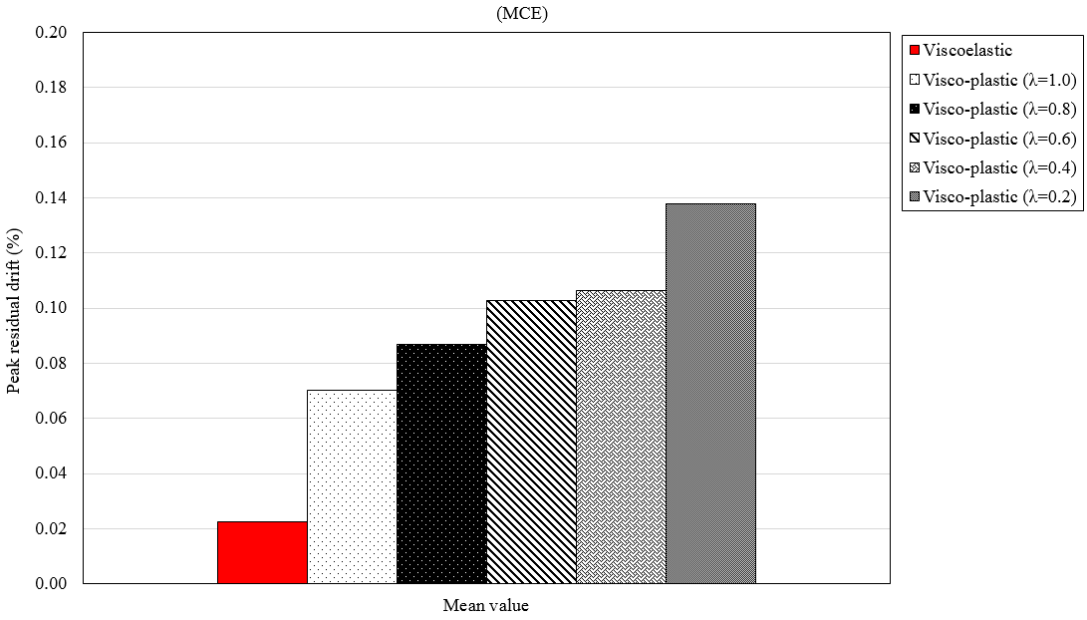

Fig. A.32 20-storey peak residual drift(%) mean value for 20 seismic records under MCE

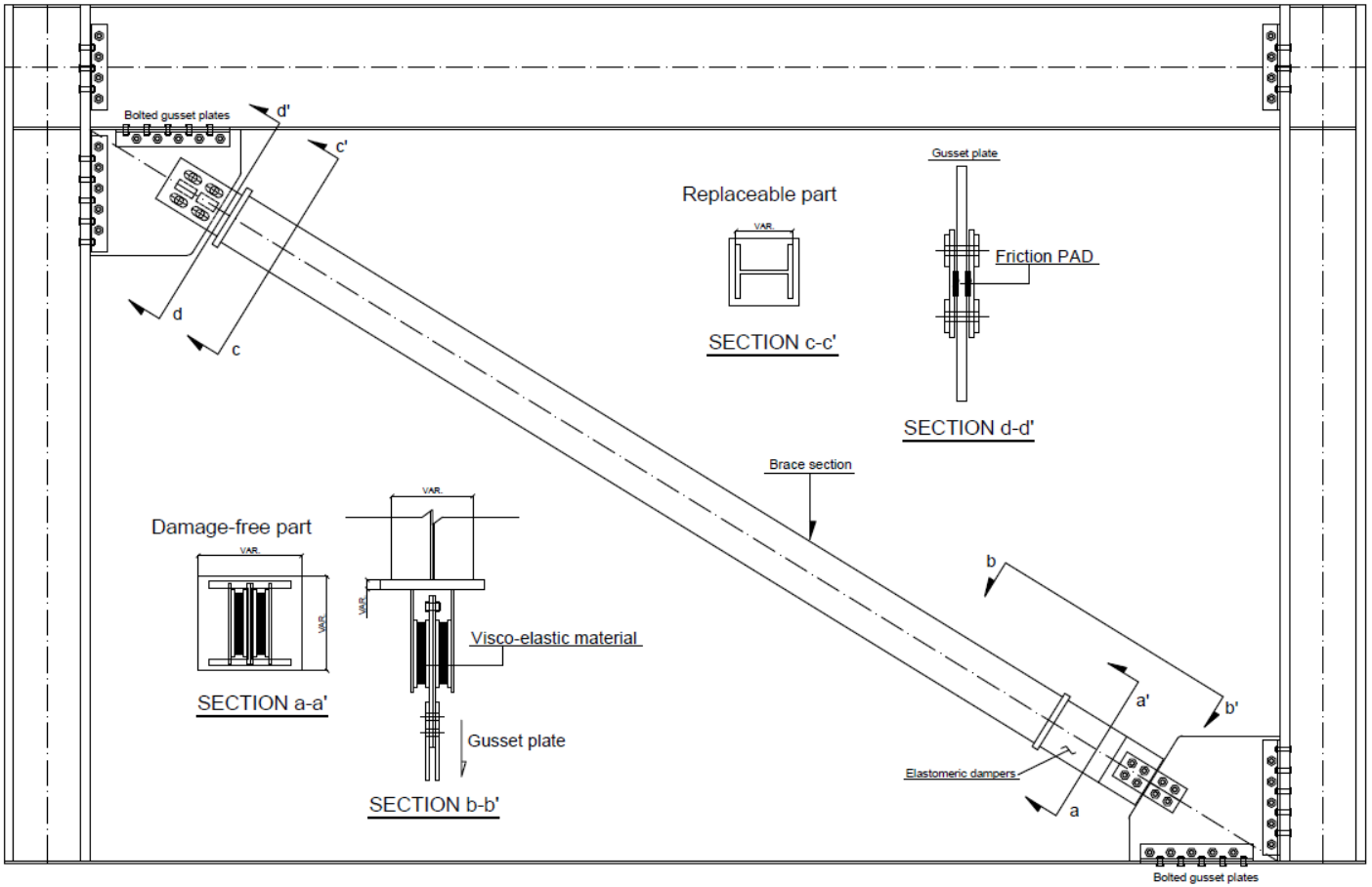

Fig. A.33 VPD (Viscoelastic & Friction devices) tentative application details (Brace-type)

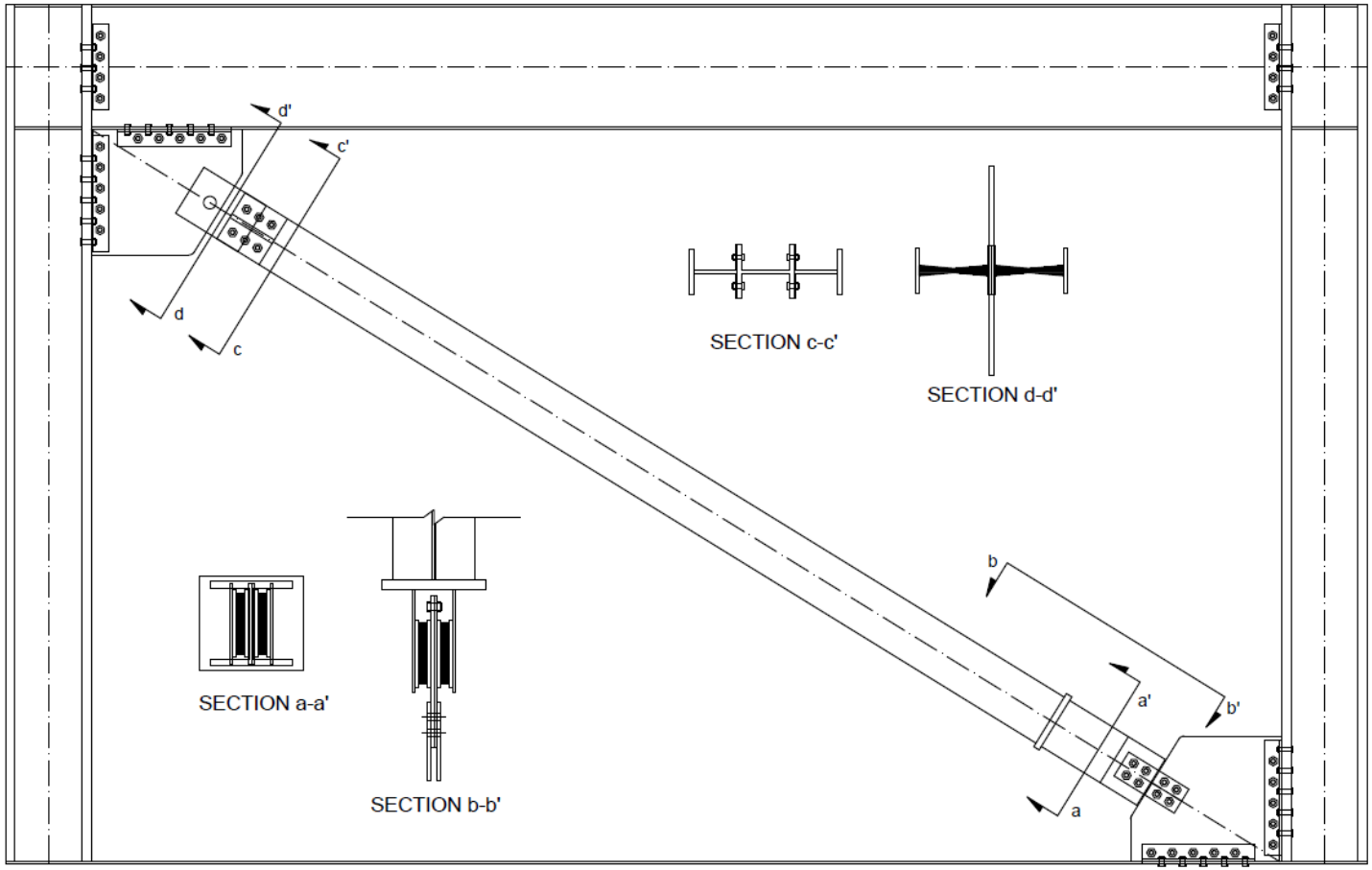

Fig. A.34 VPD (Viscoelastic & Friction devices) tentative application details (Brace-type)